INTERFACIAL INTERACTIONS IN ARAMID FIBRE COMPOSITES

By

Daryl Robert Williams

A dissertation submitted to the University of London for the degree of Doctor of Philosophy.

Department of Chemical Engineering and Chemical Technology

Imperial College of Science, Technology and Medicine

London SW7 2BY

December 1989

PREFACE

The work described in this dissertation was carried out in the Department of Chemical Engineering and Chemical Technology, Imperial College, London between March 1986 and November 1989. Except where acknowledged, the material is the original work of the author and includes nothing which is the outcome of work in collaboration, and no part of it has been submitted for a degree at any other university

I am extremely grateful to Dr. B.J. Briscoe for his support and encouragement during my time at Imperial College. His advice, guidance and friendship have been invaluable.

The important and varied contributions of a number of individuals is also acknowledged. The technical assistance provided Mr. L.Moulder, Mr.S.Roach, Mr. G. Senior and Mr. R. Wilkins at Imperial College is acknowledged, as are discussions with Dr. G. Godokian and library support provided by Mrs. S. Dibley. The generous help provided by Dr. G. George and Miss H.Willis from the Surface Analysis facility, University of Queensland is acknowledged. The assistance and friendship of the members of the Particle Technology Group is also acknowledged.

I am especially grateful for the generous financial support provided by Materials Research Laboratories, DSTO and the Public Service Board of the Australian Government, in the form of a Postgraduate Study Award. Financial assistance for materials and equipment provided by Fibers Department, Du Pont, USA is also gratefully acknowledged.

I would also like to thank my parents and Mary Simmons for their support of my studies.

Finally I would like to thank my wife Kate for her untiring love, patience and support though-out my time at Imperial College.

Daryl Williams

December 1989

For Hugh

ABSTRACT

This thesis describes an experimental study of the influence of fibre surface modifications on the mechanical performance of aramid-epoxy composites. Fibre modifications were chosen so that a range of interface adhesive strengths could be prepared, from potentially weak to potentially strong. Fibres were coated with a range of polymers to make weak interfaces, whilst a novel solution graft route was developed for introducing new functional groups onto the fibre surface so as to make stronger interfaces. Successful grafting of various groups onto the fibre surface was confirmed and quantified by X-ray photoelectron spectroscopy, gas adsorption and wettability. The transverse compressional properties of the unimpregnated fabrics were studied and appeared to be strongly dependent on the fibre-fibre friction within the fabric assembly. The modified fabrics were found to have a wide range of frictional, and thus compliance, properties. The compressional properties of the fabrics were in general agreement with the deduced mutual interfacial shear stresses of the fibre surfaces predicted on the basis of literature data.

Epoxy laminates were manufactured from the modified aramid fabrics and examined in a variety of modes of mechanical deformation. The tests used were short beam shear, flexural, mode I interlaminar fracture, high speed ballistic impact and micro-mechanical measurements. The results obtained from the short beam shear test, the flexural test and the micro-mechanics showed that the nature of these types of mechanical responses was essentially independent of the fibre surface treatments.

In contrast, the interlaminar fracture behaviour of the laminates, as determined by a new analytical method, was found to be markedly dependent on the presence of a fibre bridging phenomenon which involves filaments spanning the crack zone. The interlaminar fracture results and the derived sizes of the fibre bridging zone, a_b, were found to be clearly dependent on the nature of the fibre surface treatments. The larger values of a_b were found for those materials with the largest interlaminar fracture energies which were also observed to have the most fibre pull-out during fracture. Those fibre surfaces which

produced the lowest fibre-fibre friction in the weave appeared to promote the fibre-bridging process. The ballistic deformation experiments produced data which broadly confirmed the importance of the bridging phenomenon .

The mechanical tests did *not* produce the anticipated correlations between the fibre surface energetics and the composite performance. A stronger and more physically significant correlation between the interlaminar fracture energy and the fibre-fibre friction was deduced. It is argued that the fibre-fibre friction directly controls the fibre migration process which in turns determines the extent of fibre bridging. This fabric-matrix interpenetration in the resin interlayers appears to have a pronounced influence on the interlaminar fracture energy. Fibre migration and hence the extent of fibre bridging was apparently the greatest for the least compliant fabrics which were composed of relatively low friction fibre-fibre junctions.

The primary conclusion of this thesis is that, in the case of aramid-epoxy laminates at least, the structure within the composite materials is of a greater significance than the fibre-matrix interfacial adhesion in determining the material performance.

CONTENTS

FIGURE LEGENDS		10
TABLE LEGENDS		16
LIST OF SYMBOLS		20
CHAPTER 1		
INTRODUCTION		27
1.1	FIBRE-MATRIX INTERFACE: CURRENT STATUS OF RESEARCH	27
1.2	RESEARCH STRATEGY ADOPTED IN CURRENT WORK	28
1.3	GENERAL FORM OF THE THESIS	31
CHAPTER 2		
INTERFACIAL ADHESION		
2.1	INTRODUCTION	33
2.2	THEORIES OF ADHESION	33
2.2.1	Mechanical Theories of Adhesion	33
2.2.2	Diffusion Model of Adhesion	34
2.2.3	Adsorption Theory of Adhesion	35
2.2.4	Chemical Bonding Theory of Adhesion	36
2.2.5	Electronic Theory of Adhesion	36
2.3	ADHESION IN FIBROUS COMPOSITES	37
2.4	CONCLUSIONS	39
CHAPTER 3		
ARAMID FIBRE SURFACE MODIFICATION		
3.1	INTRODUCTION	40
3.2	FIBRE SURFACE MODIFICATION	40
3.2.1	Gas Phase Chemical Plasmas	40
3.2.2	Solution Graft Reactions	42
3.2.3	Polymeric Coatings	44
3.2.4	Conclusions	46
3.3	EXPERIMENTAL SURFACE MODIFICATION	46
3.3.1	Cleaning of Aramid Fibres	46
3.3.2	Experimental Solution Graft Reactions	46

3.3.3	Preparation of Modified Fabrics via Graft Reactions	49
3.3.4	Preparation of Modified Fabrics via Polymer Deposition	52
3.3.5	Nature of Surface Modifications	53
3.3.6	Discussion	53
3.3.7	Conclusions	53

CHAPTER 4

X-RAY PHOTOELECTRON SPECTROSCOPY

4.1	INTRODUCTION	55
4.2	A LITERATURE REVIEW OF XPS	55
4.2.1	Introduction to XPS	55
4.2.2	Photoelectron Emission	56
4.2.3	Valence Band Photoelectron Studies	57
4.2.4	XPS Apparatus	57
4.2.5	Core Level Photoelectrons	60
4.2.6	Satellite Peaks	62
4.2.7	Surface Chemical Derivatives	62
4.2.8	Depth Profiling	63
4.2.9	Recent Advances in XPS	64
4.2.10	Application of XPS	65
4.2.11	XPS of Aramid Polymers	65
4.2.12	Conclusions	69
4.3	EXPERIMENTAL XPS STUDY	70
4.3.1	XPS Experiments	70
4.3.2	XPS Results	72
4.3.3	Surface Analysis of Cleaned and "As received " "Kevlar" Fibres	77
4.3.4	Surface Analysis of Polymeric and Oligiomeric Coated"Kevlar" Fibres	79
4.3.5	Surface Analysis of Functionally Grafted "Kevlar" Fibres	79
4.3.6	Conclusions	85

CHAPTER 5

WETTABILITY AND SURFACE ENERGETICS

5.1	INTRODUCTION	86
5.2	WETTING, ADHESION AND SURFACE ENERGETICS	86
5.2.1	The Young Equation	86
5.2.2	Work of Adhesion	88

5.2.3	The Equilibrium Spreading Pressure	89
5.2.4	The Critical Surface Tension Method	90
5.2.5	Semi-Empirical Surface Energy Models	91
5.2.6	Acid-Base Interfacial Interactions	95
5.2.7	Contact Angle Hysteresis	100
5.2.8	Equilibrium Contact Angle	102
5.2.9	Fibre Wettability by the Drop Profile Method	102
5.2.10	Fibre Wettability by the Wetting Force Method	104
5.2.11	Aramid Fibre Wettability	107
5.2.12	Conclusions	109
5.3	EXPERIMENTAL CONTACT ANGLE STUDY	109
5.3.1	Drop Profile Measurement of Contact Angles	109
5.3.2	Wilhelmy Balance Measurement of Contact Angles	112
5.3.3	Wetting Force Measurements	114
5.3.4	Contact Angle Data	119
5.3.5	Fibre Surface Energetics	123
5.3.6	Conclusions	126

CHAPTER 6
INVERSE GAS CHROMATOGRAPHY

6.1	INTRODUCTION	128
6.2	SURFACE CHARACTERISATION USING GASEOUS PROBES	128
6.2.1	Gas-Solid Interactions	128
6.2.2	Basic Gas Chromatography	129
6.2.3	The Gas Chromatographic Adsorption Process	130
6.2.4	Chromatographic Peaks and the Adsorption Isotherm	133
6.2.5	Non-Linear Adsorption Studies on Polymers using IGC	136
6.2.6	Linear Adsorption Studies on Polymers using IGC	139
6.2.7	Adsorption Studies on Aramid Fibres using IGC	144
6.3	EXPERIMENTAL IGC STUDY OF ARAMID FIBRES	146
6.3.1	Materials and Equipment	146
6.3.2	IGC Results	149
6.3.3	Discussion	155
6.3.4	Conclusions	158

CHAPTER 7
INTERLAMINAR BEHAVIOUR OF LAMINATES
7.1 INTRODUCTION 159
7.2 INTERLAMINAR PERFORMANCE OF COMPOSITES 159
7.2.1 Interlaminar Shear in Composites 159
7.2.2 Interlaminar Shear and Fibre-Matrix Adhesion 160
7.3 INTERLAMINAR EXPERIMENTS 162
7.3.1 Sample Preparation 162
7.3.2 Sample Cutting 164
7.3.3 Sample Polishing 166
7.3.4 Interlaminar Testing 166
7.3.5 Flexural Results 168
7.3.6 Short Beam Shear Results 169
7.3.7 Discussion 171
7.4 CONCLUSIONS 174

CHAPTER 8
FRACTURE IN COMPOSITES
8.1 INTRODUCTION 175
8.2 A REVIEW OF THE FRACTURE OF MATERIALS 175
8.2.1 Linear Elastic Fracture Mechanics 175
8.2.2 Brittle versus Ductile Fracture 177
8.2.3 Elastic Stresses Near the Crack Tip 178
8.2.4 Modes of Fracture Failure 179
8.2.5 Measurement of Fracture Energies 180
8.2.6 Fracture Behaviour of Epoxy Resins 183
8.2.7 Theoretical Fracture Mechanics of Composite Materials 184
8.2.8 Energy Absorption Mechanisms in Composites 185
8.2.9 Experimental Fracture Studies of the Composites 186
8.2.10 Fibre Bridging Effects in Composite Fracture 187
8.2.11 Experimental Studies of Fibre Bridging 188
8.3 EXPERIMENTAL FRACTURE MECHANICS STUDY 189
8.3.1 Specimen Preparation 189
8.3.2 Determination of G_{IC} 193
8.3.3 Fracture Mechanics Results 196
8.3.4 Modelling the Effects of Fibre Bridging 201

8.3.5	"Kevlar"-Epoxy G_{IC} Results	201
8.3.6	Fracture Energy Analysis using the Reduced Crack Length Approach	203
8.3.7	Discussion of Fracture Results	210
8 3.8	Presence of an Fibre Bridging Zone	210
8.3.9	Microscopy of Fracture Surfaces	213
8.3.10	Mechanism of Laminate Failure	217
8.3.11	Conclusions	218

CHAPTER 9

BALLISTIC PERFORMANCE OF ARAMID COMPOSITES

9.1	INTRODUCTION	219
9.2	ADVANCED POLYMERS AND BALLISTIC PERFORMANCE	219
9.2.1	Literature Review	219
9.2.2	Conclusions	222
9.3	EXPERIMENTAL BALLISTIC STUDY	223
9.3.1	Equipment	223
9.3.2	Results	227
9.3.3	Discussion	227
9.3.4	Conclusions	232

CHAPTER 10

INTERFACIAL MECHANICS

10.1	INTRODUCTION	233
10.2	INTERFACIAL SHEAR STRENGTH OF POLYMERS.	234
10.2.1	Introduction	234
10.2.2	Friction	235
10.2.3	The Adhesive Component of Friction	237
10.2.4	Factors Affecting Adhesive Component of Friction	238
10.2.5	Conclusions	240
10.3	A REVIEW OF INTERFACIAL FIBRE MICROMECHANICS	240
10.3.1	Introduction	240
10.3.2	Interfacial Rupture by use of the Poisson Ratio	240
10.3.3	Experimental Fibre Pull-out Techniques	242
10.3.4	The Shearing of Microdroplets on Fibres	253
10.3.5	The Microdebonding Method	256
10.3.6	Determination of Single Fibre Critical Length	257

10.3.7	Raman Spectroscopic Studies of Micro-strain	260
10.3.8	Theoretical Aspects of Fibre-Matrix Micro-mechanics	262
10.3.9	Conclusions	268
10.4	A REVIEW OF FIBRE FRICTION	269
10.4.1	Introduction	269
10.4.2	Single Fibre Friction Studies	269
10.4.3	Fabric Mechanics	270
10.4.4	Conclusions	271
10.5	EXPERIMENTAL FIBRE MECHANICS STUDY	272
10.5.1	Introduction	272
10.5.2	Micro-debonding Experiments	272
10.5.3	Compressional Properties of "Kevlar" Fabrics	277
10.5.4	Conclusions	281

CHAPTER 11
CONCLUSIONS 282

JANUS 287

APPENDIX A 288
XPS Spectra of Surface Modified "Kevlar" Fibres

REFERENCES 308

FIGURE LEGENDS

CHAPTER 3

Figure 3.1 Some reaction routes studied for the modification of "Kevlar" fibre surfaces: (a) Keller *et al.* 1983 (b) Wake 1972 (c) Allred 1983

Figure 3.2 Reaction scheme for aramid graft reaction via dimethyl sulphinyl carbanion (DMSC).

CHAPTER 4

Figure 4.1 Schematic diagram of XPS equipment.

Figure 4.2 Binding energy shifts for carbon 1s photoelectrons as a function of the chemical substituent attached to the carbon nucleus.

Figure 4.3 Carbon 1s spectrum of a plasma polymerised vinylidene fluoride film. The deconvoluted component curves for the four chemical environments of the carbon atom are shown.

Figure 4.4 X-ray photoelectron spectrometer with a cylindrical mirror energy analyser.

CHAPTER 5

Figure 5.1 The equilibrium contact angle, θ, in relation to the liquid-vapour surface tension, $\gamma_{L\text{-}V}$, the solid-liquid interfacial tension ,$\gamma_{S\text{-}L}$, and the solid surface tension, $\gamma_S{}^o$. $\gamma_S{}^o$ consists of two components, the solid-vapour interfacial tension, $\gamma_{S\text{-}V}$, and the equilibrium film spreading pressure π_e.

Figure 5.2 Drop shape profile parameters where $\mathbf{x}_2$ is the drop radius, $\mathbf{x}_1$ is the fibre radius and **L** is the droplet length (Carroll 1976).

Figure 5.3 Schematic diagram of the apparatus for Wilhelmy plate measurement of surface tension or contact angle.

Figure 5.4 Microdroplets of water on a clean "Kevlar" monofilament.

Figure 5.5 Histogram of contact angles versus frequency of measurements using the drop profile method.

Figure 5.6 Successive wetting force traces for a water-air interface advancing against an "as received" " Kevlar" monofilament.

Figure 5.7 Receding (upper) and advancing (lower) wetting traces for water with a diol grafted fibre.

Figure 5.8 A model asperity on a fibre in profile with an angle α and a height Δh.

Figure 5.9 Wetting force fluctuations as a function of the liquid surface tension for polyethylene terephthalate fibres (Kremnitzer 1978).

Figure 5.10 Wetting (advancing and receding) traces for hexadecane with a "Kevlar" fibre.

CHAPTER 6

Figure 6.1 Chromatogram for a methane, hexane, heptane and octane. t_M represents the elution of non-adsorbed species, whilst t_{R1} , t_{R2}, t_{R3} represents the time for the elution of adsorbed species hexane, heptane and octane respectively.

Figure 6.2 The relationship between the isotherm shape and the chromatographic peak-shape at infinite dilution concentrations. Case (a) represents the case of concave BET type isotherm with a skewed Gaussian chromatographic peak ($S< 0$), case(b) represents an essentially linear isotherm with Gaussian chromatographic peak and case(c) represents a convex Langmuirian shaped isotherm with skewed Gaussian peak ($S>0$) (Condor and Young 1979).

Figure 6.3 Overlaid chromatograms for dioxane on cellulose fibres at 25.7°C obtained via the elution of a characteristic point technique. Note the movement in the superimposed boundaries from the rear chromatogram boundary to the front boundary (Mohlin and Gray 1974).

Figure 6.4 Layout of apparatus for inverse gas chromatography.

CHAPTER 7

Figure 7.1 Schematic representation of the flexure experiment.

Figure 7.2 "Kevlar"-epoxy laminate samples after flexure and short beam shear tests.

CHAPTER 8

Figure 8.1 Modes of failure by fracture.

Figure 8.2 Experimental methods for the measurement of G_{IC}.

Figure 8.3 Schematic diagram showing crack growth with and without fibre bridging.

Figure 8.3 Schematic diagram of fracture mechanics specimen.

Figure 8.4 Fracture mechanics sample in loading jig of Instron Testing machine.

Figure 8.5 G_{IC} values as a function of the crack length, **a**, for two different "Kevlar"-epoxy laminates.

Figure 8.6 Fracture energy versus crack length for the amine treated fabric.

Figure 8.7 Fracture energy versus crack length for the "as received" fabric.

Figure 8.8 Fracture energy versus crack length for the clean fabric.

Figure 8.9 Fracture energy versus crack length for the diol grafted fabric.

Figure 8.10 Fracture energy versus crack length for the epoxy grafted fabric.

Figure 8.11 Fracture energy versus crack length for the epoxy coated fabric.

Figure 8.12 Fracture energy versus crack length for the PDMS coated fabric.

Figure 8.13 Fracture energy versus crack length for the PEG fabric.

Figure 8.14 Fracture energy versus crack length for the metallated/clean fabric.

Figure 8.15 Bending Force versus crack length for the amine coated fabric.

Figure 8.16 Bending force versus crack length for the "as received" fabric.

Figure 8.17 Bending force versus crack length for the clean fabric.

Figure 8.18 Bending force versus crack length for the diol grafted fabric.

Figure 8.19 Bending force versus crack length for the epoxy grafted fabric.

Figure 8.20 Bending force versus crack length for the epoxy coated fabric.

Figure 8.21 Bending force versus crack length for the PDMS coated fabric.

Figure 8.22 Bending force versus crack length for the PEG coated fabric.

Figure 8.23 Bending force versus crack length for the metallated/cleaned fabric.

Figure 8.24 Experimental and predicted values of G_{IC} versus crack length, **a**, for the laminate made from the cleaned fabric. The predicted values were computed using the reduced crack length concept.

Figure 8.25 Fractography of the laminate based on the "as received" fabric.

Figure 8.26 Fractography of the laminate based on the diol grafted fabric.

Figure 8.27 Fractography of the laminate based on the epoxy grafted fibres.

Figure 8.28 Fractography of the laminate based on the metallated/cleaned coated fabric.

CHAPTER 9

Figure 9.1 Schematic diagram of the high speed gas gun equipment.

Figure 9.2 Diagram of the laminate specimen and the flight of projective.

Figure 9.3 Frontal view of the gas gun apparatus.

Figure 9.4 Three different laminate samples showing different extents of delamination on the sample rear face following impact. The samples are from left to right: clean, metallated/clean specimens and epoxy grafted laminates.

CHAPTER 10

Figure 10.1 A schematic diagram of a rigid asperity sliding against a soft polymer. Energy is dissipated in the shear interfacial zone as well as the bulk deformation zone.

Figure 10.2 Schematic diagrams of two tests designed to measure (a) the interfacial transverse tensile strength, **S**, and (b) the interfacial shear debonding strength, τ_i .

Figure 10.3 A schematic diagram of the single fibre pull-out experiments developed by Broutman (1963). In figure (a) the fibre is pulled from a block of matrix, whilst in figure (b) the fibre is pulled from a thin matrix film.

Figure 10.4 A typical load versus displacement curve for a single fibre pull-out experiment.

Figure 10.5 A typical force, **F**, versus displacement, **u**, trace for a single fibre pull-out experiment as a function of the externally imposed pressure, $\mathbf{P}_a$ (Chua and Piggott 1985c).

Figure 10.6 Adhesion force, $\mathbf{F}_a$, for a polyester matrix with glass fibres as a function of embedding depth **L** and external pressure $\mathbf{P}_a$. The data points represented by an (x) and an (o) denote fibre breakage and fibre pull-out respectively (Chua and Pigggott 1985c).

Figure 10.7 Measurement of τ_i using the microdroplet shearing technique (Miller *et al.* 1985).

Figure 10.8 Schematic diagram of the micro-indentation method for measuring τ_i .

Figure 10.9 In the critical fibre length experiment a single fibre is embedded into a matrix phase. Upon matrix straining, fibre fragmentation occurs resulting in a distribution of fibre fragment lengths $\mathbf{L}_{c1}$, $\mathbf{L}_{c2}$ ... $\mathbf{L}_{cn}$.

Figure 10.10 σ_f, and τ_i , as a function of position, **x**, for a single embedded fibre subject to elastic stress transfer between the fibre and the matrix (Cox 1952; Piggott 1980).

Figure 10.11 σ_f and τ_i , as a function , **x**, for a single embedded fibre with plastic yielding between fibre and matrix (Kelly and Davies 1965; Piggott 1980).

Figure 10.12 σ_f and τ_i , as a function of, **x**, for a single embedded fibre with interfacial slippage between fibre and matrix Piggott (1978).

Figure 10.13 Typical trace of **F** versus **d** obtained by debonding an epoxy micro-droplet from a "Kevlar" fibre.

Figure 10.14 Apparatus for conducting the micro-debonding experiments.

Figure 10.15 Compression loading and unloading of a range of surface modified "Kevlar" fabrics.

Figure 10.16 First and second compression loading/unloading cycles for the metallated/clean "Kevlar" fabric.

TABLE LEGENDS

CHAPTER 4

Table 4.1 Surface C, O and N composition for various "Kevlar 49" fabrics (Allred 1983).

Table 4.2 Experimentally observed and predicted carbon 1s peak positions, as well as the surface composition of a number of model aramid compounds (Chappell *et al.* 1989).

Table 4.3 C, O and N surface composition, the entropy of adsorption for n-octane ($-\Delta S_A^o$) and the dispersive component of the surface free energy (γ_S^d) for various "Kevlar" fibres (Chappell *et al.* 1989).

Table 4.4 Comparison of the XPS peak positions (and peak width at 1/2 height) for clean "Kevlar 49" fibres.

Table 4.5 Surface composition of the "Kevlar" fibres as determined by XPS analysis

Table 4.6 Position of peak maximum (and peak width at 1/2 height) for the principal XPS spectral peaks of the "Kevlar 49" fibres

Table 4.7 Experimental and predicted atomic surface composition for the polymeric and oligiomeric coated "Kevlar" fibres.

Table 4.8 Experimental and predicted atomic surface composition of the surface grafted "Kevlar" fibres.

CHAPTER 5

Table 5.1 Surface tension of a number of contact angle liquids, and their polar and dispersive components at 25°C. Taken from the work of Fowkes and co-workers (Fowkes 1964; Fowkes and Maruchi 1977; Williams and Fowkes 1989).

Table 5.2 Surface tension data via geometric, harmonic mean equations and Zisman's Critical Wetting Tension for a range of polymers (Wu 1982).

Table 5.3 Advancing work of adhesion for untreated and plasma modified aramid monofilaments with water and methylene iodide (Allred 1983).

Table 5.4 Advancing and receding contact angles for "Kevlar 49" monofilaments. The dispersive component of the surface tension was calculated from the methylene iodide contact angle data (Penn and Miller 1980).

Table 5.5 Advancing and receding contact angles for "Kevlar 49" fibres.

Table 5.6 Surface energetics of modified "Kevlar 49" fibres.

CHAPTER 6

Table 6.1 Surface chemical characterisation of carbon fibres by IGC and wettability measurements (Schultz *et al.* 1987a,b).

Table 6.2 Comparison between surface analysis using XPS and thermodynamic data from IGC experiments for a range of "Kevlar" materials (Chappell and Williams 1989a,b ; Chappell *et al.* 1989).

Table 6.3 V_N (cm^3 /gm) as a function of T (^oC) for clean and "as received" "Kevlar" fibres.

Table 6.4 V_N (cm^3/gm) as a function of T (^oC) for diol and octane grafted "Kevlar" fibres.

Table 6.5 Heats of condensation and adsorption for alkane vapours (kJ/mol). The results in brackets are the uncertainties in the adsorption heats (kJ/mol).

Table 6.6 The dispersive component of the surface energy, γ_S^d (mN/m).

Table 6.7 Total and estimated dispersive component of the heats of condensation for the acid-base probes (kJ/mol).

Table 6.8 Experimental heats of adsorption (kJ/mol) and their estimated acid-base component for various vapours. The results in brackets are the uncertainties in these heats (kJ/mol).

Table 6.9 The estimated $\Delta H_{complex}$ (kJ/mol) for the interaction between dimethyl-formamide with the acid-base probes and the experimental values of ΔH_{ad}^{a-b}.

CHAPTER 7

Table 7.1 Flexural Modulus **E**, strength **S**, and the relative energy to failure **T** for various "Kevlar"-epoxy laminates.

Table 7.2 Short beam shear strength, **D**, for various "Kevlar"-epoxy laminates manufactured from surface modified fabrics.

CHAPTER 8

Table 8.1 G_{IC} values as a function of epoxy and crosslinking chemicals (Kinlock and Young 1983).

Table 8.2 Experimental and numerical estimation of dC / da and G_{IC}.

Table 8.3 Pre-crack length for laminate samples.

Table 8.4 Mode I fracture energy G_{IC} and the effective crack zone length a_{eff} for various "Kevlar"-epoxy laminates. R denotes the co-efficient of fit for the linear regression data analysis.

CHAPTER 9

Table 9.1 Data from the ballistic impact experiments.

Table 9.2 Mode I fracture energy, G_{IC}, area of delamination, D_Z ,total ballistic energy absorbed, E_a , and the energy dissipated due to mode I impact fracture for each ply, E_l , for various "Kevlar"-epoxy laminates.

CHAPTER 10

Table 10.1 Interfacial shear strengths, τ_i, and frictional shear strengths, τ_f, for a number of "Kevlar" fibres with various thermoplastic matrixes (Eagles *et al.* 1976).

Table 10.2 Interfacial mechanical properties obtained from a single fibre pull-out experiment. Glass fibres were embedded in epoxy and polyester matrixes (Chua and Piggott 1985b).

Table 10.3 The coefficients of friction and the shrinkage pressures for a series of polyester/glass fibre and epoxy/glass fibre systems (Chua and Piggott 1985c).

Table 10.4 Measurement of τ_i using the shear micro-droplet debonding technique for a range of fibres with an epoxy polymer (Miller *et al.* 1985; Gaur and Miller 1989).

Table 10.5 Individual measurements of τ_i using the shear droplet debonding technique for a range of surface treated "Kevlar" fibres with an epoxy polymer.

Table 10.6 List of predicted values of τ_i decreasing in magnitude from the top of the list. Approximate values for τ_i are also shown.

LIST OF SYMBOLS

CHAPTER 2

W	=	work of adhesion

CHAPTER 4

BE	=	binding energy
$h\nu$	=	X-ray energy
KE	=	measured kinetic energy
ϕ	=	work function correction

CHAPTER 5

θ	=	equilibrium contact angle
$\gamma_{L\text{-}V}$	=	liquid-vapour interfacial tension
$\gamma_{S\text{-}L}$	=	solid-liquid interfacial tension
γ_S^o	=	solid surface tension
$\gamma_{S\text{-}V}$	=	solid-vapour interfacial
π_e	=	equilibrium film spreading pressure
W_{AB}	=	work of adhesion between phases A and B
W_{AA}	=	work of cohesion between phases A and A
ΔG	=	Helmholtz free energy
γ_A	=	interfacial tension for phase A
$W_{S\text{-}L}$	=	solid-liquid work of adhesion
γ_S	=	solid surface tension
$\gamma_{L\text{-}V}$	=	liquid-vapour surface tension
$\gamma_{S\text{-}L}$	=	solid-liquid interfacial tension
Γ	=	surface concentration of adsorbed species
p^o	=	saturated vapour pressure of adsorbate
p	=	vapour pressure of adsorbate
b	=	empirical constant
γ_c	=	critical wetting tension
γ	=	surface tension for any phase
γ^d	=	dispersive component of the surface tension
γ^p	=	polar component of the surface tension
γ^i	=	induction component of the surface tension
γ^h	=	hydrogen bonding component of the surface tension

n	=	the number of acid-base pairs per unit interface
W	=	work of adhesion
W^d	=	dispersive component of the work of adhesion
W^p	=	polar component of the work of adhesion
γ_S^d	=	dispersive component of the solid surface tension
γ_S^p	=	polar component of the solid surface tension
C_A, E_A	=	Drago's acid-base constants for species A
C_B, E_B	=	Drago's acid-base constants for species B
f	=	constant normally equal to 1
W^{a-b}	=	acid-base component of the work of adhesion
n_a	=	concentration of acid groups per unit area
n_b	=	concentration of base groups per unit area
γ^{LW}	=	long range (dispersive) component of the surface tension
γ^+	=	acid surface energy parameter
γ^-	=	basic surface energy parameter
θ_A	=	advancing contact angle
θ_R	=	receding contact angle
r	=	roughness factor
θ_w	=	Wenzel's contact angle
θ_0	=	real contact angle.
θ_C	=	Cassie's angle
A_1	=	area fractions of a region whose contact angle is θ_1
A_2	=	area fractions of a region whose contact angle is θ_2
x_2	=	drop radius
x_1	=	fibre radius
L	=	droplet length
S_c	=	critical spreading coefficient
F	=	change in the wetting force
P	=	perimeter of plate
Δw	=	wetting force fluctuations
Δc	=	diameter fluctuations
Δh	=	asperity height
α	=	angle of inclination made by an asperity to the fibre surface.

CHAPTER 6

t_M	=	elution time of a non-adsorbed species
t_{Rx}	=	elution time of an adsorbed species x
F	=	carrier gas flow rate dead volume
V_M	=	dead volume
V_R'	=	adjusted retention volume
j	=	gas compressibility correction factor
p_i	=	column inlet pressure
p_o	=	column outlet pressure
V_N	=	net retention volume
W_s	=	mass of stationary phase
T	=	column temperature
V_g	=	specific retention volume
K_S	=	slope of the isotherm at infinite dilution
A	=	surface area of sample
c	=	solute concentration in the gas phase
q	=	solute concentration in the stationary phase
dq/dc	=	slope of the adsorption isotherm
y_o	=	mole fraction of solute in the gas phase at the column outlet
m	=	mass of sample
p/p_o	=	relative vapour pressure
π_e	=	equilibrium spreading pressure
γ_S^d	=	dispersive component of the surface tension of solid surface
N	=	Avagadro's constant
$a_{(CH2)}$	=	surface area of a $-CH_2-$ group
$\gamma_{(CH2)}$	=	surface energy of hypothetical $-CH_2-$ liquid
$-\Delta G_{(CH2)}$	=	free energy of adsorption for a $-CH_2-$ group
T	=	temperature
R	=	universal gas constant
A	=	surface area of the probe molecule
c	=	a constant term for the loss of entropy on adsorption
S	=	specific surface area of the adsorbent
C	=	a measure of dispersive surface energy of adsorbent
C'	=	a measure of acid(acceptor) properties of adsorbent

C''	=	a measure of base(donor) properties of adsorbent
ΔG	=	free energy
ΔH	=	enthalpy
K_A	=	acidity constants
K_B	=	basicity constant
$\Delta H_{acid\text{-}base}$	=	enthalpy of acid-base interaction
DN	=	donor number
AN	=	acceptor number
γ_S^p	=	polar component of the surface tension of solid surface
γ_S	=	surface tension of solid surface
E_A, E_B	=	Drago's acid-base constants
C_A, C_B	=	Drago's acid-base constants
ΔS^o	=	entropy
q_d	=	isosteric heat of adsorption
V_W	=	retention volume for adsorption onto the column walls
ΔH_{con}	=	heat of condensation
$\Delta H_{con}^{a\text{-}b}$	=	acid-base component of the heat of condensation
ΔH_{con}^{d}	=	dispersive component of the heat of condensation
$\Delta H_{ad}^{a\text{-}b}$	=	acid-base component of the heat of adsorption
ΔH_{ad}^{d}	=	dispersive component of the heat of adsorption
$\Delta H_{self\ assn}$	=	heat of self association
$\Delta H_{complex}$	=	heat of complexation

CHAPTER 7

E	=	flexural modulus
L	=	support span distance
m	=	initial slope of stress/strain curve
b	=	sample width
d	=	sample thickness or depth
S	=	flexural strength
P	=	maximum load
T	=	energy to failure
D	=	short beam shear strength

CHAPTER 8

$\mathbf{U}$	=	elastic strain energy per unit thickness
σ	=	failure stress
$\mathbf{a}$	=	half crack length
$\mathbf{E}$	=	Young's modulus
ν	=	Poisson's ratio
γ	=	surface energy
$\mathbf{G}$	=	fracture energy
$\mathbf{G_C}$	=	critical rate of fracture energy release
σ_{tip}	=	stress near the crack tip the bulk
σ_{∞}	=	stress the bulk material stress
$\mathbf{K}$	=	stress intensity factor
$\mathbf{r}$	=	the crack tip radius
$\mathbf{a}$	=	the half crack length
$\mathbf{K_I}$	=	the stress intensity factor for mode I fracture
$\mathbf{K_C}$	=	the critical stress intensity factor
$\mathbf{G_{IC}}$	=	fracture energy for mode I fracture
$\mathbf{G_{IIC}}$	=	fracture energy for mode II fracture
$\mathbf{G_{IIIC}}$	=	fracture energy for mode III fracture
$\mathbf{V_f}$	=	volume fraction
σ_f	=	ultimate tensile strength of fibre
$\mathbf{y}$	=	average debonded length of fibre
$\mathbf{E}$	=	Young's modulus
τ_i	=	interfacial frictional shear stress
$\mathbf{L_c}$	=	critical transfer length of fibre
$\mathbf{d}$	=	fibre diameter
$\Delta\varepsilon$	=	differential failure strain between fibre and resin
$\mathbf{N}$	=	force
$\mathbf{d}$	=	loadline displacement
$\mathbf{a}$	=	crack length
$\mathbf{B}$	=	specimen width
$\mathbf{C}$	=	beam compliance
ε	=	error function
$\mathbf{C(a)_i}$	=	beam compliance as a function of crack length for *i* th datum point

ß	=	polynomial co-effecients
a_{eff}	=	reduced crack length
a_b	=	length of fibre bridging zone

CHAPTER 9

V_i	=	impact velocity
V_e	=	exit velocity
E_a	=	total ballistic energy absorbed
E_l	=	energy absorbed by interlaminar fracture per interply
D_z	=	size of delamination zone

CHAPTER 10

W	=	normal load
n	=	load index
k	=	constant
τ_o	=	material constant
α	=	material constant
τ_i	=	interfacial shear stress
D	=	fibre diameter
L	=	length of the cylindrical section of fibre embedded in resin
F	=	frictional force
A	=	area of interfacial contact
S	=	transverse tensile strength
σ_m	=	axial compressive stress on specimen
ν_m	=	Poisson ratio for matrix
ν_f	=	Poisson ratio for fibre
E_f	=	Young's elastic modulus for fibre
E_m	=	Young's elastic modulus for matrix
τ_f	=	frictional force for fibre pull-out
G_i	=	work of fracture of the interface
τ_a	=	adhesion shear stress
τ_{iy}	=	interfacial yield stress
τ_w	=	average (interfacial) shear stress

r	=	fibre radius
Q	=	area under the stress-strain pull-out curve
$(dF/du)_L$	=	steepest slope of the fibre pull-out stress strain curve at $u=L$.
u	=	displacement
P_a	=	external pressure
L_c	=	critical fibre length
μ	=	coefficient of friction
P_o	=	shrinkage pressure
P_a	=	applied pressure
n^2	=	$E_m / \{E_f (1 + \nu_m). \ln(R / r)\}$
s	=	L / r
R	=	distance to nearest fibre
r	=	radius of fibre
σ_f	=	stress for fibre failure
x	=	distance from the matrix surface to the fibre

CHAPTER 1

INTRODUCTION

This thesis describes a broad experimental study of interfacial interactions in aramid fibre reinforced epoxy composites. A prime objective of the study has been to determine the interrelationship between fibre-matrix interactions and the mechanical performance of aramid fibre based composites. The research strategy adopted in this thesis has involved a systematic study of fibre surface modification and surface characterisation, coupled with a range of mechanical evaluations of the performance of the materials manufactured from these fibres. It was anticipated at the inception of the study that this approach would allow the interrelationships between interfacial interactions and composite performance to be established. At the conclusion of this study the value of this correlation is addressed.

1.1 Fibre-Matrix Interface: Current Status of Research

Whilst the initial research and development in fibre reinforced composites concentrated on the matrix and fibre components, research on the fibre-matrix interface has become more prominent during the last 10 years. It is now generally agreed that the performance of fibre reinforced composites depends on the fibre, the matrix and the interface. However the effect of interface properties on the performance of composites is far from being fully understood.

The primary role of the interface is to provide a means by which load may be transferred from the "stiff" anisotropic high modulus fibres to the "softer" isotropic matrix materials. The fibre-matrix adhesion determines the essential efficiency of this stress transfer process and thus influences both the shear and the off-axis mechanical properties of the composite.

Because of the interdisciplinary nature of the science of composite interfaces,

scientists and engineers have found it necessary to consider the implications of several disciplines such as surface chemistry, micro-mechanics, stress analysis, adhesion science, mechanics of anisotropic materials, polymer chemistry and surface physics. In many cases research laboratories have not had the wide experience necessary in this range of disciplines to tackle comprehensively the fundamental role of the interfaces on composite mechanics. Consequently the appropriate experimental techniques required to probe the fibre-matrix interface have developed relatively slowly.

It has only been during the last 5 years that research has significantly focussed on the interface in fibre reinforced composites. Increased interest in this area is reflected in the growth of international meetings, for example the International Conference on Composite Interfaces held biennially at Case Western University since 1986, and more recently the European based conference series on Interfacial Phenomena in Composite Materials. These meetings have helped in the development of the necessary interdisciplinary research skills.

1.2 Research Strategy Adopted in the Current Work

In developing the research strategy for this thesis a wide ranging assessment of the reported literature in the area of interfacial interactions and composites was undertaken. This review identified a number of specific experimental limitations in previous studies. In particular these limitations included:

(i) the use of a limited range of techniques for fibre surface characterisation. Many studies only refer to X-ray photoelectron spectroscopy measurements.

(ii) limited reporting of both the results of fibre surface characterisation and also of fibre composite performance. In many cases composite testing was restricted by the limited amount of laminate manufactured.

(iii) the over-dependence on the results obtained from single fibre micromechanical measurements. Clear correlations between these measurements and either the fundamental fibre-matrix adhesion or macroscopic composite performance are not well established.

Consequently, the experimental research program reported in this thesis was specifically devised to avoid these problematic areas. A broad range of relevant surface characterisation experiments has been utilised in this study. These experiments allowed wettability, gas adsorption, frictional and surface spectroscopic information to be obtained on a range of modified fibres. In addition, fibre modification was undertaken on a sufficient scale so that large laminate panels could be manufactured from the various aramid fabrics. This approach allowed a sufficient number of composite laminate specimens to be fabricated for a wide range of relevant mechanical tests. Finally, micromechanical measurements were not given the prominence in this thesis that has been the case in other similar studies.

In deriving this research strategy, the experimental precedents and concepts developed and used by other researchers working in the area of composite interfaces have been critically appraised. The two dominant concepts which are encountered in the literature relate to adhesion and the structure within a composite laminate. Much of the research reported is based on these premises.

The concept of adhesion within fibre reinforced materials is essentially presumed to be fundamentally the same as the adhesion in structural bonding applications. That is, the adhesion between the fibres and the polymeric matrixes is likened to the adhesion between a polymer and an immobile planar substrate. The structure of laminated composites is essentially based upon the assumption that the material may be considered as a series of quasi-rigid two dimensionally anisotropic layers. Thus, the transverse properties of the laminate, orthogonal to the initial orientation of the fibres, are assumed to be essentially the result of fibre-matrix adhesion. The primary recognition that fibre reinforced composites require a unique experimental approach is illustrated by the extensive development of single fibre micromechanical experiments. Whilst these techniques seemed potentially useful in relating macro-mechanics to fibre-matrix bonding, the results obtained and reported in the

literature have been disappointing.

This thesis presents experimental justification for the inclusion of another concept which is relevant to the understanding of the behaviour of fibre reinforced composites; fibre migration. This concept is best understood by considering the fundamental processes which occur during the fabrication of the laminate. During the initial stages of laminate fabrication a complex three dimensional polymerisation process occurs which involves mixing and interpenetration of two separate polymeric phases. This process, in many ways, is similar to the formation of an interpenetrating polymer network (IPN) as it also involves solubilisation, migration and reaction of polymeric/monomeric species. Research on IPN type materials has shown that mechanical performance of these materials depends on the structure and the dual phase continuity of the phases in the final product, which is a direct result of the creation and interpenetration of the two polymer networks. In the case of fibre reinforced composites their fabrication similarly involves the simultaneous interpenetration of two polymeric phases, a polymeric liquid and a fibrous network. The overall procedure may be viewed as consisting of two separate, but simultaneous, processes. The first process involves wicking or wetting of the fibre network by the polymeric liquid and is well characterised by wettability studies on monofilaments. The second process is the migration or penetration of the fibres, within the fabric layers, through the polymeric liquid. Fibre migration in composite materials has not been previously identified as a significant factor in controlling the behaviour of fibre reinforced composites. This thesis will argue that this migration of fibres from within the fabric layers to the interlaminar or other lamella regions of the laminate results in the occurrence of fibre bridging during interlaminar fracture. This process seems to have a major influence on the mechanical properties of the laminate and, in the current work, seems to negate the expected correlations between adhesion and mechanical performance.

1.3 General Form of the Thesis

The thesis layout is as follows. Chapters 2 through 6 consider the various interfacial phenomena and the surface characterisation of fibres which are used to construct reinforced composites. Chapters 7 to 9 report on the macroscopic mechanical performance of fibre reinforced laminates whilst Chapter 10 is concerned with fibre and fabric mechanics.

Chapters 2 to 10 comprise the primary Chapters of this thesis and share a common structure. The first part of each Chapter consists of a literature review and the second part reports the results of an experimental investigation of this same research topic undertaken in the present study.

Chapter 2 consists of a review of adhesion and interfacial interactions. This review concentrates on a number of the fundamental and applied concepts which have developed in this area. Specific references to adhesion and interfacial interactions in composite materials are introduced. It is this Chapter which introduces the established belief that the adhesion between a fibre and a matrix is a critical factor in determining the mechanical response of the composite.

Chapter 3 contains a detailed review of the aramid fibre surface chemistry. In particular, research on the surface modifications of aramid fibres and their effect on composite performance is discussed. Experimental work is reported on the modification of aramid fibres using both polymeric coatings as well as the grafting of functional groups onto the fibre surface via carbanion chemistry.

In Chapter 4 the use of X-ray photoelectron spectroscopy (XPS) as a surface analytical technique for studying polymers is presented. XPS has been used to assess the success of the attempted aramid fibre surface modifications and these results are reported within this Chapter.

Polymer wettability and surface energetics are reviewed in Chapter 5. This review initially considers flat polymeric substrates and later deals with fibre systems. Experimental wetting techniques and methods for data analysis are presented in detail. The

experimentally measured wettability results and the computed surface energetics for a number of the surface modified aramid fibres are presented in this Chapter.

Chapter 6 contains a detailed survey of the use of chromatographic gas-adsorption methods for the surface characterisation of materials, especially polymers. The experimental adsorption results obtained for a number of the surface grafted aramid fibres using inverse gas chromatography are presented in this Chapter and are related to the acid-base character of the fibres.

Chapter 7 reports on the interlaminar and flexural performance of aramid-epoxy composites. Results reported in the literature are surveyed and these are compared with experimental results obtained in this study from both short beam shear and flexural tests.

In Chapter 8 interlaminar fracture in isotropic and anisotropic materials is surveyed. The results of the current experimental study of mode I fracture of aramid-epoxy laminates are reported in this Chapter. The nature of the fracture process is discussed, especially in terms of fibre-bridging effects which appear to constrain crack propagation.

Chapter 9 reports on the ballistic performance aramid-epoxy laminates. The ballistic performance of composite materials is reviewed and the experimental results obtained from the high speed impact with a range of aramid-epoxy laminates are reported and discussed.

Chapter 10 consists of three sections which deal with interfacial shear strength, fibre micro-mechanics and fabric mechanics. These three areas are reviewed and experimental results for micromechanical and fabric mechanics experiments are presented.

In Chapter 11 the conclusions of this thesis are presented. This discussion draws together the conclusions of the various Chapters presented previously and in addition makes specific suggestions for future study. The major conclusion emerges is that, for the systems studied here at least, there is a poor correlation between the expected fibre-matrix adhesion with the mechanical properties of the composite. In many cases the converse of what is expected was found. This result is attributed to the influence of the fibre surface properties on the structure of the composite.

CHAPTER 2

INTERFACIAL ADHESION

2.1 INTRODUCTION

Chapter 2 briefly reviews the concept of interfacial adhesion and the present theoretical understanding of this phenomenon. The current understanding of the origins of bonding between fibres and polymeric matrix phases is also reviewed in this Chapter.

2.2 THEORIES OF ADHESION

Adhesion is loosely described as the affinity of one phase for another. In practical terms it is quantified by the work or energy required to separate two phases and thus create an interface. Generally the work done comprises a part due to the creation of new surface and a part due to work done in the regions adjacent to the interface. The essential point is that forces must operate across the the interface when the interface is ruptured. The origin of these forces is briefly described below.

2.2.1 Mechanical Theories of Adhesion

In a number of specific material systems, the importance of a mechanical mechanism for adhesion has been well established. The most important mechanical model for adhesion is interlocking. Mechanical interlocking refers to the process by which the keying or interlocking of one phase into irregularities or surface features of the other results in the creation of a mechanical link for the adhesive force. The creation of this mechanism is best achieved by the use of surfaces which contain microscopic undercuttings or root-like cavities which can be penetrated and subsequently interlocked by the second phase. Mechanical interlocking can be an important mechanism for the adhesion between metallic

and polymeric phases. Metallic substrates are ideal materials for etching, or other methods of surface preparation, in which significant interlocking sites can be created. Interlocking is the critical factor in strong adhesion between polyethylene (PE) and anodised aluminium in which chemical adhesion is minimal due to the inert nature of the PE (Packham *et al.* 1974; Malpass *et al.* 1974). Similarly, interlocking is important in the adhesion between acrylo-butadiene-styrene copolymers with polypropylene (Finchmun *et al.* 1970; Mijovic and Koutsky 1977). Other workers who have reported on this mechanism include Bascom *et al.* (1975), Jennings (1972), Arrowsmith (1970), Borroff and Wake (1949) and Siegmund and Kukanskis (1976). This topic has been reviewed by Evans and Packham (1977).

2.2.2 Diffusion Model of Adhesion

When one or more fluid phases meet at an interface intimate contact between these phases can be followed by diffusion of molecular species into the interfacial region. In the case of polymeric liquids macromolecular inter-diffusion can contribute to the creation of an entangled interphase. The adhesive force is transmitted via molecular chains which bridge the interface. The local diffusion of polymeric species can lead to the creation of an interfacial layer of between 1.0nm and 100nm in thickness. This layer results in an enhanced mechanical strength of the interface due to the intrinsically high adhesion of polymers to themselves. Voyutskii (1963) has discussed in detail this specific mechanism for adhesion and the requirements that the phases must possess both sufficient mobility and mutual solubility to promote diffusion.

A number of workers have reported experimental evidence for polymeric inter-diffusion both directly, via diffusion coefficients measurements, and indirectly by electron microscopy or luminescence techniques. Klein and Briscoe (1979), and Rhee *et al.* (1977) for example have reported the diffusion coefficients for the diffusion of a number of

polymeric materials via IR absorption and ^{14}C labelling techniques respectively. Molecular entanglements have been described by Bueche (1952) as leading to increased resistance to motion of the diffusing chain and thus resulting in a decreasing diffusion coefficient with increasing molecular weight. More recently de Gennes (1976) has proposed a reptation model of polymer diffusion which has been experimentally substantiated (Klein and Briscoe 1979).

A number of workers have reported a good correlation between the molecular compatibility as predicted by solubility theory with the fracture bond strength. Iyengar and Erickson (1967) have presented a correlation between the peel strength of various polymers adhered to polyethylene terephthalate and the solubility parameter of the adherent. Deryaguin *et al.* (1956) have reported a similar relationship between the adhesive strength and the polymer compatibility.

2.2.3 Adsorption Theory of Adhesion

The adsorption theory of adhesion is the most generally accepted adhesion model. The forces involved are surface forces of the classical type. This theory presumes that interfacial adhesion is the result of equilibrium surface forces between the atoms at the interface. These adhesive interactions may be quantified by the thermodynamic work of adhesion, **W**, between the surfaces as defined in Chapter 5. Thus wetting measurements, for example, are sufficient to quantify **W** and thus should correlate with the interfacial adhesion. A number of researchers, in particular Andrews and Kinloch (1973) have reported correlations between **W** and the adhesive bond strength. The adsorption model is equally valid for systems in which specific surface chemical interactions, such as chemisorption, occur.

Recently Fowkes (1978, 1980) has proposed that acid-base interactions are an important contribution to interfacial adhesion. This proposition has resulted in the

development of new semi-empirical expressions for **W** for use with wetting data which contain the additional terms due to acid-base interactions. These expressions are reviewed in detail in Chapter 5. Preliminary work by Fowkes has confirmed the success of this approach in correlating these new expressions for **W** with mechanical tests of adhesion. Much more work needs to be undertaken to verify the general validity and/or limitations of this approach.

2.2.4 Chemical Bonding Theory of Adhesion

The creation of covalent bonds across an interface can promote adhesion. Since a covalent bond requires at least 10 times the energy of a secondary van-der Waals to induce interfacial failure, covalent bonding can substantially increase the failure energy of an interface. The importance of strong chemical bonds as a method for improving interfacial adhesion is well established and has been reviewed in detail (Wu 1982).

2.2.5 Electronic Theory of Adhesion

Deryaguin and his co-workers have established that the different electronic structures of the adhesive components can lead to electronic interactions across the interface (Deryaguin and Smilga 1969; Deryaguin *et al.* 1957). These interactions can take the form of electrostatic double layer interactions which can lead to enhanced adhesion. The coulombic interactions which occur at the interface were argued to contribute to the adhesion. However these interactions do not lead to significant increases in the adhesion and are comparable to the effects of secondary van der Waals interactions. This theory is not currently a topic of active research in Western science.

It is interesting to note that this model requires the presence of separated charges at the interface. Charge redistribution, which is most likely, and whose omission is the main weakness of this model, provides the basis of the chemical bonding models such as the

Fowkes acid-base model.

2.3 ADHESION IN FIBROUS COMPOSITES

The fundamental nature of the fibre-matrix adhesion process within composite materials has been a topic of interest since their earliest development. The earliest engineering composite materials manufactured were based on glass fibres. The mechanism of adhesion between the glass fibres and with polyester and epoxy polymers has been a topic of significant research interest during the last 25 years. The topic has been reviewed by Erikson and Plueddemann (1974) and more recently by Jones (1989).

Strong fibre-matrix adhesion for glass fibre composites has been industrially achieved by the use of various surface treatments for the glass fibres. The primary role of these treatments is to create strong interfacial adhesion between the fibres and the matrix. This adhesion is achieved by the use of coupling agents which:

(i) remove the chemisorbed water from the fibre surface.

(ii) improve fibre wetting.

(iii) promote strong interfacial bonds between the fibres and the matrix phase.

These requirements have led to the development of a class of fibre surface treatments known as coupling agents whose primary role is to create strong interfacial bonds. The mechanism which allows these agents to improve interfacial bonding is conceptually simple. A coupling agent is essentially a bifunctional chemical moiety in which one functional group is designed to bond to the matrix phase whilst the other functionality is designed to attach to the glass fibre surface. They are most commonly silanes of the type $R\text{-}(CH_2)_n\ Si\ (OCH_3)_3$. Thus a chemical bond is made between the fibre and the matrix in

which the silane functionality hydrolyses onto the fibre surface and a suitably chosen chemical group, R, reacts with the matrix phase.

However, the exact role of the coupling agent in promoting adhesion is more complicated than the above description would suggest. Glass fibres have a complex surface chemistry due to the range of high energy oxide/hydroxide sites present. Consequently the nature of the exact hydrolysis reaction which occurs between the coupling agent and the glass surface is unclear. It has been established that the coupling agents form structured multimolecular layers on the fibre surface and their existence is clearly important in achieving adhesion. Erikson and Plueddemann (1974) have argued that the good adhesion due to the presence of coupling agents is due to the formation of a softer deformable layer at the interface. This layer results from the adsorption/hydrolysis of the coupling agent on the fibre surface. A number of models have been proposed which consider both the chemical linking of the two phases by the coupling agent and also the presence of a deformable inter-phase. All that can be clearly concluded is that the adsorption and interfacial interactions between the coupling agent and the glass fibre surface are critical in achieving successful adhesion in glass fibre reinforced composites.

The relatively more recent advent of carbon fibres has resulted in greater uncertainty regarding the nature of the adhesion between these fibres and epoxy matrixes. A number of workers such as Harvey *et al.* (1987), Walterson (1982, 1985a,b) Fitzer (1988) and Garton *et al.* (1988) have recently investigated the fundamental aspects of adhesion between various carbon fibres with epoxy resin materials. Most of these authors have concluded that the irreversible adsorption of the bi-functional amines, used to cure the epoxy polymer, was a potentially critical factor in determining the interfacial adhesion. This adsorption occurs on the acidic hydroxyl and carboxyl groups present on these relatively high energy fibre surfaces. Fitzer (1988) has studied the surface chemistry of carbon fibres in considerable detail and has ascribed the major portion of the interfacial adhesion to be

due to strong specific interactions or covalent bonding at these acidic sites on the carbon fibre surface. Harvey *et al.* (1987) have suggested that mechanical interlocking may be important for carbon fibre epoxy materials, though no direct evidence for this conclusion was presented. Carbon fibre based composite materials generally have sufficient fibre-matrix adhesion and in some cases there is an interest in decreasing the extent of fibre-matrix bonding.

Very little fundamental work has been reported on the adhesion between aramid fibres and matrixes though such adhesion is generally regarded as being weak (Piggott and Reboredo 1980). Chapter 3 contains a discussion of this topic.

2.4 CONCLUSIONS

Although a number of models for adhesion have been proposed, it appears that the fundamental nature of adhesion in fibre reinforced composite materials is predominantly chemical in nature. The most likely mechanism involves a broad range of chemical interactions which is a combination of the adsorption and covalent modes of adhesion. Topographical models have been excluded. In the aramid systems investigated in this thesis the highly anisotropic state of the fibres provides a serious potential complication. Sub-surface failure approximates to interfacial rather than cohesive failure.

CHAPTER 3

ARAMID FIBRE SURFACE MODIFICATION

3.1 INTRODUCTION

The poor performance of aramid fibre reinforced composites under loading directions normal to the orientation of the fibres is primarily attributed in the literature to poor adhesion between the fibres and the matrix. Consequently there exists a substantial interest in improving this adhesion. This Chapter consists of two sections. The first section reviews a range of chemical approaches which have been used in an attempt to increase the fibre-matrix adhesion by modifying the surface properties of aramid fibres. These surface modifications and their effects on the mechanical behaviour of composites and/or the interface are discussed. In the second part of this Chapter the experimental methodology for the surface modification of "Kevlar" fibres adopted in the current study is described.

3.2 FIBRE SURFACE MODIFICATION

3.2.1 Gas Phase Chemical Plasmas

At pressures between 0.1 torr and 20 torr, gases and vapours which are subject to strong electric fields form gaseous plasmas. In this unique state of matter, a complex mixture of positive, negative and radical gas phase species is created which exhibits a characteristic plasma glow or discharge. Whilst the gas temperatures are often barely above ambient, and thus the term cold plasmas is commonly used, the effective electron energies are orders of magnitude higher. These conditions result in an unique reaction media in which both homogeneous and heterogeneous reactions can take place. Plasmas can be used to polymerise a wide range of organic vapours in the gas phase, often resulting in the formation of new or novel materials. Organic polymers can be exposed to plasmas without the risk of thermal degradation, allowing the highly reactive plasma medium to interact with and thus chemically modify the exposed polymer surface.

Allred *et al.* (1979) have employed gas phase O_2 plasmas for the oxidation of "Kevlar

49" fibres. Filament wound vessels made from these fibres exhibited a 30% improvement in their transverse tensile strength.

A wide range of plasma treatments was used by Wertheimer and Schreiber (1981) to modify "Kevlar 29" fibres. They included :

(i) argon ion plasma.

(ii) an argon ion plasma used to activate the substrate surface, which was then exposed to polymerisable vapours, resulting in a surface graft reaction.

(iii) plasma exposure to non-polymerisable vapours such as N_2, NH_3 and air.

(iv) plasma activated polymerisation of vapours such as propane,epoxy and hexamethyl siloxane.

Two ply laminates were then fabricated with the "Kevlar" fabric within a very short time of the plasma reaction using a triazine based epoxy resin system. The mechanical performance of these materials was evaluated using a 180^{o} peel test. It was concluded that a majority of these treatments led to some increase in the peel performance. For example, the organo-siloxane polymerised system led to a 100% increase in the peel strength. The performance was found to be strongly dependent on the lapsed time between plasma reaction and sample fabrication. Surface activity after the plasma reactions decreased with increasing exposure time to the ambient environment. Electron spin resonance measurements confirmed that the activity of the plasma treated surfaces is significantly dependent on the presence of free radical species. It was not clear whether the free radical species detected were created in the gas phase and deposited onto the surface or whether the plasma itself acted as an excitation source for species already on the polymer surface.

Petrie and Chottiner (1982) have used helium and nitrogen plasmas to modify "Kevlar". Some wettability changes were noted and laminates fabricated from the "Kevlar" fabrics with epoxy matrixes were tested via short beam shear tests. Increases in the short beam shear strength of between 15% and 36% were observed.

A detailed study of the use of plasmas to aminate "Kevlar" fabrics has been undertaken by Allred (1983). Amine group surface concentrations were successfully monitored using dye adsorption studies following exposure of the fabric to ammonia or monomethyl amine

plasmas. However contact angle measurements showed no differences between the modified and unmodified fibres. XPS spectra revealed a linear relationship between the nitrogen content (nitrogen 1s electron intensity) and the surface amine concentration as determined by the dye adsorption studies. The mechanical performance of composites manufactured from these materials was also briefly reported. The longitudinal tensile behaviour of [0/90] "Kevlar"-epoxy laminates showed a 9% increase in modulus and showed a similar decrease in strain to failure and strength relative to the control specimen. The interlaminar shear strengths of the composites were measured and found to be 31% higher for the aminated fabric laminate. T-peel tests of two ply fabric/epoxy laminates showed substantial increases in the peel strength of the aminated fabric composites. The water absorption for these two composite materials was also found to be very different. Laminates made with the amine modified fabric exhibited water absorption behaviour very similar to that of the epoxy resin and consistent with a Fickian type diffusion mechanism. The laminates fabricated from the "as received" "Kevlar" fabrics exhibited water absorption rates about three times higher than that of the aminated sample. This absorption behaviour was non-Fickian and consistent with some type of interfacial transport mechanism. Such a mechanism is thought to occur in aramid composites when poor fibre-matrix adhesion exists (Scola 1974, Allred and Lindorse 1979).

Recently Penn *et al.* (1987) have examined the effect of amine plasmas on "Kevlar" fibre adhesion and wettability. Micro-mechanics measurements suggested an increase of 25% in the bond strength, though this value is based on statistical averages in which the standard deviation was about 20% of the average result. Thus, there exists considerable unreliability in this claim. The authors concluded that the increased adhesion was due to additional hydrogen bonding and not due to direct covalent bonding between the fibre and the matrix.

3.2.2 Solution Graft Reactions

The first attempt to modify the surface properties of aramid fibres by a solution technique was an isocyanate graft reaction proposed by Wake (1972). This approach had been previously applied to Nylon 6 by Ulrich (1971). More recently this route was used by Penn *et al.* (1987) to grafted functional groups on the surface of "Kevlar" fibres. The

authors reported that quantitative analysis showed a pendant group attachment of 1.5 to 4.5 groups per 100 $Å^2$ of fibre surface, a level which agrees well with the theoretical amount predicted for the reaction. However, specific chemical tests for covalent bond formation between the terminal amine of the pendant group and the epoxy molecules showed that covalent bonding did not occur. The results of mechanical tests showed no improvement in the fibre-matrix interface strength. The authors claimed that the other factors that could affect interfacial adhesion were kept constant, such as the surface energy and surface topography. It is not clear how this control could be achieved since both the surface energy and surface topography are intrinsically related to the reactive modification of the material surface.

Keller *et al.* (1983) have studied a solution reaction scheme for "Kevlar" fibres based on the aqueous hydrolysis of the amide linkages with strong aqueous acidic and basic solutions. Following hydrolysis, a bifunctional epoxy monomer was reacted with the amine groups released by the hydrolysis reaction. This reaction resulted in a free terminal epoxy group which could then react with an amine functionality. The epoxy reaction was monitored via the XPS of chlorine following chemical derivatisation of the epoxy group with HCl. A dye assay was also used to confirm the existence of a hydrolysis reaction. Whilst the reaction scheme was successful, the aqueous hydrolysis step led to the fibre tensile strength decreasing by over 20%.

Recent work has shown that normal substituted polyphenylene terephthalamide polymers, such as N-alkylated, N-arylated and N-carboxymethylated can be synthesised (Takayanagi and Katayose 1981). It was previously found that NaH and dimethyl sulphoxide (DMSO) react to form sodium methyl sulphinylcarbanion which can ionise the proton of the amide group of aramid molecules resulting in homogeneous dissolution in DMSO. Following the metallation of poly(phenylene terephthalamide) (PPTA), a nucleophilic substitution reaction allowed the normal substitution to be accomplished. Metallated PPTA fibre surfaces were reacted with alkyl halides and epoxy compounds so that N substituted epoxy and alkyl groups were grafted onto the fibre surface (Takayanagi *et al.* 1987). The interfacial shear strength and the critical fibre length were determined between the various fibre surfaces and an epoxy-amine matrix by the single fibre pull-out experiment. The "Kevlar" filament surface modified by polyfunctional epoxy gave the

highest interfacial shear strengths. These critical experiments were described in an abridged form and conclusions regarding the reliability of these data and the methodology employed are not possible. XPS spectra supported an enrichment of epoxy groups on the fibre surface. SEM micrographs of the pulled out filament surface suggested an increased adhesion by the grafting of epoxy groups (Takayanagi 1987). The flexural moduli of composites manufactured from the "Kevlar" materials with an epoxy-amine resin were increased by 15% for the bifunctional epoxy grafted "Kevlar" relative to the "as received" "Kevlar". Otherwise the composite flexural deformation curves were very similar for the carboxy acid, mono and bi- functional epoxy grafted fibres. However the metallisation reaction does result in a 7% loss for the strength of "Kevlar" fibres after a 10 minute reaction time. The T-peel strength of laminates incorporating the bifunctional epoxy was significantly increased relative to laminates made from the "as received" "Kevlar". SEM photographs revealed that the surface layers of the "Kevlar" fibres were dramatically damaged and support the thesis that the maximum adhesion had been achieved by the chemical grafting of bifunctional epoxy groups onto the fibre surface.

3.2.3 Polymeric Coatings

The application of polyimide, allyl glycidyl and acrylamide coatings to "Kevlar 49" fibres has been found to lead to a substantial increase in the interlaminar shear strength of "Kevlar"-polybutadiene composites (Chase 1975).

Penn *et al.* (1983) have studied the effects of various fibre coatings (including aromatic sulphonamide, aromatic polyamide and amidobenzene) in improving the adhesion with epoxy resins. None of the chemicals improved the interfacial bond strength as defined by single fibre pull-out experiments. It was concluded that an improvement in adhesion could only be obtained by the formation of direct covalent bonds between the fibre and the matrix. Mai and Castino (1984) have reported that the application of urethane coatings on to "Kevlar" fabrics led to improved mechanical performance of "Kevlar"-epoxy laminates. This improvement was related to "intermittent fibre-resin bonding". This concept pertains to maximising interfacial frictional energy absorption, though no explicit proof was offered to confirm such behaviour.

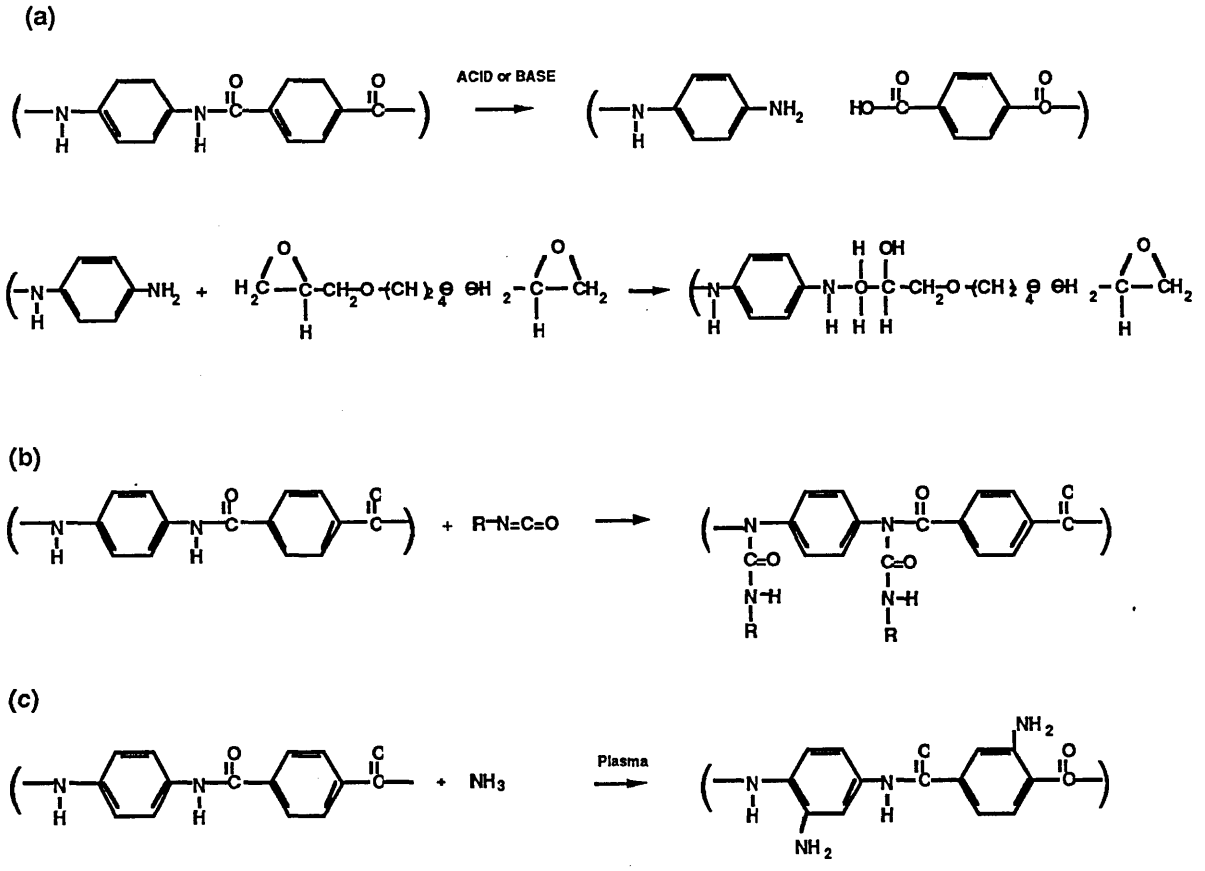


Figure 3.1 Some reaction routes studied for the modification of "Kevlar" fibre surfaces (a) Keller *et al.* 1983 (b) Wake 1972 (c) Allred 1983

3.2.4 Conclusions

A significant number of research workers have attempted to improve the performance of aramid fibre composites via the use of fibre surface modifications. Attempts to graft chemical functionalities onto the surface of "Kevlar" fibres have, on the whole, been unsuccessful, though the recent work of Takayanagi shows promise. However, none of reactive routes has dramatically improved the fibre-matrix adhesion for aramid composites. Various polymeric coatings for aramid fibres have been shown to improve the mechanical properties of the aramid composites. However, the reasons for these improvements have not been clearly established.

3.3 EXPERIMENTAL SURFACE MODIFICATION

In this section, the experimental work undertaken to modify the surface properties of "Kevlar" via both the functional group grafting route, and via the use of polymeric coatings is described.

3.3.1 Cleaning of Aramid Fabrics

Unless otherwise stated, all the "Kevlar" fabrics used in the subsequent sections of this Chapter were cleaned to remove surface contaminants prior to their use. It has been previously established that significant amounts of surface contaminants exist on the surface of even scoured aramid fabrics (Chappell and Williams 1989a,b). Cleaning was accomplished by soxhlet extracting the fabric with hot acetone. A large hot soxhlet extraction apparatus was constructed containing a glass thimble with a volume of two litres. The large thimble allowed "Kevlar" fabrics to be cleaned in 1 kilogram batches. Each "Kevlar" sample was extracted for 24 hours and the extraction process involved about 8 cycles.

3.3.2 Experimental Solution Graft Reactions

Following the work of Takayanagi *et al.* (1987), experimental studies were undertaken to confirm and extend the use of the methyl-sulphinylcarbanion graft reaction route for the modification of aramid fibre surfaces. A large volume of stock solution of the reactive

intermediate dimethyl-sulphinylcarbanion (DMSC) was produced and used for all experimental studies. Previous work (Takayanagi and Katayose, 1981) has established that DMSC is a stable species providing sufficient care is taken to prevent its degradation by water or other acidic moieties.

(a) Preparation of dimethyl sulphinylcarbanion solution

A new 500ml conical flask was fitted with septa ("Subaseal") and was dried to 130°C to remove chemisorbed water and then purged with dry nitrogen. 11.2 gram of NaH (Aldrich 80% dispersion in paraffin oil (grey in appearance)) was added to the flask in a nitrogen purged glove bag followed by the addition of 440 ml of dry dimethyl sulphoxide (DMSO) (Aldrich <0.05% water) by syringe. Under constant stirring the grey slurry was heated to 40° C for 40 minutes. Evolution of hydrogen gas commenced which was vented from the reaction flask via a syringe needle into a fume cupboard. The temperature of the slurry was slowly increased over the next 2 hours to 70°C to accelerate the liberation of hydrogen and was then continued for 1 hour at this final temperature. During this final hour the rate of hydrogen evolution dramatically decreased signifying completion of the reaction. A turbid light grey solution resulted. The reaction solution was then kept in a dry glove bag until required.

To confirm the various potential reaction routes, preliminary model reactions were conducted using an homogeneous reaction route with PPTA in solution. These experiments were designed to provide the baseline reaction rate information which was important to verify the feasibility of heterogeneous solid-liquid graft reactions to be described later.

Initial experiments revealed that DMSC in DMSO would not dissolve "Kevlar" fibres easily. Whilst Takayanagi *et al.* (1987) have reported that this dissolution process was slow, they were referring to a reaction time frame of weeks rather than hours. The extensive crystalline nature of the PPTA based "Kevlar" fibres clearly impedes the diffusion and reaction/solvation of DMSC with the PPTA molecules. Consequently to conduct the model reaction experiments, the PPTA needed to be produced in a form which was either amorphous or involved a small crystallite size so that a PPTA solution could be prepared.

(b) Preparation of amorphous Polyphenylene Terephthalamide

The general method of Gayman *et al.* (1976) was used to produce an amorphous form of PPTA. 10gm. of "Kevlar" fibres were added to 400 ml of chlorosulphonic acid and left to

stand overnight in a closed fume cupboard. A dark yellow solution of viscosity similar to glycerol resulted, with the apparent complete dissolution of the fibres. 200 ml of this liquor was added to a 1000ml beaker containing 700ml of methanol (BDH analytical grade reagent) kept at -50° C via the use of liquid nitrogen. The addition was carefully accomplished using a separation funnel through which the PPTA solution was allowed to pass slowly. A thin filament of PPTA solution resulted which was passed into the vigorously stirred methanol bath. The PPTA precipitated immediately on contact with methanol in an aggressive exothermic fashion in the form of coarse filaments. The precipitated material was washed twice with water and twice with methanol to remove residual chlorosulphonic acid. The material was then vacuum dried in an oven at 120° C overnight.

Using the amorphous PPTA, a range of spot reaction tests was performed to confirm the reactivity of the metallated PPTA with various nucleophilic reagents.

(c) Metallated PPTA

Metallated PPTA was produced by dissolving 6.0gm of the PPTA with an equi-molar amount of the DMSC solution and made up to 410ml with an additional quantity of dry DMSO. The reaction began immediately and after one hour a deep red wine-coloured solution resulted. This colouration was consistent with formation of a charge transfer complex due to the $Na^+ N^-$ species formed. Normal anhydrous reaction precautions were adopted to prevent decomposition of this intermediate.

(d) Spot Reagent Tests for Nucleophilic Reaction with Metallated PPTA

(i) To 20ml of solution (c) a molar excess of bromo-propanediol (Aldrich >95% purity) was added. Within 2 minutes a fine crystalline precipitate was observed in the test tube. The solution colour had changed from bright red to a dull yellow colour.

(ii) To 20ml of solution (c) a molar excess of chloromethyl trimethyl silane (Aldrich >98% purity) was added. No immediate reaction was evident, but a slow change in the colour of the solution to a dark yellow over a period of two hours was observed. No precipitation was observed.

(iii) To 20ml of solution (c) a molar excess of epibromohydrin was added. With 2 minutes the solution changed to a light yellow colour in appearance. No precipitate was evident.

(iv) To 20ml of solution (c) a molar excess of *p*- chloromethyl nitrobenzene (Aldrich

> 99% purity) was added dropwise in the form of a 10% solution in DMSO. A brown precipitate resulted immediately.

(v) To 20ml of solution (c) a molar excess of bromo-octane (Aldrich >98% purity) was added dropwise. Within two hours significant colour change to yellow was observed.

(vi) To 20ml of solution (c) a molar excess of water was added.The solution changed to a light yellow colour and a yellow precipitate formed.

(vii) To 20ml of solution (c) a molar excess of 4 iodo-aniline was added. After two hours only a minimal change in solution colour was observed. Increasing the temperature to 100° C led to no change in the colour of the solution .

(viii) To 20ml of solution (c) a molar excess of iodo-benzotrifluoride was added. After two hours only a minimal change in solution colour was observed. Increasing the solution temperature to 100° C led to a fading of the solution colour.

3.3.3 Preparation of Modified Fabrics via Graft Reactions

As previous discussed in this Chapter, one research objective which has eluded composite scientists is the improvement of the chemical bonding/adhesion between aramid fibres and epoxy resins. Therefore, the two reaction routes pursued for large scale surface graft modification of fabric in this study were those reactions which could be expected to lead to increased interfacial interactions and/or bonding. Thus, the diol graft and the epoxy graft reaction were utilized.

Rather than use a mono-functional epoxy as used in the model experiments, a bifunctional epoxy was chosen, as this offered increased potential for the coupling of the fibre surface with the epoxy resin system. It was also decided to include a control graft reaction experiment in which the fabric was metallated, but then neutralised with water, thus regenerating the aramid surface. This experiment allowed the effect of the changes in the surface morphology and/or surface topography to be considered

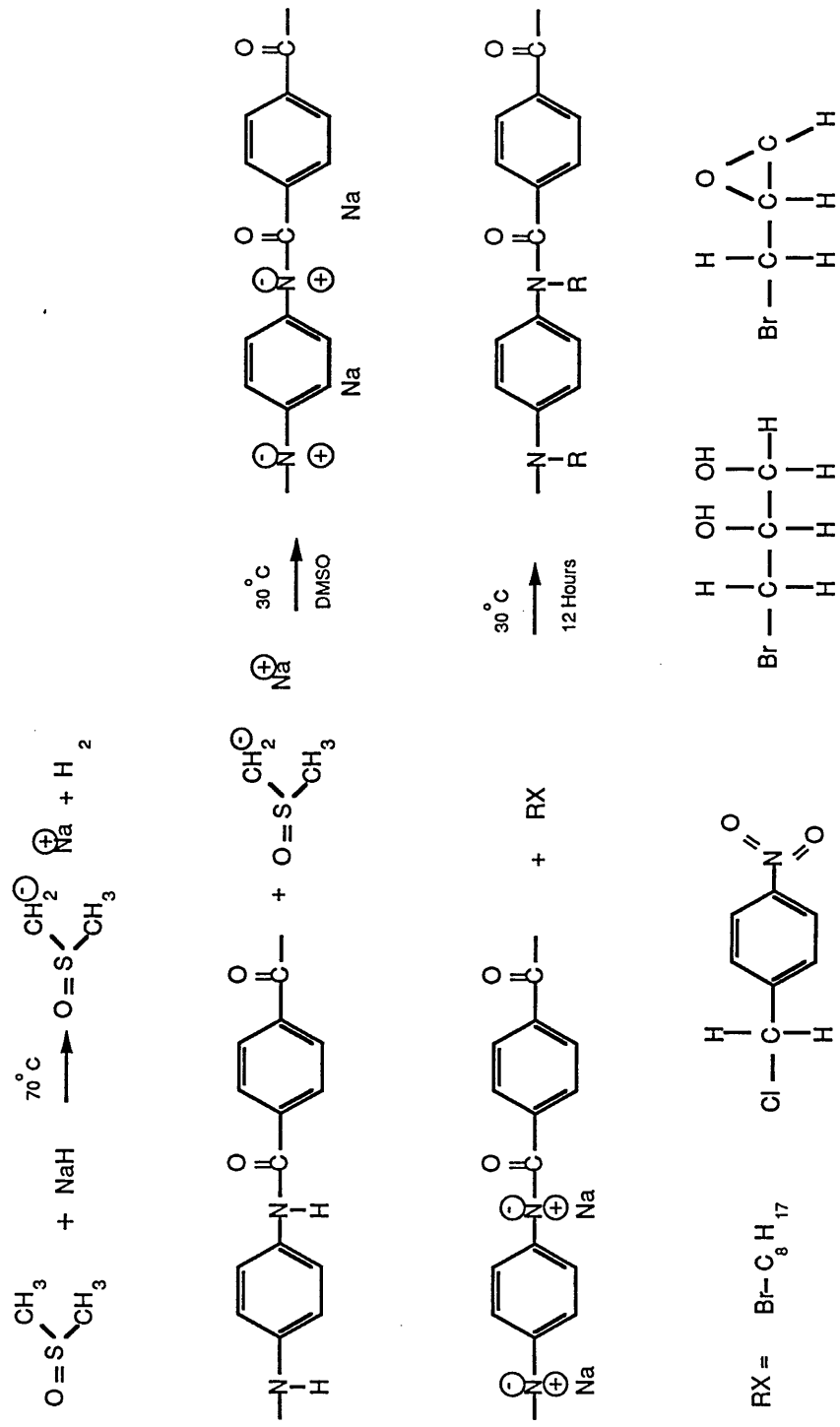


Figure 3.2 Reaction scheme for aramid graft reaction via dimethylsulphinyl carbanion (DMSC).

(i) Metallisation of "Kevlar" Fabrics

For each graft treatment, 10 pieces of "Kevlar" 49 fabric (320mm x 320mm) were pre-dried in a vacuum oven at 130° C for 2 hours prior to transfer into a dry glove bag. These pieces of fabric were place in a 3 litre closed top reaction vessel which contained 1.2 litre of dry DMSO. O.25 mole of DMSC solution was added to the vessel. Within 30 seconds of addition the solution changed colour from yellow to a deep gold. . From the model experiments discussed above, the red coloured metallated complex has a large extinction coefficient, and thus the colour change of the metallated fabric to gold is consistent with the outer regions of the fibre surfaces being metallated.

(ii) Diol Grafted "Kevlar" Fabrics

Assuming that the DMSC reactant had been completely reacted in (i) within 3 minutes, 10g of bromo-propanediol was added to the 3 litre reaction vessel. The gold colouration of the fabric virtually disappeared within 10 minutes, confirming that a reaction had occurred between the nucleophile and the metallated complex. The fabric was then removed and the excess reactants and DMSO allowed to drain. The "Kevlar" cloth was then washed with excess acetone 3 times. The fabric was then allowed to drain again followed by soxhlet extraction with acetone for 12 hours. The fabric was then vacuum dried at 160° C for 24 hours to remove any other reactants present, especially any DMSO which might have penetrated into the fibres.

(iii) Epoxy Grafted "Kevlar" Fabrics

This fabric was treated in same method as for samples (i) and (ii) above, except that the nucleophilic reactant was 25 grams of a bifunctional epoxy chemical (Polysciences 812 Epoxy resin).

(iv) Chemically Etched

In this case the DMSC solution was allowed to contact the "Kevlar" fabric for 20 minutes rather than 3 minutes. This additional reaction time was expected to result in the formation of additional metallation sites on the polymer. The reaction was quenched by the addition of 20 grams of water. The change in colour was immediate and confirmed the reaction between the water and the metallated species. Draining of the fabric of excess DMSO revealed the presence of significant amounts of gel like polymer. This observation implies that the extended period of metallation reaction had resulted in substantial penetration of the DMSC into the amorphous outer regions of the fibres. These have presumably became swollen with DMSO and resulted in the formation of the gel like reaction by-product. The fabric was washed and extracted in the same manner as described in (i).

3.3.4 Preparation of Modified Fabrics via Polymer Deposition

A number of polymeric materials were chosen for coating of the aramid fibres. The literature review of this area reveals that there exists conflicting evidence concerning the effect, in any, of polymeric sizing agents on the performance of "Kevlar" composite. Consequently a broad range of polymers was chosen to coat the fabric, prior to epoxy resin impregnation, to allow composite performance to be assessed in light of these modifications.

(i) Polyethylene Glycol

Polyethylene glycol (BDH Molecular weight 4,000) was dissolved in distilled water to make up a 2% solution. 10 pieces of fabric (300mm x 300mm) were immersed in the solution for 15 minutes. The fabric was removed from the solution and washed once with water to remove excess polymer. The fabric pieces were then vacuum dried at 100° C for 2 hours.

(ii) Polydimethyl Siloxane

Polydimethyl siloxane (Polysciences molecular weight 4,000) was dissolved in toluene (BDH Analytical Grade) to make up a 2% solution. 10 pieces of fabric (300mm x 300mm) were immersed in the solution for 15 minutes. The fabric was removed from the solution and washed once with toluene to remove excess polymer. The fabric was then vacuum dried at 100° C for 2 hours.

(iii) Epoxy Oligiomer

Ciba Geigy resin LY556, which is an epoxy oligiomer based on the diglycidyl ether of bis-phenol A, was dissolved in tetrahydrofuran (BDH Analytical Grade) to give a 2% solution. 10 pieces of fabric (300mm x 300mm) were immersed in the solution for 15 minutes. The fabric pieces were removed from the solution and washed once with tetrahydrofuran to remove excess polymer. The fabric pieces were then vacuum dried at 100° C for 2 hours.

(iv) Amine crosslinking agent

Ciba Geigy chemical LT972, which is a bifunctional amine used for crosslinking with the epoxy pre-polymer, was dissolved in tetrahydrofuran (BDH Analytical Grade) to give a 2% solution. 10 pieces were immersed in the solution for 15 minutes. The fabric was removed from the solution and washed once with tetrahydrofuran to remove excess polymer. The fabric was then vacuum dried at 100° C for 2 hours.

(v) Tin Hydrosol

A stannic/stannous chloride hydrosol solution was prepared using an established method (Briscoe *et al.* 1989). "Kevlar" fabrics were dipped into the solution for 30 seconds and then removed. The pieces of fabric were initially to drain, followed by air drying. The fabrics were finally vacuum dried to remove any residual water.

3.3.5 Nature of Surface Modifications

The range of surface modifications presented in this Chapter were chosen to result in aramid fibres with a broad range of surface properties. It would thus be anticipated that these fibre surface modifications would result in changes and variations in the properties of the fibre-matrix interface.

Some of the fibre-matrix interfaces produced would be expected to be weak due to the presence of lubricants at the fibre surface, as in the case of the PDMS and PEG coated fibres. These polymers have low shear strengths and could be expected to lead to a weak fibre-matrix interface.

In the case of diol and epoxy grafted fibres, the aim was to promote covalent bonding, or other additional chemical interactions at the interface, between the fibres and the matrix. These effects could be expected to result in an increase in fibre-matrix adhesion.

Coating the fibres with epoxy and amine chemicals was designed to evaluate the effects, if any, of high localised concentrations of epoxy or amine moieties in the fibre-matrix interfacial regions. It was noted in Chapter 1.3 that amine adsorption on the surface of carbon fibres is a critical aspect of strong fibre-matrix adhesion in those composite materials.

3.3.6 Discussion

The observed changes in the fabric colouration following addition of the metallating reagent, and also following the addition of the nucleophilic species, supported the success of both the diol and the epoxy graft reactions. The probable success of both of these reactions was supported by the test tube reactions. The test tube reactions suggested that a number of reactions occurred between the metallated PPTA and various nucleophiles. It is presumed at this stage that the anticipated reactions were the ones that proceeded. On the basis of these assumptions, a preliminary assessment of the successful reagents was

compiled. The list is as follows:

(i) bromo-octane
(ii) bromo-propane diol
(iii) trimethyl-chlorosilane
(iv) *p*-chloro methyl nitrobenzene
(v) epibromohydrin

The successful epoxidisation and alkylation reactions are directly supported by the results of Takayanagi (1987). The nitrobenzene reaction was designed as a precursor reaction to the formation of an aryl amine. This was to be accomplished via a Zinnin reduction of the nitrobenzene compound.

It is not immediately obvious that the presumed diol reaction is the reaction most likely to occur. In principle it might have been expected that the DMSC complex would exhibit a strong reactive affinity for any acidic species present such as a hydroxyl proton on the diol group. However the use of an aprotic solvent system does complicate such predictions. More significantly Takayanagi obtained product yields of nearly 20% for the reaction between bromo-acetic acid with the metallated PPTA complex. Since bromoacetic acid is significantly more acidic than bromo-propane diol, the grafting of the diol functionality onto the fibre surface seems a feasible reaction.

3.3.7 Conclusions

Preliminary experiments suggest that the grafting of diol, alkyl, nitrobenzene, epoxy and trimethyl silane groups onto the surface of "Kevlar" fibres is feasible. "Kevlar" fabrics have been coated with a range of polymer materials, as well as having diol and epoxy groups grafted onto the surface.

CHAPTER 4

X-RAY PHOTOELECTRON SPECTROSCOPY

4.1 INTRODUCTION

This chapter is divided into two major sections. The first section is a review of X-ray photoelectron spectroscopy (XPS) as a method for the surface analysis of organic polymers. The basic theoretical and experimental aspects of this technique are discussed as well as current experimental developments. Previous XPS studies of aramid polymeric materials are reviewed and discussed in detail. The second section of this chapter describes an experimental XPS study. The XPS results are presented and analysed for a range of surface modified and unmodified aramid materials. The materials characterised are:

(i) untreated "Kevlar" fibres .

(ii) "Kevlar" fibres coated with polymeric or oligiomeric species .

(iii) "Kevlar" fibres which have been modified by solution graft reactions.

4.2 A LITERATURE REVIEW OF X-RAY PHOTOELECTRON SPECTROSCOPY

4.2.1 Introduction to X-ray Photoelectron Spectroscopy

The technique known as X-ray photoelectron spectroscopy (XPS) was developed by Siegbahn and his co-workers in Sweden just over 20 years ago under the name Electron Spectroscopy for Chemical Analysis (ESCA) (Siegbahn *et al.* 1967). During the last 15 years XPS has become the technique of choice for the surface chemical analysis of polymer surfaces. The surface sensitivity and relative ease of operation of XPS has encouraged its widespread usage for studying polymeric materials.

4.2.2 Photoelectron Emission

The basis of XPS is the measurement of the binding energies of photoelectrons ejected from a molecule following excitation by a monochromatic beam of X-rays. Although the depth of penetration of the incident X-rays is many tens of nanometer, the average escape depth for a core photoelectron produced by a Mg $K_{\alpha 1,2}$ X-ray is only 1.2nm. Thus, 95% of the photoelectrons escape from a depth of less than 3.5nm from the irradiated sample's surface. This shallow depth of escape forms the basis of XPS as a surface analysis technique. The most common X-ray sources used are based on magnesium (Mg $K_{\alpha 1,2}$) and aluminium (Al $K_{\alpha 1,2}$) anodes with respective radiation energies of 1253.7 eV and 1486.6 eV.

The photoelectrons ejected from the excited sample originate from all energy levels within the molecule. Photoelectrons are emitted from both the core atomic orbitals and the valence band molecular orbitals. The energy of the ejected photoelectrons is simply defined by Equation 4.1 :

$$BE = h\nu - KE - \phi \qquad (4.1)$$

where BE = binding energy

$h\nu$ = X-ray energy

KE = measured kinetic energy

ϕ = work function correction

For both of the above X-ray sources, the cross-sections of photoionisation for the core electrons are considerably higher than those for the valence electrons. The XPS spectrum is consequently dominated by the large number of photoelectrons ejected from the core atomic orbitals. For organic molecules, the binding energies of electrons from core atomic orbitals

are typically between 200eV and 700eV, whilst for valence photoelectrons the energy range is between 5eV and 50eV.

4.2.3 Valence Band Photoelectron Studies

The use of valence band XPS for studying polymer surfaces requires additional refinement to the basic technique described above. Because of the small energies of the photoelectrons ejected typical escape depths are between 0.05nm and 0.5nm. These smaller escape depths result in this technique exhibiting an exceptional surface sensitivity. However this advantage also leads to additional problems with surface contamination. Excitation sources used for this technique are significantly lower in energy than those sources used for core photoelectron studies. The most common sources are He_{IIB} X-rays (48.3702eV) and ultra-violet lamps. XPS studies using these excitation sources are described respectively as valence band XPS and ultraviolet PS.

With normal XPS the energy of the ejected photoelectrons can be directly assigned to emissions from specific atomic orbitals. Thus, the spectral peaks detected can be assigned to specific elements. However, in the case of valence band photoelectrons, the photoelectron energy is intimately dependent on the molecular electronic energy states of the sample. In most cases, valence bond spectral peaks cannot be uniquely assigned *a priori*. Rather, they require a knowledge of the molecular orbital energies of the material under investigation. These energies would normally be computed using *ab-initio* or self consistent field molecular orbital calculations. Thus, this technique primarily attracts the interest of theoretical physicists and chemists, rather than those scientists whose interest is practical surface analysis.

4.2.4 XPS Apparatus

XPS experiments are conducted under a vacuum which is normally less than 10^{-7} torr so that the sample is kept free of surface contamination. The kinetic energy of the

photoelectrons ejected from the sample is measured using an electrostatic analyser. Two primary designs of electrostatic energy analyser are in common usage; the double focusing cylindrical mirror analyser and, to a lesser extent, the hemispherical analyser. Both analysers offer experimental advantages and these have been discussed by Orchard (1977). The photoelectron intensity detected as a function of photoelectron energy defines the XPS spectrum. XPS apparatus is schematically shown in Figure 4.1. The shaded region denotes those parts of the instrument which are maintained under high vacuum.

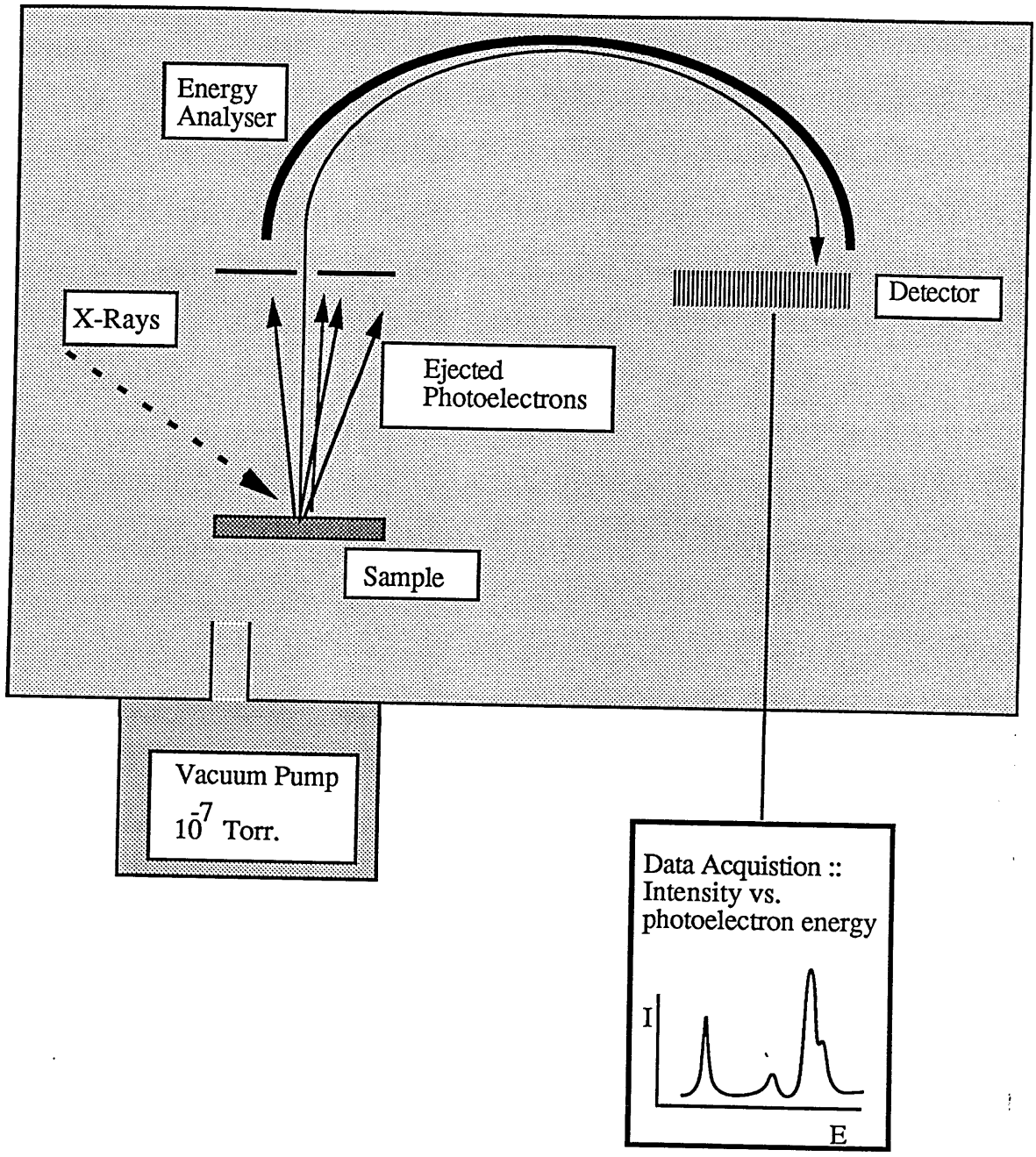


Figure 4.1 Schematic diagram of XPS equipment.

4.2.5 Core Level Photoelectrons

The energy of the core level photoelectrons ejected from a sample is a direct function of the chemical element from which they originate. Thus, elemental surface analytical information is directly ascertained from the photoelectron's energy. The core 1s orbital electrons are the most probable photoelectrons to be ejected from organic samples. The binding energy range for electrons from the 1s orbitals for the main elemental constituents of organic molecules are :

Oxygen 530-540eV : Carbon 280-290eV : Nitrogen 395-410eV

Variations in the substituents bonded to any atomic nuclei will lead to slight perturbations in precise binding energy required to eject the photoelectrons. Thus a range of binding energies, as shown above, exist for any particular atomic orbital. These chemical shifts in the binding energy, due to various substituents, have been extensively studied for a wide range of polymer systems by Clark and his co-workers (Clark 1977,1978). The sizes of these chemical shifts was found to be highly characteristic of the substituents whilst for complex molecules, with many substituents, the size of these shifts generally obeyed simple additive laws. Figure 4.2 shows the binding energy shifts for carbon 1s orbitals with various chemical substituents. These chemical shifts provide the most direct method for predicting the surface chemical structure for organic polymer surfaces. Consequently the carbon 1s spectrum is generally the most important region of the XPS spectrum for organic polymers. A typical example is shown below for plasma polymerised films of vinylidene fluoride. In this example, the four chemical environments for the carbon atom which exist are : CF_3 , CF_2, CF , C. Deconvolution of the carbon 1s spectrum for the plasma polymerised films, based on the presumed existence of all four chemical species on the polymer surface, allowed the individual curves to be summed to generate a spectrum similar to the experimental spectrum. These spectra are shown below in Figure 4.3

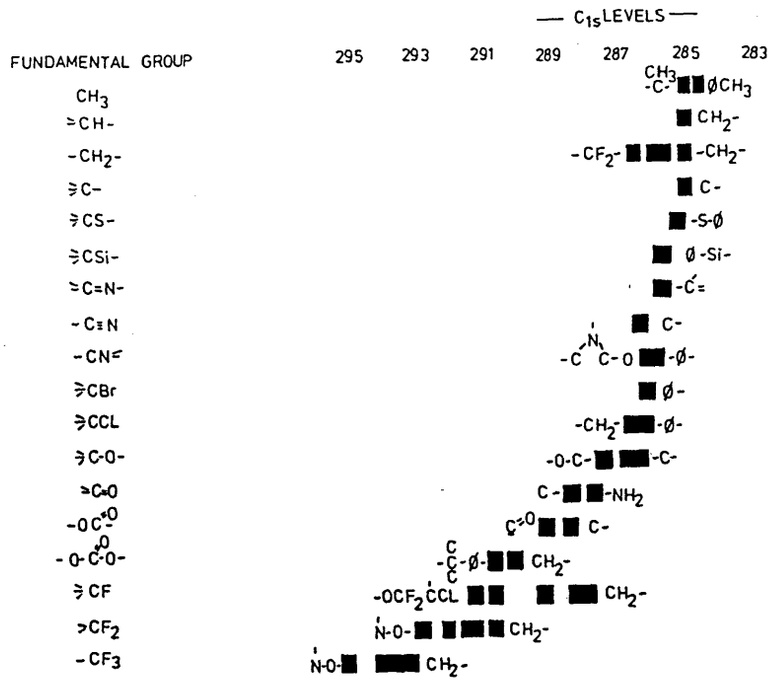


Figure 4.2 Binding energy shifts for carbon 1s photoelectrons as a function of the chemical substituent attached to the carbon nucleus.

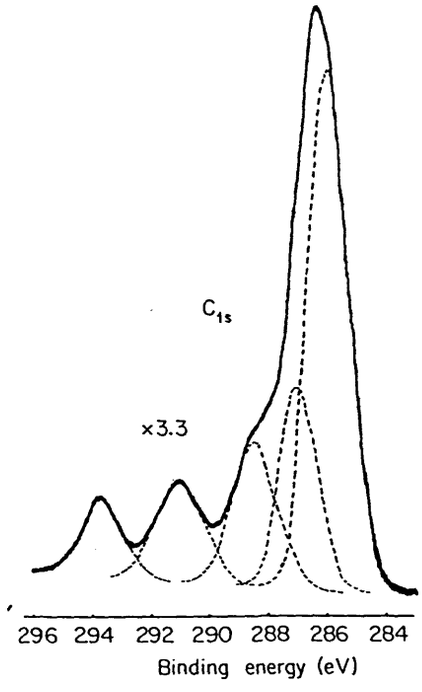


Figure 4.3 Carbon 1s spectrum of a plasma polymerised vinylidene fluoride film. The deconvoluted component curves for the four chemical environments for carbon are shown.

However, the assignment of these peaks, and the existence of the various chemical environments, could only be concluded by the authors following a large systematic study of fluorinated homopolymers and related compounds. This approach allowed a great deal of information on the positions and intensities of the various XPS bands to be accumulated. Potentially serious errors in fitting these multicomponent curves to the XPS spectra were minimised by adopting this approach.

4.2.6 Satellite Peaks

Following the loss of a photoelectron from the nucleus, the valence band electrons associated with this nucleus may relax due to an effective increase in the nuclear charge. During this relaxation process a finite probability exists for simultaneous phototelectron emission and relaxation to occur. The two most common modes of this type of electronic event involve either the ejection of a photoelectron and the excitation from an occupied molecular orbital resulting in a "shake-off" peak, or the ejection of a photoelectron and the excitation to an unoccupied orbital resulting in a "shake-up" peak. These processes result in the appearance of additional low intensity XPS peaks which are typically found up to 20 eV upfield of the main peak. Their occurrence can assist in clarifying ambiguous core photoelectron spectra and can be an especially useful method in differentiating between saturated and unsaturated organic molecules. Unsaturated molecules will normally exhibit shake-up peaks associated with $\pi \rightarrow \pi^*$ electronic transitions.

4.2.7 Surface Chemical Derivatives

There are many important polymeric materials in which the chemical shift information available, within the XPS spectra, is insufficient to permit a full analysis of the various functional groups present. In these complex systems it is very difficult to separate the close overlapping peaks due to the various chemical shifts. Spectra of this type cannot be confidently interpreted unless substantial studies with model compounds are undertaken.

Even then, all the spectral uncertainties may not be satisfactorily resolved.

A wide range of chemical techniques have been developed which, in conjunction with XPS, allows functional groups to be selectively identified. By using various selective reactions, it is possible to "tag" a specific functional group with a species which can be more easily identified in the XPS spectra than the initial moiety. This approach is described as the chemical derivatisation method. An early example of this approach was the use of bromine/carbon tetrachloride solutions (Batich and Wendt 1981). These solutions were reacted with polymers containing unsaturated alkene functionalities which resulted in the addition of bromine at carbon-carbon double bonds. Determination of the bromine concentration via XPS, which is relatively straightforward, allowed the extent of surface unsaturation to be estimated. A wide range of chemical derivative reactions have been used in XPS studies and these have been reviewed in detail by Batich and Wendt (1981).

4.2.8 Depth Profiling

The ability to profile in the depth variations in atomic composition is a major advantage of XPS. Two primary methods have been developed for depth resolved XPS. In the most common method, depth profiling may be simply accomplished by varying the angle of photoelectron collection (θ) and sample irradiation. Photoelectrons which are collected at an angle normal ($\theta = 90^o$) to the sample surface have the maximum possible escape depth. As the angle of collection, θ, decreases the escape depth becomes a minimum as θ tends to 0^o. Typical escape depths for photoelectrons are 5.0nm for $\theta = 90^o$ and 1.0nm for $\theta = 10^o$ with Mg $K_{\alpha 1,2}$ X-rays. Thus angular resolved spectra can be obtained by rotating the sample stage with respect to a constant position of the X-ray source and analyser. This technique is discussed in detail by Thomas and O'Malley (1979). The other variation of this method does not involve sample rotation but instead requires the adjustment of the energy analyser. By varying the position of the energy analyser photoelectrons with different angles of escape are analysed and thus depth profiling may be

effectively accomplished.

Another technique for obtaining angular resolved spectra requires the use of various X-ray sources with a wide range of energies (Dwight and Thomas 1981). Changing the energy of the X-ray source results in the ejection of photoelectrons with different average escape depths. The profiling of depths of up to 30nm have been achieved with this method using flat specimens. An important advantage of this approach is the ability to depth profile specimens with rough surfaces. The angular resolved methods are unsuitable for specimens with rough surfaces.

4.2.9 Recent Advances in XPS

Unlike techniques such as Auger and Secondary Ion Mass Spectroscopy, one of the most significant limitations in the use of XPS is its poor lateral spatial resolution. Normally photoelectrons from an area of many square millimetres will be analysed by most XPS detector systems. However, a number of very recent advances in the design of the photoelectron collection optics are now, for the first time, permitting XPS spectra to be obtained for regions of a few hundred square microns (Briggs 1989). Significant interest and applications are certain to follow this important development.

The lack of monochromatic X-ray sources for sample excitation has always experimentally limited the resolution of XPS spectra. The problems associated with overlapping spectral peaks, such as those shown in Figure 4.3, are primarily a result of the line width of the X-ray sources used and are not intrinsic to this experimental technique. A reduction of the experimental peak width is essential if unambigious assignments of bands due to chemical shifts are to be attained. The ideal monochromatic X-ray radiation can be obtained from a synchrotron. However the scarcity of these facilities is a serious practical limitation. X-ray radiation can be successfully filtered via the use of special molecular crystals to remove secondary wavelengths, although filtering results in a significant loss of beam intensity. Recently Briggs (1989) has reported on the use of a very high power X-ray

source. The monochromaticity of this beam was improved by filtering the radiation though a series of nine crystals which resulted in higher resolution XPS spectra being obtained.

4.2.10 Application of XPS

XPS has been widely used as a surface analytical technique. A number of areas in which the use of XPS has been particularly successful include :

Surface modification of polymers by gaseous plasmas.

Surface degradation of polymers by routes such as oxidation and weathering.

Composition of thin plasma polymerised films.

Fluoro-polymers and co-polymers.

Polymer surface cleanliness; surface etching via solvents and argon ion beams.

Segregation and morphology of block co-polymers and blends.

4.2.11 XPS of Aramid Polymers

Penn and Larsen (1979) were the first researchers to investigate, in detail, the surface composition of aramid materials using XPS. In their study of "Kevlar 49" and " Kevlar 29" fibres, they demonstrated that the atomic surface composition of both materials deviated significantly for that expected theoretically based on the bulk stoichiometry. They specifically observed that the surface nitrogen composition was less than half the bulk value expected. This variation was associated with the presence of an oxidised hydrocarbon surface.

Recently Allred (1983) has reviewed both published and unpublished work on the surface composition of aramid materials as determined by XPS. The surface compositions obtained by XPS were compared with the bulk atomic composition of polyphenylene terephthalamide. It was concluded that the "Kevlar" fibre surface contained half the amount of nitrogen and twice the amount of oxygen, relative to that theoretical bulk composition

expected. This conclusion was based on results obtained in five different studies of "Kevlar 49" fibres including his own results. His experimental results, which also reflected the averaged results obtained from his review, are shown in Table 4.1. Due to the wide range of fibre materials and sample lots examined in his review, he concluded that the oxidised surface layers observed on "Kevlar" fibres were due to the presence of a truly oxidised fibre surface and were not due to the presence of residual processing aids. This conclusion was consistent with the observation that "Kevlar 49" fibres invariably contained a lower nitrogen and higher oxygen surface content relative to "Kevlar 29" fibres. "Kevlar 29" fibre manufacture does not involve a high temperature tensioning/drawing stage (Penn and Larsen 1979). Examination of the XPS peak shapes revealed additional information about the nature of the oxidation process. The most significant information was obtained from the O_{1s} and C_{1s} spectra. Both revealed broad peaks consistent with the existence of a number of different binding energy states, and thus chemical environments, for the carbon and oxygen species. Specifically, the presence of ester and carbonyl oxidation species on the fibre surface was implied by these results.

Allred also reported on the use of ammonia plasmas for the modification of aramid fibre surfaces. This chemical modification resulted in substantial increases in the nitrogen content of the surface as measured by XPS. However the surface oxygen content did not decrease below the theoretical estimate of 11%, suggesting the existence of a real region of oxidised fibre within the top 5.0 nm of the fibre surface .

Recently Chappell *et al.* (1989) have studied the XPS of model aramid compounds as well as various "Kevlar" fibres. The model compounds studied were benzanalide (BA), N,N'-dibenzoyl-1,4-phenylenediamine (DBPD) and N,N'-diphenyl-1,4-benzene-dicarboxamide (BPBD). The XPS binding energies and surface compositions determined by these authors are shown in Table 4.2.

	C_{1s} (%)	O_{1s} (%)	N_{1s} (%)
"As received" fibres	73	22	5
Ammonia plasma 15 sec./50 watts	72	20	8
Ammonia plasma 150 sec./150 watts	73	14	13
Polyphenylene terephthalamide (bulk)	78	11	11

Table 4.1 Surface C, O and N composition for various "Kevlar 49" fabrics (Allred 1983).

Compound		C 1s Peak Position		Surface Composition		
		C-C (eV)	C=O (eV)	C_{1s} (%)	O_{1s} (%)	N_{1s}(%)
BA	(experimental)	286.2*	289.5	84.2	7.1	8.7
	(expected)	285.0	288.0	86.7	6.7	6.7
DBPD	(experimental)	285.2	288.2	85.4	8.0	6.6
	(expected)	285.0	288.0	86.7	8.3	8.3
BA	(experimental)	285.6	288.9	87.2	6.5	6.3
	(expected)	285.0	288.0	83.3	8.3	8.3

* Difference between experimental and predicted peak position is due to sample charging.

Table 4.2 Experimentally observed and predicted carbon 1s peak positions, as well as the surface composition, of model aramid compounds (Chappell *et al.* 1989).

The model compounds were studied to assist in the assignment of the spectral bands. As well as the C-C and C=O carbon 1s peaks at 285.0eV and 288.0eV, shown above, peaks due to both C-O and O-C=O would be expected to be observed at 286.8eV and 289.1eV respectively. Thus, within a range of just over 4eV, a significant amount of chemical information is contained within the carbon 1s spectrum. Chappell *et al.* (1989) observed that the C-C peak and the C=O peak dominated the XPS spectrum of the clean "Kevlar" fibres. This sample was also characterised by a relatively high surface nitrogen content. Samples which were uncleaned, and presumably contaminated, exhibited spectra with peaks characteristic of the C-O and O-C=O groups in addition to those peaks due to C-C and C=O bonds. The authors also compared the XPS analysis of the "Kevlar" fibres with thermodynamic results they had earlier obtained using inverse gas chromatography (Chappell and Williams 1989a,b). It was demonstrated that the dispersive component of the surface energy of the fibres, (γ_S^d), and the negative entropy of adsorption, ($-\Delta S_A^o$), for hydrocarbon vapours adsorbed on the fibre surface correlated well with the nitrogen 1s signal intensity.

	C_{1s} (%)	O_{1s} (%)	N_{1s} (%)	$-\Delta S_A^o$ (J/mol.K)	γ_S^d (mN/m)
Cleaned fibres	79.9	14.0	6.1	83.0	65.1
"As received" fibres	73.5	25.7	0.8	34.1	32.0
"Kevlar 49" Scoured Fabric	76.5	18.4	5.2	60.8	38.1
"Kevlar 29" Scoured Fabric	83.5	16.1	0.3	39.9	37.2

Table 4.3 C, O and N surface composition the entropy of adsorption for n-octane ($-\Delta S_A^o$) and the dispersive component of the surface free energy (γ_S^d) for various "Kevlar" fibres (Chappell *et al.* 1989).

4.2.12 Conclusions

XPS is clearly the most important technique for analysing the surface composition of organic polymers. Aramid fibres have been succcesfully studied by a number of workers using this technique. These studies reveal that aramid fibre surfaces are often comtaminated. Even when the fibres are cleaned, a higher surface oxygen content than would be expected is observed, which is consistent with a partially oxidised surface.

4.3 EXPERIMENTAL XPS STUDY

4.3.1 XPS Experiments

XPS spectra were obtained using a Physical Electronics Model 560 spectrometer. Fibre samples were mounted onto the specimen stage using copper tape and introduced into the spectrometer via a differentially pumped sample introduction lock. Spectra were obtained using a magnesium anode (Mg $K_{\alpha 1,2}$:1253.6eV) X-ray source operating at a power of 300 watts. The energy of the photoelectrons was analysed by a cylindrical mirror analyser operating in the fixed analyser transmission mode. The spectrometer is schematically shown in Figure 4.2

XPS survey spectra were initially obtained with a pass energy of 100eV. The survey spectra allowed the atomic elements present on surfaces to be identified. High resolution spectra for the species identified were then obtained using a multiplexed mode of spectral acquisition. A pass energy of 25 eV at a step size of 0.2 eV was used for obtaining these high resolution spectra. A high concentration of carbon and a relatively low concentration of oxygen and nitrogen was revealed by the survey spectra for most samples. Consequently, during the multiplexed data acquisition, four nitrogen and two oxygen spectra were acquired for every carbon spectrum collected .

The insulating nature of most organic samples leads to some positive sample charging, due to the loss of photoelectrons, during the XPS measurement. Sample charging is often confirmed by the experimentally observed binding energy of the C-C peak being found at a higher binding energy than the expected energy of 285.0 eV. In this study, the C-C peak was found to be between 2 and 5eV higher in binding energy than expected. This variation may be entirely due to sample charging, though it is more like to be due to a 2eV calibration error in the analyser, combined with a variable sample charging effect of between 0 and 3eV. This latter explanation was confirmed by comparison of the results obtained by Chappell *et al.* (1989) with the results obtained in this work.

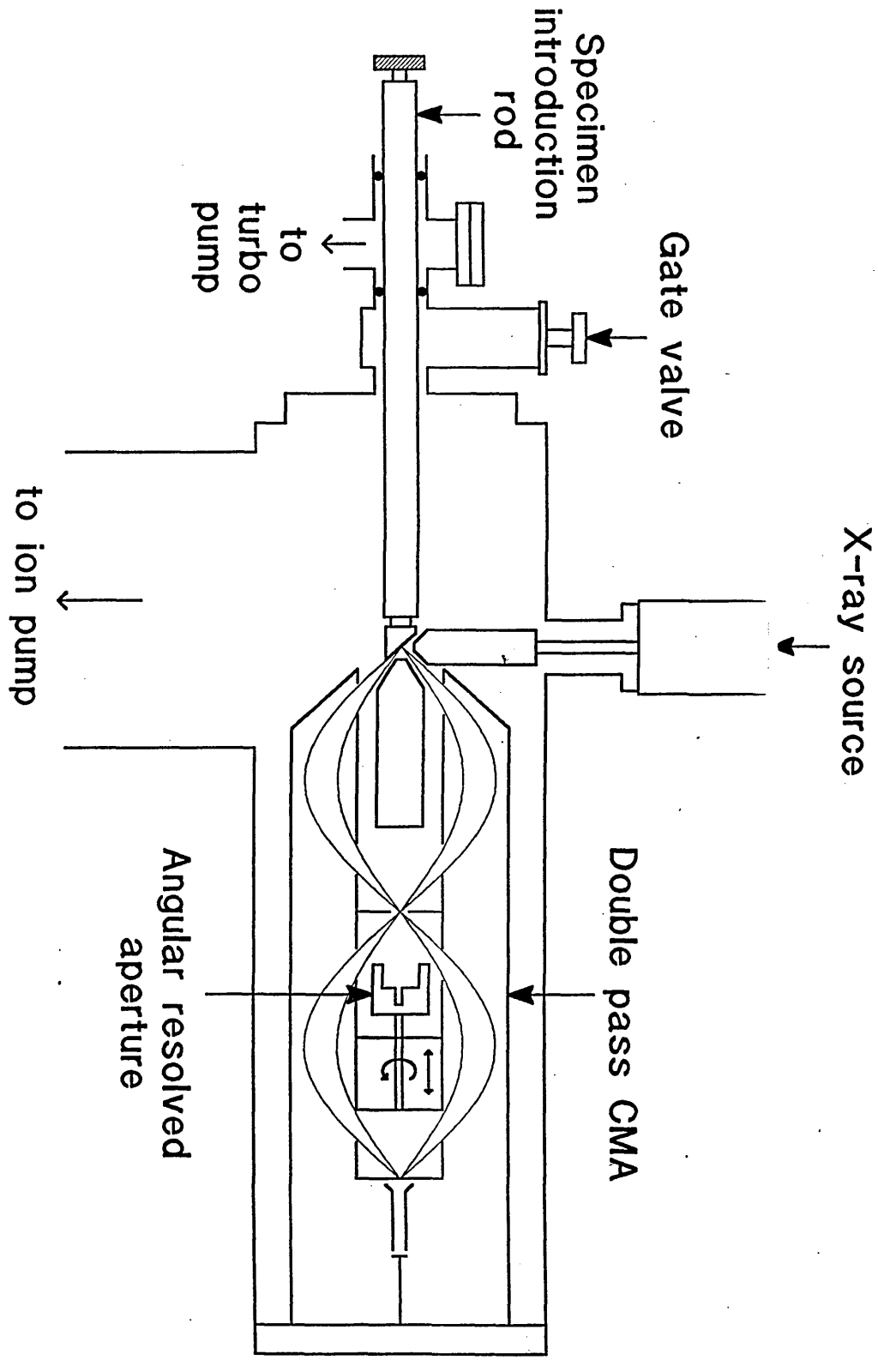


Figure 4.4 X-ray photoelectron spectrometer with a cylindrical mirror energy analyser.

The relative position of the carbon, nitrogen and oxygen 1s peaks for cleaned "Kevlar 49" fibre samples in both studies agrees to within 0.2eV.

The atomic surface composition was calculated using the software incorporated into the Physical Electronics Model 560 spectrometer system. The absolute photoelectron intensities are corrected for the photo-ionisation cross-section for the various elemental species in these computations.

	Carbon (eV)	Oxygen (eV)	Nitrogen (eV)
This study	287.3 (2.0)	534.0 (3.1)	402.5 (1.7)
Chappell *et al.* (1989)	286.0 (1.9)	532.5 (2.8)	401.3 (1.8)

Table 4.4 Comparison of the XPS peak positions (and peak width at 1/2 height) for clean "Kevlar 49" fibres.

4.3.2 XPS Results

The XPS results obtained are summarised in Tables 4.5 and 4.6. The actual spectra are included in Appendix A.

	C_{1s} (%)	O_{1s} (%)	N_{1s} (%)	$Other_{1s}$ (%)
Cleaned fibres	78.5	14.2	8.1	
"As received" fibres	71.7	21.9	6.3	
Polydimethyl siloxane coated fibres	49.2	30.7		Si 19.9
Polyethylene glycol coated fibres	64.6	32.4	2.8	
Epoxy resin coated fibres	78.8	19.8	2.1	
Tin hydrosol coated fibres	41.2	35.9	3.8	Sn 19.0
Metallisation/clean fibres	70.8	17.0	9.3	Na 2.7
Diol grafted fibres	68.5	24.8	5.1	Br 1.4
Nitrobenzene grafted fibres	76.6	14.4	8.9	Br 1.4
Octane grafted fibres	81.6	12.5	5.7	
Methyl-silane grafted fibres	70.3	19.4	6.4	Si 3.8
Epoxy grafted fibres	67.6	24.3	5.7	
Polyphenylene terephthalamide (bulk)	77.8	11.1	11.1	

Table 4.5 Surface composition of the "Kevlar" fibres as determined by XPS analysis

	Carbon (eV)	Oxygen (eV)	Nitrogen (eV)
Cleaned fibres	287.3 (2.0)	534.0 (3.1)	402.5 (1.7)
"As received" fibres	287.8 (2.3)	535.0 (3.5)	402.8 (2.0)
Polydimethyl siloxane coated fibres	287.5 (1.5)	535.0 (1.5)	
Polyethylene glycol coated fibres	287.8 (2.0)	535.4 (1.8)	402.8 (1.4)
Epoxy resin coated fibres	287.8 (2.0)	535.9 (2.5)	403.0 (1.7)
Tin hydrosol coated fibres	290.3 (2.0)	536.5 (2.8)	405.5 (2.2)
Metallisation/cleaned fibres	287.0 (2.0)	533.4 (2.2)	402.2 (1.7)
Diol grafted fibres	288.8 (1.8)	537.0 (3.3)	404.0 (1.6)
Nitrobenzene grafted fibres	286.8 (1.9)	533.3 (2.5)	402.0 (1.8)
Octane grafted fibres	287.5 (1.9)	534.5 (2.4)	402.6 (1.8)
Methyl-silane grafted fibres	287.5 (2.0)	534.5 (2.4)	402.7 (1.8)
Epoxy grafted fibres	287.8 (2.1)	535.0 (3.3)	402.9 (1.9)

Table 4.6 Position of peak maximum (and peak width at 1/2 height) for the principle XPS spectral peaks of the "Kevlar" fibres.

4.3.3 Surface Analysis of Cleaned and "As Received " "Kevlar" Fibres

The photoelectron binding energies observed in this work varied slightly from those values reported in the literature. However, for absolute agreement between these energies, it was necessary to assume that a constant offset error of -1.3eV existed for all the XPS spectra reported in this study. As previously proposed, this anomaly is probably due to a small error in the calibration of the energy analyser. The systematic error is of no consequence as far as the conclusions made in this chapter are concerned. The results presented are as experimentally obtained.

The XPS analysis of the cleaned and "as received" "Kevlar" samples provides the baseline composition of these aramid surfaces. This analysis of the clean fibres is particularly important as it allows the extent of surface modification to be gauged in later sections of this chapter. In was established in Table 4.4 that the binding energies of the XPS spectra obtained in this study for clean "Kevlar 49" fibres, agreed to within 0.2eV of those results obtained by Chappell *et al.* (1989). The good correlation between these studies is further confirmed by the consistent peak widths, as measured at half peak height, also presented in Table 4.4.

The primary spectral features of the XPS spectra of these two samples are :

(a) C_{1s} -The carbon spectrum could be expected to have bands at the 287.0eV, 288.8eV, 290.0eV due to the presence of C-C, C-O, C=O chemical environments. The close proximity of these three peaks indicates that it is unlikely that the individual peaks will be resolved in the spectrum. Experimentally, a broad peak, with some secondary "shoulders", is observed for both samples. The spectrum for the cleaned sample clearly shows a small peak due to C=O at 290.2eV as well as the primary C-C/C-O peak at 287.3eV. The "as received" fibres exhibited a slightly broader main C_{1s} peak due to the additional C-O contribution at 288.8eV to the primary C-C peak at 287.9eV, as well as a weaker C=O peak at 290.7eV.

(b) O_{1s} -A very broad XPS peak spanning between 532 and 537eV, representing a number of oxygen species, was observed experimentally for both samples. The two primary contributions to the oxygen peak will be the C-O (535.5eV) and C=O (533.5eV) chemical environments.

(c) N_{1s} -An essentially symmetric peak of weak intensity at 402.5 eV due to C-N bonds was observed for both samples.

The deduced atomic surface composition of the clean "Kevlar" fibres is in good agreement with Chappell *et al.*'s work as reported in Table 4.3. The nitrogen content of 8.1% is significantly higher than their results reported in Table 4.3. There are two possible explanations for this observation. They are that, either the cleaning procedure adopted in this study was more efficient than those utilized by Chappell *et al.*, or alternatively the clean sample used in this study was initially less contaminated. The cleaning procedure adopted in this work results in a contact time of the "Kevlar" fabric with hot acetone for 24 hours. In Chappell *et al.*'s work this time was less than 4 hours. This difference could significantly affect the solubilisation of contaminants and thus the efficiency of the cleaning procedure. The latter explanation is also reasonable since there is a substantial difference between the cleanliness of the "as received" "Kevlar" sample examined by Chappell *et al.* and the sample examined in this study. The XPS of these two samples indicated nitrogen contents of 0.5% and 5.2% respectively. This variation in the initial cleanliness could be expected to affect the final level of surface cleanliness attained.

Examination of the O_{1s} spectra for these samples reveals information on the chemical nature of the contaminants. Whilst both samples exhibit broad oxygen peaks, the asymmetry of the peaks is quite different. For the cleaned sample the peak is skewed towards a peak maximum at 533.5 eV, illustrating the dominant contribution of the C=O

peak in this spectrum. However, for the "as received" sample the peak is skewed in the opposite direction, due to the dominant presence of the C-O moieties associated with the surface contaminants.

4.3.4 XPS Analysis of Polymeric and Oligiomeric Coated"Kevlar" Fibres

The experimental XPS results and those theoretically predicted for the coated "Kevlar" materials are shown below in Table 4.7. The theoretical composition of the coated fibres was based on the bulk atomic composition of the coating excluding the presence of hydrogen atoms which are not sensed by XPS analysis. For these calculations, complete coverage of the fibres surface is assumed. The chemical structures of these coatings, from which the predicted compositions were derived, are given in Chapter 3 .

		C_{1s} (%)	O_{1s} (%)	N_{1s} (%)	$Other_{1s}$ (%)
Polydimethyl siloxane	Experimental	49.2	30.7		Si 19.9
	Theoretical	50.0	25.0		Si 25.0
Polyethylene glycol	Experimental	64.6	32.4	2.8	
	Theoretical	66.6	33.3	0.0	
Epoxy resin	Experimental	78.8	19.8	2.1	
	Theoretical	81.0	19.0	0.0	
Tin hydrosol	Experimental	41.2	35.9	3.8	Sn 19.0
	Theoretical	0.0	66.6		Sn 33.3

Table 4.7 Experimental and predicted atomic surface composition for the polymeric and oligiomeric coated "Kevlar" fibres.

The surface composition of the polydimethyl siloxane coated fibres is in good agreement with the theoretically predicted composition shown in Table 4.7. The absence of a N_{1s} signal for the coated fibres confirms the complete coating of the fibres by the polydimethyl siloxane within the sensitivity of the spectrometer. The success of this coating process is probably related to the low molecular weight, and hence low viscosity, of the polymer as well as its low surface energy. Both of these factors could be expected to contribute to complete coverage of the fibres by this polymer. The narrow peak widths for these coated fabrics reported in Table 4.6 confirms that the carbon and the oxygen photoelectrons that are detected have originated from unique chemical environments. This observation is also consistent with a surface completely covered with polydimethyl siloxane. The peak maximum of 535.0 eV for the O_{1s} spectrum confirms the presence of a single bonded oxygen species such as Si-O.

The experimentally measured surface composition for the polyethylene glycol coated fibres shows close agreement with the results predicted for a pure polyethylene glycol surface. However the origin of the 2.8% nitrogen experimentally observed for this sample is not obvious. It could be interpreted as resulting from an incompletely covered fibre surface. The fractional coverage of polyethylene glycol on the "Kevlar" fibres would in this case be 65% (1 -2.8/8.1). Alternatively, it could represent the presence of a nitrogen contaminant in the polyethylene glycol. The XPS spectra do not reveal sufficient information to differentiate between these two possible explanations. The oxygen spectrum for this sample contains a symmetric peak of width 1.8eV. The occurrence of this narrow width suggests that a single oxygen species is present on the fibre surface. A peak position of 535.5eV confirms that the oxygen is primarily bonded to a carbon atom. The carbon peak shows the significant presence of a C-O shoulder at 289.5eV, with minimal evidence of a carbonyl peak. This evidence supports the conclusion that the surface is dominated primarily by C-O and C-C species as would be expected for polyethylene glycol coating.

The non-zero concentrations of both carbon and nitrogen on the hydrosol modified fibre surfaces show clearly that incomplete coverage has occurred. From these compositions it may directly estimated that between 52% and 47% of the clean fibre surface is exposed. Using an average coverage of 50% for the surface, it is thus possible to estimate the contribution of the nude fibre surface to the O_{1s} signal assuming that the composition of the uncoated fibre surface is the same as the clean "Kevlar". On this basis, the 35.9% oxygen content of the surface is composed of 7.5% from the exposed clean fibres and 28.8% associated with the hydrosol. The total composition of 28.8% oxygen and 19.0% tin for the hydrosol surface implies a clear 3:2 stoichiometry between associated oxygen and tin species in the surface. It is difficult to predict *a priori* the composition of a tin oxide/hydroxide hydrosol once it is deposited onto a polymer surface and has dehydrated. The uncertainty in the computed ratio results from the lack of control in the preparation of the colloid which includes both stannic and stannous salts. Simply on the basis of valancy considerations, the most likely stoichiometry is between Sn:O ratio of 1:2 and 1:1. The XPS results suggest that the hydrosol is a mixed stannic/stannous material. The maximum peak in the O_{1s} spectrum corresponds to an energy of 533.4eV, after a 2.8eV correction for sample charging. The oxygen spectrum also shows the prominance of a shoulder 1eV higher in energy than the peak maximum. From the previously determined contributions to the O_{1s} spectrum, the shoulder would be expected to be due to oxygen in the underlying polymer, and the main peak to be due to the oxygen associated with the tin hydrosol.

4.3.5 Surface Analysis of Functionally Grafted "Kevlar" Fibres

Table 4.8 summarises the XPS results for the various graft reactions described in chapter 3. The theoretical compositions shown in this table are estimated on the basis of the graft reactions proceding to a 100% substitution. The experimentally determined XPS compositions are presented as well as "corrected" experimental results. Corrected

experimental results are presented in those cases where atomic species other than those which would be predicted from a completed graft reaction have been identified in the sample. In most cases these species could be tentatively identified as either unreacted chemicals or reaction products trapped within the outer regions of the fibre. The experimental results were corrected by subtracting the contributions due to these labile products. Details of these calculations are given in those cases where this correction procedure was adopted.

A number of introductory comments are appropriate with reference to results contained in Table 4.8 before the XPS data is discuussed in detail. The aggressive reactive nature of the dimethyl sulphinyl carbanion/dimethyl sulphoxide (DMSC/DMSO) solutions has been observed to result in substantial penetration of both chemical species into the crystal structure of aramid fibres (Takayangi *et al.* 1987). Indeed, over long periods of time the fibres can be completely dissolved by DMSC/DMSO solutions. Thus, the possibility of trapping substantial amounts of DMSC/DMSO in the swollen material clearly exists. However the XPS compositions determined in this study clearly indicate that the procedures developed for the cleaning and drying of the "Kevlar" fibres after the reaction were successful. Most significantly, sulphur from DMSC or DMSO was not detected by XPS in any of the samples examined. In most cases no, or minimal amounts of, unreacted chemicals were detected. In a number of cases however, the presence of these residual chemicals was confirmed by the presence of bromine or iodine in the XPS spectra. Bromine or iodine are present in the nucleophilic reagents used in these graft reactions.

		C_{1s} (%)	O_{1s} (%)	N_{1s} (%)	$Other_{1s}$ (%)
Metallated /clean	Experimental	70.8	17.0	9.3	Na 2.7
	Experimental Corr.	74.9	15.1	9.8	
	Theoretical	78.8	11.1	11.1	
Diol grafted	Experimental	68.5	24.8	5.1	Br 1.4
	Experimental Corr.	70.4	24.0	5.6	
	Theoretical	71.4	21.4	7.1	
Nitrobenzene grafted	Experimental	76.6	14.4	8.9	Br 1.4
	Experimental Corr.	77.7	13.5	8.7	
	Theoretical	73.7	15.8	10.5	
Octane grafted	Experimental	81.6	12.5	5.7	
	Theoretical	88.2	5.9	5.9	
Methylsilane grafted	Experimental	70.3	19.4	6.4	Si 3.8
	Theoretical	77.0	7.7	7.7	Si 7.7
Epoxy graft	Experimental	67.6	24.3	5.7	
	Theoretical	82.3	14.7	3.0	

Table 4.8 Experimental and predicted atomic surface composition of the surface grafted "Kevlar" fibres.

The preparation of a metallated "Kevlar" sample, which was subsequently reacted with water, provides an opportunity for the XPS analysis of a chemically regenerated poly -phenylene terephthalamide (PPTA) surface. The XPS spectra of the metallated/cleaned "Kevlar" sample revealed the unexpected presence of 2.7% of sodium on the surface. This material is likely to exist in the form of NaOH, which is the by-product of the reaction between DMSC and water and probably exists in the outer regions of the fibre surface. However, this observation does not explain why similar species were not found for the other grafted samples. The reasons for this difference are related to the reaction conditions used for these reactions. For the reaction with water, an extended metallisation reaction time, relative to the other graft reactions, was employed. It was considered that a greater extent of PPTA regeneration would be accomplished if the metallised intermediate was formed in greater quantities. The experimental results shown in Table 4.8 may simply be corrected by allowing for the contribution due to NaOH. Subtracting 2.7% sodium and 2.7% oxygen from the experimental XPS results leads to the corrected experimental surface composition. For these results the nitrogen composition is close to the theoretical value of 11.1%, but the percentage composition of both carbon and oxygen differ by about 4% from the theoretical bulk compositions. The oxygen XPS spectrum for this sample show a substantial change in the peak shape relative to both the "as received" and cleaned samples. This peak for the metallated/cleaned sample is distinctly narrower and asymmetrically skewed towards the C=O peak maximum of 534eV. The amount of C-O seems to have decreased relative to the cleaned sample simply based on obvious changes in the peak shape. It is thus concluded that the metallated/cleaned reaction route has resulted in the removal of C-O material from the fibre's surface. This conclusion supports Allred's view that oxidised PPTA polymers exist on the outer surface of these fibres.

The changes in the surface compositional stoichiometry for the diol grafted fibres are shown in Table 4.8 and strongly support the view that significant changes in the surface chemistry of these fibre have occurred. However, it is the examination of the oxygen

spectrum which reveals the most critical information. A dramatic increase in the C-O peak at 535.5eV clearly confirms that significant grafting of the diol groups onto the fibre surface has occurred. Indeed, the XPS oxygen spectrum for these grafted fibres closely resembles the contaminated "as received" materials with its pronounced C-O peak. From the oxygen spectrum it may be estimated that the ratio of the C-O to C=O intensities are about 7:6, and thus the diol reaction has achieved 58% substitution. This result reflects an average value for the whole of the surface region from which photoelectrons can escape; essentially a region 5.0nm in depth. The extent of the reaction on the outer molecular layers of the fibre might be expected to be higher than this average value due the more likely penetration of dimethyl sulphinylcarbanion, and thus the creation of the metallated PPTA species, in the outer fibre regions. The presence of bromine in the XPS analysis is presumed due to the presence of unreacted bromo-propane diol which is trapped within the outer crystalline regions of the fibre surface.

The effecient reactive grafting of octane groups on the fibre surfaces is not confirmed by the XPS compositional data. Whilst the N_{1s} theoretical and experimental data agrees, the large difference for the carbon and oxygen data is not immediately explainable. Examination of the carbon spectrum is encouraging as the C=O peak at 290.0 eV is about 0.4 intensity units in height, whereas for most other spectra, such as the "as received" and the metallated/H_2O, this peak is 0.8 intensity units high. The graft reaction would have been expected to cause a substantial decrease in the intensity of the C=O peak relative to the C-C peak. The extent of the graft reaction has been estimated by linearly interpolating the experimental surface composition between that of the clean material, representing 0% graft and the theoretical composition for a fully 100% reacted surface. This calculation predicts reaction yields of 31%, 21% and 100% using the carbon, oxygen and nitrogen composition data respectively. Whilst these results do not provide a means of estimating quantitatively the extent of the graft reaction they do support the qualitative conclusion that alkylation has occured to a significant extent on the fibre surface.

The surface composition data in Table 4.8 for the methyl silane treated "Kevlar" materials reveals a complicated spectroscopic system. The spectroscopic presence of silicon and absence of chlorine on the fibre surface is strong evidence that this graft reaction has to some extent proceeded. However the low carbon and high oxygen presence are not consistent with this explanation. The oxygen peak is only 2.4eV wide, suggesting that the spectrum is dominated by a single oxygen species, whilst the peak position at 534.4eV suggests the dominant peak to be carbonyl. The spectral evidence is inconclusive and as such does not provide a means for assessing the extent of this reaction.

The composition of the nitrobenzene grafted fibres was corrected for the presence of some residual iodo-nitrobenzene. The corrected composition of the nitrobenzene grafted fibres is similar to that theoretically predicted for a completely grafted surface as well that of the composition for cleaned a "Kevlar" fibre surface. This evidence does not substantiate the presumed nitration reaction. Most significantly, the N_{1s} peak does not show any broadening or structure as would be expected due to the different chemical environments of the amide and nitro groups.

The predicted composition for the epoxy graft reaction is based on the complete reation of the metallated "Kevlar" fibres with the difunctional epoxy bisphenol A diglycidyl ether. The surface composition of these grafted fibres shows a significant decrease in the nitrogen content from 9.8% to 5.7%. However the surface oxygen composition is unchanged and the carbon composition has increased. Examination of the actual peak shape for the oxygen spectrum reveals subtle, but more conclusive evidence. The O_{1s} peak is quite broad and the peak maximum is at 535eV. As has been previously noted, this position is normally associated with C-O groups, rather than C=O groups which tend to have a peak maximum at 534eV. In this case, the XPS results generally support some reaction between the epoxy and the fibre surface but the XPS results are inconclusive regarding the extent of this reaction.

4.3.6 Conclusions

Removal of surface contaminants from "Kevlar" fibres is confirmed via the use of soxhlet extraction with acetone. Polydimethyl siloxane, polyethylene glycol, epoxy oligiomer and a tin hydrosol coating have been successfully coated onto "Kevlar 49" fibres.

The successful grafting of alkyl and diol groups onto the surface of "Kevlar" fibres via an anhydrous reaction route has been clearly confirmed by XPS results. Spectral evidence also supports the successful grafting of functional epoxy groups onto the fibre surface. The metallated/cleaned reaction has resulted in the removal of C-O containing material from the fibre surface and results in a surface composition which is similar to that theoretically predicted.

CHAPTER 5

WETTABILITY AND SURFACE ENERGETICS

5.1 INTRODUCTION

This Chapter examines the wetting properties and the derived surface energetics of polymeric materials obtained by the use of liquids. In the first part of this Chapter, the relevant fundamental concepts and the current understanding of wettability phenomena are reviewed, especially in the context of flat polymeric substrates. The methods available for the analysis of contact angle data are discussed in detail, especially the current trend of adopting semi-empirical models which consider acid-base interactions. Recent work on the wettability of fibres is also discussed with a particular emphasis on aramid fibre materials and the experimental methods for measuring fibre wettability. Experimental wettability results for a number of surface modified "Kevlar" monofilaments, using the Wilhelmy balance technique are reported in the second part of this Chapter. These results are analysed and the surface thermodynamic properties of the fibres have been computed. The potential adhesive character of these fibre surface modifications is discussed in relation to the computed fibre surface energy characteristics.

5.2 WETTING, ADHESION AND SURFACE ENERGETICS

5.2.1 The Young Equation

The equilibrium contact angle, θ, made by a liquid drop on an ideally smooth, flat and non-deformable surface in thermodynamic equilibrium with its vapour is shown in Figure 5.1. By considering a balance of forces at the three phase contact line, Young (1805) proposed :

$$\gamma_{L\text{-}V} \cos\theta = \gamma_{S\text{-}V} - \gamma_{S\text{-}L} \qquad (5.1)$$

However, the seductive simplicity of Young's Equation hides a number of difficult conceptual and experimental problems.

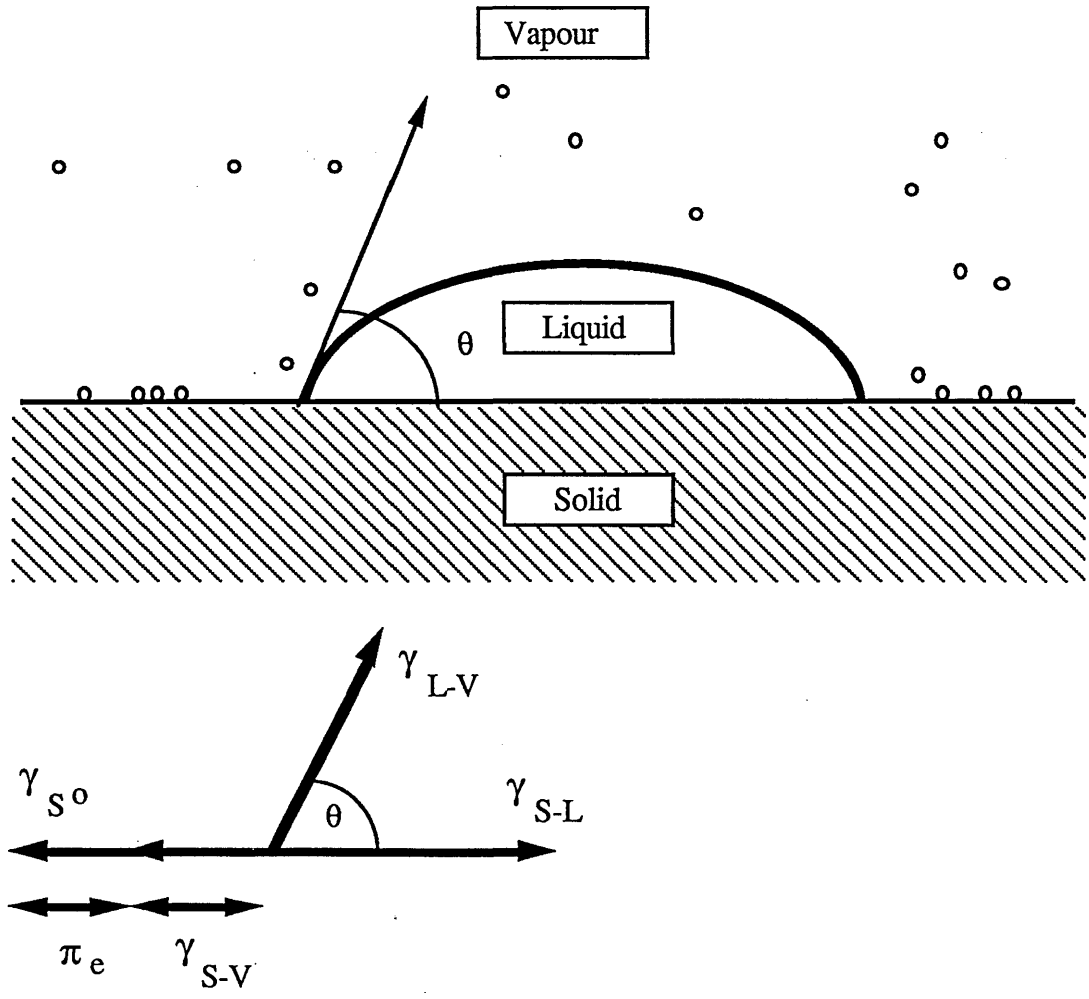


Figure 5.1 The equilibrium contact angle, θ, in relation to the liquid-vapour surface tension, $\gamma_{L\text{-}V}$, the solid-liquid interfacial tension ,$\gamma_{S\text{-}L}$, and the solid surface tension, γ_{S}^{o}. γ_{S}^{o} consists of two components, the solid-vapour interfacial tension, $\gamma_{S\text{-}V}$, and the equilibrium film spreading pressure π_e.

These difficulties have resulted in significant discussion and critical appraisal of two primary issues. Hiemenz (1977) has briefly considered these two matters which are considered below:

(i) It is implicitly assumed in the derivation of Young's Equation that the solid is sufficiently stiff so that negligible vertical displacement occurs. In the case of soft polymers, such as certain elastomers and hydrogels, this assumption is not valid and errors in the measurement of θ can occur (Andrade *et al.* 1979). A more serious argument concerns the equilibrium nature of the system and whether it is reasonable to assume that a surface which is mechanically stressed is thermodynamically equivalent to one which is not stressed.

(ii) The second issue concerns $\gamma_{S\text{-}V}$ and $\gamma_{S\text{-}L}$. Since these quantities cannot be accurately measured independently experimental verification of Young's Equation is not possible with high precision.

5.2.2 Work of Adhesion

The thermodynamic work required to separate the interface between two phases, A and B, is the work of adhesion W_{AB} and this quantity defined in terms of the final versus the initial energy states:

$$W_{AB} = \gamma_{Final} - \gamma_{Initial} = \gamma_A + \gamma_B - \gamma_{AB} \qquad (5.2)$$

The work of adhesion is a thermodynamic measure of the attraction between the phases. In the simple case in which A and B are the same phase, W_{AA} is the work of cohesion and is directly related to the Helmholtz free energy change, ΔG, and interfacial tension, γ_A:

$$\Delta G = 2\gamma_A = W_{AA} \qquad (5.3)$$

The work of adhesion between a solid and a liquid may be defined by analogy with Equation 5.2 as:

$$W_{S\text{-}L} = \gamma_S + \gamma_{L\text{-}V} - \gamma_{S\text{-}L} \qquad (5.4)$$

where $W_{S\text{-}L}$ = solid-liquid work of adhesion

γ_S = solid surface tension

$\gamma_{L\text{-}V}$ = liquid-vapour surface tension

$\gamma_{S\text{-}L}$ = solid-liquid interfacial tension

Substitution of Equation 5.1 into Equation 5.4 leads to what is commonly called the Young-Dupre Equation:

$$W_{S\text{-}L} = \gamma_{L\text{-}V} (1 + \cos\theta) + \pi_e \qquad (5.5)$$

The equilibrium spreading pressure, π_e, is the reduction in the surface energy of the solid phase due to the adsorption of the liquid phase vapour on the surface. It also defined as :

$$\int_0^{p^o} \Gamma \, d(\ln p) = \pi_e \qquad (5.6)$$

where Γ = surface concentration of adsorbed species

p^o = saturated vapour pressure of adsorbate

p = vapour pressure of adsorbate

5.2.3 The Equilibrium Spreading Pressure

For a liquid drop on a smooth homogeneous polymeric surface a finite equilibrium

spreading pressure, π_e, will exist if the contact angle $\theta = 0$. However for the case in which $\theta > 0$ it is not clear whether the assumption that $\pi_e = 0$ is generally valid.

Experimental measurements of π_e on flat substrates are difficult and normally involve thin film thickness measurements via ellipsometry. Adamson (Tadros *et al.* 1975; Hu and Adamson 1977; Tse and Adamson 1979; Nayar and Adamson 1983) has been one of the most active researchers in this area. Yet, uncertainties associated with contamination of their samples during preparation mean that his results are inconclusive. Few other studies have been undertaken in this area, except the work of Pashley and Kitchener (1979). They have demonstrated elegantly the existence of a finite value of π_e for water on hydrophobic glass surfaces.

The experimental difficulty in the measurement of π_e has encouraged workers to accept the argument that $\pi_e = 0$ if $\theta > 0$. Virtually all contact angle studies for liquids on organic polymers have presumed $\pi_e = 0$. The validity of this assumption is still an active area of current research and is yet to be experimentally verified.

5.2.4 The Critical Surface Tension Method

The first major development in the theory of contact angles was made by Fox and Zisman (1950, 1952a,b). They introduced Equation 5.7 which defined a new solid surface tension concept, the critical or limiting wetting tension, γ_c, for a solid surface:

$$\cos\theta = 1 + \mathbf{b}(\gamma_{L\text{-}V} - \gamma_c) \qquad (5.7)$$

where $\mathbf{b}$ = an empirical constant

γ_c = critical wetting tension

Fox and Zisman found a linear relationship between $\cos\theta$ and $\gamma_{L\text{-}V}$ for a homologous series of liquids tested on a particular solid surface. Plotting $\cos\theta$ versus $\gamma_{L\text{-}V}$ results in a straight line, commonly referred to as a Zisman plot. The relationship is purely empirical and may be simply stated:

$$\gamma_c = \lim_{\theta \to 0} \gamma_{L\text{-}V} \qquad (5.8)$$

However, when a non-homologous series of liquids was used the results were scattered and grouped in a curved line (Zisman 1964) and hence estimates of γ_c showed significant variations (Dann 1970; Schulman and Zisman 1952). Use of the critical tension concept is not currently in vogue.

5.2.5 Semi-Empirical Surface Energy Models

The concept that the surface tension of a phase could be considered as composed of a number of independent components was initially proposed by Fowkes (1964). This proposition led to the popular formalism:

$$\gamma = \gamma^d + \gamma^p + \gamma^i + \gamma^h \qquad (5.9)$$

where γ = surface tension for any phase

γ^d = dispersive component of the surface tension

γ^p = polar component of the surface tension

γ^i = induction component of the surface tension

γ^h = hydrogen bonding component of the surface tension

The components included in Equation 5.9 are based on the 3 types of pairwise molecular interactions considered in the Van der Waals model of gas phase molecular interactions for organic molecules. Equation 5.9 has been extended to consider other classes of molecular attractions such as ionic and metallic bonding interactions.

Examining the dispersive interactions which occur at an interface, Fowkes (1964)

showed that for two phases A and B, when either A or B could only interact via dispersive interactions, that Equation 5.10 was valid :

$$W_{A\text{-}B} = 2\sqrt{(\gamma_A^d \gamma_B^d)} \qquad (5.10)$$

This equation was based on the geometric mean arguments which were successful in non-electrolyte solubility theory (Hildebrand and Scott 1962) as well as in simple pairwise molecular potential calculations. These calculations for the dispersive interaction between two different molecules, with similar ionisation potentials, had been reported by Fowkes (1964).

This geometric mean approach was extended by Kaelble and Uy (1970) who considered an interface in which the interfacial interactions could be assumed to be due only to dispersive and polar interactions. Then the work of adhesion could be partitioned into two components (Equation 5.11). The polar interactions were described by a geometric mean equation analogous to Equation 5.10, and thus the total work of adhesion could be given by Equation 5.12 :

$$W = W^d + W^p \qquad (5.11)$$

$$W_{A\text{-}B} = 2\sqrt{(\gamma_A^d \gamma_B^d)} + 2\sqrt{(\gamma_A^p \gamma_B^p)} \qquad (5.12)$$

A similar equation was also proposed by Owens and Wendt (1969).

These approaches allowed the surface energy of a solid polymer surface to be characterised by two parameters; γ_S^d and γ_S^p. These parameters could be determined for a particular solid surface by measuring the contact angles for two different liquids with the same surface. Since γ^d and γ^p were known for both liquids, a set of linear simultaneous equations could be derived with γ_S^d and γ_S^p as the unknowns (Kaelble 1970). A simple matrix determinant solution could be obtained for γ_S^d and γ_S^p which gave acceptable

estimates for these quantities. By using a series of liquids (Kaelble 1970), various liquid pair permutations were possible, each of which gave unique estimates for γ_S^d and γ_S^p. These results were then averaged to compute a value for γ_S^d and γ_S^p.

Table 5.1 shows the dispersive and polar contributions of the surface tension of a range of contact angle liquids obtained by Fowkes and his co-workers using Equations 5.9 and 5.10. These data are commonly used to compute γ_S^d and γ_S^p using Equations 5.10, 5.11 and 5.12.

The geometric mean approach to surface energy analysis has found widespread usage due to its simple, but essentially sound theoretical basis, as well as its ease of use. It is however not without significant limitations and faults. In practical terms it is not uncommon for the multiple liquid type analysis to yield estimates of γ_S^p with errors of 100%, or indeed to predict negative values of γ_S^p. These problems are intrinsic to the multiple liquid type analysis which considers the data points for each liquid pair to be of equal quality or reliability. Since it is quite common for the estimates of γ^p in Table 5.1to have errors of +/- 5 mN/m, then clearly serious errors in the calculation of the polymer surface energies components can occur. For example, the reliability of using methylene iodide and bromonapthalene data to estimate γ^p, or to include such data in an average for γ^p, is clearly dubious. However such usage is common.

Rather than using a series of liquids, a preferred approach is the use of only two liquids, normally water and methylene iodide. Liquids which have primarily dispersive surface properties, such as methylene iodide, are best used to provide information on the dispersive surface chemical interactions. Whilst water, which has a large component of its surface tension due to hydrogen bonding (or polar interations), is best used as a wetting liquid to probe the specific interactions. The greater relative certainty in γ^d and γ^p for these liquids leads to an improved certainty in the γ_S^d and γ_S^p values (Owens and Wendt 1969).

Wu (1971) has proposed a similar equation to 5.12. Equation 5.13 uses an harmonic mean rather than the geometric mean for both the dispersive and polar components of the work of adhesion.

Liquid	$\gamma_{L\text{-}V}$ (mN/m)	γ^d (mN/m)	γ^p (mN/m)
Methylene Iodide	50.8	48.6	2.2
Bromonapthalene	44.3	44.3	0
Water	72.8	22.0	50.8
Glycerol	63.4	37.0	26.4
Formamide	58.4	39.5	18.7
Dimethyl sulphoxide	43.3	29.6	13.7
Pyridine	36.1	34.0	2.1
Pyridazine	48.9	38.9	10.0
Iodoethanol	44.9	41.1	3.8

Table 5.1 Surface tension of a number of contact angle liquids, and their polar and dispersive components at 25°C. Taken from the work of Fowkes and co-workers (Fowkes 1964; Fowkes and Maruchi 1977; Williams and Fowkes 1989).

$$W_{A\text{-}B} = \frac{4\left(\gamma^d_A \gamma^d_B\right)}{\gamma^d_A + \gamma^d_B} + \frac{4\left(\gamma^p_A \gamma^p_B\right)}{\gamma^p_A + \gamma^p_B} \qquad (5.13)$$

The use of the harmonic mean is primarily based on empirical considerations (Wu 1971), though in practical terms the advantages over the geometric mean are questionable. A comparison of the geometric and harmonic mean equations for a series of polymers based on the contact angles with water and methylene iodide is shown below. Most research workers have shown a preference for the geometric mean approach.

5.2.6 Acid-Base Interfacial Interactions

Fowkes and his co-workers have shown that the solution and surface properties of polymers as well as inorganic oxides may be understood using the concept of acid-base interactions (Fowkes 1980; Fowkes 1983; Fowkes *et al.* 1984; McCarthy and Fowkes 1985). This approach offers greater predictive capacity than the classical approach of considering specific interactions as the result of non-specific dipole-dipole (polar) interactions. These conclusions have been primarily based on experimental studies of solubility, adsorption behaviour and polymer-molecule acid-base complexes. Fowkes has argued that the energy of specific interactions at an interface could be described using Drago's E and C model which allows the heat of interaction between an acidic and a basic molecule to be predicted (Marks and Drago 1975; Drago and Epley 1969; Drago *et al.* 1971). Furthermore, Fowkes observed no correlation between the energies of interaction and the magnitudes of the dipole moments of the interacting species (Fowkes 1983).

Polymer	Contact Angle		Harmonic Mean		Geometric mean		Critical tension
	H_20	MeI_2	γ^d (mN/M)	γ^p	γ^d (mN/M)	γ^p	γ_c (mN/M)
Polyethylene	102	53	35.4	0.8	33.2	0	31
Polytetrafluoroethylene	108	77	20.5	2.0	18.5	0.5	18
Polystyrene	91	35	38.4	4.2	41.4	0.6	33
Polymethyl methacrylate	80	41	31.2	10.0	35.9	4.3	39
Polyvinyl chloride	87	36	35.8	6.1	40.0	1.5	39
Polyvinyl fluoride	82	63	27.2	11.2	31.3	5.4	28
Nylon 6	70	41	29.3	15.4	34.1	9.1	46

Table 5.2 Surface tension data via geometric, harmonic mean equations and Zisman's Critical Wetting Tension for a range of polymers (Wu 1982).

Fowkes' findings are consistent with the current classifications of bonding theories which consider hydrogen bonding to be a class of acid-base interaction. These theories recognise that partial bonding interactions are not simply the result of simple dipole-dipole interactions, but involve substantial charge redistribution within complex three dimensional electrostatic fields.

The acid-base theories of molecular interaction constitute a class of models that broadly consider all types of molecular interaction which involve charge redistribution and

electrostatic (classical and non-classical) interactions. This approach includes the intermolecular bonds and interactions which traditionally have been described as induction, polar, metallic bonding, π electron interactions, charge-transfer complexes or hydrogen bonding. These theories and concepts, such as Gutmann's donor-acceptor numbers, Drago's E and C model and Pearson's hard/soft acids and bases, have found widespread use in chemistry and chemical technology (Gutmann 1978; Jensen 1980). Fowkes' important contribution has been to introduce these concepts into interface phenomena.

Using these acid-base concepts, Fowkes and Maruchi (1977) have proposed that the work of adhesion consists of two components. The first component is a measure of the dispersive interactions and a second component describes the more specific acid-base interactions (Equation 5.14). Using Equation 5.15, these authors were able to estimate the acid-base components of the total work of adhesion for a number of polymer-liquid pairs from experimental wettability data.

$$W = W^{d} + W^{a\text{-}b} \tag{5.14}$$

$$W_{A\text{-}B} = 2\sqrt{(\gamma_A^{d}\,\gamma_B^{d})} + W^{a\text{-}b} \tag{5.15}$$

Fowkes and Mostafa (1978) have incorporated Drago's E and C model directly into an expression for the work of adhesion. The expression consists of three terms. The first term considers dispersive interactions, the second term acid-base interactions and the third term any residual polar interactions. It is the second term which utilises Drago's E and C model to compute the acid-base component of the work of adhesion.

$$W_{A\text{-}B} = 2\sqrt{(\gamma_A^{d}\,\gamma_B^{d})} + n(C_A C_B + E_A E_B) f + W_p \tag{5.16}$$

where n = the number of acid-base pairs per unit interface

C_A, E_A = Drago's acid-base constants for species A .

C_B, E_B = Drago's acid-base constants for species B .

f = constant normally equal to 1

W_p = Additional polar work of adhesion term

The values for Drago's E and C constants have been experimentally determined primarily using calorimetric data based on a large number of acid-base solution complexation studies. Drago has argued that the product C_AC_B represents the component of interaction energy due to covalent type interactions, and that the E_AE_B term relates to the electrostatic component of the interaction energy for a particular acid-base pair.

If more than one pair of acid-base interactions occurs, then additional E and C terms would need to be included in Equation 5.16. This case would arise if two amphoteric species interacted. Unfortunately, the limited number of molecules which have been characterised in terms of E and C constants has limited the extensive use of Equation 5.16.

Recently Williams and Fowkes (1989) have reported W^{a-b} values for a number of polymer-liquid pairs. These data were used to make quantitative estimations of the surface acidity/basity of polymethyl methacrylate (PMMA), polystyrene (PS), polyvinyl butyral and polyvinyl chloride. Equation 5.12 was used to predict the total work of adhesion for water-PMMA and water-PS pairs. The surface concentrations of the interacting species, **n**, were estimated on the basis of a simple bulk equivalent surface concentration calculation. The available concentration of interacting functional groups on the polymer surface, rather than the number of acid-base functionalities within the water, specified the value of **n** and thus the extent of acid-base complexation. The calculated work of adhesion correlated well with the experimental estimates, confirming the value and utilitity of acid-base theory in wettability studies.

Good (1979) has rewritten Equation 5.16 in a new format, assuming that the acid-base components can be simply defined via Equations 518 and 5.19 . These two

equations model the electrostatic and covalent acid-base interactions within a geometric mean style of argument:

$$W_{A\text{-}B} = 2\sqrt{(\gamma^d_A \gamma^d_B)} + 2\sqrt{(\gamma^i_A \gamma^i_B)} + 2\sqrt{(\gamma^{cv}_A \gamma^{cv}_B)} + 2\sqrt{(\gamma^e_A \gamma^e_B)} \qquad (5.17)$$

$$-f\,E_A\,E_B = 2\sqrt{(\gamma^e_A \gamma^e_B)} \qquad (5.18)$$

$$-f\,C_A\,C_B = 2\sqrt{(\gamma^{cv}_A \gamma^{cv}_B)} \qquad (5.19)$$

where γ^i = inductive component of γ

γ^{cv} = covalent component of γ

γ^e = electrostatic component of γ

Though this approach seems conceptually attractive, it does in fact deviate from Fowkes and Mostafa's original proposal in two significant ways. It erroneously suggests via Equations 5.18 and 5.19 that the E and C constants are characteristic of both the acid and base character of a species. However, the acid character is given by $\mathbf{C_A}$ and $\mathbf{E_A}$, and the base character by $\mathbf{C_B}$ and $\mathbf{E_B}$ for each species. Thus γ^{cv} and γ^e do not distinguish between whether the chemical species is acting as a base or as an acid. In addition, errors will be introduced by the absence of a correct specification for **n**, since it is incorporated directly into γ^e and γ^{cv}. The correct definition for **n** is given below :

$$\mathbf{n} = \min(\mathbf{n_a}, \mathbf{n_b}) \qquad (5.20)$$

where $\mathbf{n_a}$ = concentration of acid groups per unit area

$\mathbf{n_b}$ = concentration of base groups per unit area

min ( ) = minimum value within ( )

Van Oss *et al.* (1988) have recently proposed a new equation which replaces Equation

5.17 and deals with some of the inadequacies discussed above:

$$W_{A\text{-}B} = 2\sqrt{(\gamma_A^{LW}\gamma_B^{LW})} + 2\sqrt{(\gamma_A^{-}\gamma_B^{+})} + 2\sqrt{(\gamma_A^{+}\gamma_B^{-})} \qquad (5.21)$$

where γ^{LW} = long range (dispersive) component of γ

γ^{+} = acid parameter of γ

γ^{-} = basic parameter of γ

This equation defines two empirical constants γ^{+} and γ^{-} for each species as measure of their surface acidity and basicity. This model is conceptually similar to the Fowkes-Mostafa equation. This proposal is yet to be experimentally verified.

5.2.7 Contact Angle Hysteresis

It is rare for a droplet placed on a flat smooth surface to yield a unique non-zero value for the contact angle, θ. Rather, a range of stable equilibrium contact angles are observed. The upper bound contact angle is described as the advancing contact angle, θ_A, and the lower bound as the receding contact angle, θ_R. Both θ_A and θ_R are equilibrium contact angle measurements with the subscripts referring to the experimental method chosen for their measurement. The contact angle hysteresis, $(\theta_A - \theta_R)$, is not necessarily indicative of a dynamic or non-equilibrium process. θ_A is defined as the limiting contact angle made by a droplet on a substrate, such that any further increases in the contact angle will result in the three phase contact line advancing forward. Similarly θ_R is defined in terms of the minimum contact angle which will cause the three phase contact line to recede. The difference between θ_A and θ_R defines the contact angle hysteresis. The contact angles between θ_A and θ_R represent stable contact angles of non-minimum energy, and are often described as being energetically metastable. There are a number of explanations for the existence of these metastable states and the consequent occurrence of contact angle hysteresis.

One rationalisation for contact angle hysteresis is substrate surface roughness. The classical analysis of this phenomena was elucidated by Wenzel (1936) who derived a roughness factor **r** which is given by the ratio of the true surface area to the apparent two dimensional geometrical surface area. Wenzel's Equation is thus defined as :

$$\cos \theta_w = r \cos \theta_0 \qquad (5.22)$$

where θ_w = Wenzel's contact angle

θ_0 = Real contact angle.

This formula constitutes a simple relationship between the contact angle on the "rough" substrate, θ_w, and the contact angle for the equivalent flat surface, θ_0. Johnson and Dettre (1964a,b) have successfully considered, both experimentally and theoretically, contact angle hysteresis and surface topography. They concluded that hysteresis increases with increasing surface roughness.

Contact angle hysteresis can also be rationalised in terms of the energetics of a chemically heterogeneous surface. Compositional heterogeneities can lead to energy barriers between surface regions of different composition. Cassie (1948) has analysed the case of a heterogeneous surface which was composed of two regions of different composition, each with intrinsic contact angles θ_1 and θ_2. The resultant contact angle was designated Cassie's angle θ_C and is defined by Equation 5.23. A_1 and A_2 are the area fractions of the respective regions whose contact angles are θ_1 and θ_2 respectively:

$$\cos \theta_C = A_1 \cos \theta_1 + A_1 \cos \theta_2 \qquad (5.23)$$

This phenomena has also been studied by Johnson and Dettre (1964), and Dettre and Johnson (1965).

5.2.8 Equilibrium Contact Angle

Three different types of contact angles, the experimentally measured θ_A and θ_R, as well as the Young's equilibrium contact angle, θ, have been considered in this Chapter. The question clearly arises as to which experimental contact angle relates to the θ. There is no obvious answer to the question which has been much discussed in the literature (Neumann 1974). From an experimental viewpoint, current practice is to take θ_A as the value of θ. A simple justification for this viewpoint is that θ refers to a state of equilibrium of minimum energy, and that θ_A is the experimentally generated minimum energy result.

5.2.9 Fibre Wettability by the Drop Profile Method

When a drop of liquid is placed upon a surface, the drop will adopt a shape which is a result of the gravitational forces and the interfacial forces associated with the liquid-fibre -vapour interface. In the case of a fibre whose diameter is less than 20μm, droplets are typically less than 100μm in diameter and the gravitational effects become negligible relative to the interfacial forces. In these circumstances it has been observed that droplets on a fibre may adopt one of two possible conformations. These conformations are the axi-symmetric and the asymmetric ("clamshell") shapes. The former conformation is the energetically favoured case when the contact angle, θ, is between 0 and 60°, and the latter is the preferred shape when the contact angle is greater than 60° (Carroll 1976).

Carroll (1976) has considered, in detail, the first case where axi-symmetric drops are formed. He has numerically solved the Laplace equation for this case and has produced a set of tables which relate the contact angle, θ, to the two principal dimensionless drop shape parameters. These parameters are the x_2/x_1 and L/x_1 where x_2 is the drop radius, x_1 is the fibre radius and L is the droplet length as shown in Figure 5.2

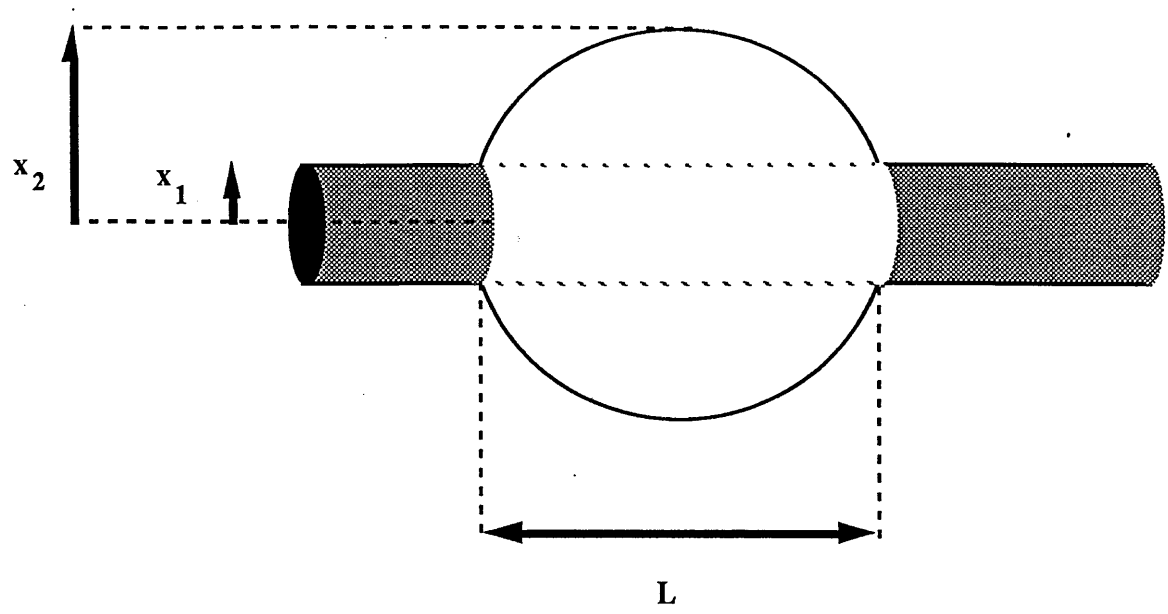


Figure 5.2 Drop shape profile parameters where x_2 is the drop radius, x_1 is the fibre radius and **L** is the droplet length (Carroll 1976).

Carroll has demonstrated that by experimentally measuring these drop shape parameters, the value of θ can be estimated by recourse to tables based on the numerical solution he generated. Yamaki and Katayama (1975) have also solved the Laplace equation for the axi-symmetric drop and have developed an analogous solution to that given by Carroll.

Recently Carroll (1984) has considered the effects of geometrical roughness on the ability of a drop to wet the fibre. He concluded that for a smooth fibre surface the droplet cannot spread along the fibre, even if θ is 0^o. Random micro-roughening or axially symmetric grooving did not lead to complete spreading. However if grooves parallel to the fibre axis were present, then spreading of the droplet would occur if the contact angle was below a critical value.

Brochard (1986) has fully considered the thermodynamics of the spreading of liquids on fibres. The critical spreading coefficient, S_c, for the conformational transition of a droplet to a droplet-sheath structure ("manchon") is defined. A detailed analysis of the "manchon" thickness and the wetting of horizontal and vertical fibres is reported by this author.

5.2.10 Fibre Wettability by the Wetting Force Method

In the Wilhelmy technique for measuring the surface tension, a thin vertical plate is suspended into a liquid interface from a suitable balance. If the plate exhibits a contact angle of θ with the liquid, then as the plate is pulled through the interface, a tare weight is sensed by the balance. This force is equal to the weight of the meniscus at the three phase contact line which is supported by the surface tension of the liquid. Resolving the gravitational and surface tension forces in the direction of the fibre axis allows Equation 5.24 to be derived :

$$F \cos \theta = P \gamma \qquad (5.24)$$

where F = change in the balance measurement

P = perimeter of plate

γ = surface tension of liquid

θ = contact angle of liquid with plate.

This equation describes the first order analysis of the Wilhelmy method, though it does not consider secondary effects such as the buoyancy force correction. It is one of the most useful experimental methods for the determination of the surface tension.

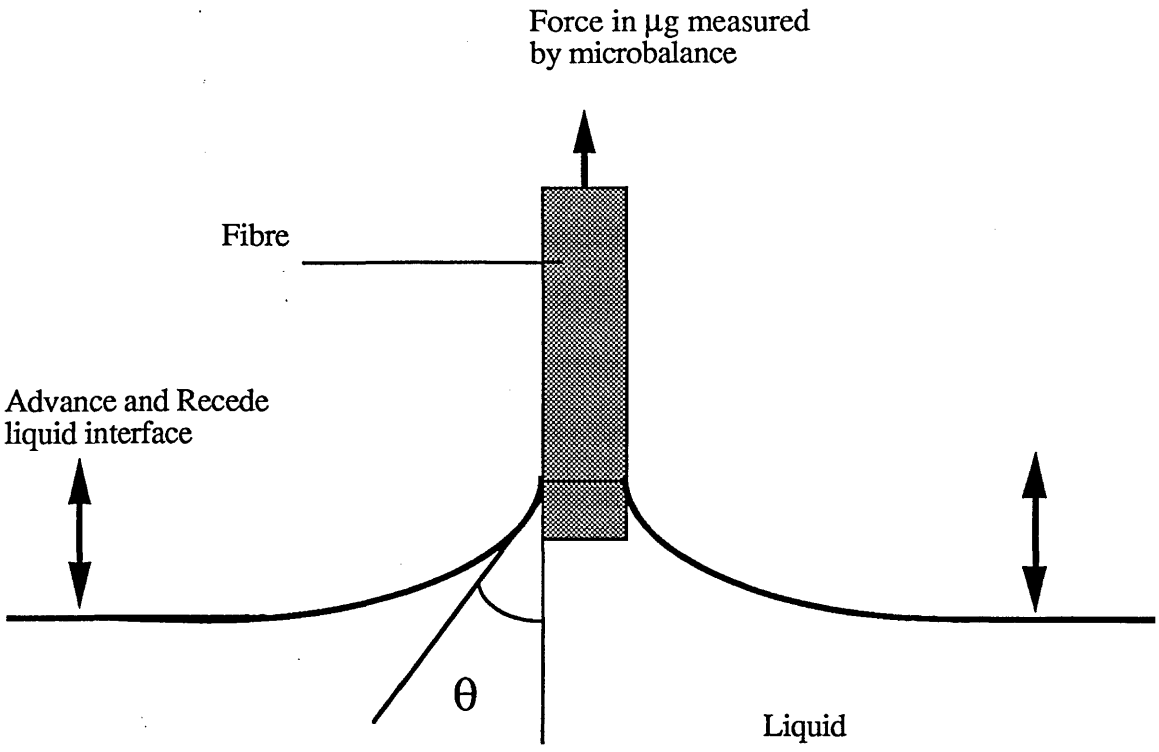


Figure 5.3 Schematic diagram of the apparatus for Wilhelmy plate measurement of surface tension or contact angle.

If the liquid surface tension is known, then the Wilhelmy method allows the contact angle to be determined directly from the wetting force measurement using equation 5.24. The use of the Wilhelmy technique for measuring the contact angles of liquids with thin fibres, was experimentally demonstrated by Collins (1947) and mathematically analysed by Allan (1958). The experimental method involves pushing, and later withdrawing, the fibre through a liquid interface to measure the advancing and receding wetting forces. Using this approach θ_R and θ_A were measured by Bendure (1973) for a number of polyester and polyamide fibres, including surface treated samples. Sell (1972) had at an earlier time adopted the same approach for determining the critical wetting tensions of carbon fibres .

Since then a large number of research workers have used this approach. Kaelble (1974a,b; 1977) has studied carbon fibre wettability in a number of investigations. He has determined the surface chemical conditions necessary for moisture insensitive and

spontaneous fibre wetting to occur. The surface properties of glass fibres have been studied by Wesson and Tarantino (1980). They have determined the wettability behaviour for a number of fibres as function of fibre treatment. Penn and Miller (1980) have considered the existence of an equilibrium contact angle for fibre wetting studies. In the case where the liquid reservoir is stationary, the nature of the contact angle is unclear. It had been suggested that it represented θ. However Penn and Miller were able to show that even when the reservoir was stationary, it was moving due to slow evaporation of the liquid and thus the contact angle sensed was θ_R. The general methodology and the experimental practice for this technique is reported in detail by Miller *et al.* (1983). Hammer and Drzal (1980) have analysed the wettability of a number of graphite fibres and compared these results with those obtained using X-ray photo-electron spectroscopy (XPS). The polar component of the fibre surface energy, γ^p, was determined using a Kaelble analysis of the wettability of a series of liquids. A correlation between the surface oxygen concentration as seen by XPS and γ^p was obtained. Chang *et al.* (1985) have studied the wettability of a number of high modulus fibres such as "Kevlar", glass and graphite with thermoplastic polymers. A special cell was constructed which allowed a polymer reservoir to be heated to 400° C. However problems associated with the high melt viscosity of the thermoplastic polymers resulted in limited success. The wettability of a series of carbon fibres with silicone oil and a low viscosity epoxy liquid was investigated by Lee *et al.* (1987). The carbon fibres examined all exhibited contact angles between 30° and 40° with the liquids and the contact angles were observed to increase by between 5° and 15° after 3 immersion cycles. The authors have argued that this result is consistent with adsorption of the epoxy and the silicone species onto the fibre surface. However, unless the authors are suggesting some type of autophobic adsorption process, which would seem unlikely, their conclusion seems incorrect. Indeed, opposite trends in the contact angle behaviour would be necessary to confirm their hypothesis. Mujin *et al.* (1989) have confirmed the sensitivity of the Wilhelmy wetting balance method for monitoring the modification of carbon fibres by plasmas.

A new, but related, wettability technique has been recently demonstrated by Kamath

et al. (1987). To scan long fibre lengths, a thin liquid film is constrained within a loop and passed up and down a single fibre. The fibre is connected to a micro-balance which measures the wetting force of the liquid film with the fibre. Whilst the technique does not allow θ_R and θ_A to be measured directly, it does measure the fibre wetting force γ_{LV} ($\cos\theta_R$ - $\cos\theta_A$). Examination of long monofilaments (300mm) using this technique has revealed unexpected periodic variations in surface energy or topography of some commercial fibres.

5.2.11 Aramid Fibre Wettability

Allred (1983) has studied the wettability of a number of "Kevlar" fibres following surface modification with ammonia and monomethyl-amine plasmas. Evidence from the associated XPS and dye adsorption studies confirmed the direct amination of the fibre surface by the plasmas. However, the reported wetting force measurements showed no differences between the fibres. The results shown in Table 5.3 indicate only small variations in both the contact angles and the computed surface energies for the fibres as a function of the surface modifications. The introduction of amine functional groups onto the fibre surface would be expected to lead to a decrease in the contact angle of the fibre with water due to the increase in the fibre's surface energy. These wetting results are difficult to rationalise coherently with the other surface characterisation results reported in this work.

The wettability of "Kevlar" fibres has also been reported by Penn and Miller (1980) in a study of contact angle hysteresis on polymeric fibres. Their results are shown below:

"Kevlar" fibre	$W_{(MeI_2)}$	θ_A	γ^d	$W_{(H_2O)}$	θ_A	W^d	W^{a-b}
Untreated	87.6	43	38.0	103.8	64	57.8	46.0
60s NH_3 Plasma	85.2	46	35.9	104.6	64	56.2	48.4
150s CH_3NH_2	87.3	43	37.7	112.9	56	57.6	55.3
150s CH_3NH_2 - HCl wash	88.2	42	38.5	94.4	72	58.2	36.2
150s CH_3NH_2 - HCl wash - Na_2CO_3 wash	81.6	52	33.0	98.1	69	53.9	44.2

Table 5.3 Advancing work of adhesion for untreated and plasma modified aramid monofilaments with water and methylene iodide (Allred 1983).

(H_2O)		(Formamide)		(MeI_2)		(Br-Napthalene)		
θ_A	θ_R	θ_A	θ_R	θ_A	θ_R	θ_A	θ_R	γ^d
63	36	55	24	47	39	18	18	36

Table 5.4 Advancing and receding contact angles for "Kevlar 49" monofilaments. The dispersive component of the surface tension was calculated from the methylene iodide contact angle data (Penn and Miller 1980).

5.2.12 Conclusions

The wetting behaviour of polymeric materials is generally well understood both theoretically and experimentally. Semi-empirical models for the estimating the surface energies of materials currently favour the incorporation of acid-base terms for estimating the energics of specific chemical interactions. Wettability results have been reported for aramid fibres and confirm the relatively high energy nature of the surface.

5.3 EXPERIMENTAL CONTACT ANGLE STUDY

5.3.1 Drop Profile Measurement of Contact Angles

The drop profile method, as described by Carroll (1976), was used in this study to determine the contact angle of liquids with "Kevlar" fibres. Single monofilaments of "Kevlar" were mounted using tweezers onto a simple glass rack. This allowed a 15mm section of fibre to be held in a taut horizontal position, as well as facilitating handling of the sample. By careful manipulation, the fibre was passed through an appropriate liquid-air interface so that a row of liquid droplets formed on the fibre. Figure 5.4 shows some typical droplets of water on a cleaned "Kevlar" fibre as seen under a microscope. Both axi-symmetric and asymmetric droplets are shown in this figure.

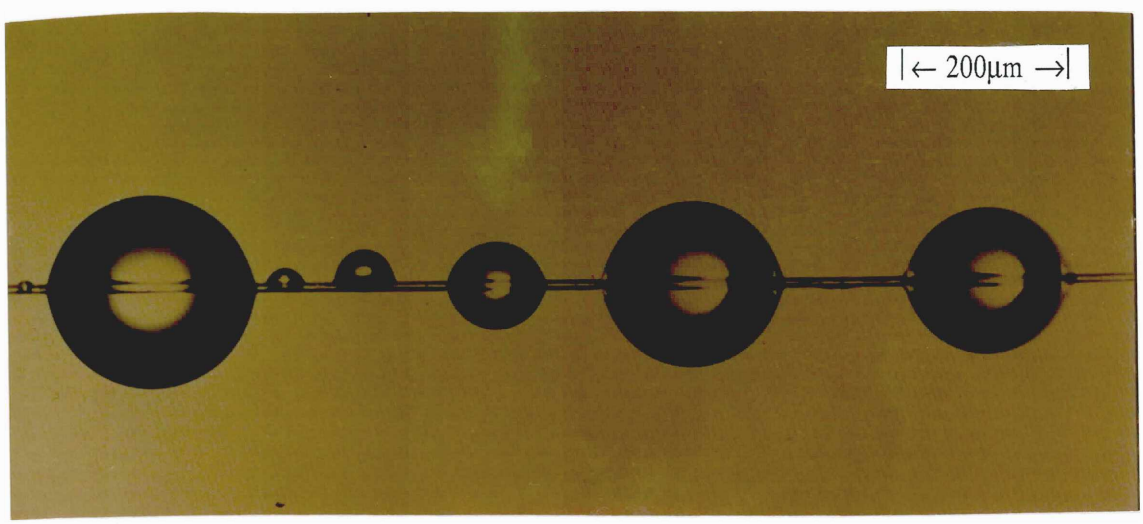


Figure 5.4 Micro-droplets of water on a clean "Kevlar" monofilament.

The droplet shape parameters were measured using a image processing system (Analytical Measuring Systems Optomax V) connected via a video camera to an research microscope (Olympus). The dimensions of the droplet images were measured using a high resolution digital image processor. The parameters x_2/x_1 and L/x_1 where x_2 is the drop radius, x_1 is the fibre radius and **L** is the droplet length were measured and the contact angle was determined using tables provided by Carroll.

The following histogram shows the contact angles measured for water on a clean "Kevlar" fibre :

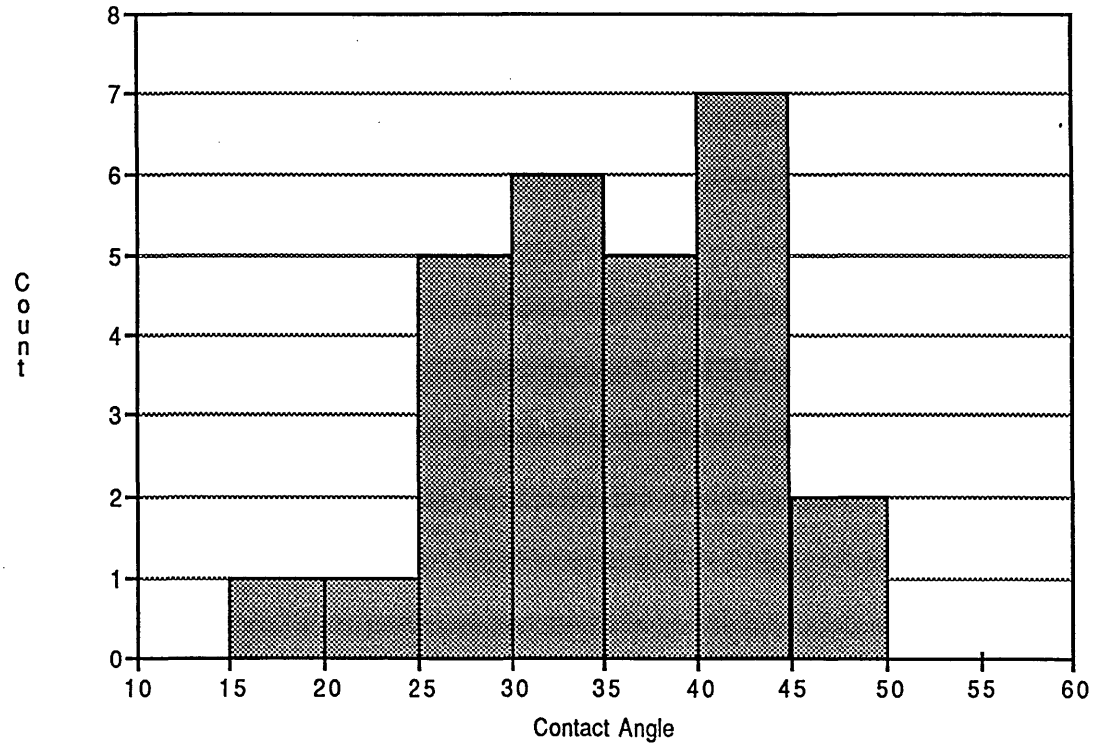


Figure 5.5 A histogram of contact angle versus frequency for measurements using the drop profile method.

The variations in these results are not due to measurement errors. The experimental error in the measurement of the drop shape parameters was estimated to lead to an uncertainty of no greater than 1^{o} in the computed contact angles. A major potential source of the large variations is the assumption that the two dimensional droplet image viewed is representative of a completely axi-symmetric droplet, and not a asymmetric droplet. However this problem would be expected to be a low frequency source of error.

The experimental results shown above highlight a number of other important aspects of this method. The wide variation in the above data is probably mainly due to the uncontrolled nature of the process in which droplets form on the fibre. Indeed the contact angle observed for a particular droplet may be viewed as being formed in a quasi-random fashion. Thus, the distribution of contact angles shown above is the result of the drop formation process in which droplets of any contact angle between θ_A and θ_R may form on the fibre.

The measurement of θ is further complicated by the small diameter of the droplets. Droplets of a diameter 50μm have a high vapour pressure as would be predicted from the Kelvin equation. This prediction was confirmed by the observation that :

(i) droplets on the fibre rapidly evaporated. In the case of water and methylene iodide droplets, evaporation occurred in less than 1 minute in most cases.

(ii) evaporation of the droplets caused a rapid decrease in droplet size. This change in size was accompanied by a receding of the three phase contact line .

The rapid droplet evaporation led to a serious problem in measuring the contact angle immediately after droplet formation. Normal procedures for measuring θ required at least 15 seconds to form the droplets, place them under the microscope, focus the image and freeze the video frame. Within this time significant droplet evaporation had already occurred. Consequently any droplets produced which might have exhibited a contact angle close to that of θ_A, would have already partially evaporated and thus their contact angle would have decreased towards θ_R .

If it is presumed that the experimental data presented above is the result of a quasi-random droplet formation process, then upper and lower bound results should be representative of θ_A and θ_R respectively. Thus 48° and 17° should correspond to θ_A and θ_R with water respectively. Whilst the estimation of 17° for the receding contact angle is close to the results obtained in the next section using the wettability balance (19°), the advancing result is nearly 20° lower. The evaporation problem previously discussed, as well as the fundamental instability of axi-symmetric droplets with contact angles greater than 60°, are reasonable explanations for this observation.

It is thus concluded that the results obtained by the drop-profile method are consistent with those obtained by the wetting balance method. However the difficulties in measuring the advancing contact angles with volatile liquids preclude the use of the drop profile method for determining the fundamental wetting behaviour of fibres. The drop profile method was not used for the major fibre surface characterisation work undertaken in this study.

5.3.2 Wilhelmy Balance Measurement of Contact Angles

A straight piece of "Nichrome" wire of length 50mm was prepared to which a small hook was shaped at one end. A single "Kevlar" monofilament was selected at random from the fabric material using tweezers and carefully attached to the other end of the "Nichrome" wire using cyanoacrylate adhesive. The fibre end was trimmed using sharp scissors to be within 5mm of the wire end. By keeping the length of the free fibre short, a relatively stiff fibre section was produced which facilitated fibre penetration through the liquid surface. These wires were suspended from a simple horizontal rack to confirm that the fibre would adopt a perpendicular position A non-normal angle between the fibre and the liquid-air interface would be expected to lead to errors in the contact angle determination. This potential error would in part result from an underestimation of the fibre's wetting perimeter.

Five fibres were taken from the samples to be examined and mounted as described above. All measurements were conducted at 25°C +/- 2°C at relative humidity of 40% +/- 3%. A Cahn Model DCA 322 wetting balance system was used to measure the wetting

forces of these mono-filaments. The micro-balance system consisted of a Model 120 micro-balance with a sensitivity of 0.1μg and a range of 3g. The liquid-air interface was moved vertically via a variable speed elevator platform. The balance and elevator platform were interfaced to an IBM personal computer which allowed the force to be measured as a function of the vertical position of the stage. The system could be programmed to cycle the liquid interface up and down the fibre between predetermined positions along the fibre length. This facility allowed the reproducibility of the results to be confirmed as well as providing a way of monitoring any time-dependent contact angle phenomena.

The fibre-wire assembly was then carefully placed onto the arm of the micro-balance. When the sample weight was constant to within 1μg, the balance was electronically tared. Experiments commenced by elevating the liquid-air interface until the fibre end just made contact (the strike position) with the liquid-air interface. The liquid was then raised a further 250μm (the start position) so that the three phase contact line was well away from the fibre end. "Kevlar" fibres have been observed to split and fibrillate during cutting and this procedure avoided the three phase contact line making contact with the damaged region of the fibre. Acquisition of the wetting force data began as the stage was moved from the start position. The stage was initially elevated to a position 3mm further along the fibre length at a rate of 20 μm per minute, and then it was returned to the start position at the same rate. This movement of the liquid-air interface 3mm up and 3mm down constituted the wetting cycle. For hexadecane and methylene iodide each experiment consisted of 2 cycles. For water, each experiment consisted of 3 or 4 wetting cycles.

Three liquids were used to characterise the surface energy of the fibres. Water was prepared from a Millipore Q system which has been established in this laboratory to be contaminant free. Methylene iodide was research grade material of greater than 99% purity (Aldrich). Visual inspection of this liquid indicated a transparent liquid with a slight yellow colouration. No signs of substantial decomposition, and the red colouration due to the presence of free iodine, were observed. Hexadecane was research grade (Kock Light) and was used as received. Surface tensions from literature sources, listed in Table 5.1, were used in the wetting force calculations. These values were corrected to the ambient

temperature where necessary using tabulated data.

The wetting forces experiments for each fibre were conducted with each liquid in the order: water, methylene iodide and hexadecane. The fibre was washed with water before the use of a each new wetting liquid and allowed to dry before measurements recommenced.The average advancing and receding wetting force was calculated by fitting a horizontal line to the experimental data.

5.3.3 Wetting Force Measurements

Figure 5.6 shows a sequence of three successive advancing wetting force traces for the water with an "as received" fibre. The highly reproducible nature of these traces confirms the validity of this method for the measurement of wetting forces.

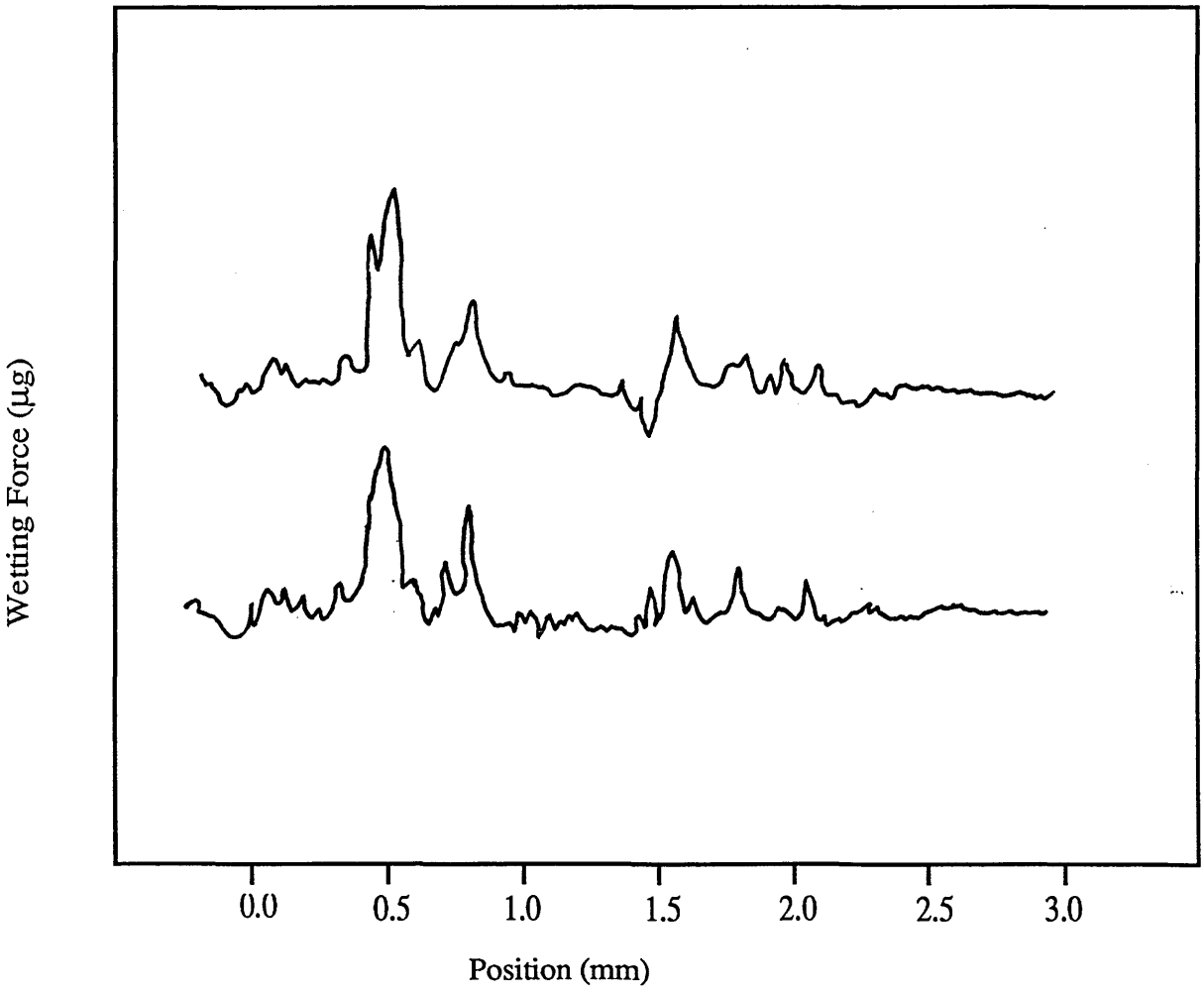


Figure 5.6 Successive wetting force traces for a water-air interface advancing with an "as received" " Kevlar" monofilament.

The fluctuations in the wetting force shown above are typical for surfaces which exhibit large advancing contact angles (>45°). There are two primary explanations for this phenomenon. Firstly, there maybe a real change in θ_A due to variations in the surface energy along the fibre length. The second explanation is a dependence of the wetting force on the surface topography.

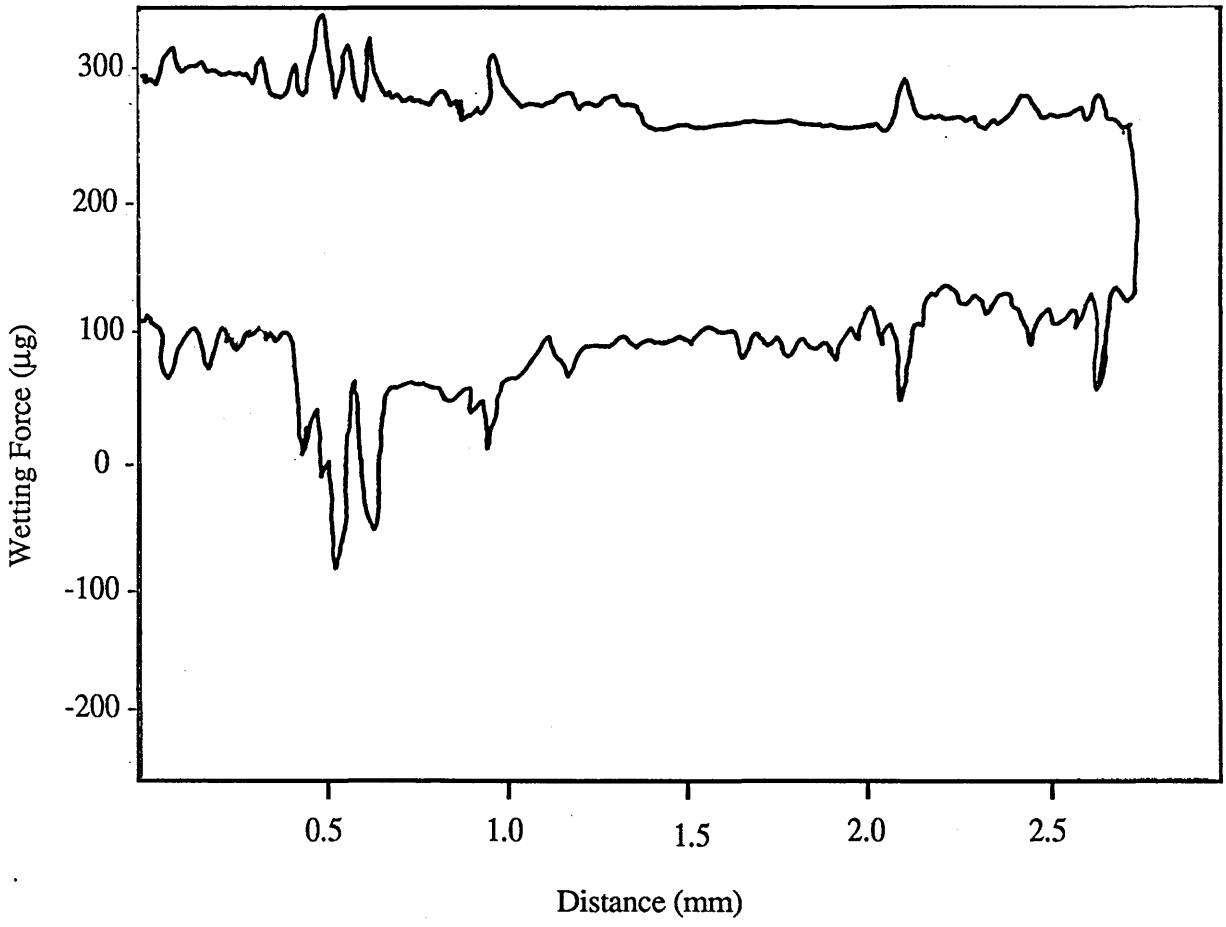


Figure 5.7 Receding (upper) and advancing (lower) wetting traces for water with a diol grafted fibre.

The above wetting traces for diol modified fibres provides information which aids in understanding of some of the factors which produce the large fluctuation in advancing wetting traces, especially with water. The receding contact angle for water with a diol

grafted "Kevlar" fibre is *ca.* 5°. This result represents effectively a case of complete fibre wetting as the wetting force is 99% of the value for the fully wetted fibre. Thus, the receding wetting force trace is effectively a direct measure of the fibre diameter. The upper trace of Figure 5.7 is such a plot. In the part of the fibre wetting trace between 0.0mm and 2.0 mm a large number of sporadic substantial diameter variations, in the region of 10-20%, are inferred. These variations are likely to be due to residual materials deposited on the fibre surface resulting from the heterogeneous surface graft reaction. However the important point to note in Figure 5.7 is the relationship between peaks in the receding traces and the troughs in the advancing trace. Indeed. there is virtually a one to one correspondence between these features. As well as being of specific theoretical interest, an understanding of this behaviour is necessary so that appropriate conditions may be established for the interpretation of this type of experimental wetting trace.

Kremnitzer (1978) has studied the wetting behaviour of alcohol/water mixtures on polyethylene terephthalate fibres. By considering the surface to be an simple idealised rough surface, he concluded that the variation in the advancing wetting force, Δw, was directly related to the diameter fluctuations Δc and the surface tension γ :

$$\Delta w = \Delta c \, . \, \gamma \qquad (5.24)$$

but was independent of the contact angle. Kremnitzer's experimental data, shown in Figure 5.9, suggests that whilst a linear relationship between Δw and Δc is apparent, the line seems to extrapolate to a finite value of γ for $\Delta w = 0$, rather than $\gamma = 0$. This extrapolation implies that his analysis is incorrect.

Figure 5.8 shows in profile a model asperity on a fibre surface where the asperity height is Δh and is inclined at an angle α to the fibre surface.

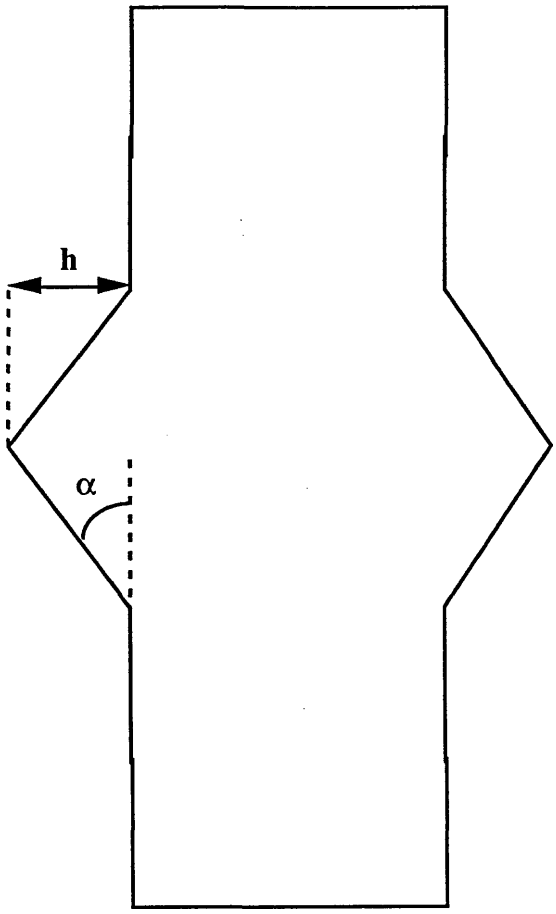


Figure 5.8 A model asperity on a fibre shown in profile with an angle, α, and height, Δh.

From simple geometrical considerations, the wetting force **W** will depend upon the effective contact angle, as modified by α, as well as the length of the three phase contact line at the liquid-air-fibre interface. A maximum and minimum wetting force will thus be defined :

$$W_{max} = \gamma \pi d (1 + 2\Delta h / d) \cos (\theta - \alpha) \qquad (5.25)$$

$$W_{min} = \gamma \pi d (1 + 2\Delta h / d) \cos (\theta + \alpha) \qquad (5.26)$$

Simplification leads to :

$$\Delta w = W_{max} - W_{min} = \gamma \pi d (1 + 2\Delta h / d) (\cos (\theta - \alpha) - \cos (\theta + \alpha)) \quad (5.27)$$

$$\equiv \Delta w = 2 \gamma \pi (d + 2\Delta h) \sin (\theta) \sin (\alpha) \quad (5.28)$$

This analysis conflicts with the work of Kremnitzer (1978) since it implies that the wetting force fluctuations, Δw, are directly dependent on the contact angle, θ, as well as the local topographical angle, α. Below are shown the experimental results for Δw obtained by Kremnitzer for a specific asperity on a PET fibre. Δw was obtained for a series of alcohol/water solutions as a function of the solution's surface tension. This graph was produced by Kremnitzer to rationalise Equation 5.24. Unfortunately the actual θ data is not reported in this work so that it is not possible specifically to fit Equation 5.26 to this data.

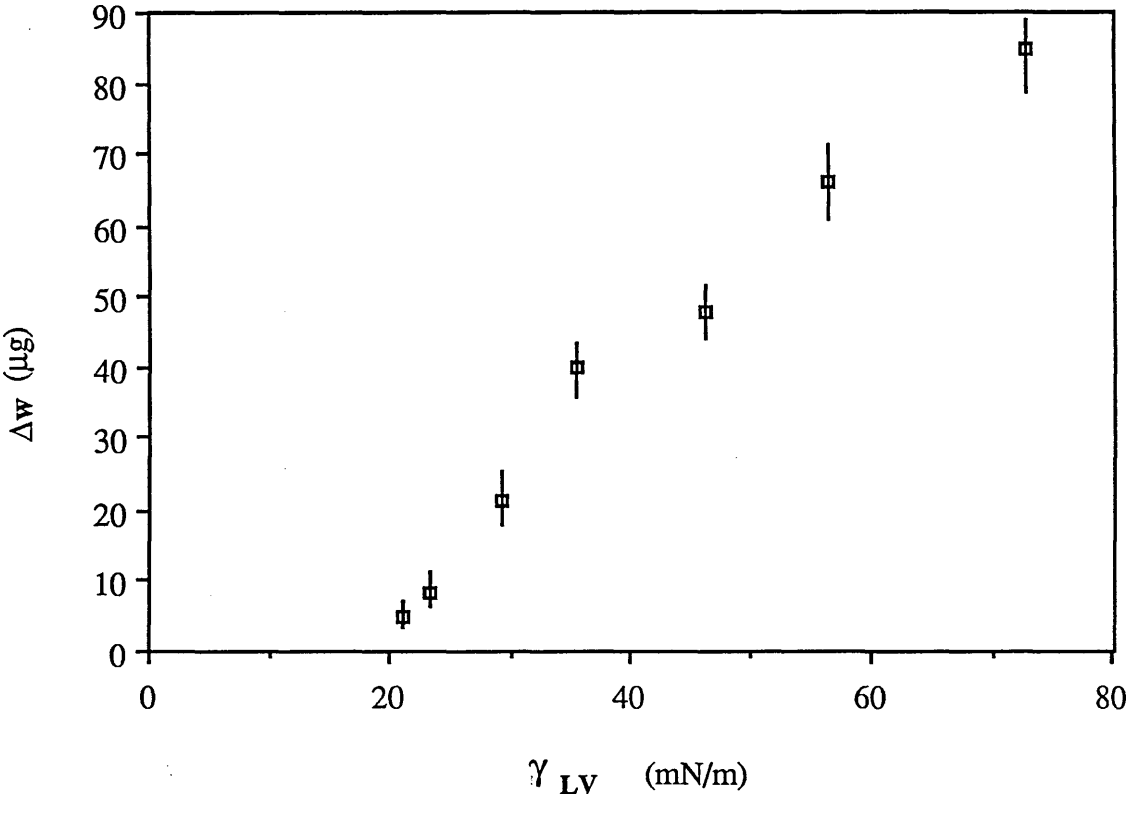


Figure 5.9 Wetting force fluctuations as a function of the liquid surface tension for polyethylene terephthalate fibres (Kremnitzer 1978).

However, it is possible to make a number of qualitative deductions. The behaviour of Δw will be dependent on γ and $\sin(\theta)$, since $\sin(\alpha)$, **d** and **h** are constant in the case described by Figure 5.8. Thus $\Delta w \rightarrow 0$ as the product $\sin(\theta)\,\gamma \rightarrow 0$. Since $\sin(\theta) \rightarrow 0$ as $\gamma \rightarrow \gamma_c$. For polyethylene terephthalate γ_c equals 27 mN/m as estimated using alcohol-water mixtures by Dann (1970). Thus it is deduced that a graph of Δw versus γ graph should intercept the γ axis at the point $\gamma = \gamma_c$. An extrapolated intercept of about 20mN/m is seen in Figure 5.9 which generally agrees with our prediction of 27mN/m. In conclusion, Equation 5.28 appears to be a more accurate representation of the behaviour of Δw for advancing liquids than Equation 5.24.

So it is now possible to account for the large fluctuations that were observed in the advancing wetting traces with water. These are concluded to be primarily associated with the localised effects of surface topography and do not necessarily reflect wide-ranging changes in the fundamental surface energetics of the fibre.

5.3.4 Contact Angle Data

The average contact angle results, obtained using the Wilhelmy balance, are shown below in Table 5.4. The uncertainty in these results is generally +/-2° for the non grafted fibres and +/-3° for the chemically grafted fibres with water. For methylene iodide the errors were +/-1° and +/-2° respectively.

Hexadecane has a surface tension lower than virtually all organic polymers and thus would be expected to wet completely the surface of most organic polymers. This prediction was observed to be true for all the "Kevlar" fibres examined in this study. For all the fibres studied, hexadecane gave force traces with a constant wetting force of 100μg +/- 2μg. Consequently results for the individual fibres are not reported. Figure 5.10 shows a typical trace obtained with hexadecane. The constant wetting force for both advancing and receding measurements is a common characteristic for fibres which are completely wetted. In some cases, small variations in the wetting trace consistent with irregularities in fibre diameter, especially in the case of the chemically grafted fibres, were observed. The

sections of fibre which exhibited these diameter variations were not included in any subsequent analysis. The wetting force measurements for hexadecane allow the fibre diameter to be accurately measured using Equation 5.24. A wetting force of 100μg equates to a fibre diameter of 12.0 μm. This measurement was subsequently used in Equation 5.24 so that the contact angles of water and methylene iodide could be determined .

The wetting force traces were used to determine the contact angles by fitting a horizontal line to the wetting force data. Regions which involved substantial force variation (ie >25μg for water and >15μg for methylene iodide) were excluded from the fitted data. These fluctuations were considered to be due to the anomalous effects of surface roughness/ fibre diameter variations as described in section 5.3.3.

For most of the samples the wetting force measurements were relatively constant as a function of the wetting cycle number. However, three of the fibre samples did exhibit consistent variations with the immersion cycle number. The diol and epoxy grafted, as well as the tin hydrolsol modified samples, exhibited significant variations in the advancing wetting force measurements between the first and subsequent cycles.

In the case of the tin hydrolsol modified fibres, the advancing contact angles decreased by 30° during the first advancing measurement cycle. This observation is consistent with that of Briscoe *et al.* (1989) who observed that a tin hydrolsol which adsorbed onto polyethylene underwent a hydrolysis reaction. Surfaces which initially exhibited hydrophobic contact angles with water of over 40° changed, soon after a short immersion time with water, to exhibit hydrophillic contact angles of less than 10°. A time dependent hydrolysis reaction with the tin particles was thought to be occurring. The diol and epoxy grafted fibres exhibited an increase in contact angle of about 10° between the first and subsequent advancing wetting force measurements with water. Both fibres exhibited receding contact angles close to zero and thus the advancing liquid front could be expected to have passed over a surface which was already wetted from the previous receding measurement. The possibility of some type of kinetic chemical process occurring in these later wetting measurements led to the assumption that the initial wetting force traces were representative of the true equilibrium advancing contact angle.

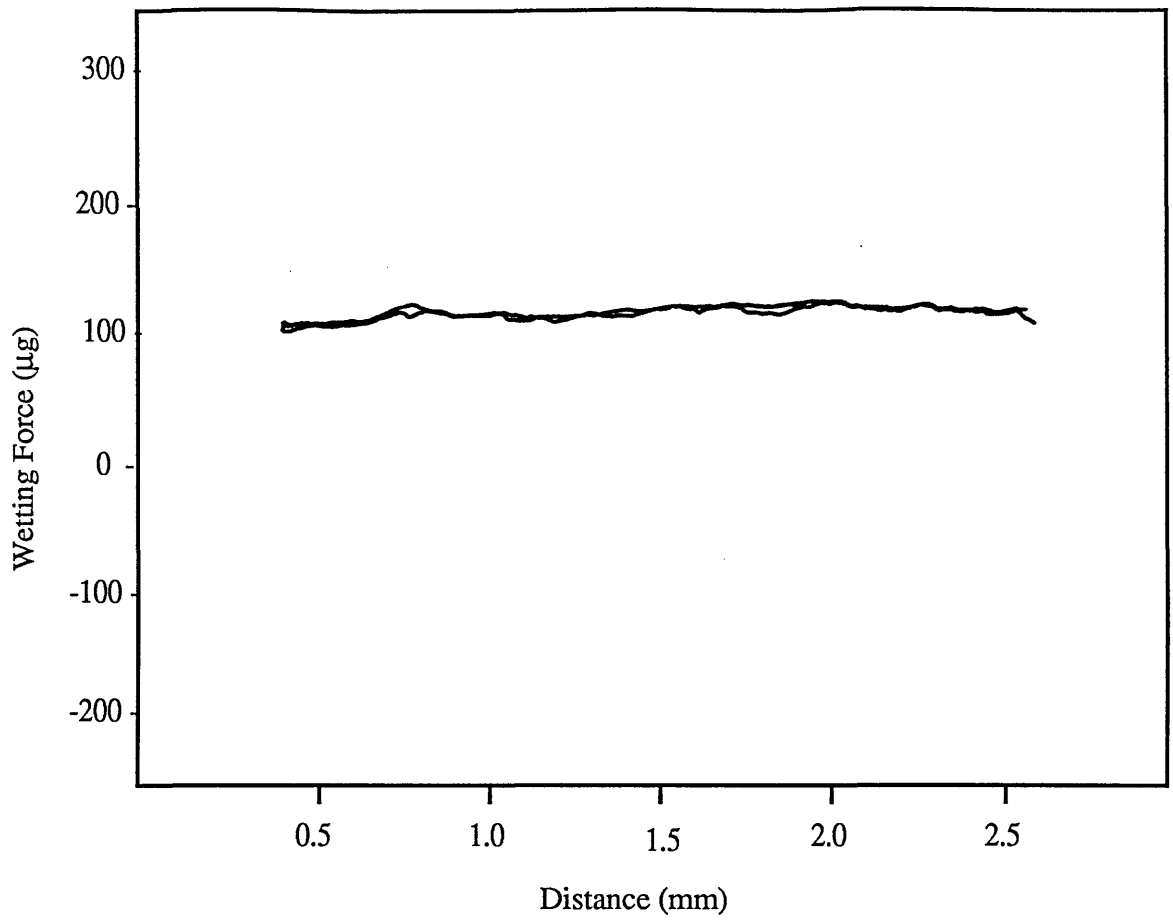


Figure 5.10 Wetting (advancing and receding) traces for hexadecane with a "Kevlar" fibre.

The contact angle results shown below are in good agreement with those literature values quoted in section 5.6. The advancing contact angle results, with both water and methylene iodide, from Allred's (1983) work on untreated fibres are in close agreement with those reported in this study. The wetting results of Penn and Miller (1980) reported in Table 5.4 also show good general agreement for both the water and methylene iodide cases, as well for the advancing and receding contact angles.

"Kevlar 49" Fibres	H_2O		Methylene Iodide	
	θ_A	θ_R	θ_A	θ_R
"As received"	71	35	45	43
Soxhlet cleaned	65	19	38	35
Octane graft	92	70	59	54
Trimethylsilane graft	77	56	45*	
Diol graft	55	<5	39	36
Nitrobenzene graft	63	15	39	33
Epoxy graft	54	<5	52	43
Tin hydrosol	<10		44	39

* Estimation

Table 5.5 Advancing and receding contact angles for "Kevlar 49" fibres.

5.3.5 Fibre Surface Energetics

As was previously reviewed, it has been common practice to use a large number of liquids in the surface energies analysis of polymer substrates. This approach is typified by the original work of Zisman which required the use of a wide range of liquids with different surface tensions so that the critical surface tension could to be estimated. However the measurement of contact angles on fine monofilaments involves a substantially greater degree of experimental uncertainty. These uncertainties are due to the very small forces which are measured and the relatively large force fluctuations which occur due to the inherent fibre roughness .

Consequently a simple set of experimental test liquids has been used in this study. The three liquids chosen for use in this study provide the following types of information:

hexadecane	-	fibre diameter
methylene iodide	-	dispersive surface chemical interactions
water	-	specific surface chemical interactions (acid-base/polar)

Methylene iodide has been extensively used in wetting studies as a means of deducing information about dispersive interfacial interactions. The value of this deduction was demonstrated originally by Fowkes (1964) who studied the dispersive interactions between mercury and liquid hydrocarbons. The results in Table 5.1 clearly show that the large surface tension of water is primarily due to the significant amount of internal hydrogen bonding interactions which are reflected in the value of 50.8 mN/m for γ^p. These specific chemical interactions would also be expected to be an important factor in the thermodynamics in many multicomponent chemical systems involving water. Indeed the strong solvation power of water and its ability to adsorb irreversibly on many solid substrates are well documented. Thus water is an ideal liquid for deducing information about acid-base interactions via wettability measurements.

"Kevlar 49" Fibres	γ^d (mN/m)	γ^p (mN/m)	W^{a-b} (mN/m)	γ (mN/m)
"As received"	36.2	7.9	39.6	44.1
Soxhlet cleaned	39.6	9.5	43.4	49.1
Octane graft	28.5	1.8	19.2	30.2
Trimethylsilane graft	36.2	5.0	31.8	41.2
Diol graft	39.2	14.4	53.5	53.6
Nitrobenzene graft	39.3	10.5	46.0	49.8
Epoxy graft	32.4	18.5	61.0	50.9
Tin hydrosol	36.7	36.7	85.4	73.4
PDMS*				20.0
PEG *				37.0
Epoxy*				44.0

* taken from the literature (Wu 1982).

Table 5.6 Surface energetics of modified "Kevlar 49" fibres.

The "as received" and the cleaned "Kevlar" fibres show some small variations in both the W^{a-b} and γ^d values. As would be expected, these results support the prediction that the cleaned fibres should exhibit higher surface energies than the contaminated fibres. However, the differences are quite small and are quite close to the experimental errors. Both of these estimates of W^{a-b} and γ^d agree with the corresponding results of Penn and Miller (1980), as well as Allred (1983) as shown in Tables 5.3 and 5.4 respectively.

The γ^d component of the surface energy of the modified fibres shows a number of small variations in surface energy. Most values are in the range of 35-40 mN/m which would be normally expected for polymeric materials. The lowest γ^d result is 28.5 mN/m for the octane grafted fibre. This value is substantially lower than all the other results and is consistent with an alkylated polymer surface. It clearly indicates the successful nature of the octane graft reaction. The epoxy grafted fibres also exhibited a lower result for γ^d than expected. The measured value of 32.4 mN/m for γ^d can be explained on the basis of the graft reaction employed. If both epoxy functional groups on the reactant species were to successfully graft onto the fibre surface, then the central hydrophobic portion of the reactant would be left exposed on the fibre surface. Such a surface could be expected to exhibit a value of 32.4 mN/m for γ^d.

The W^{a-b} results are an important indicator of the extent of interfacial acid-base interaction. The value of 43.4 mN/m for W^{a-b} with the clean "Kevlar" fibres serves as a useful reference point for comparison with the other results obtained in this study. The substantial magnitude of this result for the interaction between water and the polyamide surface could be expected since both water and PPTA are amphoteric species.

Octane grafted fibres exhibited a substantially lower result of 19.2 mN/m for W^{a-b} relative to the clean "Kevlar" fibres. The existence of a finite W^{a-b} for this sample indicates that the surface is not entirely covered by the alkyl grafted groups. It would appear that the water is sensing both the non-grafted and the grafted regions of the fibre. Indeed, the numerical results suggest that just over approximately half the surface has been covered by

grafted species. In a similar fashion the results for the trimethyl-silane grafted fibres showed a significant decrease of 11.6 mN/m for W^{a-b} compared to the cleaned sample. On the basis of this result one might predict that 27% of the fibre surface has been covered by alkyl groups.

Both the diol grafted and the epoxy grafted fibres exhibited significant increases in W^{a-b} of 10.1 and 17.6mN/m with respect to the clean sample. The diol and epoxy functionalities on the fibre surface would be expected to lead to an increase in the specific acid-base interactions. Therefore, these results directly support the success of both two graft reactions.

Both the γ^d and W^{a-b} values measured for the nitrobenzene modified fibres were very similar to those obtained for the cleaned sample. Thus it is not possible to confirm the success of this graft reaction.

Tin hydrosol coated fibres exhibited a substantially larger result for W^{a-b} relative to the clean "Kevlar" fibres. The result of 85.4 mN/m for W^{a-b} was the largest W^{a-b} value measured in this study between water and "Kevlar" fibres. The large magnitude of this result indicates that very strong interfacial interactions are occurring between the liquid and the fibre surface. The adsorbed hydrosol species would be expected to be essentially a tin oxide/hydroxide complex. These results suggest that strongly interacting groups, such as hydroxides, are present on the fibre surface. Therefore it is probable that significant amounts of the tin hydrosol species have adsorbed onto the fibre surface.

5.3.6 Conclusions

The wetting behaviour of aramid fibres has been studied using the Wilhelmy balance and Carrol drop profile methods. The Wilhelmy balance has been shown to be the best method for determining the wettability of monofilaments with a small diameter. The advancing wetting force traces for water with "Kevlar" fibres were concluded to be particularly sensitive to the fibre surface topography, as well as the fibre surface chemistry.

The wetting characteristics of a range of "Kevlar" fibres with water, methylene iodide hexadecane have been reported using this technique. The dispersive component of the fibre

surface energy and the acid-base component of the work of adhesion with water are reported for range of surface modified "Kevlar" fibres.

The contact angle and surface energy results measured for the clean and the "as received" "Kevlar" fibres were in good agreement with other work reported by other authors. The changes in the contact angle and the works of adhesions for water, and methylene iodide, with the modified fibres confirm the success of the diol, octane, trimethyl-silane and epoxy graft reactions. The adsorption of tin hydrosol species on "Kevlar" fibre surfaces was also deduced. The diol, epoxy and tin hydrosol treated fibres exhibited significant increases in their acid-base work of adhesion with water.

CHAPTER 6

INVERSE GAS PHASE CHROMATOGRAPHY

6.1 INTRODUCTION

This Chapter consists of two main sections. The first section commences with a discussion of the classical use of solid-gas adsorption as a method for the surface characterisation of powders. The gas chromatographic adsorption process is then introduced and its relationship to conventional solid-gas adsorption measurements is developed. The use of gas chromatographic techniques for measuring adsorption of gases and vapours onto polymeric substrates with low surface is reviewed. The literature for both linear and non-linear adsorption studies on polymers, as well as adsorption studies onto aramid fibres, is specifically reviewed. The second section of this Chapter describes an experimental study in which a number of different "Kevlar" fibres have been surface characterised using a gas chromatographic adsorption method.

6.2 SURFACE CHARACTERISATION USING GASEOUS PROBES

6.2.1 Gas Solid Interactions

The surface properties of powders have been traditionally studied by gas adsorption techniques. These techniques are still in common use and generally involve the physical adsorption of inert gases onto the surface of the powder. Such experiments provide important information about the surface chemistry of the substrate via the measurement of the energetics and kinetics of adsorption. Traditionally, gas adsorption experiments have involved studying the adsorption of gases, such as nitrogen, onto powders with surface areas in the range of 10 to 1000 m^2/g. By determining the amount of solute or gas adsorbed

as a function of solute concentration or gas pressure the adsorption isotherm is obtained. The isotherm is experimentally measured by following the changes in adsorbing gas pressure and the change in weight of the sample or the volume of gas adsorbed. Normal experimental apparatus would involve the use of vacuum systems incorporating pressure transducers, gas burettes or micro-balances. Adsorption isotherms allow the adsorbent surface area, the porosity and the thermodynamics and kinetics of adsorption to be measured (Gregg and Sing 1967). Most fibrous samples have surface areas which are less than $1m^2/g$ and the conventional adsorption techniques described above are not normally sensitive enough to measure the small mass or volume of the adsorbed species.

One of the most sensitive methods for studying the adsorption behaviour of low surface area samples is based on gas chromatography. Such techniques permit solid-gas adsorption to be studied for low surface area materials for a wide range of temperatures, pressures and surface areas, as well as for both chemisorbed and physisorbed species. The successful use of this technique has been pioneered by Russian research groups and their work on the chemical adsorption behaviour of catalyst surfaces has been reviewed in detail by Kiselev and Yashin (1969). The general use of gas chromatographic techniques for studying adsorption and surface thermodynamic properties is reviewed in significant depth and detail by Condor and Young (1979).

6.2.2 Basic Gas Chromatography

Chromatography is probably the most important analytical technique for measuring the chemical composition of organic mixtures. As a quantitative technique for measuring composition and concentrations, it is the technique of first choice. The fundamental phenomenon which results in the success of chromatographic methods is the adsorption process between the solutes and the stationary phase. The ability of the stationary phase to discriminate, and thus partition, the various solute species, is a direct result of differences in the molecular affinity between the stationary phase and the various solute species.

The gas chromatographic method involves the flow of an inert carrier gas, at a

constant rate, through a long column filled with a stationary solid phase. Various solute vapours are mixed with the carrier gas prior to it passing through the packed column. As the gas mixture passes through the column the solute vapours migrate along the packed column at a rate which is in part a fundamental characteristic of the adsorptive partitioning of the solute between the gas phase and the solid surface of the column packing. Different solute vapours thus travel with differing velocities along the column resulting in the separation of the vapour components. The emergence of the solute peaks from the column is sensed via a detector which is sensitive to the concentration of the solute vapours present in the carrier gas. The time versus concentration profile measured by the detector is the chromatogram. The chromatogram will contain, in principle, quantitative information on the relative amounts of the vapours detected based on the relative sizes of the solute peaks detected. Calibration is necessary to determine the compounds and their concentrations.

Analytical gas chromatography involves the use of standard commercial column packings to achieve a separation of peaks for an unknown vapour mixture. Commercial packings are optimised and calibrated for the separation of various classes of anticipated adsorbates eg.alkanes, esters, amines. The technique known as inverse gas chromatography (IGC) involves the study of an unknown packing with pure vapours whose generic adsorption properties are comparatively well understood.

IGC offers a number of advantages over conventional adsorption techniques. These are :

(i) the sample does not need to be evacuated.

(ii) temperature effects are easy to study.

(iii) the possibility of rapid measurements.

(iv) accurate measurements at low surface concentrations.

(v) the ability to study both physisorption and chemisorption.

6.2.3 The Gas Chromatographic Adsorption Process

An understanding of the chromatographic process is best accomplished by examining

a typical chromatogram. The nomenclature of Condor and Young (1979) is used here to describe this process. Figure 6.1 shows a typical chromatogram for the elution of methane, hexane, heptane and octane vapours from a GC column packed with "Kevlar" fibres at 40°C.

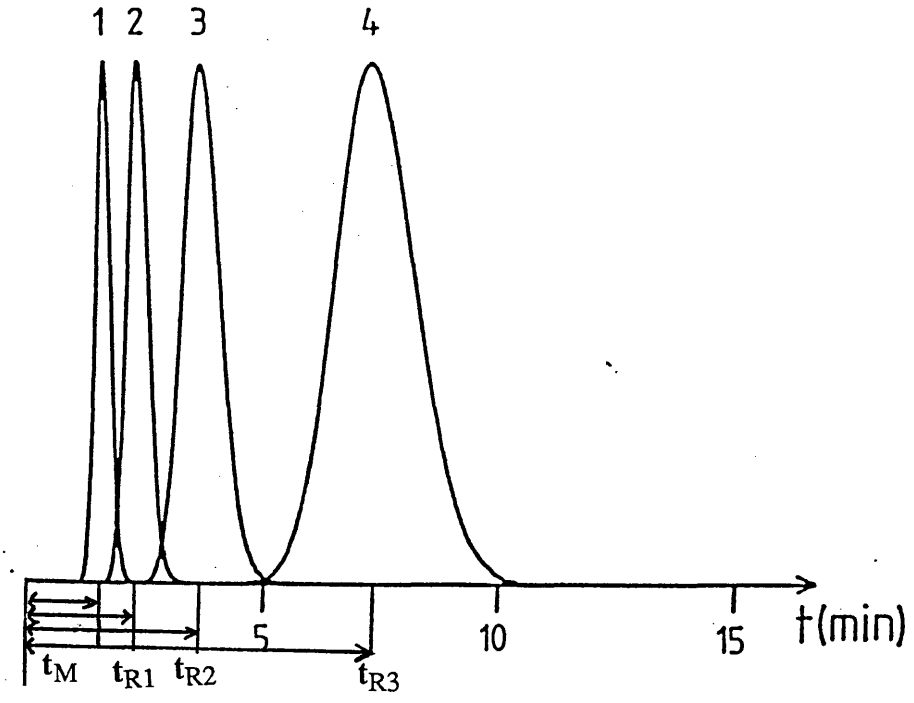


Figure 6.1 Chromatogram for methane, hexane, heptane and octane vapours. t_M represents the elution of the non-adsorbed species methane, whilst t_{R1}, t_{R2}, t_{R3} represents the time for the elution of adsorbed species hexane, heptane and octane respectively.

The time t_M represents the time required for the solute molecule to pass through the column without interacting with the adsorbent surface. Multiplying t_M by the carrier gas flow rate **F**, defines the dead volume V_M.

$$V_M = t_M F \qquad (6.1)$$

Similarly the volume associated with retention by adsorption (including V_M) can be defined

for a particular species as:

$$V_R = t_R F \tag{6.2}$$

The adjusted retention volume V_R', is a function of the adsorbate-adsorbent interaction and is defined by :

$$V_R' = V_R - V_M \tag{6.3}$$

For the carrier gas to flow through the column, there must exist a pressure gradient between the entrance of the column and the column exit. Consequently the velocity of a solute peak is less at the column entrance, where the pressure is greater, than at the column exit where the velocity is a maximum due to the conservation of mass. James and Martin (1952) have analysed this problem and have derived an analytical expression for the gas compressibility correction factor, **j**, which allows the average gas velocity in the column to be estimated:

$$j = \frac{3}{2} \frac{(p_i / p_o)^2 - 1}{(p_i / p_o)^3 - 1} \tag{6.4}$$

where p_i = column inlet pressure

p_o = column outlet pressure

The adjusted retention volume V_R' is now corrected to account for the pressure gradient, and defines the net retention volume V_N:

$$V_N = V_R' j \tag{6.5}$$

The net retention volume, or the specific retention volume, is the quantity from which all

the equilibrium thermodynamic properties are calculated. The specific retention volume V_g is referenced to 0 °C and is defined on a per unit mass basis via Equation 6.6 :

$$V_g = \frac{273\ V_N}{W_s\ T} \qquad (6.6)$$

where W_s = mass of stationary phase

T = column temperature

6.2.4 Chromatographic Peaks and the Adsorption Isotherm

The net retention volume and the slope of the adsorption isotherm are related by Equation 6.7, where the solute concentration is sufficiently low such that the isotherm is linear in shape. This region is known as the "infinite dilution" concentration region.

$$V_N = K_S\ A \qquad (6.7)$$

where K_S = slope of the isotherm at infinite dilution

A = surface area of sample

K_S is the partition, or distribution, coefficient of the solute between the mobile phase and the stationary phase where **c** is the solute concentration in the gas phase and **q** is the solute concentration in the stationary phase :

$$K_S = q/c \qquad (6.8)$$

The relationship between 6.7 and 6.8 is briefly described by Condor and Young (1979).

For higher solute concentrations where the adsorption isotherm is no longer linear, a more general expression is applicable:

$$V_N = A(1 - j y_o) \frac{dq}{dc} \qquad (6.9)$$

where dq/dc = slope of the isotherm at concentration **c**.

y_o = mole fraction of solute in the gas phase at the column outlet.

This region of higher concentrations is described as the " finite concentration" region. From Equation 6.9 the relationships between the chromatographic peak shapes and the slope of the isotherms are illustrated. Figure 6.2 shows the basic adsorption isotherm shapes and the associated chromatographic peak shapes as would be predicted on the basis of Equation 6.9 . Whilst isotherm shape is the primary cause of the peak skewness, other effects such as the non-ideality of the vapour, the "sorption effect " and other kinetic factors can also be important (Condor and Young 1979) .

Adsorption isotherms have been computed from chromatographic data in the finite concentration region of the isotherm using a number of methods of analysis. The two primary approaches involve obtaining isotherms via modified experiments or analysis respectively:

(i) Use of solute/carrier gas mixtures with (a) step function changes in solute concentration or (b) perturbation of constant solute concentration.

(ii) mathematical deconvolution of asymmetric peaks obtained with various large solute injections.

These methods and a number of other techniques for obtaining adsorption isotherms, have been reviewed in detail by Condor and Young (1979) and are illustrated by the work of Kiselev and Yashin (1969). The most popular technique for determining the adsorption isotherm using IGC is the "elution of a characteristic point" method. It is the major method described within case (b) above. This technique simply involves obtaining a series of

chromatograms via a series of separate injections with increasing amounts of a solute, typically from 0.1 μl to 20 μl of liquid. From the set of asymmetrical peaks that are obtained a common envelope or boundary in the chromatographic peaks is observed, see Figure 6.3. This curve can then be deconvoluted to produce the adsorption isotherm using Equation 6.9.

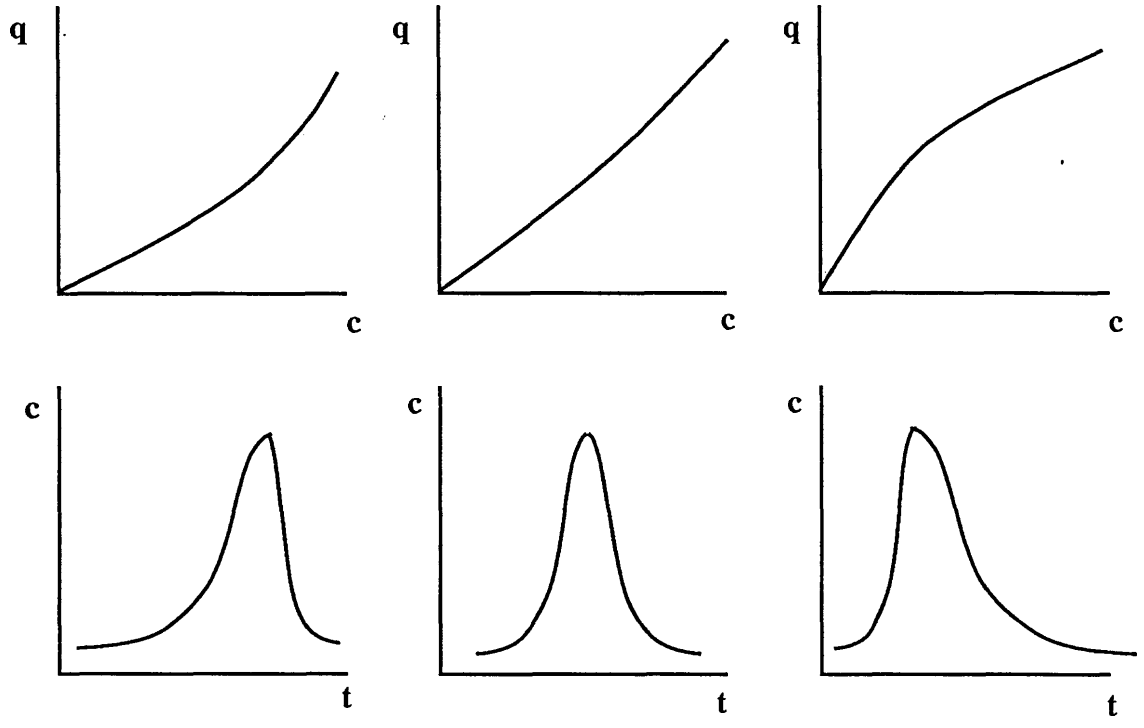


Figure 6.2 The relationship between the isotherm shape and the chromatographic peak-shape at infinite dilution concentrations. Case (a) represents the case of concave BET type isotherm with a skewed Gaussian chromatographic peak (S< 0), case(b) represents an essentially linear isotherm with Gaussian chromatographic peak and case(c) represents a convex Langmuirian shaped isotherm with skewed Gaussian peak (S>0) (Condor and Young, 1979).

6.2.5 Non-Linear Adsorption Studies on Polymers using IGC

The earliest reported studies of polymeric surfaces using IGC were the work of Chabert and Edel (1958), and Edel and Chabert (1969). They studied the adsorption of water and hydrocarbons onto Nylon 6,6 and polypropylene fibres at high solute concentrations.Gray and his coworkers have undertaken a number of major studies of polymer-solute adsorption at finite concentrations. Adsorption isotherms studies on cellulose fibres have been reported by Mohlin and Gray (1974). Their work is now discussed in detail as it is an example of sound IGC experimental technique.

The elution of a characteristic point technique (ECP) was used to determine the isotherms for octane, decane, toluene, butanone, butanol and dioxane at 25°C by Mohlin and Gray (1974). No bulk sorption effects were noted and the chromatograms gave good overlapping boundaries satisfying the conditions for the use of this technique. A typical series of these peaks is shown in Figure 6.3 .

The shift in the superimposed boundaries shown below corresponds to an inflection point in the adsorption isotherm. This point indicates the amount of solute adsorbed is equivalent to a monolayer of coverage. To determine the explicit adsorption isotherm the amount of solute adsorbed, **a**, must be determined as a function of the solute vapour pressure or concentration,**c**, for a column mass, m, as defined in Equation 6.10 :

$$a = \frac{1}{m} \int_0^c V_N \, dc \qquad (6.10)$$

Using Equation 6.10, integration of the region between the common superimposable boundary and the dead volume line in Figure 6.3 along the y direction yields the isotherm (albeit in the form of **c** versus **a**). The successful use of this method was confirmed by a good fit of the adsorption data to the BET multilayer adsorption model. All adsorbates

gave consistent surface area for the cellulose sample. The isosteric heats of adsorption were also reported for butanol, decane and dioxane via isotherm obtained at different temperatures. The heats were slightly above the heats of liquefaction for butanol and decane, for all surface coverages. For dioxane the heat of adsorption increased with decreasing surface coverage, and were 20kJ/mol higher than the heat of liquefaction. The authors suggested that specific interactions accounted for this result and these would probably result from the acid (cellulose) interactions with the base (dioxane). This same experimental approach was reported in earlier work (Gray and Guillet, 1972) which describes the measurement of adsorption isotherms for decane and hexanol on polystyrene and polymethyl methacrylate surfaces. Their later work showed little variation in the data analysis, although the experimental measurements were superior (Mohlin and Gray 1974).

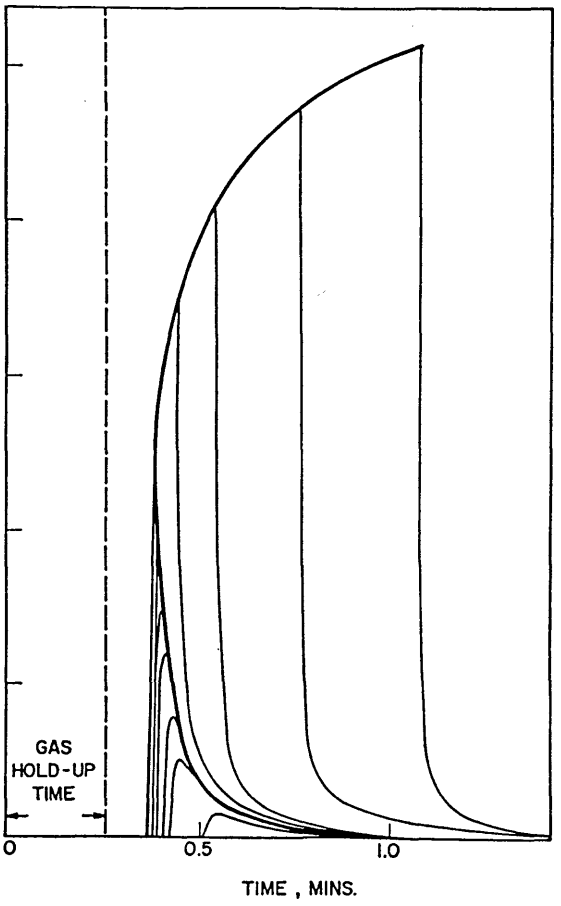


Figure 6.3 Overlaid chromatograms for dioxane on cellulose fibres at 25.7°C obtained using ECP. Note the movement in the superimposed boundaries from the rear chromatogram boundary to the front boundary (Mohlin and Gray 1974).

Using this same approach Dorris and Gray (1979) have studied cellulose fibres and pulped fibres. Recognising the likelihood of vapour condensation due to the very high values of the relative vapour pressure p/p_o these authors used, they limited their studies to values for p/p_o of less than 0.8. The isotherms were extrapolated to $p/p_o = 1.0$ and then via a fitted polynomial were integrated to allow π_e to be determined from Equation 5.6. From these measurements γ_S^d was subsequently determined.

Saint Flour and Papirer (1982a) have successfully applied IGC to the study of the adsorption of various organic molecules onto the surface of glass fibres. They have used the ECP technique as previously described in this Chapter. These authors have considered the problem of estimating the amount of solute adsorbed at monolayer coverage, q_m, in those cases where the chromatographic peaks pass though the concentration region associated with the inflection point in the adsorption isotherm. For these solute concentrations neither the rear nor front boundaries will coincide and therefore these data cannot be included in the integration process. This phenomenon was a significant problem in their study. The problem was solved by determining the isotherm in two parts. For p/p_o between 0.0 and 0.2 the isotherm was obtained from the overlapping of the rear boundaries and for values of p/p_o between 0.55 to 0.95, it was determined from the overlapping frontal boundaries. The intermediate region, in the vicinity of the q_m, was obtained by extrapolation. Using these adsorption isotherms, π_e was determined, and thus γ_S^d and W_S^{a-b} were estimated using Equation 5.10 and 5.15 respectively. This calculation yielded average estimates of 49mN/m^2 for γ_S^d based on the decane adsorption and 17mN/m^2 for W_S^{a-b} between benzene and glass fibres. The extent of the non-coincidence problem depends on the energy of the adsorbate-adsorbent interaction. For weak interactions the inflection point in the isotherm is not pronounced and thus non-coincidence is not a problem. Consequently the work reported by Gray did not exhibit this problem. For stronger specific interactions, such as those involving benzene and glass quoted above, non-coincidence is a problem.

Vokov and Gray (1989) have recently obtained the adsorption isotherms for

hydrocarbon vapours on carbon fibres. These isotherms allowed π_e and thus γ_S^d to be calculated. The γ_S^d estimates were significantly smaller than those previously determined by adsorption at infinite dilution.

6.2.6 Linear Adsorption Studies on Polymers using IGC

The majority of recent IGC studies have involved solute adsorption at infinite dilution. For low concentrations most adsorption isotherms are linear in shape and the chromatographic peak shapes obtained are thus Gaussian. These peaks are easy to analyse and, in general, infinite dilution IGC experiments can be conducted using commercial gas chromatographs (GC) with a minimum of modification.

Dorris and Gray (1980) have introduced a thermodynamic measure based on the retention of hydrocarbon vapours at infinite dilution. By experimentally estimating the free energy of adsorption for a methylene group, $\Delta G_{(CH2)}$, the dispersive component of the surface energy, γ_S^d, could be estimated via Equation 6.11:

$$\frac{-\Delta G_{(CH_2)}}{N a_{(CH_2)}} = 2 \left(\gamma_{(CH_2)} \gamma_S^d \right)^{1/2} \qquad (6.11)$$

where N = Avagadro's constant

$a_{(CH2)}$ = surface area of a $-CH_2-$ group

$\gamma_{(CH2)}$ = surface energy of hypothetical $-CH_2-$ liquid

$-\Delta G_{(CH2)}$ = free energy of adsorption for a $-CH_2-$ group

$-\Delta G_{(CH2)}$ was simply estimated from the ratio of the retention volumes V_N, and thus K_S, for alkane vapours with n and n+1 carbon atoms at a temperature T with the universal gas constant R:

$$-\Delta G^{o}_{(CH_2)} = RT \ln \left(\frac{K_S^{(n+1)}}{K_S^{(n)}} \right) \qquad (6.12)$$

V_N data were obtained at low surface concentrations in the linear region of the isotherm, and led to estimates of γ_S^d which agreed well with those determined from contact angle data. One advantage of this method is that the surface area of the sample does not need to be known.

These infinite dilution, and finite concentration, techniques were successfully applied by Katz and Gray (1981a,b) for studying the surface thermodynamics of hydrocarbon adsorption on cellophane film, and later by Anhang and Gray (1982) for their adsorption study on polyethylene terephthalate film.

These approaches have been extended to consider the adsorption behaviour at low surface coverages (Saint Flour and Papirer 1982b) for a range of neutral, acidic and basic molecules on silane treated and untreated glass fibres. For alkane vapour adsorption, the chromatographic peaks were Gaussian in shape and V_g was independent of vapour injection size. This observation confirms that the adsorption took place on the linear part of the isotherm. However for some probe vapours, such as tetrahydrofuran,the chromatographic peaks were asymmetric with neither front nor rear boundaries exhibiting coincidence. These peaks represent a complex chromatographic adsorption process in which both non-linearity of the isotherm and non-ideality (broadening) effects are dominant. The retention volume was obtained by extrapolating the retention volume to zero injection size by drawing a curve though the peak maxima for a series of decreasing injection sizes. An empirical equation based on earlier work of Snyder (1968) was proposed for modelling V_g in terms of dispersive interactions, and acid-base complexation using Gutmann's donor-acceptor model :

$$\log V_g = CA\,(\gamma_L^d) + C'(DN) + C''(AN) - c + \log(273\,R\,S) \qquad (6.13)$$

where A = surface area of the probe molecule

c = a constant term for the loss of entropy on adsorption

S = specific surface area of the adsorbent

C = measure of dispersive surface energy of adsorbent

C' = measure of acid(acceptor) properties of adsorbent

C'' = measure of base(donor) properties of adsorbent

Clearly, C is directly related to γ_S^d, C' to the acceptor number and C'' to the donor number. In many ways, this model is similar to the Fowkes-Mostafa's Equation discussed in Chapter 5. Since the adsorbates used in this study exhibited a range of acid-base properties, it was possible to test the validity of Equation 6.13 as a model for V_g. The authors concluded that experimental V_g values did indeed fit the model, based on a differential calculation for the treated versus the untreated samples. No attempt was made to estimate the values of the donor numbers and the acceptor numbers for each sample. This calculation would have been a critical test of this approach, and the absence of these results implies that the model was not successful in this more stringent evaluation. In more recent work these authors have studied silane treated, titanate treated and untreated glass fibres (Saint Flour and Papirer 1983). Attempts were made to correlate the experimentally estimated specific interaction energies with both the Gutmann and the Drago linear free energy relationships. Whilst general agreement with acid-base models was observed, a quantitative description of the acid-base properties of the fibres was not attempted. The reasons for this failure are most probably related to the experimental technique the authors have employed. Their injection sizes were in the non-linear concentration region of the adsorption isotherm as a result of using a thermal conductivity GC detector. Consequently their chromatographic peaks exhibited significant asymmetry which required an arbitrary empirical approach for the extrapolation of V_g values.

Recently Schultz *et al.* (1987a,b) have used IGC for studying carbon fibre surfaces. Adsorption results for a range of acidic, basic and neutral molecules were used to determine

both ΔG and ΔH at infinite dilution for a number of different surface modified substrates. From the measurement of ΔH they have calculated the acidity and the basicity constants K_A and K_B for the carbon fibre via Equation (6.14) :

$$\Delta H_{acid\text{-}base} = K_A . DN + K_B . AN \qquad (6.14)$$

Using the IGC data and the results of wettability experiments, the authors were able to provide a comprehensive description of the fibre surface chemistry as summarised in Table 6.1. This study is a good example of the type of analysis of a polymer surface which is most likely to succeed in predicting accurately interfacial bonding interactions.

Carbon Fibre	Wettability Experiments			IGC Experiments		
	γ_S^d	γ_S^p	γ_S	K_A	K_B	γ_S^d
Untreated	50	7	57	6.5	1.5	49
Oxidised	48	15	63	10.0	3.2	49
Coated	34	13	47	8.6	13.0	34

Table 6.1 Surface chemical characterisation of carbon fibres by IGC and wettability measurements (Schultz *et al* .1987a,b).

Further work by these authors (Schultz and Lavielle 1989) has concluded that the interfacial shear strength, τ_I, for carbon fibre interfaces, determined by the fibre fragmentation test, correlated with the strength of the acid-base interactions and not with the work of adhesion determined by wetting measurements. Since both IGC and wettability measurements sense the same type of chemical information, it is unclear as to the significance of this conclusion.

However in both these two papers, relatively minimal experimental details are reported. Specifically, the authors make no mention of the peak shapes encountered in the IGC measurements, nor the size of the normally quite large errors in the τ_t measurements. Whilst the conclusions of these studies seem to be significant, omission of these fundamental experimental details makes it difficult to assess the reliability of their conclusions.

Chen (1988) has analysed of the IGC data of Tseng *et al.* (1985) and Casterls and Mazza (1986), via the Fowkes' theory of acceptor-donor (acid-base) interactions. The ΔH of donor-acceptor interaction, as described by Drago's equation, was calculated for various probes with low density polyethylene (LDPE). However, there are a number of serious problems with the analysis developed by the author. The first problem was that large positive values of $\Delta H_{acid\text{-}base}$ were calculated. This problem was solved by assuming that E and C constants could be negative, and would thus eliminate the positive $\Delta H_{acid\text{-}base}$ values. Secondly, due to a lack of reported Drago constants, it was assumed that $E_A = -E_B$ and $C_A = - C_B$. Both of these assumptions are seriously flawed and invalidate the author's analysis.

Menard *et al.* (1987) have measured the adsorption isotherms of various organic molecules on asbestos fibres using IGC. Their results show that the adsorption mechanism lies somewhere between physisorption and chemisorption. This conclusion supports the importance of acid-base interactions in such adsorption phenomena. The extent of adsorption was observed to be toluene > tetrahydrofuran> benzene> CH_2Cl_2.

Wesson and Allred (1989) have studied the surface properties of carbon fibres using IGC with various acid-base probes. From the skewed chromatograms obtained, the authors have determined histograms of surface area fraction versus adsorption energy for a range of plasma and non-plasma treated materials. Their results were found to correlate with both XPS and wetting data. The authors concluded that acid-base chemisorption interactions are important for carbon fibre materials. Bolvari and Ward (1989) have also studied carbon fibres with acid/base probes using IGC and have concluded that acid-base interactions were

a factor in determining the extent of fibre-matrix adhesion.

Recently Osmont and Schreiber (1989) have reported on the IGC behaviour of E-glass fibres, both unmodified and modified by coupling agents. The acid-base properties of the fibres were determined by IGC as well as by solution adsorption studies with PMMA and PVC. The sensitivity of IGC to subtle changes in the surface properties of silica powders has been demonstrated by Papirer *et al.* (1989)

6.2.7 Adsorption Studies on Aramid Fibres using IGC

IGC has been used to study the surface properties of a number of fibrous materials including "Kevlar 49" fibres (Gozdz and Weighman, 1984). Using various organic vapours they determined adsorption isotherms for "Kevlar 49" fibres. From their BET plots the authors estimated that the surface area of "Kevlar 49" fibres was $0.233 m^2/gm$ which was in close agreement with geometrical estimates.

Chappell and Williams (1989a,b) have reported on the successful use of IGC for determining the extent of contamination of "Kevlar" fibre. They have studied a number of "Kevlar" fibre materials using an homologous series of hydrocarbon probes at infinite dilution. From the temperature dependence of V_g, they calculated ΔG^o, ΔH^o and ΔS^o for a range of "Kevlar" materials, including samples cleaned via soxhlet extraction and contaminated "as received" materials. The isosteric heat of adsorption, q_d, and γ_S^d were also measured. These thermodynamic measurements were found to be very sensitive to cleanliness of the surface (see Table 6.2). More recently these authors have reported the XPS results for those same samples studied by IGC (Chappell *et al.* 1989). A strong correlation was found between the nitrogen 1s peak intensity and the values of q_d (the isosteric of adsorption), γ_S^d and the negative values of the entropy of adsorption, ΔS^o. These results supported the conclusion that the clean surfaces were polyamide in composition with relatively high surface energies (by organic polymer standards) due to the crystalline nature of the surface. The entropies measured were directly related to the relatively local adsorption of the hydrocarbon probes.

Sample	q_d (kJ/mol)	ΔS^o (J/mol.K)	γ_S^d (mJ/m^2)	N_{1s} (% surface)
"Kevlar 49" - as received	32.6	34.1	32.0	0.8
"Kevlar 49" - water washed and dried	46.7	78.4	52.5	3.3
"Kevlar 49" - acetone washed and dried	50.1	83.0	65.1	6.1
"Kevlar 29" -finish (scoured)	34.5	39.9	37.2	0.3
"Kevlar 29" - finish (scoured) and acetone washed	46.9	77.5	43.4	6.8

Table 6.2 Comparison between surface analysis using XPS and thermodynamic data from IGC experiments for a range of "Kevlar" materials (Chappell and Williams 1989a,b; Chappell *et al.* 1989)

The above results showed consistently that commercial "Kevlar" materials, including those commercially scoured, have significant levels of surface contamination. The small negative values of ΔS^o are due to a positive entropy of mixing associated with absorption of the hydrocarbon vapours into the contaminant layer.

6.3 EXPERIMENTAL IGC STUDY OF ARAMID FIBRES

6.3.1 Materials and Equipment

The solute vapours used in this study were taken from the headspace of liquid samples. The vapours used were n-nonane (>99% purity), n-decane (>99% purity), butyl acetate (>99% purity), *sym*-tetrachloroethane (>98% purity), ethanol (HPLC grade), 1-4 dioxane (>99.5% purity). All the chemicals were obtained from BDH. A single 100cm x1/4" stainless steel column was cleaned with acetone prior to use for all the chromatographic measurements. Parallel strands of yarn were pulled through the column resulting in a 30-35% packing by volume and a typical sample weight of 5 gm. The packed column was then placed in a Hewlett Packard model 5300 gas chromatograph fitted with a flame ionisation detector. Since the GC oven was not suitable for experiments in the temperature range 20°C-40°C, the column was enclosed in a plastic tubing jacket through which water was circulated from a refrigerated water bath (Grant LTD). This jacketing allowed the column temperature to be controlled to within 0.1°C. For temperatures above 40°C the GC oven was used, though the thermal gradients in this case were larger.

The carrier gas was high purity helium which was passed through molecular sieves to remove residual water. The carrier gas flow rate was controlled and measured at the column inlet by a double pattern fine metering valve (Nupro) and a thermal conductivity mass flow transducer (MKS FM-360) respectively. The carrier gas flow rate was usually 10.0 standard cubic centimetres per minute (sccm) and the drift in flow rate was less than 0.05 sccm during the course of an experiment. The column inlet gauge pressure was measured by a differential pressure transducer (MKS 223BD) with a typical pressure drop along the packed columns of between 1 and 5 torr. Aramid fibres were placed into the columns and dried at 80°C under flowing helium for between 2 and 4 hours prior to commencing experiments. The chromatograms were recorded on IBM compatible computer (Amstrad) with a analogue to digital converter (μMicro Science Card). The retention time was taken as the first statistical moment of the chromatographic peaks. The results were corrected for

gas compressibility, column temperature, dead volume, and column wall retention. V_N is given as :

$$V_N = j.F(T/273.15)\,(t_R - t_M - t_W) \qquad (6.15)$$

where t_R = total retention time in minutes

t_M = methane retention time in minutes

t_W = wall retention time in minutes

T = column temperature

V_M was estimated from the retention time of methane, a non-adsorbing species. V_W was measured for all probes at all the temperatures studied using an empty column. It was observed that for nonane and decane, V_W was found to be significant and could account for up to 5% of the retention time for packed columns. For the acid and base probes used in this study V_W, did in some cases rise to 10% of V_N for the packed columns, though generally it was about 2-3%. A more significant complication was that some elution peaks exhibited skewness and thus V_W exhibited a dependence on the volume of the injection. The apparatus used for the inverse gas chromatography is shown in Figure 6.4.

Most of the chromatographic peaks were observed to be essentially Gaussian in shape. A purely Gaussian shaped chromatographic peak is evidence of an equilibrium adsorption process, as well as confirming the linearity of the adsorption isotherm in the concentration region being studied. Furthermore, for the linear portion of the adsorption isotherm, V_N will be independent of vapour injection size. For the nonane and the decane vapours this behaviour was observed to be true. However, some slight skewness, and thus injection size dependence, was observed with the tetrachloroethane, the butyl acetate and the dioxane. The results for ethanol exhibited a significant level of tailing. This peak skewness was probably due to adsorption on a non-linear region of the adsorption isotherm, as well as a result of the relatively heterogeneous nature of the interaction between the polymer surface and this strong acid-base molecule. The shape of the peak

skewness indicated that this adsorption isotherm was Langmuirian.

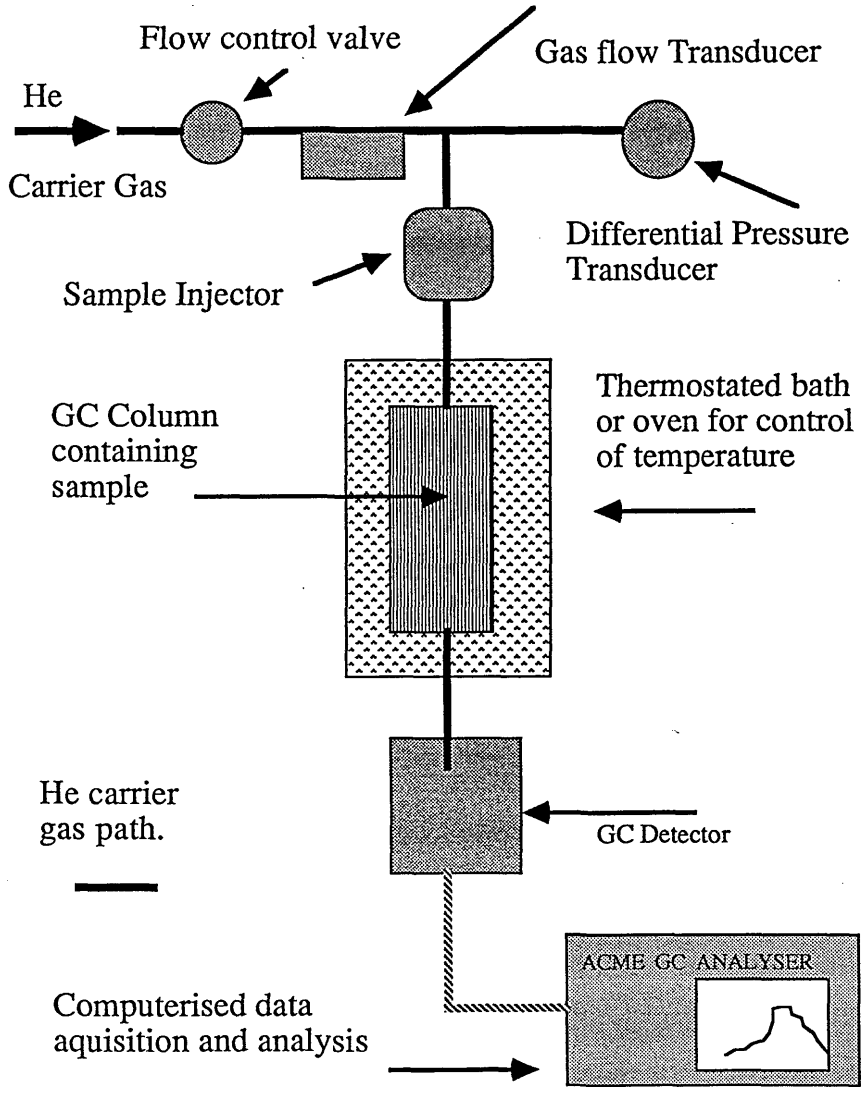


Figure 6.4 Apparatus for inverse gas chromatography.

To minimise the effects of this problem, the size of vapour injections was carefully chosen so that an equimolar amount of the vapours, and thus surface coverage, were adsorbed in all experiments. The resultant retention data were thus comparable between the different samples and the different probe vapours. The injection sizes used corresponded to approximately 0.1% of nominal monolayer coverage.

6.3.2 IGC Results

The retention behaviour for the six probes previously listed (two acidic, two basic and two neutral) were measured for four samples at a range of temperatures. The temperatures were chosen so that peak elution occurred between 2 and 20 minutes after the solute injection. The retention volume data is presented in Tables 6.3 and Table 6.4. These results are corrected for both V_M and V_W.

	Clean			" As Received"		
	20°	30°	40°	20°	30°	40°
Nonane	8.10	4.40	2.42	9.52	5.79	3.45
Decane	25.4	12.5	6.58	27.3	15.3	8.74
Tetrachloroethane	29.0	14.0	6.83	46.1	24.2	13.3
Dioxane	2.59	1.49	0.872	2.66	1.87	1.24
Butyl acetate	12.0	5.33	2.51	6.57	3.77	2.51
Ethanol	7.59	3.98	1.80	8.15	4.42	3.00

Table 6.3 V_N (cm^3/gm) as a function T (°C) for clean and "as received" "Kevlar" fibres.

	Diol Grafted				Octane Grafted			
	50°	60°	70°	80°	50°	60°	70°	80°
Nonane		16.1	10.4	6.73	7.33	4.14	2.67	1.58
Decane		24.4	15.4	9.93		9.47	5.31	3.07
Tetrachloroethane		29.9	18.0	10.9		39.9	22.6	12.5
Dioxane	8.50	6.36	4.46		5.52	3.30	2.189	1.46
Butyl acetate	14.95	9.15	6.13		9.44	5.25	3.75	1.93
Ethanol	15.0	9.85	6.55		3.593	2.15	1.35	0.786

Table 6.4 $\mathbf{V_N}$ (cm^3/gm) as a function T (°C) for diol and octane grafted "Kevlar" fibres.

From the temperature dependent behaviour of $\mathbf{K_S}$, $\Delta\mathbf{H_{ad}}$ can be calculated using the following expression :

$$\mathbf{q_d} = -\Delta\mathbf{H_{ad}} = R\, d(\ln \mathbf{K_S})/\, d(1/T) \qquad (6.16)$$

where K_S = partition coefficient

q_d = isosteric heat of adsorption

R = Gas constant

T = Temperature

"Kevlar" fibres have a diameter of 11.9 μm and a density of 1.44 gm/cm^3. These values yield a geometrical surface area of 0.233 m^2/gm and are in agreement with experimental estimates (Allred 1983; Gozdz and Weighman 1984).

The experimental heats of adsorption, ΔH_{ad}, have been calculated using Equation 6.16 with the data from Table 6.3 and 6.4 for a constant surface coverage. The results for the alkane vapours are shown in Tables 6.5. The values of γ_S^d are shown in Table 6.6 and have been calculated via Equation 6.11 using the retention data for nonane and decane. The values of $a_{(CH_2)}$ and $\gamma_{(CH_2)}$ used in this calculation were those chosen by Chappell and Williams (1989a).

		Cleaned	"As received"	Diol graft	Octane grafted
	ΔH_{con}	ΔH_{ad}	ΔH_{ad}	ΔH_{ad}	ΔH_{ad}
Nonane	46.4	45(2)	39(3)	40(1)	49(3)
Decane	51.4	51(1)	43(1)	44(1)	55(1)

Table 6.5 Heats of condensation and adsorption for alkane vapours (kJ/mol). The results in brackets are the uncertainties in the adsorption heats (kJ/mol).

γ_S^d (mN/m)	Cleaned	"As received"	Diol graft	Octane grafted
	42	32	28	23

Table 6.6 The dispersive component of the surface energy, γ_S^d (mN/m).

	ΔH_{con}	ΔH_{con}^d
Tetrachloroethane	44.7	44.7
Dioxane	38.4	31.7
Butyl acetate	43.6	34.7
Ethanol	41.8	10.0

Table 6.7 Total and estimated dispersive component of the heats of condensation for the acid-base probes (kJ/mol).

acid-base probes (kJ/mol).

Probe	Cleaned		"As received"		Diol graft		Octane grafted	
	ΔH_{ad}	ΔH_{ad}^{a-b}	ΔH_{ad}	ΔH_{ad}^{a-b}	ΔH_{ad}	ΔH_{ad}^{a-b}	ΔH_{ad}	ΔH_{ad}^{a-b}
Tetrachloroethane	55(2)	10	47(1)	2	46(1)	1	53(2)	8
Dioxane	42(2)	10	30(3)	-2	30(3)	-2	41(2)	9
Butyl acetate	59(1)	10	36(2)	7	41(3)	-2	50(4)	7
Ethanol	47(2)	37	33(6)	23	38(1)	28	48(4)	38

Table 6.8 Experimental heats of adsorption (kJ/mol) and the estimated acid-base component for various vapours. The results in brackets are the uncertainties in these heats (kJ/mol).

So that the acid-base component of the heat of adsorption, ΔH_{ad}^{a-b}, could be estimated, the dispersive component, ΔH_{ad}^{d}, of ΔH_{ad} must be firstly evaluated:

$$\Delta H_{ad}^{a-b} = \Delta H_{ad} - \Delta H_{ad}^{d} \qquad (6.17)$$

Assuming that ΔH_{ad}^{d} will be equal to the dispersive component of the heat of condensation, ΔH_{con}^{d}, this quantity may be defined in an analogous fashion to Equation 6.17:

$$\Delta H_{con}^{a\text{-}b} = \Delta H_{con} - \Delta H_{con}^{d} \qquad (6.18)$$

Experimental values of ΔH_{con} are well tabulated in the literature (Stull *et al.*, 1969), however experimental values of $\Delta H_{con}^{a\text{-}b}$ have not been reported. Assuming that the non-dispersive contributions to ΔH_{con} are acid-base in nature, donor-acceptor theory has been used to estimate these energies. Whilst such a calculation could only be expected to give first order estimates for $\Delta H_{con}^{a\text{-}b}$, it is however acceptable due to a lack of appropriate experimental data for more reliable determinations. Errors in this estimation will affect the absolute values of $\Delta H_{con}^{a\text{-}b}$, and thus $\Delta H_{ad}^{a\text{-}b}$, though they will not affect the underlying trends in the values for $\Delta H_{ad}^{a\text{-}b}$ for the range of fibre surfaces examined.

Values of $\Delta H_{con}^{a\text{-}b}$ were estimated via the Gutmann donor-acceptor theory (Gutmann 1978) as shown below. The self-association within these liquids is assumed to be due to the amphoteric nature of the liquids and $\Delta H_{con}^{a\text{-}b}$ and is defined below in Equation 6.19.

$$\Delta H_{con}^{a\text{-}b} = \Delta H_{self\ assn} \qquad (6.19)$$

Donor and acceptor constants have been reported for both dioxane, butyl acetate and ethanol, and these values have been used to calculate the extent of the self-association. For tetrachloroethane, only acceptor constants have been reported and it is thus presumed that no self-association occurs. The values of these constants used in this calculation of $\Delta H_{self\ assn}$ are listed in Table 6.9.

	DN	AN	$\Delta H_{self\text{-}assn.}$
Tetrachloroethane	0	23.1	0
Dioxane	14.8	10.8	6.7
Butyl acetate	17.1	12.5	8.9
Ethanol	20	37.1	31

Table 6.9 Donor (DN), acceptor (AN) numbers and the estimated $\Delta H_{self\text{-}assn}$ (kJ/mol) for the acid-base probes.

6.3.3 Discussion

The experimental values of ΔH_{ad} for nonane and decane show variations for the different fibre surfaces. For the cleaned fibres the values ΔH_{ad} are close to the heats of condensation as would be expected. The lower values for the "as received" fibres suggest a lower enthalpic interaction between the surface and the vapours. These values are consistent with the presence of contaminants on the fibre surface as previously reported (Chappell and Williams, 1989a). The diol grafted and the "as received" fibres exhibited similar values for ΔH_{ad}. It has been previously observed (Chappell and Williams, 1989a) that the "as received" materials were contaminated with polymeric glycol species which are chemically similar to the surface groups on the diol grafted fibres. Consequently, the observed similarity in the ΔH_{ad} values is reasonable. The increased values for ΔH_{ad} on the octane grafted fibres suggest that adsorption occurred on a relative high energy portion of

the surface which is probably chemically similar in nature to that of the cleaned materials. Lower values might have been expected, considering the probable presence of octane groups, adsorption on non-reacted portions of the fibre seems likely to have occurred.

The γ_S^d values reported in Table 6.6 are in agreement with those values reported for cleaned and "as received" "Kevlar" fibres (Chappell and Williams, 1989a). The low value of 23mN/m for γ_S^d on the octane grafted fibres would be expected for adsorption onto a alkylated surface. The intermediate value of 28mN/m for the diol grafted fibres is significantly lower than the value of 42mN/m for the clean fibres. A lower value would be expected for an amorphous graft surface compared with a highly crystalline clean fibre surface.

All of the fibre surfaces showed significant amount of acid-base interaction as reflected in the values of ΔH_{ad}^{a-b} reported in Table 6.8. The cleaned and octane grafted fibres showed similar behaviour with most of the probe vapours. Ethanol exhibited the largest values of ΔH_{ad}^{a-b} due to its strong amphoteric properties.Strong interactions were registered with the other vapours confirming the amphoteric nature of the PPTA surface. Considering that the primary polymer chains in the fibres are held together by intermolecular hydrogen bonding this observation is to be expected. The ethanol molecules would be expected to interact with the non-bonding orbitals of the carbonyl oxygen whilst the butyl acetate would be expected to interact with the amide hydrogens. Whilst it may have been expected that the alkylated fibre surface would have low acid-base interaction energies, experiments at infinite dilution are sensitive to those high energy areas on the fibre surface. Unless the octane groups completely covered the fibre surface, then similar values of ΔH_{ad}^{a-b} for both treated and clean materials are quite reasonable.

The diol grafted fibres showed very little interaction with three of the acid-base probes. This result implies that not only were the underlying PPTA molecules unable to interact with the adsorbate specifically, neither were the diol groups. The first premise implies that the fibre surface has been substantially covered with the diol groups and thus the PPTA chains are effectively screened from the adsorbates. In this case, the diol groups

could possible interact with the adsorbents. These interactions might be physically possible, however they are not energetically favoured. The strong self association energy between the hydroxyl groups in each diol functional groups is greater than the expected interaction energy between a single hydroxyl group with either the dioxane, butyl-acetate or the tetrachloroethane. Only in the case of another hydroxyl group, as in the case of ethanol, is a significant ΔH_{ad}^{a-b} observed.

The acid-base complexation enthalpies for dimethyl-formamide with the acidic and basic molecules used in the experimental study, have been calculated and are shown in Table 6.10. These results were determined using the Gutmann equation with a donor and an acceptor constant of 26.6 and 16.0 respectively for dimethyl-formamide. Dimethyl-formamide was chosen for this calculation as it has a similar chemical structure to PPTA and the donor-acceptor constants for this molecule are known. Thus the acid-base interactions between dimethyl-formamide and the adsorbate vapours should model the ΔH_{ad}^{a-b} results observed for PPTA with those same species.

	DN	AN	$\Delta H_{complex}$	ΔH_{ad}^{a-b}
Tetrachloroethane	0	23.1	25.6	10
Dioxane	14.8	10.8	12.0	10
Butyl acetate	17.1	12.5	11.4	10
Ethanol	20	37.1	41.0	37

Table 6.10 The estimated $\Delta H_{complex}$ (kJ/mol) for the interaction between dimethyl-formamide with the acid-base probes and the experimental values of ΔH_{ad}^{a-b}.

The calculated results, shown in Table 6.10, generally show a good agreement with the predicted complexation energies. In all cases the experimental results are slightly lower than the predicted enthalpies, though they are within experimental error. This correlation confirms that the acid-base properties of PPTA are similar to those of dimethyl- formamide due to the common dominant influence of the amide group. Furthermore, this correlation confirms the applicability of the Gutmann approach to modelling the acid-base adsorption enthalpies of organic polymers.

6.3.4 Conclusions

The sensitivity and usefulness of IGC for studying the surface properties of fibrous materials has been demonstrated. The measured acid-base and dispersive thermodynamic properties of a number of "Kevlar" fibres have been reported based on the temperature dependent retention volumes. Clean and octane grafted "Kevlar" fibres exhibited similar adsorption energies. This observation was due to the low adsorbate concentrations used in these infinite dilution experiments. The "as received" and diol grafted fibres surface also exhibited similar adsorption enthalpies which was probably the result of the presence of hydroxyl groups on both fibre surfaces. As would have been predicted, "Kevlar" fibre surfaces were found to be amphoteric due to the chemical nature of their amide constituents. The acid-base component of the adsorption enthalpy for these fibres was in good agreement with the acid-base complexation energies predicted by the Gutmann equation.

CHAPTER 7

INTERLAMINAR BEHAVIOUR OF LAMINATES

7.1 INTRODUCTION

The mechanical properties of fibre reinforced composites under deformations orthogonal to the direction of fibre orientation is an area of current research interest. These properties are an important consideration in composite design as in many cases they constitute the weakest link in the material strength. It could be anticipated that an improvement in these off-axis properties would result in an overall improvement in composite performance.

This Chapter consists of two sections. In the first section the interlaminar performance of "Kevlar"-epoxy composites is reviewed. Failure in flexural and short beam shear testing is often the result of interlaminar failure, and recent attempts to improve fibre-matrix adhesion and thus increase the interlaminar shear strength are discussed. In the second section, the results of an experimental study of interlaminar performance of "Kevlar"-epoxy laminate samples is presented. The effect of fibre surface modification on the flexural and interlaminar properties of "Kevlar"-epoxy laminates is then discussed.

7.2 INTERLAMINAR PERFORMANCE OF COMPOSITES

7.2.1 Interlaminar Shear in Composites

A composite specimen subject to flexural bending will contain a maximum interlaminar shear stress through the mid-section of the specimen. The maximum tensile stresses will develop on the convex side of the deformed specimen, whilst on the concave side of the specimen, the maximum compressive stresses will be developed. A composite specimen will normally fail via one of these three pure stress modes, or in a combination of these modes, depending upon the materials and the test configuration.

The interlaminar shear properties of fibre reinforced composites are generally thought to depend largely on the adhesion between the fibre and the matrix resin. This argument has

been used extensively during the last 20 years as the rationale for a large number of experimental studies. These studies have attempted to correlate changes in fundamental fibre-matrix adhesion characteristics with the interlaminar shear strength as measured via flexure or short beam shear experiments. The basic assumption in this argument is that a condition of plane shear exists in both these types of experiments, and that the resultant deformations cause failure by matrix shear yielding, debonding or some combination of both. In reality, tests such as short beam shear and flexure simply generate a numerical result which can partially, or entirely, correspond to the interlaminar shear properties of the laminate. The actual correspondence depends upon whether the mode of failure of the material is observed to be completely or partially interlaminar. In those cases where interlaminar failure does contribute to failure, many authors have sought to correlate these properties with fibre-matrix adhesion. A number of workers have reported a satisfactory correlation between these properties.

7.2.2 Interlaminar Shear and Fibre-Matrix Adhesion

It has been generally assumed that an improvement in the interlaminar strength of a fibre reinforced composite can be achieved by improving the adhesion between the fibre and the matrix resin. Consequently a substantial research effort has been directed at modifying the surface chemistry of various reinforcement fibres to attain this goal.

Drzal and Rich (1983) have investigated the shear strength of carbon fibre based laminates. They observed a relationship between the low apparent shear strength of the laminates and the fibre-matrix adhesion as determined from single fibre fragmentation experiments. In earlier work Drzal *et al.* (1982) proposed that the oxidative treatments used to improve adhesion in carbon fibre composites removed the weak outer layers of the fibre surface as well as adding oxygen groups to the fibre surface which could interact with the matrix phase. In a subsequent study Drzal *et al.* (1983) studied the effect of polymeric sizings on the interfacial shear strength of carbon fibre composites. He concluded that these coatings did improve the shear strength by creating in a brittle interphase region around the fibres. Varma *et al.* (1983) have observed a linear relationship between the interlaminar shear properties of the carbon fibre composites and the interfacial shear as measured via single fibre micro-mechanics.

Verpoest (1987) has recently considered the effects of a proprietary aramid fibre surface modification on the mechanical performance of aramid-epoxy composites and their moisture sensitivity. He concluded that the extent of moisture uptake of the laminate and the mechanical performance of the laminate were related to the fibre surface modifications. However he also noted that the effect of the fibre surface treatment on the initial interlaminar shear strength prior to exposure to moisture resulted in less than a 10% change in both the flexural modulus and the flexural strength.

Takayanagi *et al.* (1987) have reported that significant changes in the surface chemistry of aramid fibres were accompanied by dramatic changes in the interfacial shear strength as measured using the micro-mechanic methods. These changes were accomplished via a selective grafting of chemical groups onto "Kevlar " fibres. However, these modifications resulted in a maximum increase of only 15% for the flexural modulus and 20% for the flexural strength as measured in three point bending experiments for "Kevlar"-epoxy laminates.

Penn *et al.* (1983) have reported on the interlaminar shear performance of "Kevlar"-epoxy laminates in which the aramid fabrics were surface modified and then surface characterised. The authors used a wide range of organic and inorganic species to modify the fibre surface chemistry in an attempt to improve adhesion with the epoxy matrix. These modifications included species which could undergo hydrogen bonding, metal ion co-ordination, increased dispersion interactions as well as direct covalent interaction with the matrix phase. Whilst wetting experiments verified a number of the surface modifications, both the micro-mechanical measurements and the short beam shear experiments showed no statistically significant results for five out of the six surface modifications. Only the presence of poly(dimethyl siloxane) coating on the fibres showed a change in the laminate mechanical behaviour. This polymeric coating resulted in a dramatic decrease in mechanical strength as sensed by both the short beam shear results and the micro-mechanically measured interfacial shear strength.

Peters and Springer (1987) have investigated the effect of a fibre surface treatment on the flexural behaviour of carbon fibre epoxy laminates. The carbon fibres were coated with a commercial size prior to fabrication into uniaxial laminates. The flexural strain to failure was measured for two different levels of epoxy sizing as well as for uncoated samples as a

function of degree of the epoxy cure. Some small variations in the strain to failure of the laminates fabricated from these different surface treated fabrics were observed. In all of the four cases investigated these differences were not statistically significant at the 2σ level of error. However, the authors have preferred to argue that these small differences in the strain to failure were statistically significant and are the result of improvements in fibre-matrix bond strength. This conclusion is based entirely on the strain to failure data.

Clearly, the evidence for a correlation between the interlaminar shear strength of a composite and the fibre-matrix adhesion is not conclusive. In some cases the only evidence for changes in adhesion are based on micro-mechanics measurements. These types of measurements are later concluded to have a large experimental uncertainty (see Chapter 10).

The supposed importance of a relationship between interlaminar shear strength of a composite and the fibre-matrix adhesion has recently attracted some criticism. The primary criticism of this concept is that it is a simplistic, and consequently an unrealistic, description of a complex mode of material failure. Bascom and Drzal (1987) have concluded that shear tests for composite materials do not provide an unambiguous measure of fibre-matrix bond strength. They also state that a low shear strength measurement for a composite does not imply a low interfacial strength since a number of other modes of failure may be operative. These include shear cohesive failure of the fibres or matrix yielding in the resin-rich regions between the plies. They also recognised that the type of shear tests used is also a factor as additional modes of failure can occur in the various test methods for determining the interlaminar shear strength.

7.3 INTERLAMINAR EXPERIMENTAL STUDY

7.3.1 Sample Preparation

The fabric used in this study was a 4x4 satin weave of "Kevlar 49" fibres as supplied by Du Pont. "Kevlar 49" is the high modulus version of a class of aramid fibres manufactured by Du Pont under the regiestered trade name "Kevlar". In this thesis references to "Kevlar" will refer to "Kevlar 49" unless otherwise indicated.

This fabric was cut into 320mm x 320mm pieces and cleaned via soxhlet extraction with acetone and then surface treated as described in Chapter 3. The fabric pieces were then

vacuum dried 100° C prior to impregnation with an epoxy resin. Epoxy prepreg film (Ciba-Geigy type 913) was then impregnated with each layer of the "Kevlar" fabric by melt pressing two sets of two layers of the prepreg film with each piece of fabric at 110° C at a pressure of 0.7MPa. Eight layers of the fabric were then stacked together to form a [0,90] laminate. The panels were then trimmed to a size of 300mm x 300mm and cured by autoclave at the manufacturers' recommended curing conditions of 120° C and 0.7MPa for 1.5 hours. The laminates had a nominal fibre volume of 55%.

The unique physical properties of "Kevlar" fibres, especially their high tensile strength and the low compressive strength, results in a number of difficulties in the machining of these materials relative to composites containing carbon or glass fibres. The most commonly encountered problem is the difficulty in fabricating clean, "fuzz-free" specimen edges. This problem has been noted by various authors and a range of solutions has been proposed (Wardle and Steenkamer 1987). These solutions invariably involve the use of a specialist methods of sample machining. Special helical routers, high power lasers and high pressure water jets are some of the more recent techniques which have been evaluated for cutting the laminate. Wet grinding techniques are generally used for the final machining of the sample for both the correct shape and for preparing sample edges (Rueda *et al.* 1988; Wardle and Steenkamer 1987)

As has been discussed in Chapter 3, water is known to modify the mechanical performance of aramid-epoxy composites. This effect has been reported by a number of authors and is known to depend especially on the nature of the fibre-matrix adhesion (Allred 1978; Verpoest 1987). Since a number of common machining techniques for composites involve the use of water as a lubricant and/or coolant, the possibility of water absorption was considered to be a general problem. Since the current study is especially concerned with investigating the fibre-matrix interface, it was deemed to be essential that direct contact with water should be avoided. Consequently a number of dry machining methods have been evaluated and compared with other "wet" machining methods for the preparation of "Kevlar"-epoxy test specimens.

7.3.2 Sample Cutting

A number of methods for the cutting of "Kevlar" laminates, both 8 ply and 24 ply, have been reviewed and evaluated. The methods and the observations on their suitability for machining "Kevlar"-epoxy laminates are reported as follows:

(i) High Pressure Water Jet.

Operating at 4000 bar, very fine water jets can cut through many strong engineering materials, such as 1" sheet steel, with great ease. This method has been found to be suitable for cutting glass and carbon fibre laminates with good accuracy and edge finish. However preliminary experiments conducted with such a system in the Department of Mechanical Engineering, Imperial College, revealed a number of problems in cutting "Kevlar"-epoxy laminates. Although the edge finish of the laminates was acceptable in quality, especially for the thicker laminates, the water jet did penetrate between the laminae. Especially for the thinner laminates serious delamination between the plies of "Kevlar"-epoxy was observed. These delaminations resulted in this technique being excluded as a potential method for sample preparation.

(ii) Diamond Tipped Abrasive Wheel

A more common method for cutting involves the use of a diamond tipped abrasive wheel in conjunction with water as a coolant. Whilst the use of this method is established, it was considered that the significant immersion of the sample in water during the machining might result in significant water absorption.

(iii) High Power CO_2 Laser

Previous investigations have established that high power CO_2 lasers can accurately cut laminate samples (Tagliaferri *et al.* 1987). However, significant charring of the sample edge occurs and the associated thermal effects of sample heating on the laminate performance is a matter of some concern and uncertainty. Consequently this technique was not directly evaluated in this study.

(iv) Radial Saw

A common method for cutting simple samples geometries is the use of a radial saw equipped with an appropriate blade. Unfortunately, "Kevlar"-epoxy laminates prepared using this method result in samples which have a significant amount of "fuzziness" along

the cut edges due to fibre material not severed by the saw. The resulting layer of fibrous material, which is up to 1mm thick, then needs to be removed during a later preparation step. In addition, contact between the radial saw and the composite sample can lead to very significant heating of the laminate. This heating can result in thermal degradation of the laminate as well as the release of noxious odours.

(v) High Speed Router

It has been claimed that the optimum tool for the preparation of a laminate sample of "Kevlar"-epoxy laminates is a high speed router with a specially designed fluted router bit. Du Pont (in "Cutting and Machining Kevlar"), have supported the use of such a tool for use with "Kevlar" fibre based composite. Such a router was purchased and evaluated in this study (Aramid Fibre Cutters, Basingstoke, UK). The ability of this router to cut laminate samples was judged to vary between acceptable and fair. However this average performance was partially the result of inexperience in the use of the router, as well as other non-optimised operating conditions employed. It was concluded that the use of this router system for sample preparation was not justified based on the quality of the specimens it produced.

(vi) High Speed Power Jigsaw

Eventually it was concluded that the most successful method for the cutting of "Kevlar"-epoxy laminate samples was the use of a power jigsaw (Bosch PDT50) operating with an appropriate blade (type T119A). The reciprocating nature of the blade motion seems to be a factor which results in sample edges with minimal edge "fuzzing". Furthermore, the small blade/laminate contact area minimised the thermal heating and associated problems encountered with those radial saws. This method, although not fully optimised, was able to cut 24 and 8 ply laminates without difficulty.

This technique seems to offer a number of significant advantages over the other techniques considered such as:

(i) relies on a simple technology with a low cost.

(ii) having the ability to cut complex shapes which is important for the fabrication of certain test specimens.

(iii) Portability of the saw means that this method can be used on real composite structures or systems.

7.3.3 Sample Polishing

After the samples were cut from the laminate panels using the jigsaw, the edges were polished to remove the small amount of fibrous materials which remained. Initially an industrial belt sander with Al_2O_3 abrasive belt was used to polish the specimen edges. However these edges did not exhibit the crisp edge finish which is easily obtained with laminates such as those containing carbon or glass fibres. Edge "fuzziness" still remained and seemed to be regenerated in this method of polishing. It was observed that samples which were polished by hand exhibited a significantly improved edge finish. This improvement was thought to be due to two factors. Firstly, significant heating of the specimen which occurred during the mechanical polishing procedure was avoided by using slow polishing rates by hand. The resultant lower temperatures led to less fibre fibrillation along the specimen edges. Secondly, the reciprocating motion associated with polishing by hand led to a cleaner sample edges as less fibrous material was generated. Any residual fibrous materials left along the sample vertices were removed by one pass of the sample vertex, at an angle of about 70°, over the Al_2O_3 paper. Hand polishing with various grades of Al_2O_3 paper allowed rectangular shaped specimens to be prepared. A high quality of sample finish was obtained.

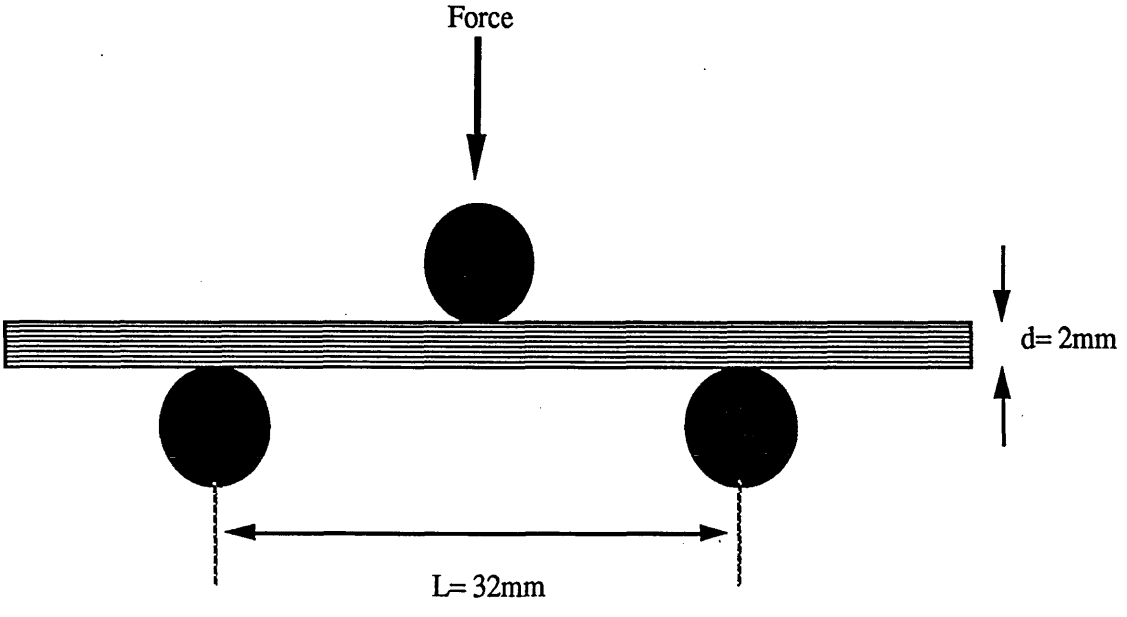
7.3.4 Interlaminar Testing

Two different mechanical tests have been used to evaluate the interlaminar behaviour of the laminates. These tests are the flexural and the short beam shear test.

Flexural samples were prepared with dimensions of 50mm x 25mm, with a nominal depth, **d**, of 2mm using the methodology described in sections 7.1. and 7.1.2. Sample dimensions were measured to 0.05mm using Vernier callipers. The samples were mounted onto a flexure testing apparatus with a load span, **L**, of 32mm which corresponded to a **L/d** ratio of 16:1. The samples were loaded in three point bending with the apparatus schematically shown in Figure 7.1. All rollers in the flexure apparatus had a diameter of 6mm.

Short beam shear samples were prepared with dimensions of 10mm x 20mm. All samples had a depth of between 2.00mm and 2.20mm.The sample loading geometry is virtually the same for the flexure test as for the short beam shear test, except that the span to depth ratio is far smaller in short beam shear. In this study the ratio of **L/d** was 5:1, thus the loading span was 10mm. The loading rollers all were 3mm in diameter.

The flexure and the short beam shear test apparatus were mounted into a Instron 1122 Mechanical Testing Machine, equipped with a 5kN tension/compression load cell. The test speed was 1mm/minute as recommended in the ASTM Standard D790M for the Flexural Properties of Unreinforced and Reinforced Plastics (ASTM 1984). Five specimens of each sample type were tested in flexure and the average results are shown in Table 7.1. Six samples were tested in the short beam shear test according to ASTM Standard D2344 for the Apparent Horizontal Shear Strength of Reinforced Plastics and the average results and their standard deviation, σ, is shown in Table 7.2.



Sample width b= 25mm

Sample span L= 32mm

Sample depth d = 2mm

Figure 7.1 Schematic representation of the flexure experiment.

7.3.5 Flexural Results

The experimental results obtained are listed below in Table 7.1. The test method and calculations were performed in accordance with ASTM Standard D790M. The flexural modulus was calculated using Equation 7.1, and the flexural strength by Equation 7.2:

$$\mathbf{E} = \mathbf{L}^3 \mathbf{m} / \mathbf{b}\, \mathbf{d}^3 \qquad (7.1)$$

$$\mathbf{S} = 1.5\, \mathbf{P}\, \mathbf{L} / \mathbf{b}\, \mathbf{d}^2 \qquad (7.2)$$

where **E** = flexural modulus (GPa)
L = support span distance (mm)
m = initial slope of stress/strain curve (N/mm)
b = sample width (mm)
d = sample thickness (mm)
S = flexural strength (MPa)
P = maximum load (N)

The initial slope of the stress/strain curve was estimated from the chart recorder trace. In most cases a region of non-linear behaviour was observed at the commencement of the experiment due to the take-up of slack and alignment or seating of the sample. This artifact is described as the "toe region" and its presence was compensated for via a simple linear extrapolation of the linear region of the stress/strain curve to give a corrected zero strain. This corrected value for the displacement was used in all calculations. The relative energy to failure, **T**, was estimated by integrating the stress/strain curve up to the stain of failure for the load **P**. The errors in the flexural modulus were very close to 0.1GPa for all the samples at the 1σ confidence level and similarly for **S** the error was 10MPa for all samples. The strain to failure of the convex face for all the composite samples was 2.3% +/- 0.1%.

Fabric Treatment	E (GPa)	S (MPa)	T
"As received"	21.0	450	2.40
Clean	20.0	449	2.30
Amine coated	21.0	454	2.25
Epoxy resin coated	21.0	450	2.30
Polydimethyl siloxane coated	22.0	455	2.40
Polyethylene glycol coated	23.5	470	2.25
Diol grafted	20.5	465	2.40
Epoxy grafted	21.5	465	2.50
Metallated/cleaned	20.0	450	2.60

Table 7.1 Flexural modulus, **E**, flexural strength ,**S**, and the relative energy to failure, **T**, for various "Kevlar"-epoxy laminates.

7.3.6 Short Beam Shear Results

The short beam shear strength, **D**, were calculated using Equation 7.3 and are listed below in Table 7.2.

$$\mathbf{D} = 0.75.\mathbf{P}/\mathbf{b}. \qquad (7.3)$$

Fabric Treatment	**D** (MPa)	σ (MPa)
"As received"	39.7	0.9
Clean	41.7	1.4
Amine coated	39.2	1.4
Epoxy resin coated	43.0	0.6
Polydimethyl siloxane coated	40.4	1.0
Polyethylene glycol coated	39.6	0.7
Diol grafted	40.3	1.5
Epoxy grafted	44.0	1.2
Metallated/cleaned	31.1	1.6

Table 7.2 Short beam shear strength, **D**, of "Kevlar"-epoxy laminates manufactured from surface modified fabrics.

7.3.7 Discussion

All of the flexural samples exhibited an apparent failure on the tensile side of the samples as shown in Figure 7.2.

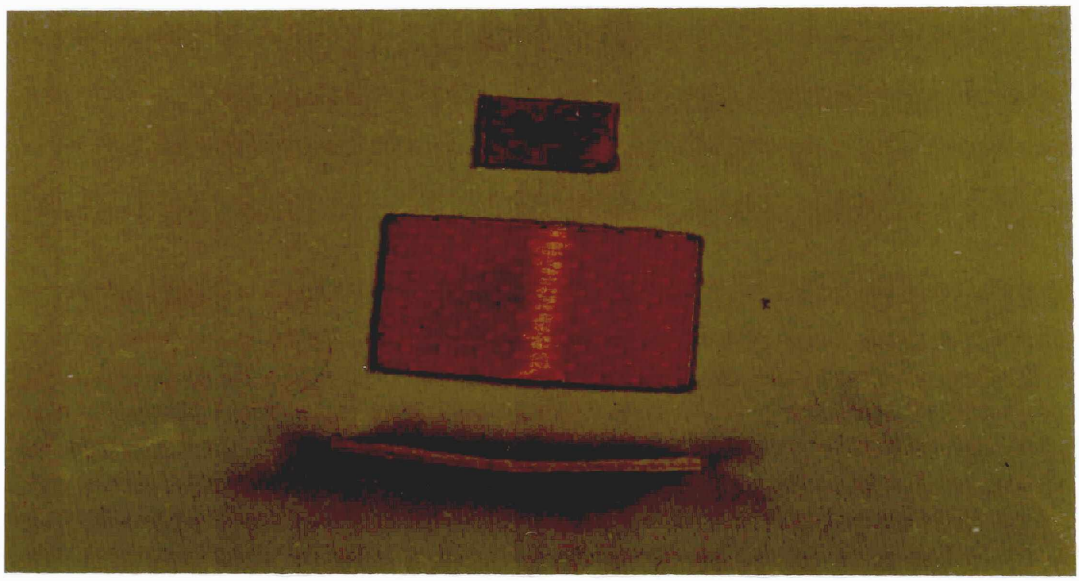


Figure 7.2 "Kevlar"-epoxy laminate samples after the flexure and the short beam shear tests.

A "whitened" damage zone was observed in the region where the fibre bundles have undergone tensile failure (see Figure 7.2). On the compressively loaded side no damage seems apparent except an area where the loading roller has indented the laminate surface. The flexural test traces of the load versus displacement were all very similar in appearance and showed the typical non-linear variations in their shape as have been previously noted by Zweben (1978).

Gueda *et al.* (1988) have reported on the flexural performance of 2mm thick "Kevlar"-epoxy laminates. The material used in their study was an 8 ply 0/90 "Kevlar"-epoxy laminate of the same type used in the current study. They obtained values of 18 +/- 0.5 GPa and 425 +/- 5 MPa for the flexural modulus and the flexural strength respectively using ASTM standard D790M for samples with a **L/d** ratio of 16:1. They observed that increasing the **L/d** ratio to 40:1 resulted in the flexural modulus increasing to a value of 31GPa. Their results are within 10% of the results obtained in this work for laminates based on clean "Kevlar" fabric. The small differences between the results obtained in these

two studies are most probably related to the differences in the thickness of the samples. On average the thickness of the "Kevlar"-epoxy laminates prepared in the current study was close to 1.9mm, thus resulting in a **L/d** ratio larger than 16:1. Based on Gueda *et al.*'s conclusion, this increased value for **L/d** would account for the slightly larger result for the flexural moduli determined. In conclusion, the flexural performance of "Kevlar"-epoxy laminates fabricated by the hand lay-up method used in this study, compare very favourably with materials commercially manufactured.

The flexure samples used in the current study were observed to fail in a tensile mode on the convex side of the sample as reported by Gueda *et al.* (1988). The sample strain at failure on the convex face of the specimens was 2.3% which is very close to the failure strain for "Kevlar 49" fibres of 2.5% (Dupont, 1977) and supports the observation of tensile failure on convex loaded specimen face.

The flexural strength and modulus results reported in Table 7.1, in general, show a small variation with the type of fibre surface treatment adopted. However, these variations are mostly within the experimental errors associated with the measurement. Consequently, virtually all flexural strength and moduli results were observed to be independent of the fibre treatment. The only samples in which significant variations in performance were observed were those manufactured with a polyethylene glycol coated fabric. This material exhibits an apparent 10% increase in the flexural modulus and a 5% increase in the flexural strength.

Thus it is concluded that the modification of the fibre surface chemistry for "Kevlar" fibres influenced neither the flexural modulus, strength nor the strain to failure of "Kevlar"-epoxy laminates. The mode of failure for all samples was tensile fibre failure. In no cases did the attempts to introduce a modification of the fibre-matrix bond strength result in a change in this failure mode. Even the use of a lubricant, such as poly(dimethyl siloxane), which has a low interface yield stress and could be expected to weaken significantly the fibre matrix bonding, did not effect the flexural behaviour of these composites. A decrease in the the fibre-matrix bond strength might be expected to promote failure due to interlaminar shear rather than tensile or compressive failure at the sample's faces.

A number of other authors have reported results which are consistent with these

conclusions. A number of workers have studied in detail the failure for "Kevlar"-epoxy laminates in flexure. Zweben (1978) has suggested that whilst the deformation of these laminates in tensile deformations was elastic, the compressive deformations was elastic-plastic in behaviour. This deformation was thought to be a direct consequence of the low compressive strength of "Kevlar" fibre relative to their tensile strength. The non-linearity of the flexural stress/strain curves supported the argument that elastic plastic deformation had occurred on the compressively loaded side of the specimen. This deformation resulted in a shifting of the neutral axis of bending towards the specimen face in tension.

Marom and his co-workers have studied this argument in some detail and have looked further into the elastic-plastic deformation mode. Davidovitz *et al.* (1984) observed that "Kevlar"-epoxy laminates in flexural loading failed via a tensile and/or delamination modes. The authors concluded that a transition from interlaminar to tensile failure occurred at a critical fibre volume of about 46% for a **L/d** ratio of 8:1. Fisher *et al.* (1987) have also considered the variation in the apparent interlaminar shear strength of "Kevlar"-epoxy laminates in flexural loading. They have observed that the apparent interlaminar shear strength increased with a decreasing **L/d** ratio due to compressive plastic deformations which occur. Modelling of this deformation behaviour allowed the authors to correct the experimentally estimated values to give a correct measure of the apparent flexural strength.

The failure mechanism of the samples tested with the short beam shear test differed considerably from that of the flexurally tested. No apparent exterior damage was visible on the compressive or the tensile loaded sides of these specimens after sample failure. This observation suggests that the mode of failure was within the sample interior and thus was likely to be partially interlaminar in character.

The results shown in Table 7.2 show a number of clear trends. Both samples which were treated so that epoxy functionalities were present on the fibre surface prior to laminate fabrication showed clearly the largest values for **D**. Most of the other specimens exhibited shear strength of about 40 MPa, except the metallated/cleaned laminates which showed substantially lower values for **D**. A detailed discussion of the trend in these values of **D** is given in Chapter 11.

7.4 CONCLUSIONS

The flexural performance of "Kevlar"-epoxy composites is independent of fibre surface treatments. Flexural moduli and strength do not exhibit any interlaminar characteristics and presence of a polymer lubricant does not cause a change in the mode of failure to that of interlaminar shear. Failure occurs by fibre fracture on the tensile loaded face of the flexure sample and is promoted by elastic-plastic deformation on the compressively loaded side of the specimen. These results are similar to those described by other workers.

The short beam shear test yields data which seems to be characteristic of the interlaminar shear properties of the composite. No mechanism for failure was apparent visually in failed specimens and it was assumed that the mechanism was to some extent interlaminar in nature. The experimental results imply that epoxy surface treatments can increase the interlaminar shear strength by about 10%, whilst etching of the fibre surface led to a significant decrease in the interlaminar strength. In the former case the increase in **D** is most likely due to some increased interactions between the fibres and the matrix.

CHAPTER 8

FRACTURE IN COMPOSITES

8.1 INTRODUCTION

An important mode of failure in composite laminates is the propagation of cracks in planes parallel to the lamina structure. In some circumstances, this process may lead to catastrophic failure of the component. Because of the relatively low fracture energies involved in this mode of failure, the study of interlaminar fracture of composites has important practical engineering implications as well as being of fundamental interest as a research topic.

This Chapter considers in two sections the fracture behaviour of materials. In the first part, the analysis of crack propagation though homogeneous isotropic and anisotropic materials via linear elastic fracture mechanics is reviewed. The various modes of material failure and the experimental methods for their characterisation will also be reviewed and discussed. The specific fracture performance of epoxy resins, and their modified variants, is also considered. Particular attention is paid to the various studies of the fracture toughness of the composite laminates which have been reported in the literature. In the second part of this Chapter experimental results for the mode I fracture of "Kevlar"- epoxy laminates will be reported and discussed.

8.2 A REVIEW OF THE FRACTURE OF MATERIALS

8.2.1 Linear Elastic Fracture Mechanics

One of the most successful approaches for the characterisation of the fracture energy of homogeneous materials has been the use of linear elastic fracture mechanics (LEFM).

Griffith (1921, 1924) postulated that all materials contain an intrinsic distribution of flaws, and that this distribution, coupled with the stress state in the material, determined its

fracture strength. Using an energy balance approach, he was able to explain why the theoretical strength of a wide variety of materials, based on atomic force considerations, was far greater than those experimentally observed. Development of this analysis was possible following the work of Inglis (1913) who had explicitly analysed the stresses around an elliptical crack and defined the elastic strain energy per unit thickness, **U**, for plane stress and plane strain respectively as :

$$\mathbf{U} = \frac{\pi \sigma^2 \mathbf{a}^2}{\mathbf{E}} \tag{8.1}$$

$$\mathbf{U} = \frac{\pi (1 - \nu^2) \sigma^2 \mathbf{a}^2}{\mathbf{E}} \tag{8.2}$$

where the failure stress is σ, the half crack length is **a**, **E** is Young's modulus and ν is Poisson's ratio. These solutions allowed Griffith to propose Equations 8.3 and 8.4 which equate the elastic energy **U**, in terms of the fracture surface energy per unit area, γ, required to produce a fracture surface:

$$\sigma^2 \pi \mathbf{f} = 2 \mathbf{E} \gamma \tag{8.3}$$

$$\pi (1 - \nu^2) \sigma^2 \mathbf{a}^2 = 2 \mathbf{E} \gamma \tag{8.4}$$

Equations 8.3 and 8.4 refer to the cases of plane stress and plane strain respectively, and apply to the critical condition in which the energy released by the crack propagation equals the energy required to create additional fracture surface ie. $\mathbf{dU/da} = 0$. This equation leads to the fundamental premise that fracture may occur when sufficient energy is released by crack growth process (from the highly stressed crack tip zone) to permit the creation of the associated additional fracture surface area.

Griffith's γ parameter refers to a mechanical process by which significant numbers

of primary chemical bonds are broken in a clearly irreversible way. It is consequently quite distinct from the surface free energy γ referred to in the context of equilibrium surface thermodynamics in Chapter 5 which pertains to a reversible process involving the formation and breakage of secondary chemical bonds. However, this distinction was not always made. Indeed, in Griffith's early work he presumed these two quantities to be same, though this simplification was later recognised as inappropriate.

It is worth briefly considering the energies associated with the creation of an interface. If purely covalent bonds are broken at a polymeric interface, then an energy of approximately 1 J/m^2 would be predicted, which compares with the surface free energies of polymers which are 50 mJ/m^2. Yet the energy of fracture for polyesters and phenolic based polymers is normally in the range of 20 to 50 J/m^2. Clearly other modes of energy dissipation are operative in the zones around the propagating crack front in addition to those simply due to the creation of new fracture surface and hence the surface free energy of the system.

8.2.2 Brittle versus Ductile Fracture

Griffiths' (1920) original work on glassy materials provided a nearly ideal brittle substrate for the evaluation of his linear elastic model for fracture strength. However, there exist other modes of energy absorption in inelastic systems. These modes of dissipation include crazing, shear band formation, viscoelastic losses and plastic yielding or flow. The most important of these processes is plastic yielding or flow in the crack tip zone.

Plastic yielding of the materials creates two problems for the LEFM approach. Firstly, it leads directly to a blunting of the crack, and secondly it results in an additional energy absorption process which absorbs significantly more energy than that required to create new surface area **A**, γ.A. For small zones of yielding, Irwin (1947) has shown the Griffith approach is still valid. For such cases, the term 2γ is replaced by the quantity G_C which includes the energetic contributions of plastic yielding. The G refers to Griffith and the C stands for the critical energy release condition. In many cases the yield energy

component is many orders of magnitude greater than the surface free energy component and is generally 10^3 times greater.

The two most important mechanisms which contribute to plastic yielding are crazing and shear yielding. Shear yielding manifests itself in the formation of shear bands. These are regions of localised bulk yielding of the matrix in the direction of the maximum shears stresses which are usually disposed at 45° to the maximum tensile stresses. Crazing is a process by which material locally cavitates to form microvoids which are in turn spanned by orientated fibrillar material. The resultant systems may be described as a network of fibrils and voids.

The detailed approaches for constrained yielding, fully yielded and diffuse dissipation are discussed by Williams (1984) and other authors (Kinloch and Young 1983), and are beyond the scope of this introductory review.

8.2.3 Elastic Stresses Near the Crack Tip

For a crack within a homogeneous medium, Inglis (1913) showed that the stresses close to the crack tip were far greater than those in the bulk remote from the crack tip. The stresses, both normal and tangential to a crack, are directly dependent on the crack tip geometry and the externally applied stresses. The sharper, or less circular, the crack tip then the greater are the stresses. The ratio of the stress near the crack tip, σ_{tip}, to the bulk stress (at a relatively infinite distance away), σ_{∞}, defines the stress intensity factor **K** (Irwin 1957):

$$\mathbf{K} = \frac{\sigma_{tip}}{\sigma_{\infty}} \qquad (8.5)$$

Analysis of the stress around an elliptically shaped crack, subject to a constant bulk tensile stress normal to the principle axis of the crack, leads to a simple first order estimation for **K**:

$$K_I = \frac{\sigma_{tip}}{\sigma_\infty} = 1 + 2\sqrt{(a/r)} \qquad (8.6)$$

where the crack tip radius is **r**, **a** is the half crack length and K_I is the stress intensity factor in the plane normal to the crack.

Whilst examining the elastic stress distribution around a crack tip, Irwin (1957) derived an expression which contained the stress intensity factor, **K**. This expression relates the elastic stress field in the neighbourhood of the crack tip to the system loading and the geometrical configuration. **K** is thus a material independent property. However under conditions of fracture, **K** takes on a constant value, K_C, which is the critical threshold value for which fracture will proceed. K_C thus becomes a material dependent property. Irwin later demonstrated that **K** was intrinsically linked to Griffith's fracture energy **G** :

$$K^2 = \frac{E\ G}{(1 - \nu^2)} \qquad (8.7)$$

$$K^2 = E\ G \qquad (8.8)$$

for plane strain and plane stress respectively. Like the **K** values, the **G** parameters are material independent constants. Thus the energy approach of Griffith and the stress intensity method of Irwin are intrinsically equivalent and fundamentally linked together by Equations 8.8 and 8.9.

8.2.4 Modes of Fracture Failure

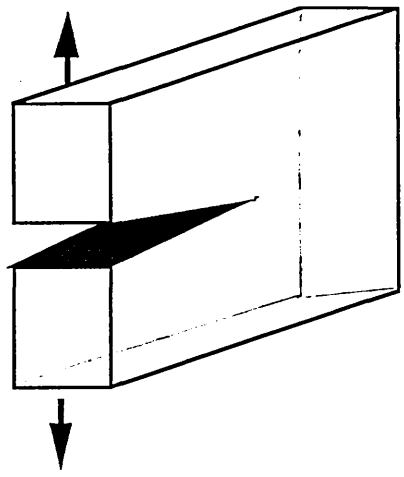
A number of modes of fracture failure for isotropic materials are possible and are shown in Figure 8.1. The mode of lowest fracture energy is usually the tensile, or the mode I mechanism, in which the crack propagates in a normal path to the maximum

principal tensile stress direction. In mode II failure, the crack propagates by the action of a plane shear stress parallel to that motion of the crack. Mode III failure is uncommon, but refers to an out of plane shear, or tearing, behaviour. Mixed modes of fracture failure are possible and mixed modes I/II have been found to be particularly important in practice.

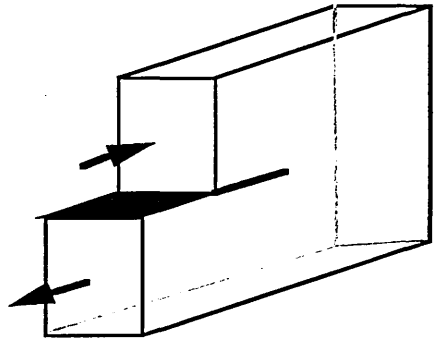
8.2.5 Measurement of Fracture Energies

A number of experimental methods have been developed for the measurement of G_C and K_C values. The specimen geometries shown Figure 8.2 illustrate some of the more common experimental configurations used for studying isotropic materials. For anisotropic materials these configurations are not always satisfactory and other special configurations have been developed for fibre laminates.

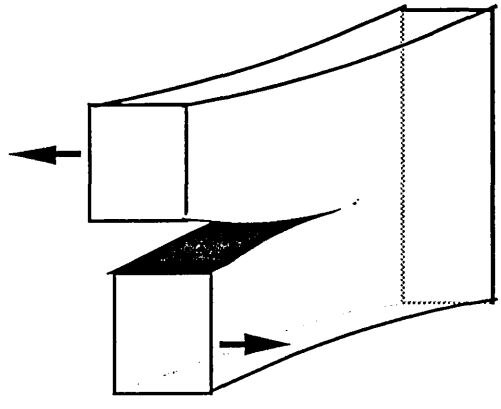
In virtually all of the test geometries shown in Figure 8.2 a starter crack or defect is introduced into the sample prior to the sample being stressed. During testing the change in the stored energy of the specimen is monitored as a function of deformation so the energy release rate G_C can be calculated. In the case of double cantilever beam specimens, parameters such as the crack lengths, the applied force and the displacements are measured. These experimental methods have been reviewed by Williams (1984) and other authors. Some of the experimental methods designed specifically for the study of fracture in fibre reinforced composites will be introduced later in this Chapter.



Mode I Fracture
Tensile Failure -K_I

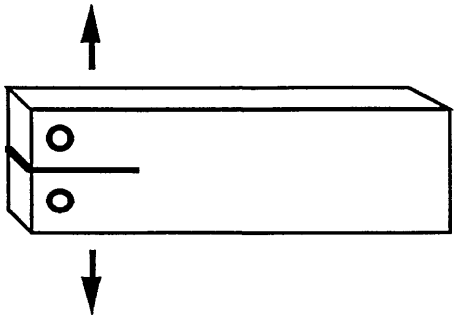


Mode II Fracture
Shear Failure - K_{II}



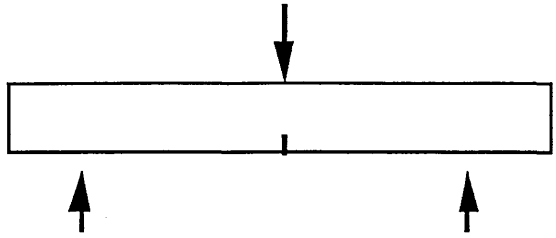
Mode III Fracture
Failure by Tearing- K_{III}

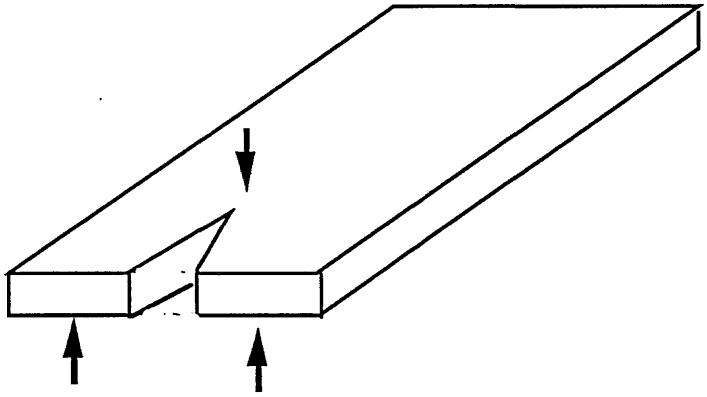
Figure 8.1 Modes of failure by fracture



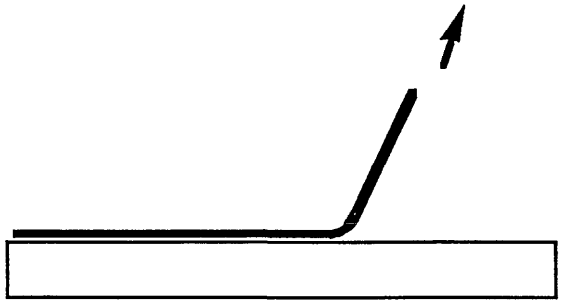
Double Cantilever Beam

Three Point Bend

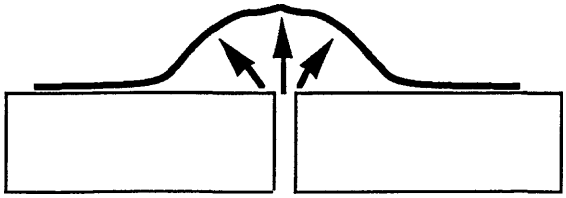




Double Torsion



Peel Test



Blister Test

Figure 8.2 Experimental methods for the measurement of G_C.

8.2.6 Fracture Behaviour of Epoxy Resins.

Prior to the consideration of the fracture mechanics of anisotropic composite materials it is appropriate to consider the fracture behaviour of epoxy resins. Epoxy polymers are the matrix phases in many advanced composite materials, including the materials explicitly studied in this thesis. A number of the important features of their fracture behaviour are now discussed.

The chemistry of the epoxy resin plays an important role in determining the G_{IC} values for these materials. The choice of epoxy moiety, crosslinking (hardener) chemical as well as the reaction stoichiometry can lead to significant changes in the material performance as shown in Table 8.1

The fracture performance of the epoxy resins can be significantly improved by the creation or addition of secondary phases in the resin. Significant increases in performance have been achieved via the addition of rubber particles and glass beads to epoxy resins. These additional phases can have dramatic effects on the micro-mechanics operating at the crack tip, as well as effecting the fundamental nature of the crack propagation process. Increases in G_{IC} of up to a factor of 10 can be attained via use of these additives.

The additional modes of energy absorption include cavitation in the rubber particles, or at the matrix-particle interface. However the most important process is the development of localised shear plastic yielding zones. The rubber particles interact with the stress field ahead of the crack front. The inclusion of glass particles, which can strongly adhere to the epoxy resin, results in another mechanism for energy absorption. In this case, the constraint of the propagating crack by the strongly bonded filler particles causes the crack to be deflected along secondary fronts which leads to additional energy dissipation. Epoxy polymers, which are used in most composite applications, are not normally toughened and usually exhibit fracture energies of between 200 and 300 J/m^2.

Epoxy Resin (Based on diglycidyl ether of bisphenol A.)	Crosslinking Chemical (Parts per hundred)	G_{IC} (J/m^2)
Epikote 828	diethylenetriamine (10)	172
	diphenyldiaminomethane (27)	340
MY 750	diethylenetriamine (11.5)	130
	tetramethylenediamine (12.2)	489
	hexamethylenediamine (16.5)	575

Table 8.1 G_{IC} values as a function of epoxy and crosslinking chemicals. (Kinloch and Young 1983)

8.2.7 Theoretical Fracture Mechanics of Composite Materials

The methods of stress analysis applied to isotropic materials have also been applied to anisotropic materials. Green and Taylor (1945) were two of the earliest workers to consider these anisotropic effects. They showed that the general effect of the anisotropy was to increase the local normal tensile and shear stresses and decrease the corresponding normal tensile stresses relative to the direction of loading. Wu (1968) has derived expressions for the stress distribution around a crack tip in an anisotropic material. He concluded that the stress intensity factor depended not only on the product $\sigma_\infty . \sqrt{a}$, but also on the orientation of the crack relative to the principle stress axes and the direction of the material's anisotropy. Other authors who have been involved in the pioneering work of applying fracture mechanics to fibre reinforced composites include Tetelman (1969) and Corten (1967) who have considered micro-mechanics aspects, Sih and Chen (1973) who

have considered mixed mode fracture and Konist *et al.* (1972) who applied the concepts of fracture mechanics to laminates. Olster (1970) has confirmed the validity of the stress intensity factor approach for composites and Irwin (1962) has derived the more complex relationships between **K** and **G** for anisotropic materials.

Other authors have considered the intrinsic mechanism for failure and energy absorption. Kelly (1966) has considered the case of a unidirectional composite under loading with a notch. He concluded that the laminate would fail in shear parallel to the fibre direction before it splits in the same direction in tension. Cook and Gordon (1964), and also Kelly (1966) have argued that the primary mechanism by which the stress intensity at the crack tip is reduced is by a process of fibre splitting. For a weak or brittle interface, the high matrix shear stress can result in splitting parallel to the fibres and perpendicular to the direction of crack propagation. However the dominant energy absorption mechanisms have not been generally explained.

8.2.8 Energy Absorption Mechanisms in Composites

These concepts have been reviewed separately in Chapter 10 which deals with the micro-mechanics of failure. However, the processes are presented here in an abbreviated form for convenience. Beaumont (1989) has recently reviewed in detail the micro-mechanics of composite fracture. He analysed a number of primary mechanisms by which fibres can absorb energy in a crack zone. They are :

(1) fibre debonding

(2) interfacial fibre friction

(3) fibre strain

The equations which describe the respective energy absorption mechanisms are :

$$E_d = \frac{V_f \cdot \sigma_f^2 \cdot y}{4E} \qquad (8.9)$$

$$E_s = \frac{V_f . \tau . y^2 . \Delta \varepsilon}{d} \qquad (8.10)$$

$$E_d = \frac{V_f . \sigma_f . L_c}{24} \qquad (8.11)$$

where V_f = volume fraction

σ_f = ultimate tensile strength of fibre

y = average debonded length of fibre

E = Young's modulus

τ = interfacial frictional shear stress

L_c = critical transfer length of fibre

d = fibre diameter

$\Delta \varepsilon$ = differential failure strain between fibre and resin

Details of the derivation and the origin of these equations are given in Chapter 10.

Using these equations, Beaumont has produced fracture maps which graphically represent Equations 8.9-8.11 and describe the regions wherein the various failure modes are dominant. Whilst this approach is fundamentally attractive, a lack of appropriate constants to input into these equations limits their widespread use.

8.2.9 Experimental Fracture Studies of Composites

One of the earliest reports on the fracture of composite laminates was by Wu (1965) who showed that K_{IC} was a material property for glass reinforced laminates. Schultz (1970) and Hamilton (1975) made the same conclusion for the fracture of glass fibre reinforced composites in Mode I failure. McKenna *et al.* (1975) and Mandell (1971) have also studied the fracture of glass fibre composites using various experimental model systems. One of the first studies of fracture in carbon fibre based composites was reported

by Larsen (1971) and also by Sidney and Bradshaw (1971). Later work has been reported by a number of workers including Scott and Phillips (1975) and more recently by Kageyama *et al* .(1987).

The previous work cited has concentrated on mode I fracture, though more recently a greater interest in Modes II and III fractures is becoming apparent. This interest has arisen primarily as a recognition that in anisotropic materials the crack is not constrained, in the same fashion as in isotropic materials. It may grow in a mode I manner, but also may propagate in directions other than those normal to the maximum principal tensile stress. For these types of measurements a number of new experimental sample geometries have been used in addition to the traditional specimen geometries. The cracked lap shear test has been used by Wilkins *et al.* (1982) and also by Johnson and Mangalgiri (1986). Benzeggah (1985) has used a cantilever beam specimen with an enclosed notch whilst Saczalski (1989) has studied modes I and II fracture in carbon fibre epoxy laminates using double cantilever beam (DCB) specimens. Hashemi *et al.* (1987) have also studied mode I, mode II and mixed mode I/II fracture of carbon fibre with PEEK and epoxy matrices using DCB specimens. Mode II fracture of a range of fibre-matrix systems has been reported by Prel (1987). O'Brien and his co-workers (1984) have used an edge delamination specimen for determining composite fracture toughness.

8.2.10 Fibre Bridging Effects in Composite Fracture

Fibre bridging refers to the phenomena of fibres being interconnected or bridging across the zone behind the propagating crack front. This phenomena is shown schematically below in Figure 8.3. Clearly the presence of fibre bridges constrains the growth of the cracks and thus represents a potentially important mechanism for preventing composite failure by interlaminar fracture.

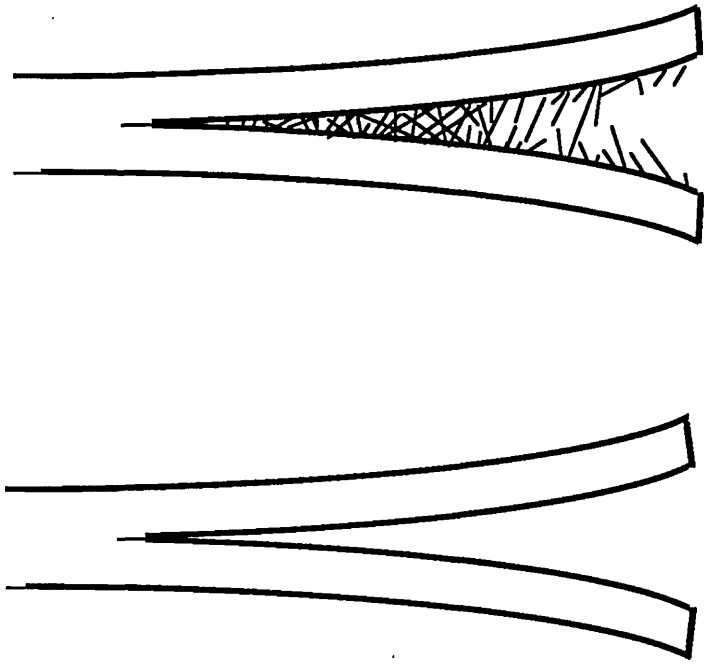


Figure 8.3 Schematic diagram showing crack growth with and without fibre bridging.

8.2.11 Experimental Studies of Fibre Bridging

A number of authors have reported the occurrence of fibre bridging in various studies of composite fracture.The earliest report is the work of Sidney and Bradshaw (1971) who studied carbon fibre epoxy laminates in mode I fracture. Slepetz and Carlson (1975) have reported that G_{IC} vales for unidirectional S-glass-epoxy composites increased with increasing crack length for compact tension specimens. The G_{IC} values increased by a factor of two from the initial values before reaching a plateau. Using double cantilever beam specimens, Phillips and Wells (1982) have reported an increase of over 5 in G_{IC} for unidirectional composites of carbon and glass fibres. Johnson and Mangalgiri (1986) have also described the occurrence of fibre bridging.

Huang and Hull (1989) have recently reported the effects of fibre bridging on G_{IC} for unidirectional S-glass-epoxy composites. They observed that the values of G_{IC} increased

with crack length by over a factor of six from those values where fibre bridging did not occur. The values for G_{IC} in the absence of fibre bridging were obtained using a novel solution technique in which the stressed (bridging) fibres were chemically induced to fracture. This induced rupture was possible since the E-glass fibres fracture at low stresses when exposed to dilute acid. The unbridged G_{IC} value of 235 J/m^2 was comparable to the values obtained for the pure epoxy resin.

Hunston *et al.* (1985) have concluded that fibre nesting and bridging can led to an increased resistance to interlaminar crack propagation and postulated that weak fibre-matrix bonding would decrease this resistance. De Charentenay *et al.* (1987) have briefly reviewed work on composite fracture and recently Saczalski (1989) has applied a factorial analysis to fracture toughness measurements which involved substantial fibre bridging in carbon fibre-epoxy laminates.

Since G_{IC} can increase very rapidly with crack length there is a current trend to attempt to measure G_{IC} very close to the starter crack. Davies *et al.* (1989) have carefully studied the nature of the crack initiation as function of method of pre-cracking. They concluded that thin single and folded aluminium foil gave reproducible G_{IC} values which were independent of starter crack length.

8.3 EXPERIMENTAL FRACTURE MECHANICS STUDY

8.3.1 Specimen Preparation

Eight ply laminates as described in Chapter 7 were used in the manufacture of specimens for the current fracture mechanics study. Prior to autoclaving, a starter crack or pre-crack was implanted between the fourth and fifth plies of the composite, near one of the outer free edges. The starter crack consisted of a 25mm x 200mm strip of aluminium foil which had been double folded and was aligned with the major axis of the laminate. The foil was coated with release agent (Frekote 44) which resulted in the creation of a non-bonding interface between the foil and the composite lamella.

Preliminary experiments verified that the relatively high compliance of the cross-ply "Kevlar"-epoxy (KE) composite necessitated the fabrication of 24 ply laminates to produce composites of sufficient stiffness to provide linear beam bending. However the significant wastage of material, and the effort required to produce laminates of this thickness, did not make it experimentally viable to use this approach for the main study. Williams (1987) has commented on this type of problem and has suggested a number of analytical routes for dealing with thin laminates to enable an improved estimation of the crack length to be made as well as better determination of the beam moments in LEFM. In this study it was decided to decrease the sample compliance by re-fabricating the sample. Sample fabrication was accomplished by bonding the KE laminate between two supporting glass reinforced epoxy (GRE) panels. This fabrication was effected by bonding onto both the top and bottom face of the KE laminate, 2mm sheets of GRE laminate. As well as significantly increasing the stiffness of the laminates, this process provided some practical advantages during the machining of the final samples.

The bonding of the GRE to the KE laminates was begun by roughening all the surfaces to be bonded with Al_2O_3 paper followed by degreasing and removal of surface debris via a solvent wipe with toluene. Both the GRE sheet and the KE laminate were precut into 140mm x 150mm pieces. For optimal adhesion, an epoxy "prepreg" film (Ciba-Geigy 913) was used as a thin film adhesive for the bonding. Four film layers were hot melt pressed onto the KE laminates. The GRE layers were then placed on the top and bottom and the bonding was accomplished by curing the epoxy within this new laminate in a hot press at 120°C at 0.7 MPa for 70 minutes.

The presence of these GRE layers minimised the common problems of edge "fuzzing" which occurs during the machining of KE laminates. Laminate fracture samples of nominal dimensions 130mm x 25mm x 6mm were cut using a radial saw. The cut edges of the individual fracture samples were then polished using various grades of Al_2O_3 to produce flat smooth edges.

Fracture mechanics tabs were machined from aluminium to a size of 25mm x 25mm x

10mm with a 5mm hole placed though the centre for the loading pins. The tabs, and the portions of the laminate sample to which they were to be bonded, were roughened with Al_2O_3 paper and solvent wiped prior to bonding the tabs onto the laminate with a toughened epoxy adhesive (Permabond Type E38). The laminates and tabs were aligned in a simple jig prior to curing at 70° C for 2 hours. Excess adhesive was removed after curing. Figure 8.3 shows the form of these specimens.

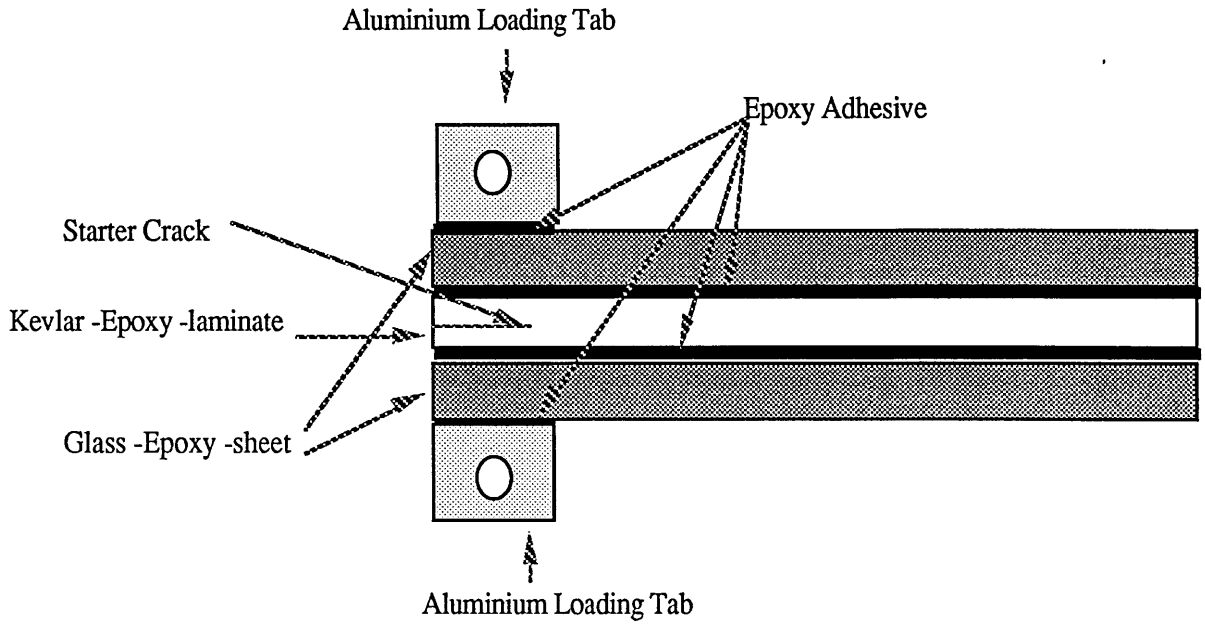


Figure 8.3 Schematic diagram of fracture mechanics specimen

To aid in the observation of the crack propagation, the laminate edge was coated with a thin layer of white liquid paper. A thin brittle coating resulted which gave high contrast between the cracked and non-cracked portions of the laminate. 25mm from the loadline position, lines were ruled vertically on the laminate's white coated edge at intervals of 5mm. These markings were used to locate the length the crack had travelled in the sample.

The samples were loaded in the the test jig (as shown in Figure 8.4) in an Instron Model 1022 Universal Testing Machine. A constant crosshead speed of 1mm/minute was

used in all experiments, with a full scale load of 50kg. Calibration was effected using 10kg weights.

The crack growth though the laminate was observed using a travelling microscope. As the crack passed over the sequence of crack length markers, an event marker on the Instron's chart recorder was tripped so that a simultaneous record of the loadline displacement, the imposed force and crack length was obtained. Four samples of 25mm in width were prepared and tested, as well as one of 15mm.

Crack propagation from the starter crack did not proceed satisfactorily for all samples. The primary problem which occurred with some samples was the transfer of the crack tip from the starter crack to the KE-GRE laminate interface, resulting in catastrophic delamination at that interface. It was particularly a problem for the laminates manufactured from diol grafted fibres. Inspection of the failed interface indicated that poor wetting and adhesion at this interface was the probable explanation. Poor adhesion was normally the explanation in these cases of KE-GRE delamination. No experimental results are reported for these cases.

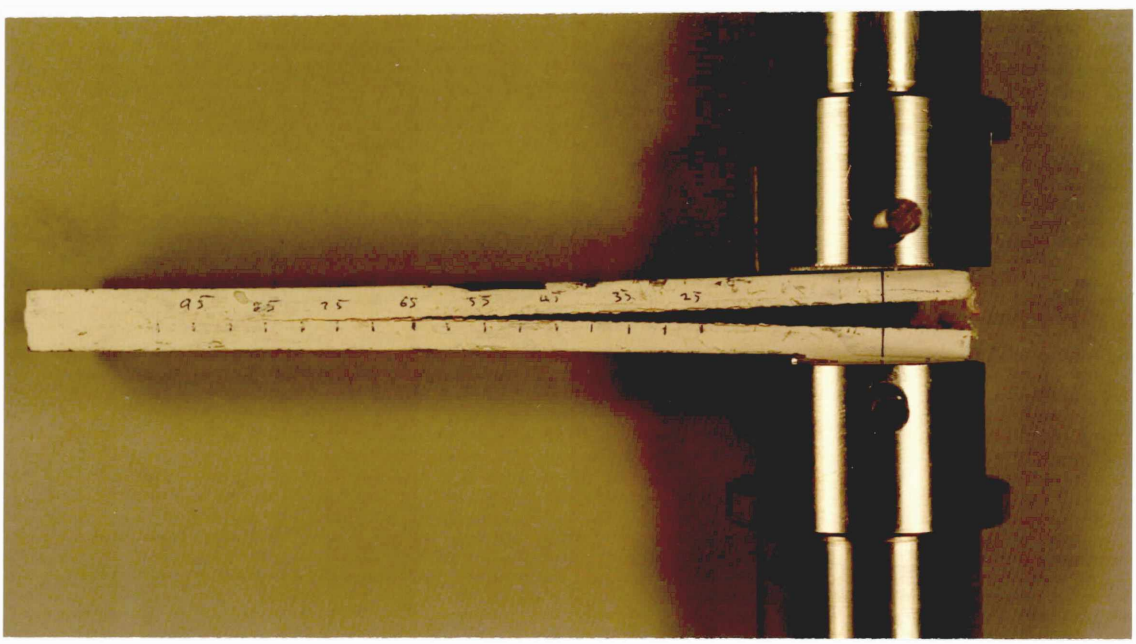


Figure 8.4 Fracture mechanics sample in loading jig of Instron Testing machine.

8.3.2 Determination of G_{IC}

For the simple double cantilever beam, the energy release rate G_{IC} is given by:

$$G_{IC} = \frac{3\,N\,d}{2\,a\,B} = \frac{N^2}{2B} \cdot \frac{dC}{da} \qquad (8.12)$$

where **N** is the force in Newton, **d** is the loadline displacement in mm, **a** is the crack length in mm, **B** is the sample width in mm and **C** is the compliance (**d / N**). This method for the determinations of G_{IC} is one of several alternatives and has been use extensively for measuring G_{IC} of polymeric materials at Imperial College (Williams 1988; Kodokian and Kinloch 1988; Hashemi *et al.* 1987). This method and other alternatives have been reviewed in detail by Guedra *et al.* (1987) and De Charentenay (1987).

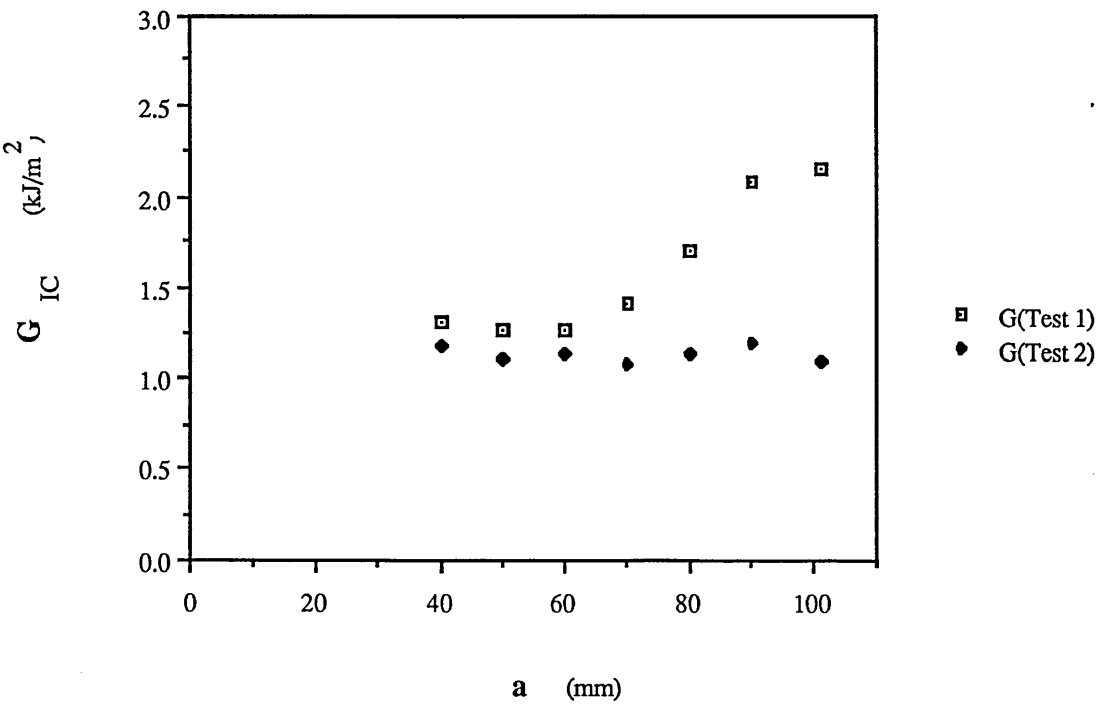


Figure 8.5 G_{IC} values as a function of crack length **a** for two different "Kevlar"-epoxy laminates.

G_{IC} is theoretically independent of the crack length for isotropic materials, and preliminary experiments were conducted to investigate whether the KE laminates behaved in the same manner. These preliminary experiments revealed two types of behaviour. For some systems it was observed that G_{IC} was clearly independent of crack length, whilst for other samples, this behaviour was not the case. Figures 8.5 illustrates the two types of behaviour observed. There are at least two possible reasons for the observed variations of the G_{IC} with crack length.

It is possible that the variation was related to errors introduced in the computed beam compliance **C**. Consequently a numerical method was evaluated for the estimation of the **C(a)** using a polynomial of fourth order Thus **dC/da** could be numerically estimated with the additional constraint that :

$$\frac{dC}{da} = 0 \quad \text{for } a = 0 \tag{8.13}$$

The beam compliance is simply the ratio of the loadline displacement **d** to the force, **N**,

thus : $$C(a)_i = \beta_0 + \beta_2 a_i^2 + \beta_3 a_i^3 + \beta_4 a_i^4 \tag{8.14}$$

Defining an error function ε :

$$\varepsilon = (C(a)_i - \beta_0 + \beta_2 a_i^2 + \beta_3 a_i^3 + \beta_4 a_i^4)^2 \tag{8.15}$$

Minimisation of ε with respect to β_0 , β_2 , β_3 and β_4 leads to the following relationships:

$$\frac{\partial \varepsilon}{\partial \beta_0} = 0 \quad \frac{\partial \varepsilon}{\partial \beta_2} = 0 \quad \frac{\partial \varepsilon}{\partial \beta_3} = 0 \quad \frac{\partial \varepsilon}{\partial \beta_4} = 0 \tag{8.16}$$

These equations constitute a linear algebra problem which can be expressed in matrix form as:

$$\begin{bmatrix} 1 & a_i^2 & a_i^3 & a_i^4 \\ a_i^2 & a_i^4 & a_i^5 & a_i^6 \\ a_i^3 & a_i^5 & a_i^6 & a_i^7 \\ a_i^4 & a_i^6 & a_i^7 & a_i^8 \end{bmatrix} \begin{bmatrix} \beta_0 \\ \beta_2 \\ \beta_3 \\ \beta_4 \end{bmatrix} = \begin{bmatrix} \Sigma_i C(a)_i \\ \Sigma_i C(a)_i a_i^2 \\ \Sigma_i C(a)_i a_i^3 \\ \Sigma_i C(a)_i a_i^4 \end{bmatrix} \qquad (8.17)$$

where the summations are from i=0 to i= n, for (n-1) data points.

This matrice problem was solved using a IBM microcomputer running a Fortran program which uses a triangular reduction method for determining the inverse matrix. These results and those using Equation 8.12 are shown below:

Crack Length a (mm)	Compliance C		dC / da		G_{IC}	
	Experimental	Numerical	Experimental	Numerical	Experimental	Numerical
40	0.0203	0.0191	0.00152	0.00178	1.12	1.30
50	0.0365	0.0379	0.00219	0.00201	1.39	1.27
60	0.0573	0.0596	0.00286	0.00237	1.54	1.27
70	0.0896	0.0862	0.00384	0.00300	1.82	1.41
82	0.130	0.129	0.00474	0.00423	1.91	1.70
91	0.170	0.172	0.00560	0.00562	2.07	2.08
102	0.248	0.247	0.00715	0.00800	1.97	2.15

Table 8.2 Experimental and numerical estimation of dC / da and G_{IC}

The results in Table 8.2 indicate that the crack dependence on G_{IC} is not an anomalous result associated with uncertainty in C. Though the numerical analysis was successful it was not used in the final data analysis as another methodology for estimating G_{IC} values was derived.

8.3.3 Fracture Mechanics Results

Figures 8.6 to 8.14 show the fracture energy, G_{IC}, as a function of the crack length, a, for a range of samples. The legend on the right hand side of the results figures denotes the specimen's number (G(1), G(2), G(2), G(2)) in the case of 25mm wide sample and G(T) for the 15mm wide specimen.

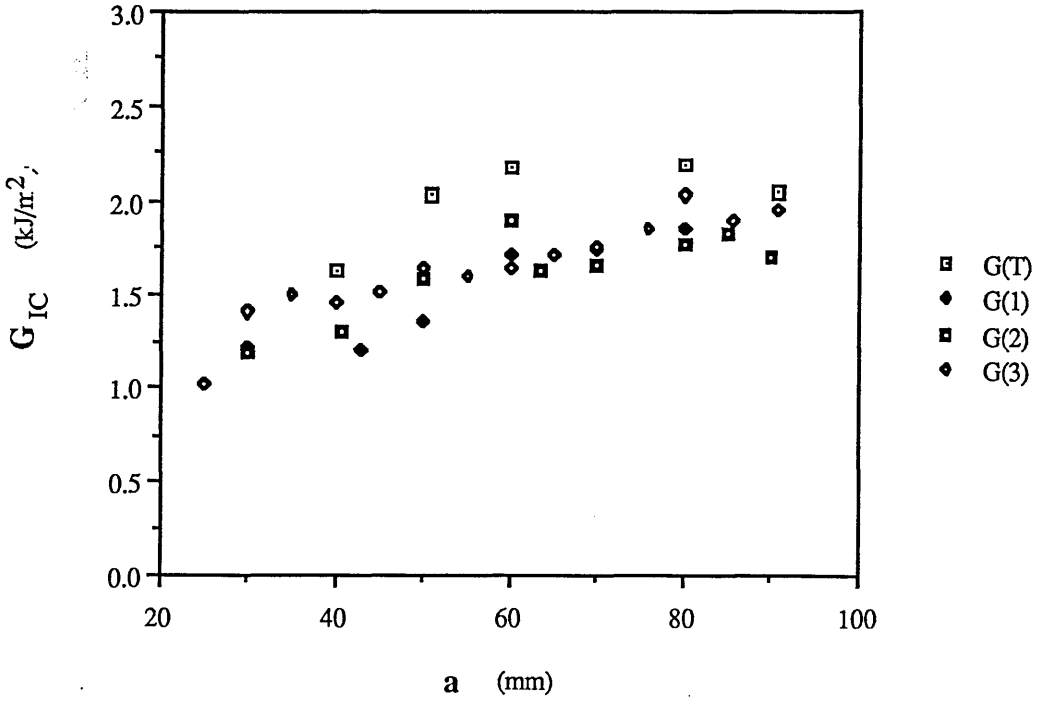


Figure 8.6 Fracture energy versus crack length for the amine treated fabric

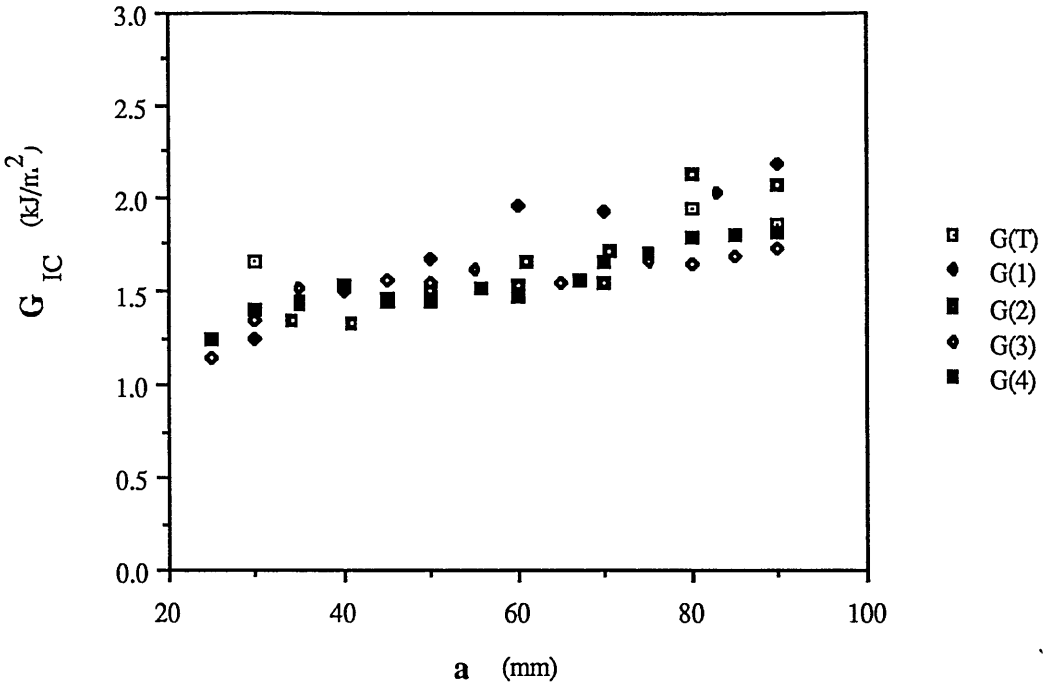


Figure 8.7 Fracture energy versus crack length for the "as received" fabric

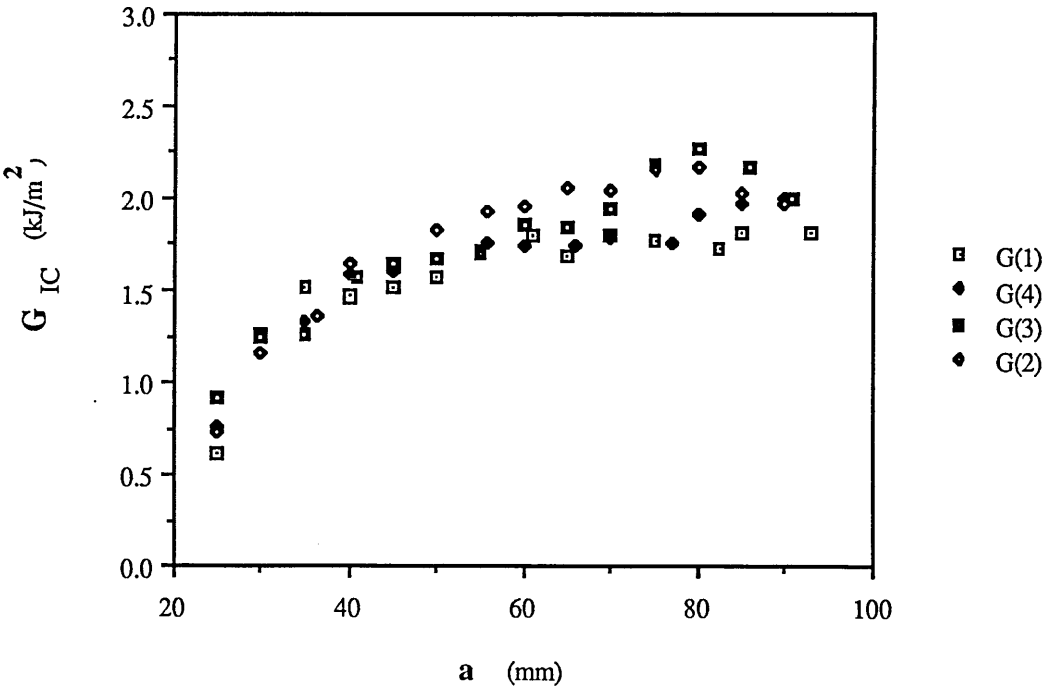


Figure 8.8 Fracture energy versus crack length for the clean fabric.

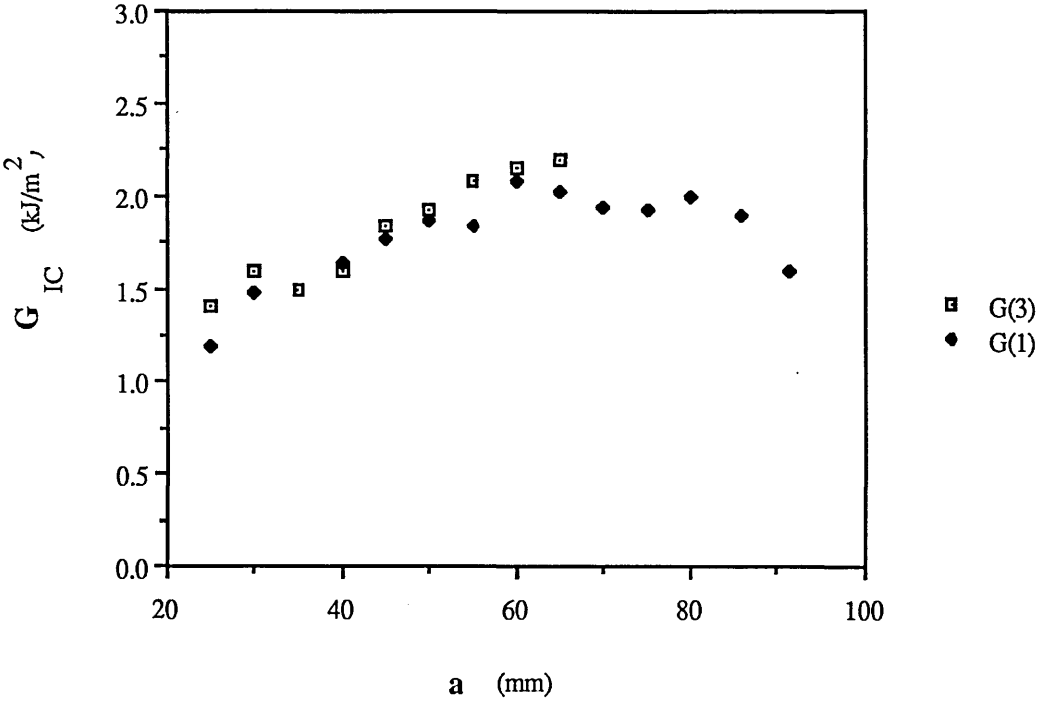


Figure 8.9 Fracture energy versus crack length for the diol grafted fabric

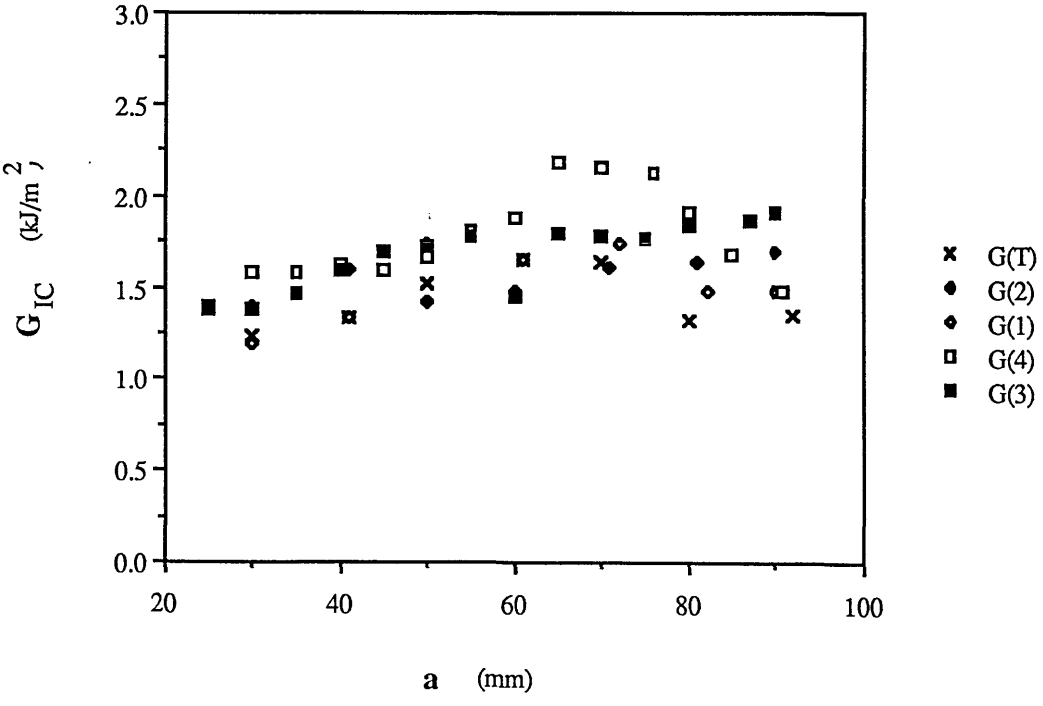


Figure 8.10 Fracture energy versus crack length for the epoxy grafted fabric

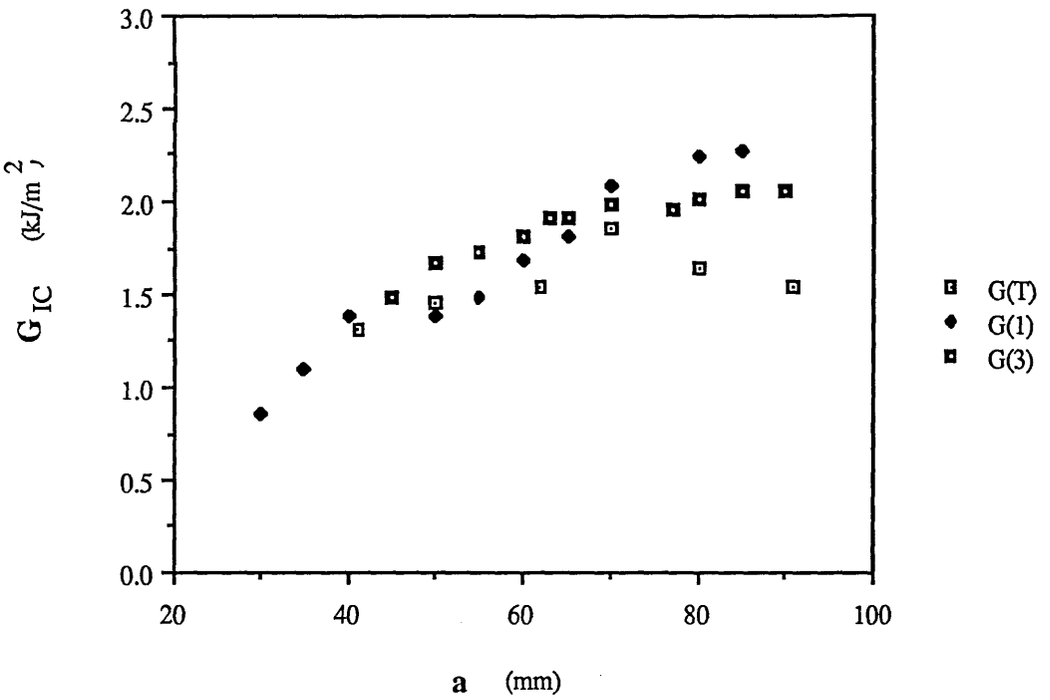


Figure 8.11 Fracture energy versus crack length for the epoxy coated fabric

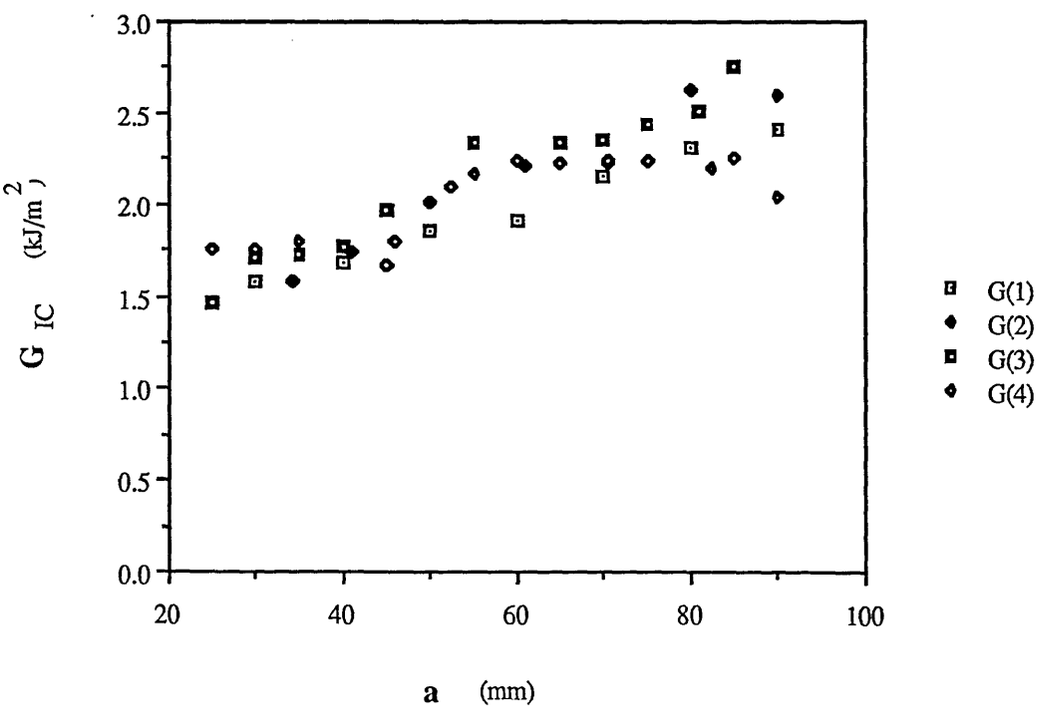


Figure 8.12 Fracture energy versus crack length for the PDMS coated fabric.

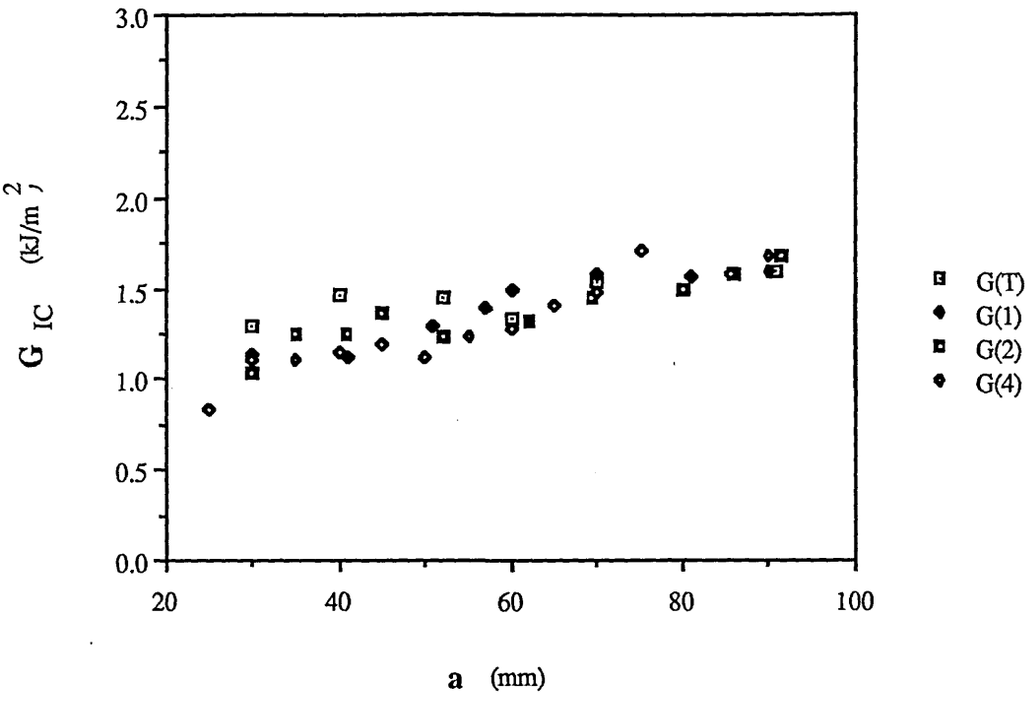


Figure 8.13 Fracture energy versus crack length for the PEG fabric

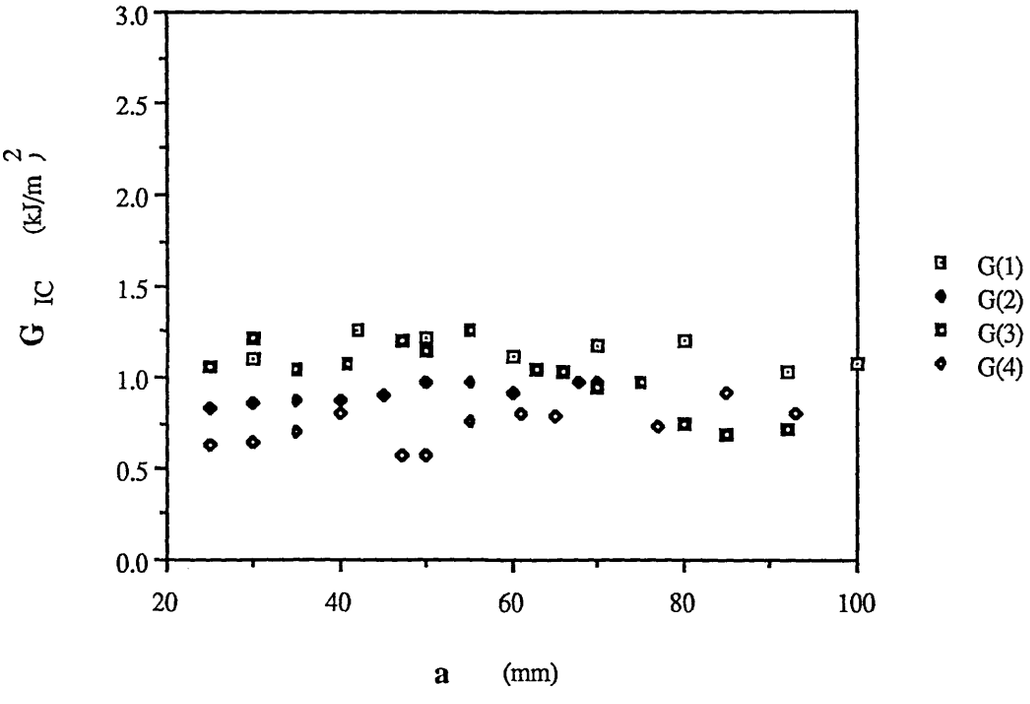


Figure 8.14 Fracture energy versus crack length for the metallated/clean fabric

8.3.4 Modelling the Effects of Fibre Bridging

Figures 8.6 to 8.14 clearly show that virtually all of the samples tested exhibited a pronounced dependence of the computed values of G_{IC} on the crack length, **a**. Visual inspection of the samples both during and after fracture indicated that substantial fibre bridging had occurred across the crack zone. The potential effects of fibre bridging on the interlaminar fracture process are now considered.

The effect of fibre bridging is to absorb some of the elastic strain energy of the strained cantilever beam specimen. Two primary approaches have been adopted for modelling the effects of fibre bridging on the observed G_{IC} values. These approaches are the reduced crack length concept and the uniformly distributed normal compressive force model.

In the reduced crack length concept, it is argued that the fibre bridged sample behaves like an unbridged sample with a reduced crack length a_{eff}, where a_b is a hypothetical negative crack length due to the fibre bridging constraint. Simply stated the argument is that a_{eff} is given by:

$$a_{eff} = a - a_b \qquad (8.18)$$

This approach was successfully used by Huang and Hull (1989) who determined that a_b varied with crack length with a constant rate of between 0.69-0.84 a_b units per apparent crack length. The authors concluded that the fibre bridging zone continuously increased in size during the crack growth process.

Wu (1985) has developed a model which equates the effect of fibre bridging with an effective uniformly distributed normal compressive force which closes the crack tip. Huang and Hull (1989) have also demonstrated that this method can be successfully applied to glass-epoxy composites to model the crack length dependence of G_{IC}.

8.3.5 "Kevlar"-Epoxy G_{IC} Results

Figures 8.6-14 show that the G_{IC} values increased with **a** (and a_{eff}) for all samples except the metallated/clean sample. Typically the G_{IC} values are in the range of 1.0 to 2.0

kJ/m^2. In a number of cases, such as for the clean fabric composites, it was observed that the values commenced well below 1.0 kJ/m^2 and rose sharply to the 1.0-2.0 kJ/m^2 range with the increasing of **a**. Later in this Chapter, a detailed analysis of the G_{IC} versus **a** graphs will be presented.

Examination of the samples revealed an important factor which may be relevant in the analysis of these data. Whilst the measurement of G_{IC} of the double cantilever beam samples commenced at 25mm or 30mm from the loadline position, the edge of the aluminium foil pre-crack varied between the various samples. It was planned that the pre-crack edge would be in close vicinity to the 25mm position. However a number of samples showed significant deviations from the optimum position as shown below:

Fabric used in laminate	Length from loadline to pre-crack edge (mm)
"As received"	13mm
Clean	20mm
Polyethylene glycol coated	18mm
Epoxy coated	14mm
Amine coated	18mm
Polydimethyl siloxane coated	11mm
Diol grafted	4mm
Epoxy grafted	13mm
Metallated/cleaned	3mm

Table 8.3 Pre-crack length for laminate samples

In the analysis of the fracture mechanics of homogeneous polymers the position of the pre-crack is of no real consequence. In contrast, for the accurate computation of G_{IC} values for materials in which substantial fibre bridging occur, appropriate measurements within 5 mm of the pre-crack are important.

8.3.6 Fracture Energy Analysis using the Reduced Crack Length Approach

An analysis of the G_{IC} values was undertaken using the reduced crack length concept as introduced in section 8.2.11.

To determine the validity of this approach for the analysis of the experimental data, the reduced bending force, **d.N/B**(see section 8.3.2), was plotted as a function of the crack length **a**. G_{IC} is given by the slope of the experimental data when plotted in this form. The intercept on the **a** axis would normally be zero for homogeneous materials. However in the case of fibre reinforced composites this crack length axis intercept will confirm, or negate, the validity of the negative crack length concept for describing the effects of fibre bridging.

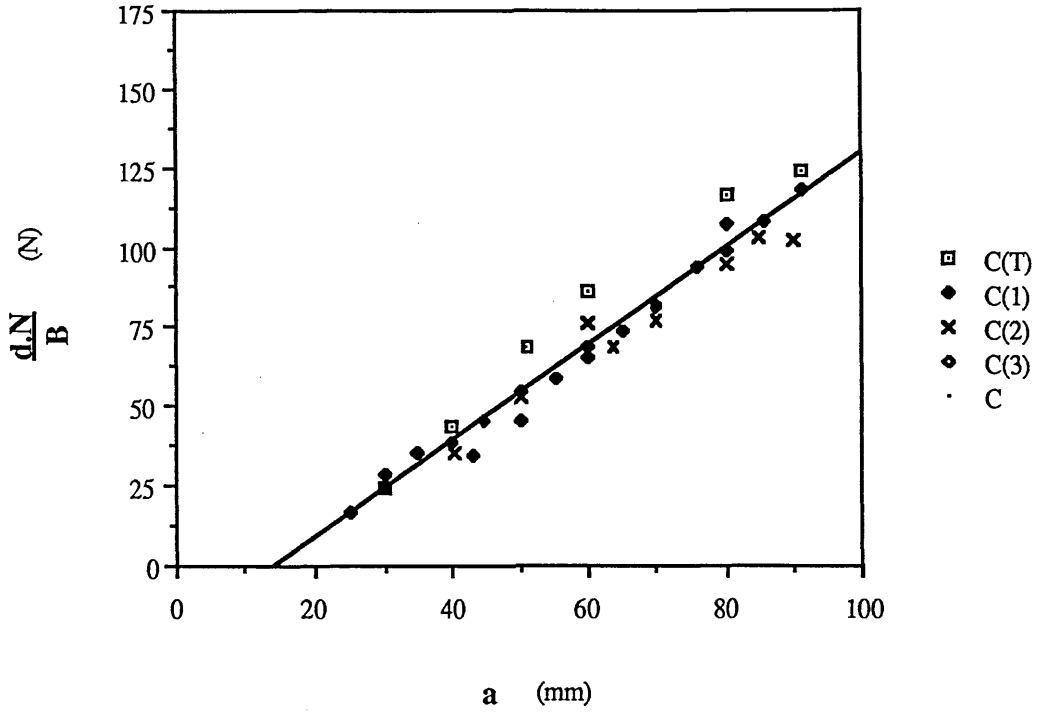


Figure 8.15 Bending Force versus crack length for the amine coated fabric

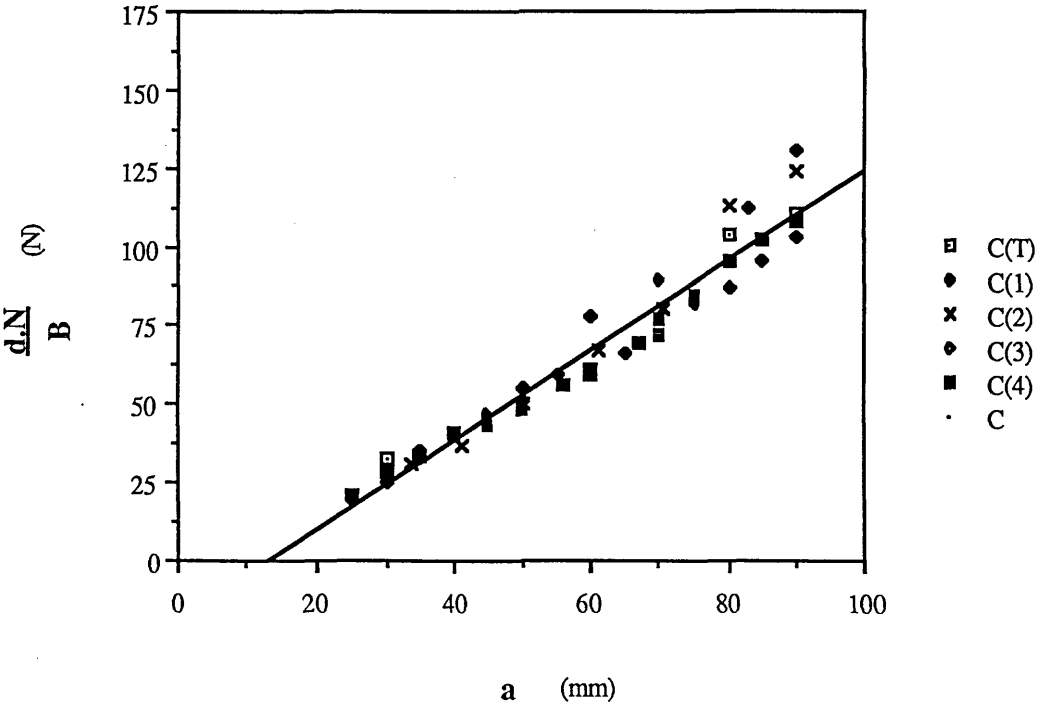


Figure 8.16 Bending force versus crack length for the "as received" fabric

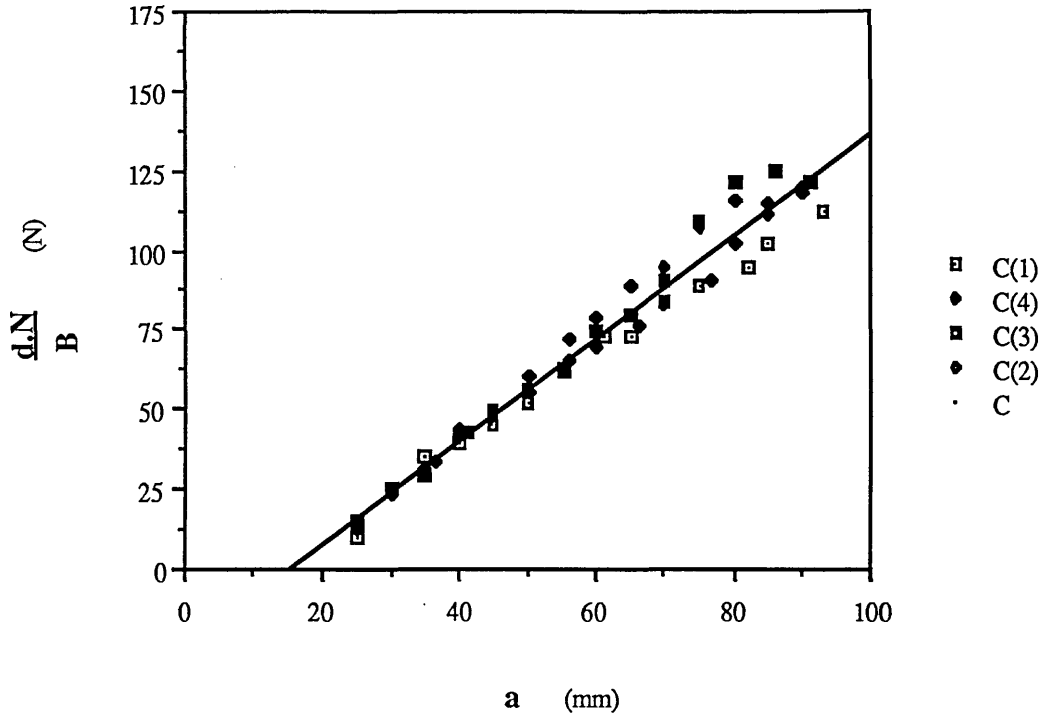


Figure 8.17 Bending force versus crack length for the clean fabric

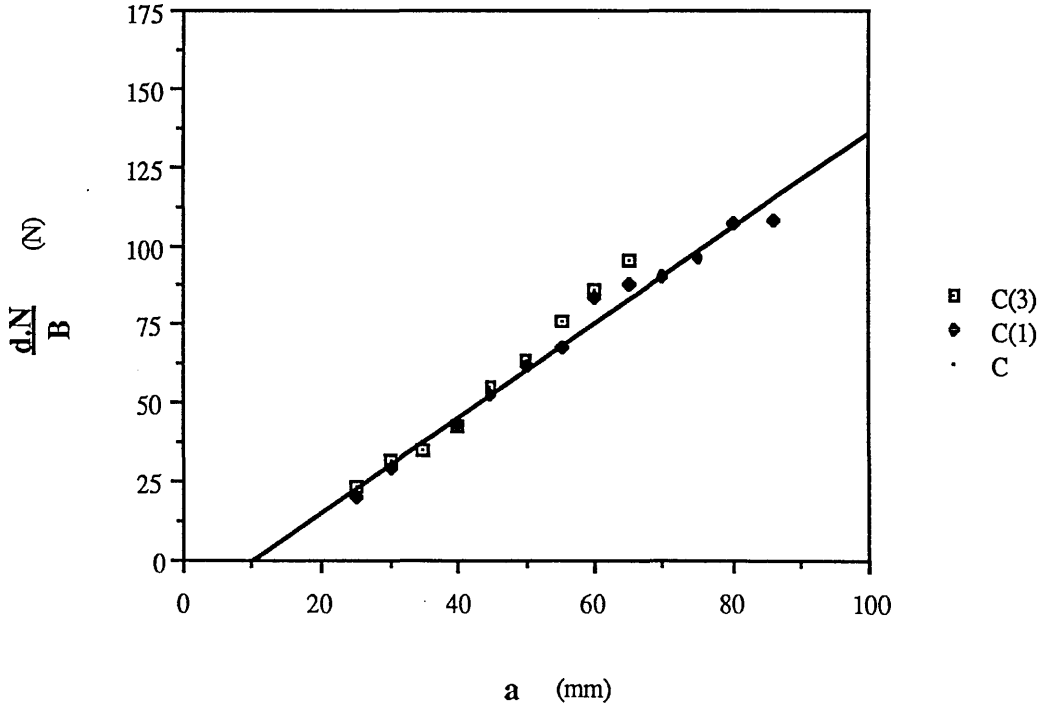


Figure 8.18 Bending force versus crack length for the diol grafted fabric

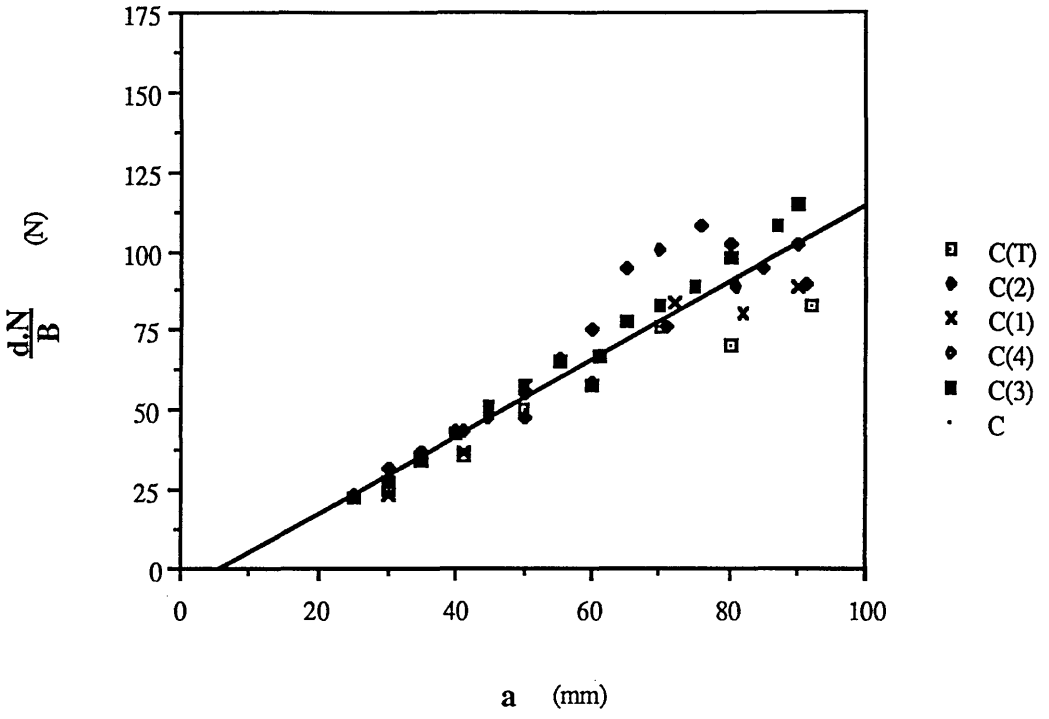


Figure 8.19 Bending force versus crack length for the epoxy grafted fabric

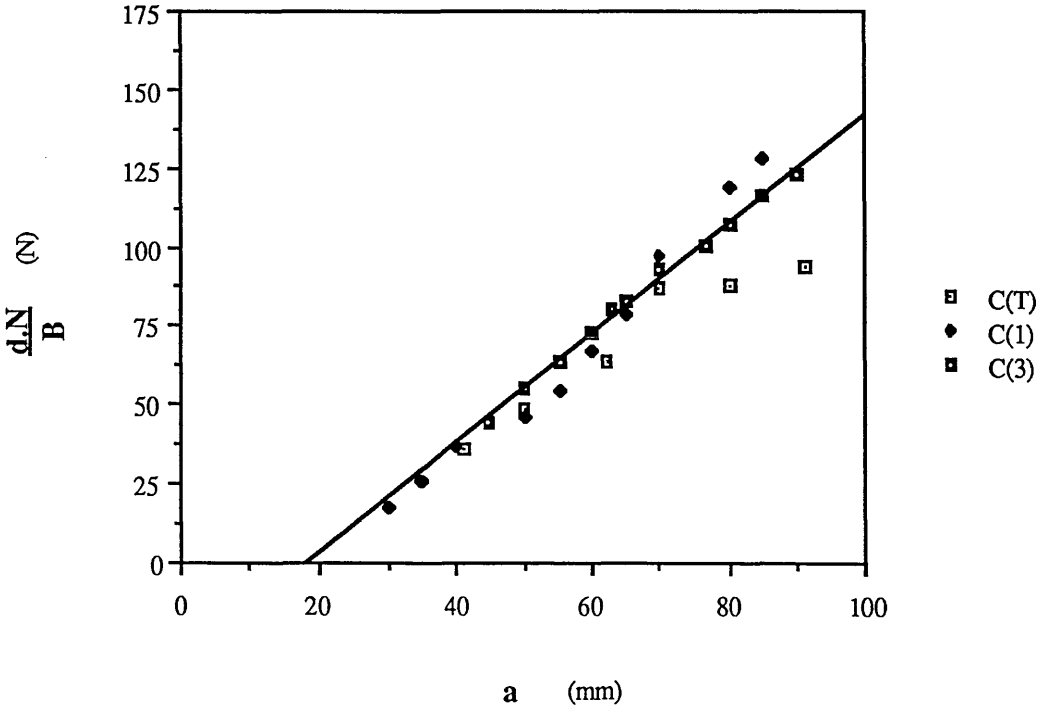


Figure 8.20 Bending force versus crack length for the epoxy coated fabric

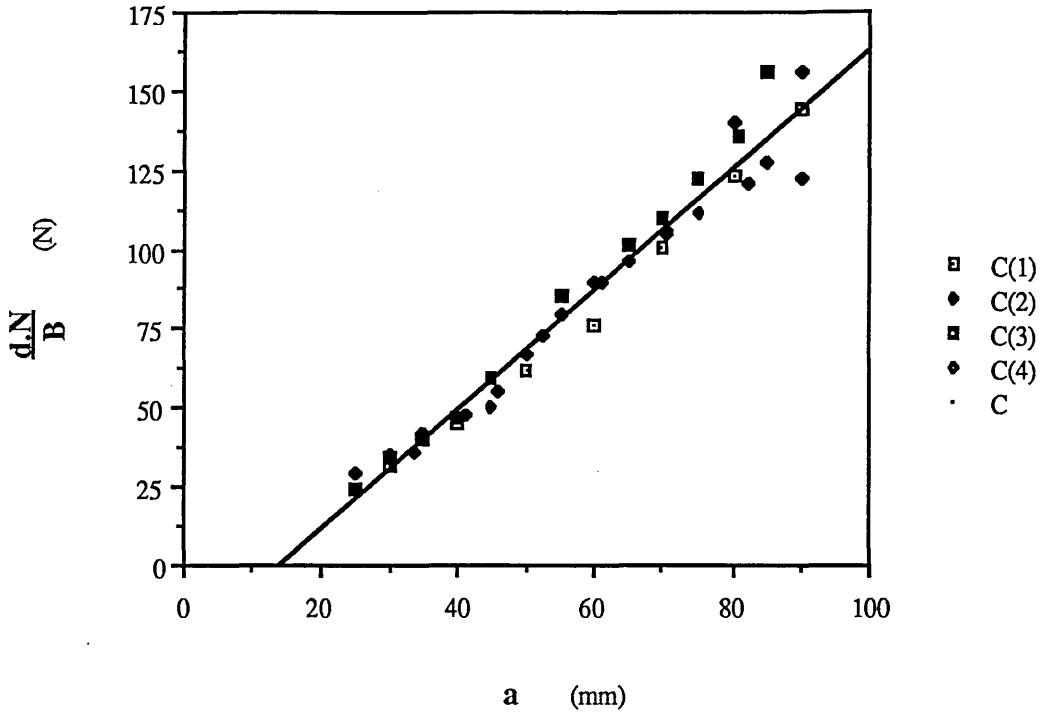


Figure 8.21 Bending force versus crack length for the PDMS coated fabric

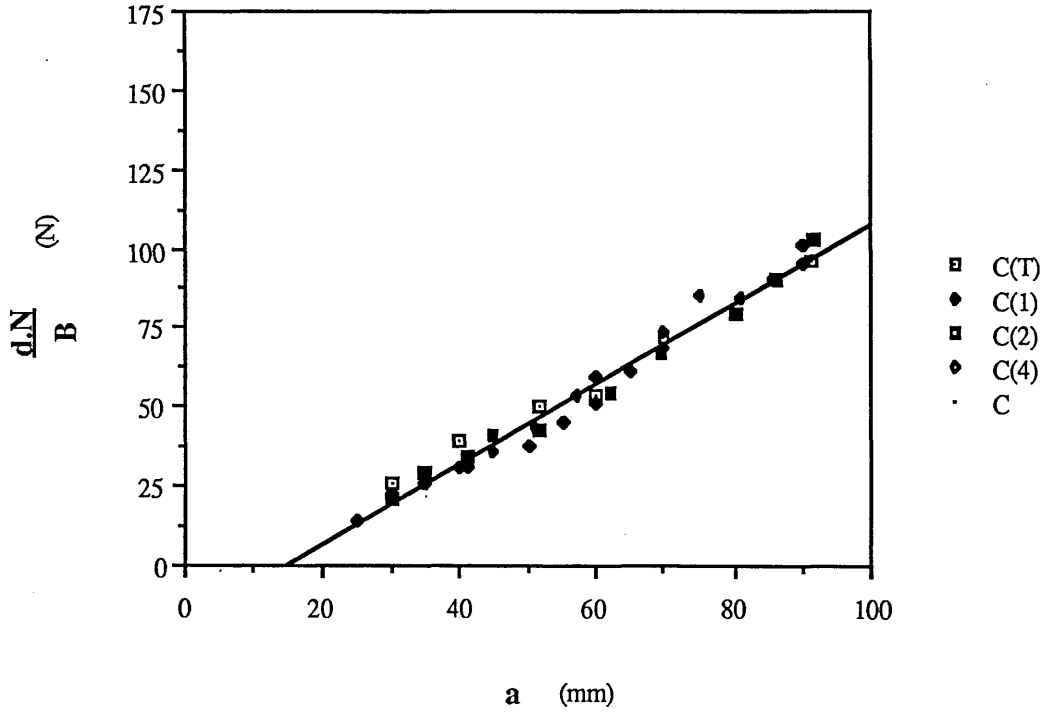


Figure 8.22 Bending force versus crack length for the PEG coated fabric

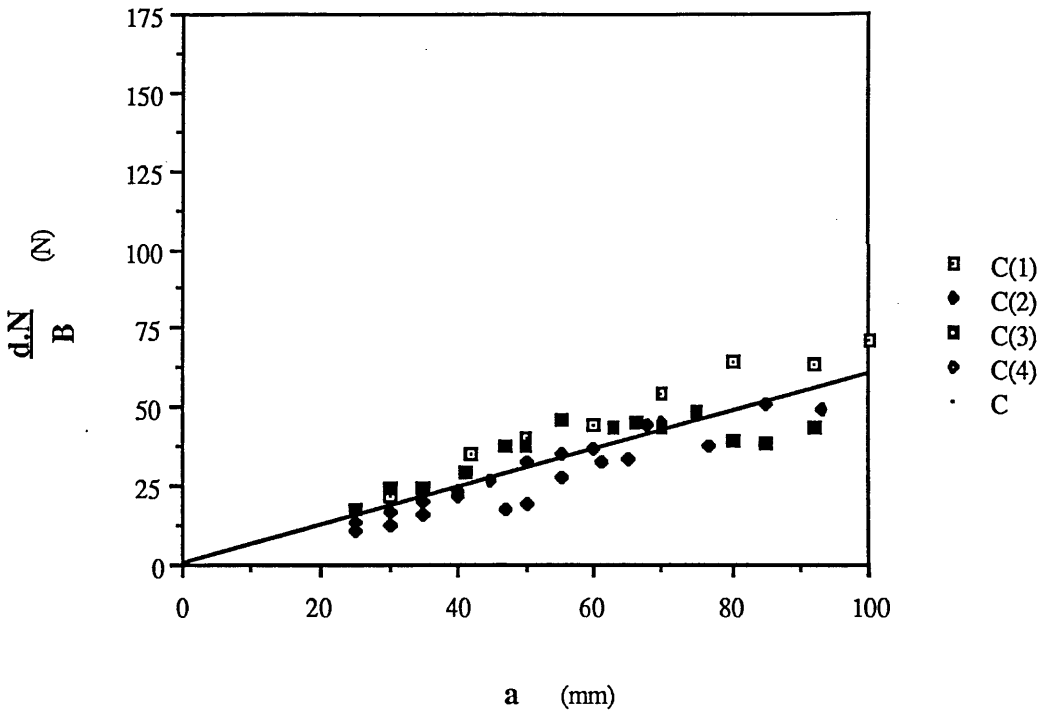


Figure 8.23 Bending force versus crack length for the metallated/cleaned fabric

	G_{IC} (kJ/m^2)	a_b (mm)	R
"As received"	2.15	13	0.97
Clean	2.41	15	0.98
Amine coated	2.25	14	0.98
Epoxy resin coated	2.58	19	0.96
Poly(dimethyl siloxane) coated	2.85	14	0.98
Poly(ethylene glycol) coated	1.89	14	0.99
Diol grafted	2.32	10	0.99
Epoxy grafted	1.83	5	0.94
Metallated/cleaned	0.90	-2	0.87

Table 8.4 Mode I fracture energy, G_{IC}, and the effective crack zone length, a_b , or various "Kevlar"-epoxy laminates. R denotes the co-efficient of fit for the linear regression data analysis

8.3.7 Discussion of Fracture Results

In summary, the results shown in Figures 8.15 to 8.23 indicate the existence of both :

(1) well defined non-zero values of a_b as deduced from the abscissa intercept of the graphs. These values typically exhibit lengths in the range between 10mm to 20mm.

(2) a linear slope of the bending force, **d.N/B**, with crack length, **a**, which defines the fracture energy G_{IC} .

This analysis leads to a number of significant conclusions. The practical validity of the use of an effective crack length concept is clearly demonstrated by the unique values of a_b presented in Table 8.4. The large coefficients of correlation for the data justify the choice of fitting a linear function to the data. The unique values for a_b support the premise that fibre bridging may be modelled on the basis of the effective crack length argument. The consistent values of a_b strongly support the contention that the fibre bridging zone progressively propagates itself in the wake of the true crack tip zone and in doing so absorbs a substantial amount of the fracture energy.

An equally important matter is the physical significance of a_b. There are two different concepts of this quantity. The first is that the length a_b is a true presentation of the fibre bridging, and thus energy absorption, zone. Alternately a_b may be considered as a quantity which directly scales with the true size of the deformation zone. It was visually observed during the fracture experiments that no fibre bridges were observed 50mm from the crack tip. Thus an upper bound estimate for a_b is 50mm.

In the following section, evidence which relates to this issue will be discussed in greater detail.

8.3.8 Presence of a Fibre Bridging Zone

The variations in the length of the pre-crack for different samples can result in differing values for G_{IC} at a particular value of **a**. This behaviour is not related to the

intrinsic energy of fracture, but is a direct consequence of the development of fibre bridging. For example, in the clean sample the first G_{IC} value is taken at 25mm from the loadline position.The pre-crack length for these specimens was 20mm, and thus a bridged crack length of 5 mm, out of the calculated crack bridge zone of 13mm, is included within the G_{IC} value calculated. This accounts for the dramatic increase in G_{IC} with **a** shown in Figure 8.24 as the fibre bridging zone is still increasing to the limiting value of 13mm. However for the case of PDMS coated samples, the pre-crack length of 11mm means that the first G_{IC} measurement at 25mm corresponds to a fully developed crack bridging zone since the fibre bridging zone is 14mm in length for these specimens. Thus for the PDMS samples, relatively constant G_{IC} values were measured which are not sensitive to the pre-crack length.

The non-chemically grafted fabrics gave consistent values of a_b in the range between 13 and 19mm. For the double cantilever beams fracture mechanics samples used in this study the separation of the fracture surfaces, corresponding to a position furthest from the crack tip (but within the fibre bridging zone) is about 200μm. Fibre bridging as a crack constraining mechanism for these materials is only effective across distances less than 200μm.

In summary, the reduced crack length concept may be used to predict the variation of G_{IC} with **a**. Figure 8.24 shows a good agreement between the experimental results and the predictions based upon this model.

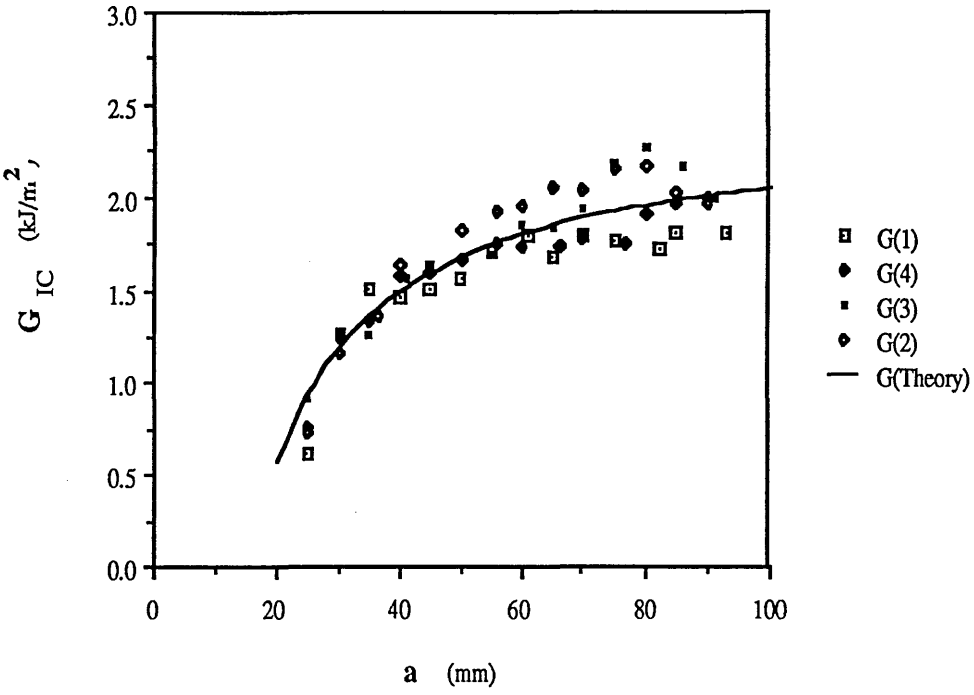


Figure 8.24 Experimental and predicted values of G_{IC} versus crack length, **a**, for the laminates made from cleaned fabric. Predicted values were estimated using the reduced crack length concept.

The success of the reduced crack concept in the interpretation of this data directly supports the proposition that a finite energy release rate is associated with the failure of the composite, even when significant fibre bridging occurs. Thus the energy absorption processes associated with fibre bridging are constant throughout the failure process and therefore fibre bridging may be viewed as a mechanism by which additional energy is dissipated during crack propagation. Certain quantitative aspects of the experimental results given in Table 8.4 are discussed after the examination of the fracture surfaces.

8.3.9 Microscopy of Fracture Surfaces

The fracture surfaces of the laminate samples were examined under both optical and electron microscopes so that the micro-mechanics of the failure process in the laminate could be examined. Figures 8.25 to 8.28 show both fracture surfaces for a range of samples as viewed under an optical microscope. The comments given in the following section on the appearance of the fracture surfaces are based on observations made using a stereo microscope. This microscope gave superior information compared with the photographic images shown in the Figures below. A number of clear trends and observations may be made from the inspection of the fracture surfaces. These are summarised below:

(i) Laminates based on the "As received" fabric

These fracture surfaces exhibited substantial amounts of exposed "Kevlar" fibres. These fibres were apparently free of epoxy resin and appear to have been both pulled away from the fabric layer which lies below. Some of these fibres have fractured but the vast majority of the fibres are simply debonded from the epoxy resin. These fibres maybe the ones involved in the fibre bridging effect. The epoxy fracture surface shows the "beddings" from which the fabric has fractured, with a small number of fibres still embedded.

(ii) Laminates based on diol grafted fibres.

The fracture surface of this sample was different from those described above. The exposed fibres show considerable evidence of less fibre "pull-out" and thus disruption of the fabric network. The epoxy surfaces show some fibres still embedded as in (i).

(iii) Laminates based on epoxy grafted fibres.

A further significant change in the nature of the fracture surface of this sample is clearly shown above. On the fibre dominant fracture surface, the extent of fibre pullout is significantly less than (ii) and substantially less than (i). The fibre bundles seem to exhibit a

strong affinity for the epoxy resin and in fact it seems that the fibre-epoxy bundles have actually fractured from the other fracture surface in an integral process. These fracture surfaces generally show a considerable amount of exposed epoxy, suggesting a brittle epoxy rather than a fibre based, fracture process. The epoxy fracture surface exhibits a well defined topography from where the fabric bundles have been removed. Where significant fibre pull-out and debonding has occurred on the fabric yarn it has occurred predominantly for the fibre bundles which pass over only one yarn, rather than those which pass over three yarns.

(iv) Laminates based on metallated/cleaned fibres.

Some exposed fibres are observed but essentially both fracture surfaces are similar to (iii). The fibre dominated fracture surface indicates that the fibres are well wetted and that the relatively few fibres that have been pulled out, leave behind what is essentially a brittle epoxy fracture surface. As previously noted, the surface treatment of this fabric has caused the fibre bundles to wick together resulting in gaps or holes in the cloth weave. Epoxy resin has penetrated through these macroscopic holes and the brittle fracture of these epoxy sections is shown especially well in the epoxy dominated fracture surface.

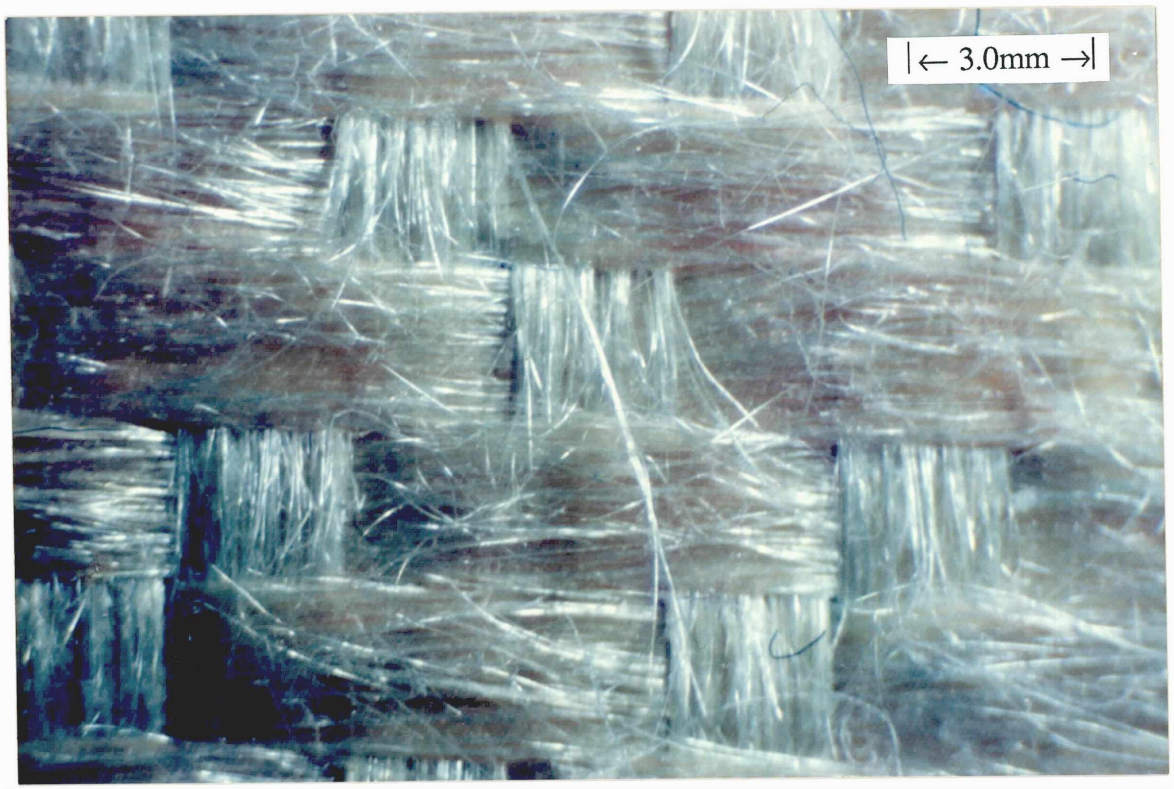


Figure 8.25 Fractography of the laminate based on the "as received" fabric



Figure 8.26 Fractography of the laminate based on the diol grafted fibres.



Figure 8.27 Fractography of the laminate based on the epoxy grafted fibres.

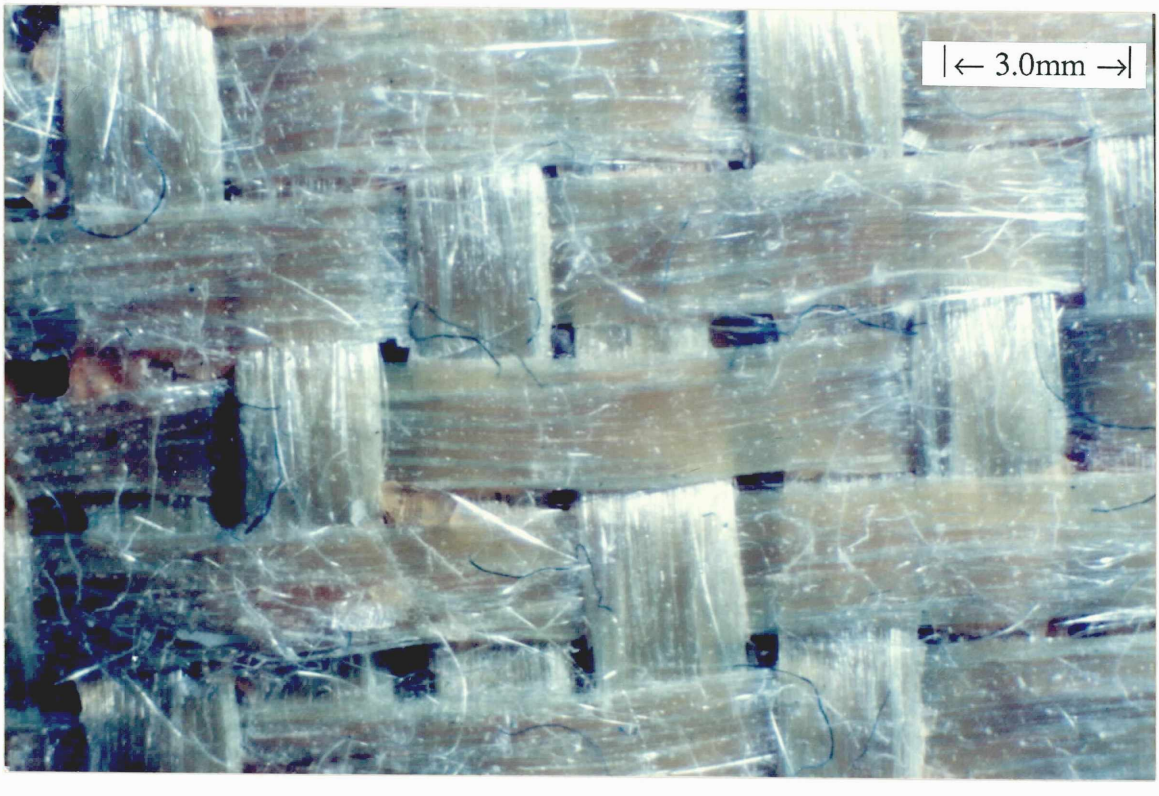


Figure 8.28 Fractography of the laminate based on the metallated/cleaned fibres.

8.3.10 Mechanism of Laminate Failure

Combining analyses of both the fractography observations and the fracture mechanics allows a number of interrelationships between the failure micro-mechanics and the material's performance to be proposed:

(i) the fractography figures confirm the presence of substantial fibre debonding and fibre pull-out on the fracture surfaces. There is a good qualitative correlation between the extent of the fibre debonding and the fibre pull-out, the G_{IC} values and also the extent of fibre bridging as indicated by the negative crack length parameter a_b (shown in Table 8.4).

(ii) composites fabricated using chemically grafted "Kevlar" fabrics showed little propensity to undergo fibre debonding and/or fibre pullout. These fracture surfaces show a fundamentally brittle epoxy mode of failure. The epoxy grafted and metallated/cleaned "Kevlar" fabrics show this brittle failure especially and it is these two samples which exhibit the lowest G_{IC} values and the smallest a_b values. There are two possible reasons for this observation which are discussed in the following section.

The first explanation is an increase in the intrinsic adhesion between the fibre and the epoxy resin. This argument is directly supported by the large value of G_{IC} obtained for the epoxy grafted fibres even though fibre bridging zone, as indicated by a_b, was significantly less than for many of the other samples. The other explanation considers the two grafted fabrics in terms of fabric mechanics. As previously noted, these two grafted fibre samples exhibited a different fabric structure and appearance. The fibre bundles within these fabrics were wicked together, resulting in a more open fabric weave, and the fabric also had a stiffer "feel" compared with the other samples. These changes in the fabric and yarn mechanics might be expected to constrain the migration of fibres across the laminae boundaries during fabrication. This constraint would thus restrict the fibre interpenetration anticipated to be necessary for the creation of significant fibre bridging. Indeed the high G_{IC} values obtained for the PDMS treated fabrics strongly suggest that interfilament and

interyarn friction are important factors in controlling the extent of fibre bridging. This aspect of fabric and yarn mechanics is considered in Chapter 10.

8.3.11 Conclusions

The following conclusions concerning the fracture of lamines may be made :

(i) the practical validity of using an effective crack length model for describing fibre bridging effects in the mode I fracture of "Kevlar"-epoxy laminates is clearly demonstrated. This model suggests that a uniquely defined zone exists in which fibre bridging occurs and that this zone progressively propagates in the wake of the true crack tip

(ii) a plot of bending force, **d.N/B**, versus crack length, **a**, is a new and useful way of estimating G_{IC} and the effective size of the fibre bridging zone, a_b.

(iii) substantial toughening with respect to mode I fracture, can be achieved via extensive fibre bridging across the crack zone. The topographical features of the fracture surfaces show a strong correlation between the computed length of the crack bridging zone and the extent of debonded and pulled out fibres observed. The extent of this fibre bridging effect is be thought to related to fibre-fibre friction and/ or the fibre-epoxy bond strength.

(iv) fibre bridging can lead to G_{IC} values of nearly 3 kJ/m^2 for the crack propagation. Thus, these materials exhibit a toughness performance similar to thermoplastic based matrix-fibre composites.

CHAPTER 9

BALLISTIC PERFORMANCE

9.1 INTRODUCTION

Polymer composites incorporating man made fibres are important materials for providing protection from high speed projectiles. As well as the more obvious military applications, ballistic performance is an important consideration for the design of structures likely to be subject to foreign object damage such as turbine engine casings and space vehicles. The superior ballistic performance of organic materials is due to the high strength and modulus of the reinforcing fibres. The superior strength and stiffness of aramid and polyethylene fibres results in their use in composite materials designed for ballistic protection.

In this Chapter the ballistic performance of advanced fibre reinforced composites is reviewed and discussed. In the second part of this Chapter, an experimental study of the ballistic performance of "Kevlar"-epoxy laminates is presented.

9.2 ADVANCED POLYMERS AND BALLISTIC PERFORMANCE

9.2.1 Literature Review

The use of organic materials for ballistic protection parallels the development of advanced engineering polymers. The development of nylon 6,6 ultimately led to the use of this material, in a fabric form, for the protection of aircraft crews during the Second World War. At the same time glass fibre reinforced polyester laminates began to be used to provide ballistic protection. The successful use of glass fibre reinforced composites for

providing ballistic protection was unexpected, since both the glass fibres and the epoxy resin individually offer poor performance under ballistic impact. The success of this composite systems was due to the presence of a weak fibre-matrix interface. This synergistic benefit was ascribed to the intrinsically weak interface which allowed significant deflection of the propagating cracks. Later research showed that optimum performance of these laminates was obtained when the resin level was kept to a minimum. This level was normally defined by the structural performance required of the material and was typically between 15% to 25% of resin by volume (Rugger and Fenter 1971).

During the 1950's improved ballistic armour was manufactured based on nylon fibres. In most cases these materials consisted of nylon fabrics impregnated by a polyvinyl-butyral/phenolic resin system. However for this particular material, its ballistic performance could be understood simply on the basis of the nylon content of the composite. No advantage associated with presence of a fibre-matrix interface was observed for this material (Lastnik 1962).

The development of high strength and high stiffness organic fibres during the 1970's led to a new generation of ballistic materials. The three classes of fibres which were developed during this time were carbon, aramid and polyethylene fibres. All three of these fibres were candidate materials for use in ballistic protection applications.

As has been previously shown for nylon reinforced materials, it was established that the ballistic performance of aramid composites is a linear function of the fabric weight per unit area incorporated into the laminate (Bowyer 1980). Kruger (1983) has investigated the ballistic performance of aramid based laminates and has considered specifically the effect of the fibre-matrix interface on ballistic performance. A number of laminate materials whose adhesion strength varied, as determined by T-peel tests, were evaluated using ballistic impact experiments. Although the adhesion varied considerably amongst the laminates, the ballistic performance of all the different materials was very similar. However, the laminate with the poorest adhesion gave slightly better ballistic performance. Kruger also concluded

that tough thermoplastic matrixes, such as polycarbonate, gave superior performances to those given by thermoset matrixes such as epoxies and polyurethane polymers.

Shepherd (1983) has studied the ballistic performance of both aramid fabric and aramid laminate materials. This study compared the ballistic performance of free "Kevlar" fabric with two different "Kevlar" laminate systems; one had a silicon rubber and the other a polyester matrix phase. He concluded that the free fabric offered better performance than the laminate with the silicon rubber matrix, which was in turn superior to the laminate with the polyester matrix. This author has also studied specifically the delamination behaviour of aramid composites under ballistic loading. It had been previously suggested that delamination during ballistic deformations is a beneficial process due to the absorption of additional energy. However, Shepherd has observed that composites which contained a number of separately impregnated plies, relative to a composite in which the plies are all simultaneously impregnated, gave inferior ballistic performance.

Dorey *et al.* (1978) have reported on the impact performance of carbon/"Kevlar" hybrid materials. The inclusion of "Kevlar" plies within the carbon fibre composites was found to improve the laminate's impact performance. Dorey (1987) has also reviewed in detail the impact performance of carbon fibre reinforced composites. In carbon fibre reinforced composites the interfacial bond strength is increased by a oxidative surface treatment, resulting in a significant increase in the interlaminar shear strength and the most brittle material failures. However most of the work discussed relates to low velocity impacts of less than 50m/s which can inflict critical damage to these materials. This damage is a result of the brittle nature of composite and the size of the damage zone has been established to be dependent on the interfacial bond strength. Pure carbon fibre composites fail catastrophically at impact velocities of 80m/s and thus are of not useful in primary ballistic protection applications.

The development of high modulus polyethylene fibres such as "Spectra" which are manufactured from an ultra high molecular weight polyethylene has resulted in a number of

recent reports. Bhatnagar *et al.* (1989) have studied the ballistic performance of "Kevlar", glass, and "Spectra" fibre reinforced composites, as well as a number of hybrid variants. The materials evaluated in this study were commercial or potentially commercial in their fabrication and composition. The authors concluded that "Spectra" reinforced vinyl ester composites gave better ballistic performance relative to those given by "Kevlar" phenolic/polyvinyl butyral, as well as the other materials examined, in addition to a significant weight saving. Prevorsek (1989) has recent reported on the ballistic performance of "Spectra" fibre reinforced elastomers. These materials consisted of 0/90^{o} orientated unidirectional fibre layers held in place by a soft polymeric matrix. These materials were observed to offer superior ballistic performance to "Kevlar 29" fabrics due to the additional modes of energy absorption associated with fibre flattening, the compression of the impact zone and the longitudinal straining of the fibres.

Briscoe *et al.* (1989) have recently shown that the ballistic performance of aramid fabrics could be modelled on the basis of static fabric mechanics. The fibre-fibre friction was established as an important factor in the absorption of impact for fabrics subject to high speed ballistic impact.

9.2.1 Conclusions

Aramid and polyethylene fibres are currently the most suitable high modulus fibres for the inclusion in materials designed to withstand ballistic impact. Whilst the fibre-matrix interface has been shown to be important for glass fibre polyester composites, the importance of the interface for aramid fibre laminates has not yet been established.

9.3 EXPERIMENTAL BALLISTIC STUDY

9.3.1 Equipment

Ballistic impact experiments were conducted using a high speed gas gun. The gas gun test equipment consists of two major components. The first section of the apparatus fires the projectile and the second part consists of a sealed cavity in which the specimens are impacted. Using high pressure gas, the gas gun fires a high speed ball bearing into the sample cavity. This cavity is essentially a rectangular steel box, with polycarbonate windows and contains sensors for measuring the projectile velocity and apparatus for holding the test specimen .

Figures 9.1 and 9.3 show the high speed gas gun schematically and pictorially. The gas gun relies on a pulse of high pressure gas to accelerate a cylindrical polyethylene sabot (40mm length x 25mm diameter) containing a small stainless steel ball bearing (diameter of 6.35mm) through the gun barrel (1 metre long, bore 25.4mm). The gas pulse is obtained via the use of a low and high pressure gas chambers, and an electromagnetic release valve. The sabot is stopped by a steel plate at the end of the barrel which contains a small hole, large enough to allow the ball bearing to pass through. Entering into the test cavity, the ball bearing passes through a pair of infrared beams which permits the projectile velocity to be measured prior to impact . After impact with the specimen, if the projectile passes through the specimen, the exit velocity will be sensed by a second pair of infrared beams. The signals generated by the projectile crossing though the infrared light beams were electronically differentiated and smoothed. These signals were captured with a 20 MHz digital storage oscilloscope (Hameg oscilloscope model HM205) and retrieved after the impact to compute the velocities.

Samples were cut from the aramid-epoxy laminate panels into 75mm x 75mm specimens as previously described in Chapter 7. Four specimens of each laminate type were prepared. Specimens were supported by four 15mm ball bearings which formed a

square pattern of 50mm in length as shown below on the vertical sample support assembly (see Figure 9.2). The sample rested against the support structure. This assembly was held rigidly against the main apparatus super-structure within the closed test cavity.

In this study, a gas pressure of 3 MPa was used for the main gas chamber pressure. This pressure resulted in projectile velocities of between 180m/s and 200m/s. Impact velocities and exit velocities were normally subject to experimental uncertainty of less that 2%. The impact energy was approximately 15J.

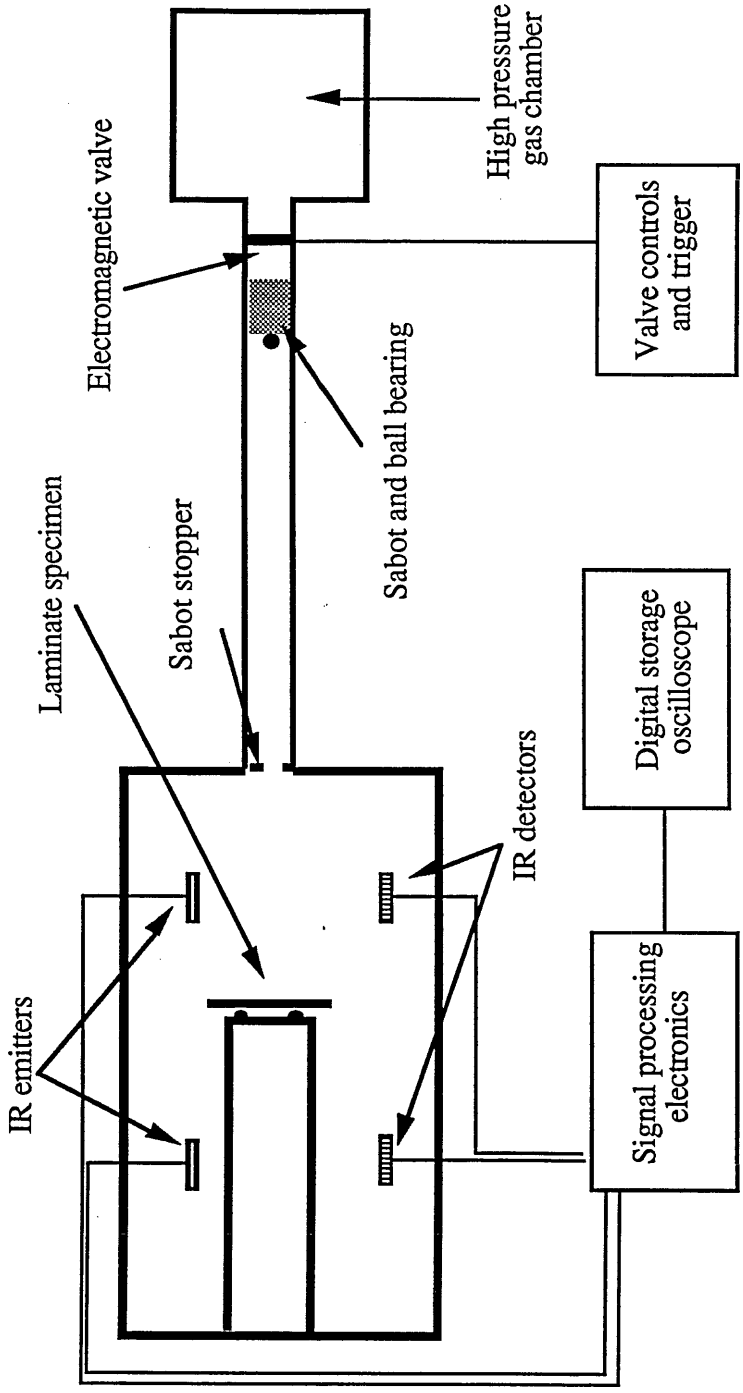


Figure 9.1 Schematic diagram of the high speed gas gun equipment.

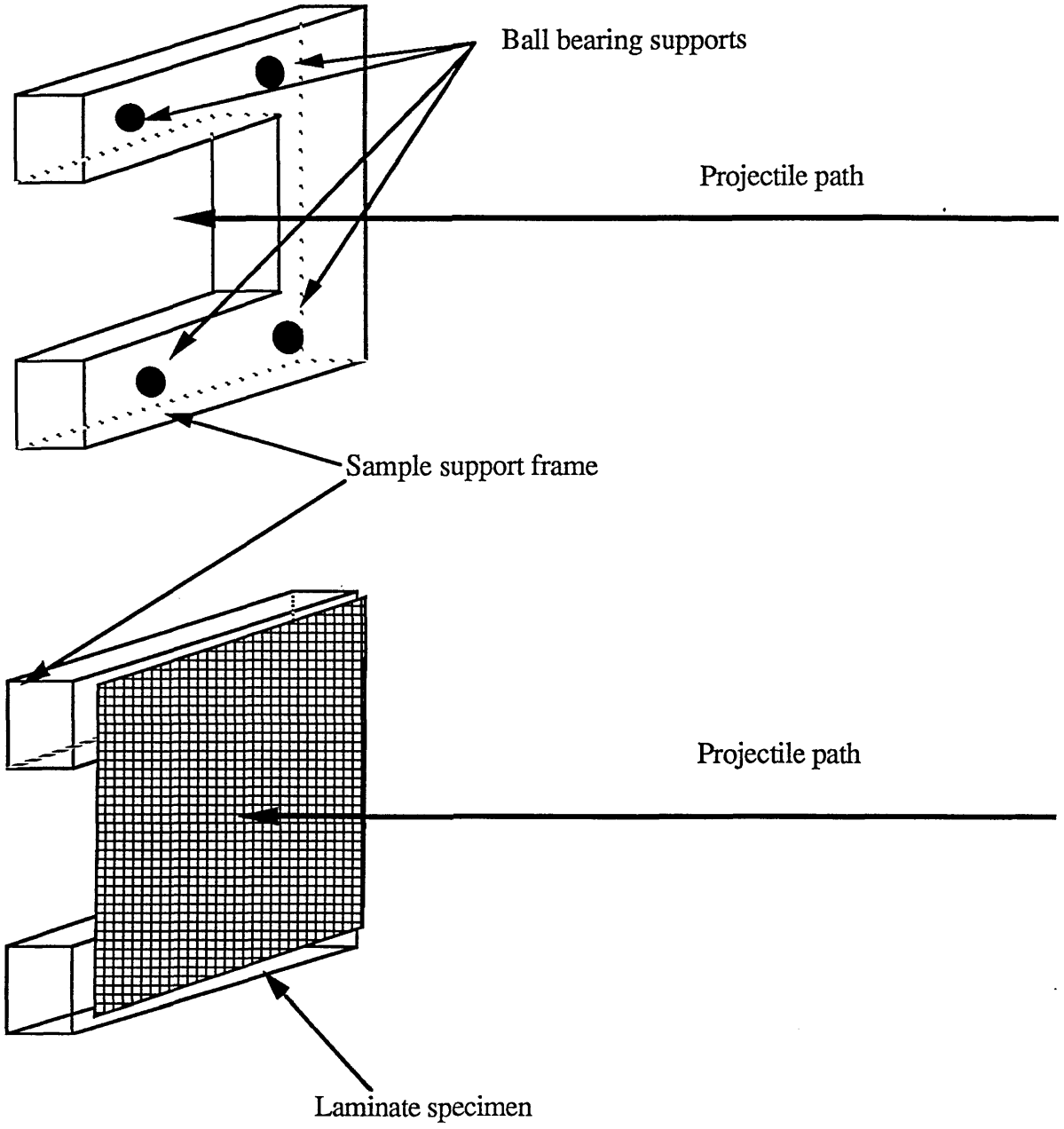


Figure 9.2 Diagram of the laminate specimen holder and the projectile path .

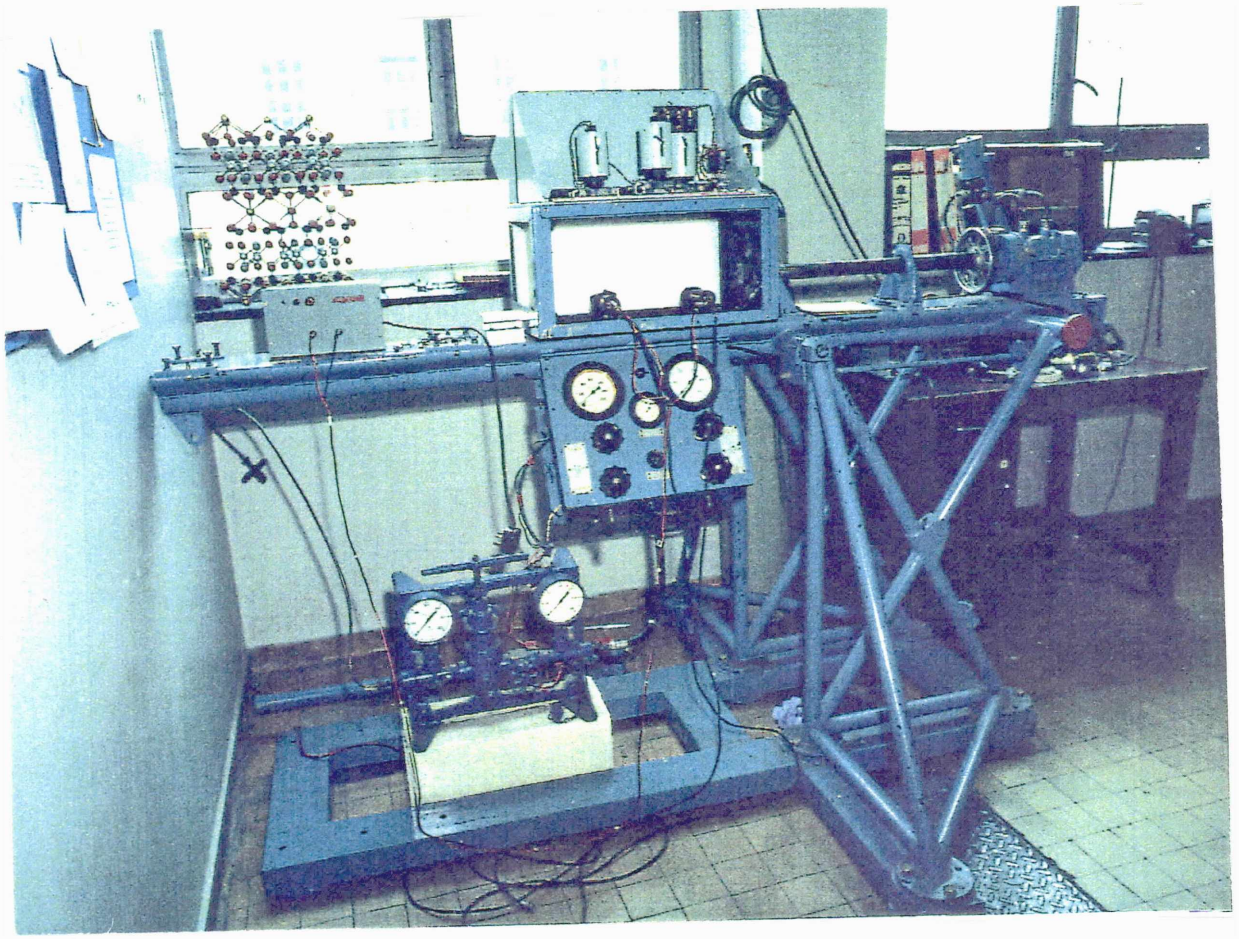


Figure 9.3 Frontal view of the gas gun equipment.

9.3.2 Results

The results obtained from the high speed gas gun experiments are shown below in Table 9.1. $\mathbf{V_i}$ and $\mathbf{V_e}$ refer to the impact and the exit velocities respectively and $\mathbf{D_z}$ refers to the average area of the delamination zone following impact on the exit side of the sample. $\mathbf{E_a}$ is the energy absorbed by the laminate on impact and was estimated from the change in the kinetic energy of the ball bearing.

9.3.3 Discussion

Figure 9.4 illustrates the most significant difference between the various impacted laminates. The size of the delamination zones clearly varies between the different laminate samples. The average size of the delaminations zones on the rear face of the specimens are given in Table 9.1. Sample delaminations were observed for both the rear and the front faces of the specimens. The size of the delamination zone for the front face of the sample

are not reported but were approximately half the size of those apparent on the rear faces.

The largest delamination zones were observed for the metallated/cleaned specimens, whilst the smallest zone is found on the PDMS treated fabrics. Most of the other laminate samples have delamination zones significantly smaller than the metallated/cleaned specimens but slightly larger than the PDMS laminates. The size of the delamination zones seems to give a good general correlation with the values of G_{IC} as shown in Table 9.2.

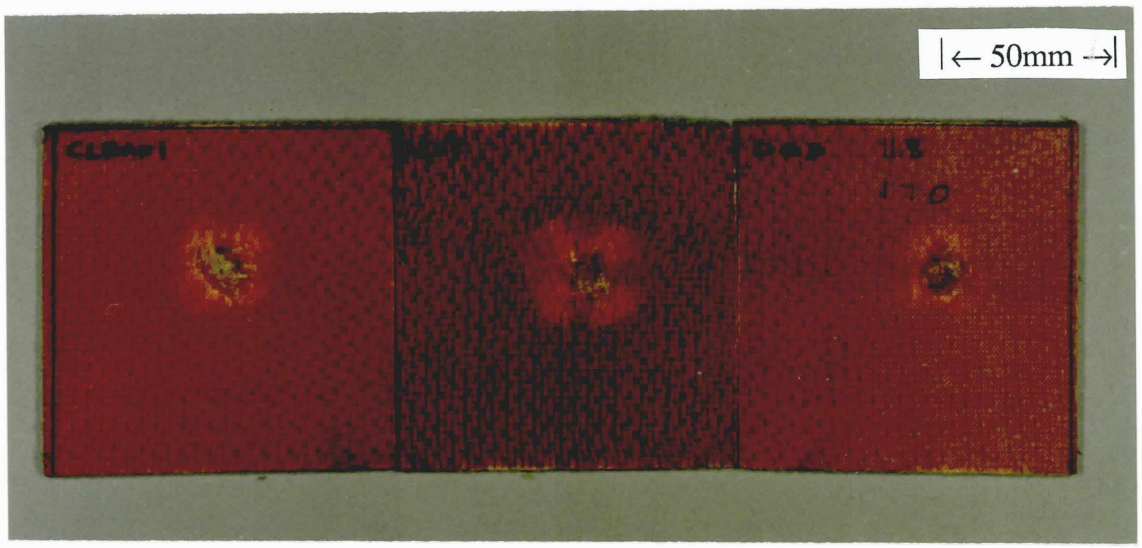


Figure 9.4 Three different laminate samples showing different extents of delamination on the sample's rear face following impact. The samples are, from left to right: clean, metalled/cleaned and epoxy grafted laminates.

This correlation is consistent with the nature of the impact event, as the propagation of the delamination crack during the ballistic deformation may be viewed as intrinsically a mode I fracture process.

Most of the aramid laminates absorb approximately between 10 and 11 J of energy on impact, which corresponds approximately to two-thirds of the incident kinetic energy of the projectile. However the epoxy grafted and the metallated/cleaned laminates absorbed a

Sample	V_i (m/s)	V_e (m/s)	E_a (J)	D_z (mm^2)
PEG	172	93	10.5	200
PEG	179	110	10.0	
PEG	182	117	9.7	
PEG	168	87	10.3	
"As recieved"	179	115	9.4	150
"As recieved"	187	113	11.1	
"As recieved"	180	108	10.4	
"As recieved"	182	114	10.1	
Metallated/clean	182	123	8.9	350
Metallated/clean	175	118	8.3	
Metallated/clean	179	118	9.0	
Amine	170	111	8.3	200
Amine	177	99	10.7	
Amine	180	97	11.4	
Epoxy Graft	170	118	7.5	150
Epoxy Graft	164	116	6.7	
Epoxy Graft	172	116	8.0	
PDMS	172	90	10.7	100
PDMS	178	102	10.6	
PDMS	165	89	9.6	

Table 9.1 Data from the ballistic impact experiments.

smaller amount of energy, approximately 8 and 9 J of energy respectively on impact. In the case of the metallated/cleaned laminates the decrease in energy absorption is of particular interest. The increased size of the delamination zone observed for those samples did not result in additional energy absorption. Rather, as suggested by Shepherd (1983), stratification of the ply layers in the composite led to a decreased efficiency in the energy absorption processes.

The results presented in Table 9.2 show the estimated energy associated with delamination of the ballistically impacted laminates. These are based on the simple product of G_{IC} and D_Z and assume that G_{IC} is constant with crack length. Though this was shown not to be the case in Chapter 8, it serves as a simple first order upper bound approximation. In most cases the fracture energy is less than 5% of the total energy absorbed assuming that only one delamination zone is created. Since delaminations are evident from examination of both the front and rear specimen faces, it seems likely that significant delamination between all seven inter-ply layers has occurred. So the delamination energy could account for up to a maximim of 35% of the energy absorbed. Again this estimate is an upper bound result and the true result is likely to be significantly lower due to the variation of G_{IC} with crack length and the variations in D_Z through the laminate thickness. However, the delamination energies per interply for the various types of laminate are similar in magnitude.

Consequently maximum energy absorption would seem to be best accomplished by ensuring that the maximum degree of three dimensional structure is introduced into the laminate. This premise is supported by the results in Table 9.1 which show that the PDMS specimens which were previously shown in Chapter 8 to have significant fibre bridging, exhibited the smallest delamination damage zone.

	G_{IC} (kJ/m^2)	D_z (mm^2)	E_l (J)	E_a (J)
"As received"	2.15	150	0.3	10.3
Amine coated	2.25	200	0.45	10.1
Polydimethyl siloxane coated	2.85	100	0.3	10.3
Polyethylene glycol coated	1.89	200	0.4	10.1
Epoxy grafted	1.83	200	0.35	7.4
Metallated/cleaned	0.90	350	0.35	8.7

Table 9.2 Mode I fracture energy, G_{IC}, area of the ballistic delamination zone, D_z, total ballistic energy absorbed, E_a, and the energy dissipated due to mode I impact for each interply, E_l, for various "Kevlar"-epoxy laminates.

Figure 9.4 shows that a number of other failure mechanisms in the materials are operative during impact. Tensile fibre failure, shearing of the matrix phase, flexural bending of the laminate would all be expected to absorb energy during impact.

9.3.4 Conclusion

The size of the delamination zone observed for aramid-epoxy laminates after high speed ballistic impact is inversely related to the mode I fracture energy. Increasing size of the delamination zone does not lead to increased energy absorption on impact. Rather the converse behaviour seems to be true. The impact behaviour of aramid laminate specimens is sensitive to the internal structure of the composite as manifest in the fibre-bridging effects noted in interlaminar fracture. Interlaminar fracture accounts for less than a third of the energy absorbed on impact by aramid laminates.

CHAPTER 10

INTERFACIAL MECHANICS

10.1 INTRODUCTION

The primary role of the interface in composite materials is to transfer the load from the "stiff" anisotropic high modulus fibres, to the "softer" isotropic matrix materials. The adhesion between the fibre and the matrix defines the essential efficiency of this stress transfer process. Thus, the adhesion directly influences both the shear and the off-axis properties of fibre reinforced composites.

Model mechanical studies involving single fibres could be expected to help bridge the gap in understanding between the macroscopic engineering properties of composite materials and the fundamental chemical and physical interactions which occur between a fibre and the matrix. Consequently, during the last 10 years a significant number of techniques have been developed for studying the micro-mechanics of interfaces. Experimental studies using these techniques have assisted in the development of a number of theoretical models for the fibre-matrix interface. However, the validity of these models and their relationship to the macroscopic properties of composites is still uncertain.

Whilst significant interest in fibre-matrix micro-mechanics is evident from the large number of papers which have been reported on the topic, a number of related but important topics seem to have received minimal interest. Specifically, the frictional properties of fibres and the interfacial shear properties of thin polymers films, both of which are clearly relevant to composite materials, have rarely been reported. Furthermore, the mechanics of the high modulus fabrics, which form the load bearing part of the laminate, have not been reported at all.

This Chapter consists of two major sections. The first section reviews the literature published on the interfacial mechanics of polymeric materials and consists of three

sub-sections. The first sub-section reviews the interfacial mechanics of thin polymer films, especially in the context of adhesion and friction. The second part of this section reviews the interfacial micro-mechanics of fibre-matrix systems. The wide range of experimental techniques which has been developed to study the single fibre-matrix interface are described and current models of the fibre-matrix interface are presented. The final sub-section reviews the mechanical properties of fabrics and fibres.

The second section of this Chapter describes two experimental studies. In the first part preliminary experimental micro-mechanics results for "Kevlar" fibres with an epoxy matrix are reported. In the second part, the compressive mechanical properties of "Kevlar" fabrics are reported and discussed.

10.2 INTERFACIAL SHEAR STRENGTH OF POLYMERS.

10.2.1 Introduction

The interfacial shear properties of polymeric films are of fundamental importance in any system of contacting bodies which involves the movement of one surface over another. The primary quantity which characterises such movements is the interfacial shear strength, τ_i. The interfacial shear strength may be described as the interfacial force per unit area of contact, or alternatively as the energy dissipated per unit area of contact per unit sliding length.

In fibre reinforced composites, τ_i is a critical quantity as it defines the conditions at which fibre-matrix debonding may occur under the application of shear stress at the interface. Interfacial failure marks a critical transition in the mechanical performance of a composite as the stress transfer mechanism changes from being elastic in nature,to becoming one which is dependent on interfacial frictional forces. Fibre-matrix debonding can directly result in material failure via interfacial crack propagation, or material failure may occur as result of the interfacial load bearing mechanism not being able to support the

increased loading.

In the following sections the nature of friction and its relationship to the interfacial shear strength will be discussed.

10.2.2 Friction

The coefficient of friction, μ, is defined as the ratio of the frictional load, **F**, to the normal load, **W**:

$$\mu = F / W \qquad (10.1)$$

This equation is commonly known as Amonton's first Law. Since it is known that μ decreases with increasing **W**, a number of expressions relating **F** to **W** have been proposed. The most successful relationship is Equation 10.2:

$$F = k W^n \qquad (10.2)$$

where n = load index ($^2/_3 < n < 1$)

The frictional interactions between solid bodies is generally the result of two main mechanisms for energy dissipation. The first mechanism involved the dissipation of energy in the interfacial layers between the two phases, and results from interfacial shearing of the bodies at the points of adhesive contact. The second mechanism involves the energy dissipation in relatively large sub-surface volumes within the interacting bodies. Energy dissipation in this case is the result of the surface asperities of the harder solid deforming the surface of the softer solid phase. Localised energy losses occur due to viscous, visco-elastic or plastic processes. This model of interfacial friction has been reviewed in detail by Briscoe (1985), and Briscoe and Tabor (1978).

These two mechanisms result in adhesive and bulk deformation components of the total frictional work. Both processes are generally treated as independent and additive energy dissipation mechanisms (Bowden and Tabor 1950; Briscoe and Tabor 1978) and may also be distinguished by the differing sizes of the energy dissipation region. In the case of adhesive friction, the zone for energy dissipation will correspond to the distances though which the surfaces forces propagate and will thus be less 10nm in thickness, whilst for ploughing type deformations, the depth would be many millimetre in size depending on the size of the bodies and the contact area. The diagram below shows the two primary zones for energy dissipation for a rigid asperity on a soft polymer.

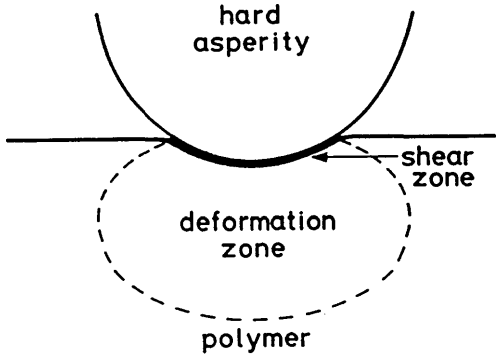


Figure 10.1 A schematic diagram of a rigid asperity sliding against a soft polymer. Energy is dissipated in the shear interfacial zone as well as the bulk deformation zone (Briscoe 1978).

The relative importance of these two mechanisms is dependent on the chemical and physical properties of the materials, as well as the surface roughness and the type of motion between the bodies. For relatively smooth surfaces, such as high modulus fibres, in contact with a glassy matrix phase, the adhesive component of the friction would be expected to be the dominant term.

10.2.3 The Adhesive Component of Friction

The total adhesive contribution to the interfacial friction is given by Equation 10.3:

$$\mathbf{F} = \mathbf{A}\ \tau_i \qquad (10.3)$$

where $\mathbf{F}$ = frictional force per unit area

τ_i = interfacial or adhesive shear stress

For the case of static friction, the conditions most relevant to the debonding of fibres within a matrix phase, τ_i relates directly to the force required to initiate motion. In this situation, τ_i is best approximated to a rupture stress or to a mode II type fracture stress.

10.2.3 Measurement of τ_i for Thin Polymeric Films

A number of experimental techniques have been utilised for the measurement of τ_i of thin polymer films. Bridgeman (1935) has described equipment for measuring τ_i consisting of a metal disc with a thin polymeric film coated on each side, which is sandwiched between two flat anvils. Pressure was applied to the anvils and the torque required to rotate the metal disc was used to calculate τ_i. Another technique was developed by Scruton (1971) following earlier work by Tabor (Rabinowicz and Tabor 1951; Bowden and Tabor 1964). By sliding a rigid elastic indentor over a flat elastic substrate with an

interposed polymeric film, τ_i could be estimated from the force required to move one surface over another, at a constant velocity. The third type of experiment used to measure τ_i involves the use of thin sheets of cleaved mica with have a molecularly smooth surface. Bailey and Courtney-Pratt (1955) coated monolayers of stearate materials onto two mica sheets which were bowed and mounted orthogonally with the monolayers in contact. The force required to rupture the junction was measured and used to calculate τ_i. More recently, Israelachvili and Tabor (1973) used a similar experimental approach to detect a slight pressure dependence on τ_i for calcium stearate monolayers.

10.2.5 Factors Affecting the Adhesive Component of Friction

The most important variable affecting the adhesive component of friction is the contact pressure, **P**. A number of studies of τ_i as a function of **P** for polymers have been reported (Briscoe *et al.* 1973; Briscoe and Tabor 1974; Amuzu 1976). Amuzu has reported that for glassy polymers such as poly(methyl methacrylate), poly(styrene) and nylon 6, τ_i increased with **P** over the contact pressure range of 3 to 20 MPa. The τ_i values determined were typically half the value of the imposed contact pressure. Briscoe *et al.* (1973) have demonstrated that this dependency is well modelled by the expression:

$$\tau_i = \tau_o + \alpha \mathbf{P} \qquad (10.4)$$

where τ_o = material constant

α = material constant

Values for τ_o and α have been reviewed in detail by Smith (1979).

More recently the use of Equation 10.4 led to an alternate expression for the coefficient of friction:

$$\mu = \tau_o / P + \alpha \qquad (10.5)$$

For large contact pressures, this Equation reduces to :

$$\mu \approx \alpha \qquad (10.6)$$

A small number of studies have been reported on the effect of temperature on values of τ_i . Amuzu (1976) has observed that τ_i decreased or was constant in value as temperature increased. Only a few studies of the relationship between the morphology and chemistry of the substrate and the values of τ_i have been undertaken. Amuzu *et al.* (1977) have reported on the variations in τ_i for a homologous series of poly(n-alkyl methacrylates). The trend in the shear strength of these materials was rationalised in terms of the molecular engagements of protruding segments of the different size pendant alkyl groups. Pooley and Tabor (1972) have interpreted the interfacial shear properties in terms of the molecular profile or "roughness" of the polymer molecules. Poly(tetrafluoro ethylene) (PTFE) has a smooth helical structure which can be perturbed by the introduction of perfluoromethyl groups in place of the fluorine atoms. The frictional forces of PTFE were observed to increase significantly with the introduction of these large substituents. Recently Smith (1979) has studied the effects of polymer conformation and morphology on the interfacial shear behaviour of a wide range of polymeric films. The polymer morphology was varied by using different solvents for casting the films, by preparing polymers with different thermal histories and by varying the polymer tacticity. Smith's work highlighted the importance of sample preparation in determining the shear properties of the film, and consequently demonstrated the sensitivity of τ_i to the polymer morphology. The subtle, but significant, differences between the bulk yielding of organic polymers and the interfacial yielding of thin films were also discussed by this author, although the specific nature of the relationship between these properties could not be elucidated.

10.2.6 Conclusions

The basic surface mechanics of thin organic polymeric films has been well established both experimentally and theoretically. Whilst some of the basic trends in τ_i have been empirically determined, the fundamental structure property-relationships have not been established. The relationship between bulk and surface shearing processes is not yet fully understood nor is the intrinsic nature of the energy dissipation mechanisms. Work has not yet been reported on organic materials which are directly relevant to fibre reinforced composite materials.

Typical interface rheological parameters (Equation 7.4) for a wide range of organic materials have been published by Smith (1979). The τ_i parameters are usually between 1 MPa and 10 MPa for organic polymers. The values of α vary from between 0.05 to 0.8, but typical values are in the range of 0.2 to 0.4.

10.3 A REVIEW OF INTERFACIAL FIBRE MICRO-MECHANICS

10.3.1 Introduction

Micro-mechanical studies could be expected to help bridge the lack of understanding between the macroscopic engineering properties of composite materials, and the fundamental chemical and physical interactions which occur between a fibre and the matrix. Consequently, during the last 10 years a significant number of techniques have been developed for studying the micro-mechanics of interfaces. Experimental studies using these techniques have assisted the development of a number of theoretical models for the fibre-matrix interface.

10.3.2 Interfacial Rupture by use of the Poisson Ratio

Broutman (1966, 1970) has pioneered the use of a number of innovative experimental

sample geometries for the measurement of the interfacial mechanical properties. Figure 10.2 shows the sample geometries for two tests designed to measure the interfacial transverse tensile strength, **S**, and the interfacial shear debonding strength, τ_i. In both tests the samples are deformed under compressive loading and the stress required to rupture the interface is measured.

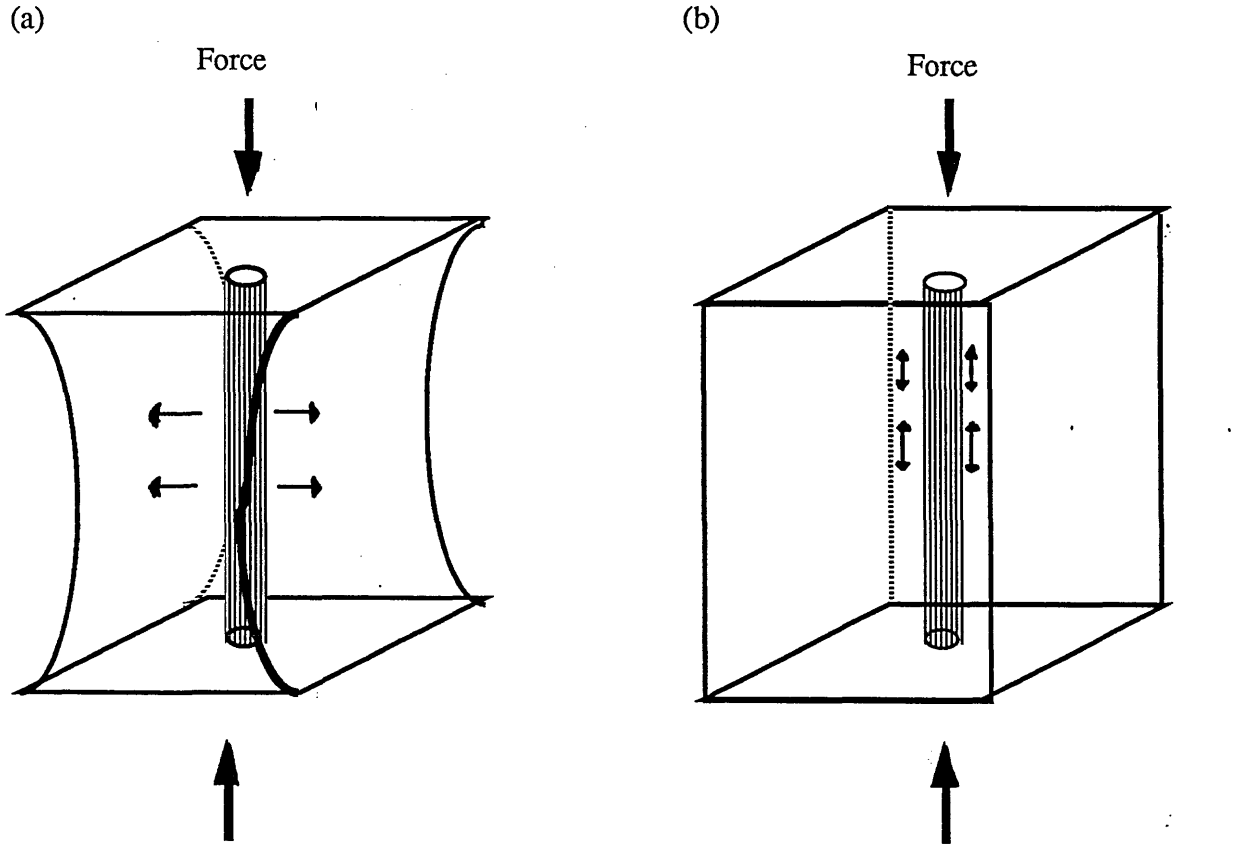


Figure 10.2 Schematic diagrams of two tests designed to measure (a) the interfacial transverse tensile strength, **S**, and (b) the interfacial shear debonding strength, τ_i .

These tests allow S and τ_i to be calculated via Equations 10.7 and 10.8:

$$S = - \frac{\sigma_m (\nu_m - \nu_f) E_f}{(1 + \nu_m) E_f + (1 - \nu_f - 2 \nu_f^2) E_m} \quad (10.7)$$

$$\tau_i = 2.5 \sigma_m \quad (10.8)$$

where S = transverse tensile strength

σ_m = axial compressive stress on the specimen

ν_m = Poisson ratio for the matrix

ν_f = Poisson ratio for the fibre

E_f = Young's elastic modulus for the fibre

E_m = Young's elastic modulus for the matrix

Although these tests were initially successful with glass fibres, various experimental have led to their infrequent use during the last 10 years (Varma *et al.* 1983).

10.3.3 Experimental Fibre Pull-out Techniques

The earliest measurements for τ_i between a reinforcing fibre and a matrix phase were reported by Broutman (1963). His simple, and relevant, measurements, involved embedding part of a glass fibre into a section of a polymeric matrix. Two experimental methods were devised for pulling an embedded fibre out of a polymeric matrix. Sample preparation involved passing the fibre through a thin button of matrix materials or, alternatively, embedding of a short length of a fibre into a larger section of matrix. Both types of sample are shown below in Figure 10.3. Measurement of the force as a function of displacement allows the critical load for interface rupture to be determined. The force to

rupture the cylindrical fibre-matrix interface is then used to determine τ_i using Equation (10.9) :

$$\tau_i = F / A = F / \pi D L \qquad (10.9)$$

where τ_i = interfacial shear stress

D = fibre diameter

L = length of the fibre-matrix interface

F = force to rupture interface

A = area of interfacial contact

Using a range of film thicknesses, Broutman determined τ_i (the debonding strength) of a number of glass/epoxy materials. Although these experiments allowed the debonding strength to be estimated, large variations in the experimental results were observed. These variations resulted from the experimental difficulties and errors associated in conducting experiments with embedded fibre lengths of less than 1mm, fibre diameters of less than 20μm and resultant debonding forces of only a few grams. Four specific problems identified with these experiments are:

(i) estimation of **A** is one of the primary problems. Since it is not possible to measure the true mechanical area of interfacial contact, it must be assumed that the geometrical contact area is appropriate for the calculation of τ_i . A more significant practical problem is that the matrix and fibre do not form a geometrically regular system in the vicinity of the matrix-fibre-air contact line. Because of the capillary forces associated with the liquid polymer prior to curing, liquid polymer wicks up the fibre periphery, resulting in the formation of a meniscus well above the planar surface which constitutes the bulk matrix surface. Consequently, neither the film thickness, nor the nominal fibre embedding depth, agree with the true embedded length.

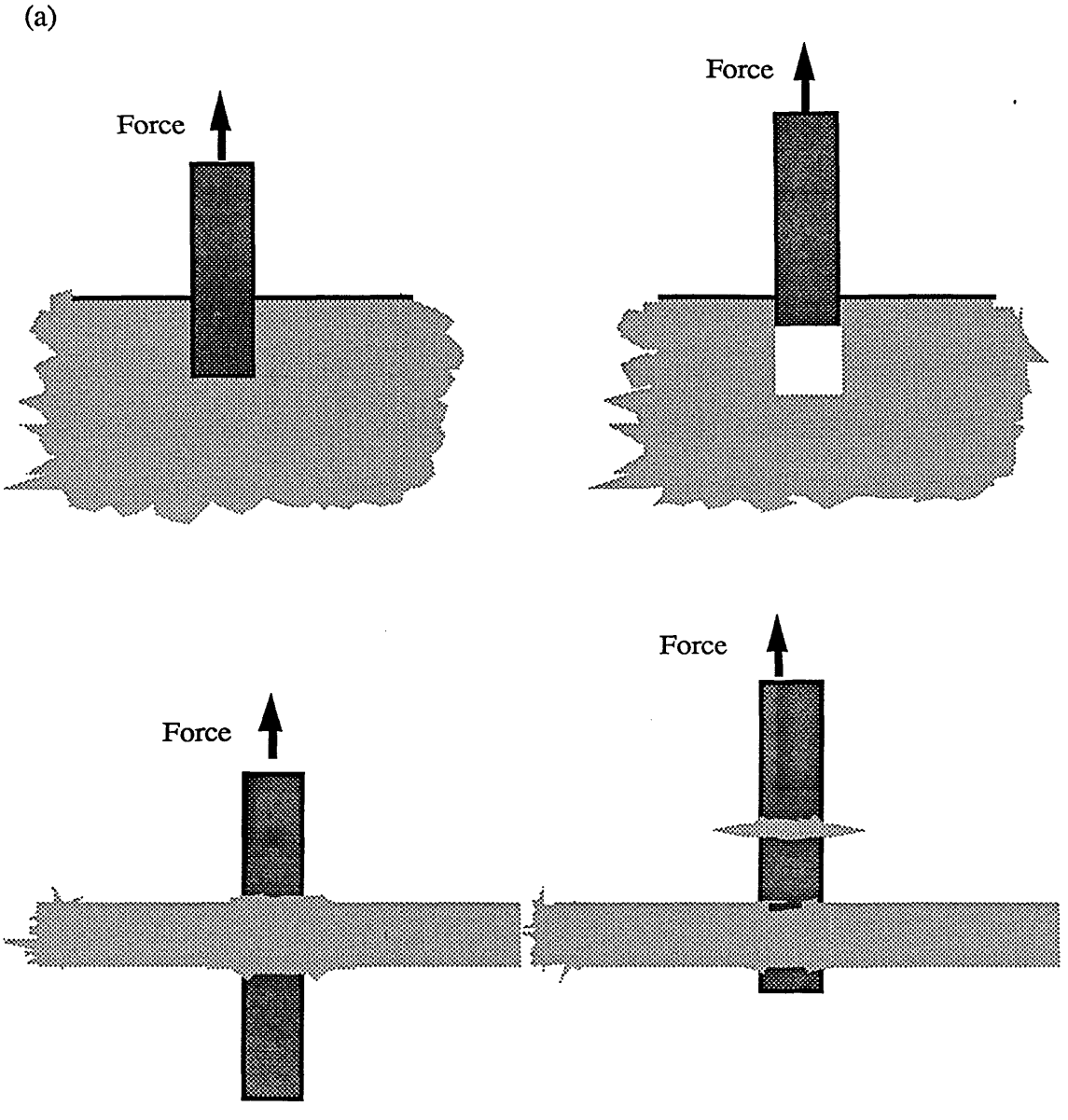


Figure 10.3 A schematic diagram of the single fibre pull-out experiments developed by Broutman (1963). In figure (a) the fibre is pulled from a block of matrix , whilst in figure (b) the fibre is pulled from a thin matrix film.

(ii) that it is quite common for the fibre not to debond cleanly from the matrix during these types of experiments. There is a tendency for fibre-matrix fracture to also involve additional matrix failure, especially fracture of the matrix meniscus or the matrix region immediately surrounding the fibre (see Figure 10.3). As well as resulting in an additional unknown contribution to **F**, this matrix fracture also leads to an additional uncertainty in estimating **A**.

(iii) Equation 10.9 assumes that the interfacial shear stress is uniformly distributed along the fibre interface and hence that τ_i is simply defined by Equation 10.9. Recently work by Gray (1984) has shown that the assumption of stress uniformity is erroneous.

(iv) the Poisson ratio effect results in the fibre diameter shrinking away from the interface as the elongational fibre strain increases during the experiment. This behaviour complicates the measurement of τ_i.

The first researchers to use the single fibre pull-out experiment were Shiriajeva and Andreevskaya (1962). Favre and Perrin (1972) have also used this technique to study carbon fibre interfaces by embedding short fibre lengths into a thermoset matrix. Their study however, met with limited success due to the same sample fabrication problems encountered by Broutman.

One of the earliest studies of aramid fibre systems was by Eagles *et al.* (1976) who studied various surface treated "Kevlar 49" fibres in a range of thermoplastic matrixes. Their results are summarised below. τ_i was calculated using Equation 10.9, whilst the frictional shear strength, τ_f was determined from the experimental plateau values observed for the fibre pull-out frictional force. This study confirmed the importance of the fibre

surface chemistry in determining the values of τ_i between fibres and thermoplastic resins. The authors also proposed a correlation between the tensile strength of short fibre reinforced composites and the interfacial shear strength τ_i.. However, only 20 individual pull-out experiments were performed for each fibre-resin system and the variance in their results was not reported. Whilst errors of up to 10 MPa in τ_i could be expected, based on the observations of Piggott (see Table 10.2), such errors would not be expected to alter the authors' primary qualitative conclusions.

	Fibre Preparation					
	Unsized		Sized		Water Treated	
Matrix	τ_i (MPa)	τ_f (MPa)	τ_i (MPa)	τ_f (MPa)	τ_i (MPa)	τ_f (MPa)
Ionomer	6.0	0.7	9.2	1.2	10.6	1.1
Polyethylene	8.0	1.5			12.6	1.5
Nylon 12	45.8	2.0				
Poly carbonate		8.9	2.1	38.6	2.6	
Polymethyl methacrylate	11.4	2.8	53.8	3.1	14.8	2.9

Table 10.1 Interfacial shear strengths and frictional shear strengths for a number of "Kevlar" fibres with various thermoplastic matrixes (Eagles *et al.* 1976).

Using the single fibre pull-out experiment, Penn and Lee (1982) have analysed the adhesion between "Kevlar" fibres and epoxy resins. These authors observed the slip/stick nature of the force versus displacement traces following the primary debonding event and have discussed in general terms, the debonding mechanism. No quantitative results were reported by these authors. In later work Penn reported that fibre surface modifications did not change the values for τ_i . For both polymeric coated "Kevlar" fibres (Penn *et al.* 1983) and covalently grafted fibres surfaces (Penn *et al.* 1987) values of 32 MPa were reported for "Kevlar" fibres with an epoxy matrix. Recently Chua and Piggott (1985a) have analysed, in detail, the mechanics of the fibre pull-out test. They concluded that satisfactory results could only be obtained by using embedded fibre lengths of less than 1mm and free fibre lengths of less than 2mm. These conditions would minimise both the errors due to the stored elastic strain in the fibres and due to the Poisson shrinkage. Reasonable measurements of τ_i and the work of fracture of the interface, G_i , were obtained from preliminary experiments using glass fibres and an epoxy matrix.

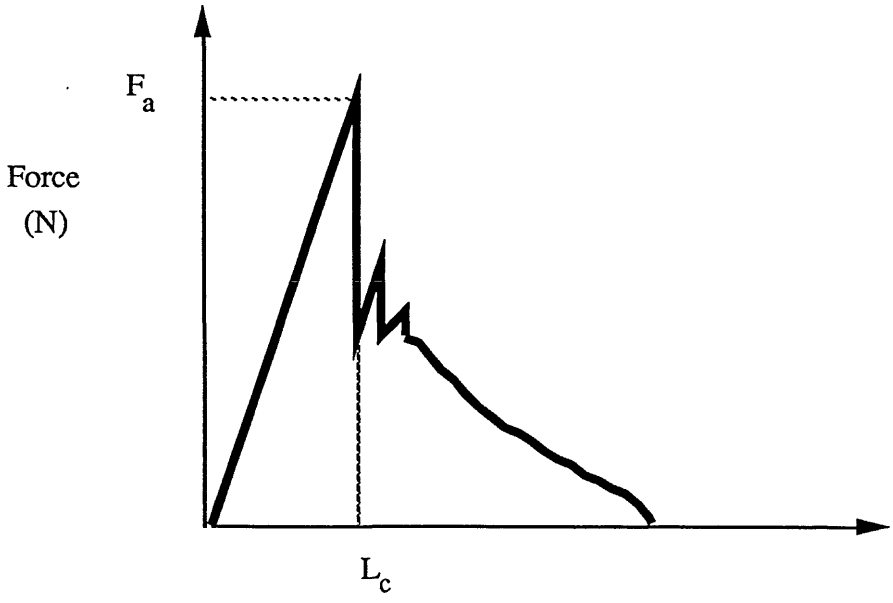


Figure 10.4 A load versus displacement curve for a single fibre pull-out experiment.

More successful experimental procedures were later developed by the same authors (Chua and Piggott 1985b) which allowed a series of glass/epoxy interfaces to be systematically studied by the single fibre pull-out test. τ_i was not evaluated via Equation 10.9, since τ_i values did not appear to be a simple linear function of the embedded length, **L**, as would be predicted on the basis of this Equation. It was assumed by the authors that the experimental data could be fitted by two linear segments. The first segment had a positive slope which allowed an interfacial yield stress, τ_{iy}, to be evaluated via Equation 10.10 :

$$\tau_{iy} = (dF_a / du) / 2 \pi r \qquad (10.10)$$

The second segment was a linear force plateau region of force F_p , with a slope of zero for which:

$$F_a = F_p \qquad (10.11)$$

The existence of this plateau region was argued to be the result of continuous interface fracture which has been previously cited as an important contributing mechanism to the fracture energy of a composite material. More recently, Piggott and Dai (1988) have shown, via model experiments, that the assumption of two linear regions is incorrect and that the debonding force is a function of the square root of the embedded length. Equation 10.12 defines the energy absorption per unit fracture energy, G_i.

$$G_i = F_p^{\,2} / 4\pi^2 r^3 E_f \qquad (10.12)$$

These authors also defined a maximum (interfacial) shear stress τ_{if} and average

(interfacial) shear stress τ_w respectively as :

$$\tau_{if} = (dF / du)_L / 2 \pi r \qquad (10.13)$$

$$\tau_w = 2Q / \pi r L^2 \qquad (10.14)$$

where r = fibre radius

Q = area under the stress-strain pull-out curve.

$(dF/du)_L$ = steepest slope in the pull-out curve at $u=L$.

The experimental results for a number of epoxy-glass and polyester-glass fibre systems were examined using these expressions and are summarised in Table 10.2. The values for τ_i show a number of interesting trends. For both thermoset matrixes, coating the fibres with a silicone release agent led to an increase in τ_i relative to the uncoated fibre of between 20% and 50%. A significant decrease in τ_i would have been expected due to the presence of the lubricant. No explanation is given for this unexpected observation. Only the parameters τ_{if} and τ_w varied in the expected manner due to the presence of the lubricant. This work was later extended to consider the effects of interfacial pressure (Chua and Piggott 1985c). By clamping a circular polymeric sample within an aluminium ring, a range of external pressures could be imposed by tightening the ring progressively. Increases in the external pressure led to increases in F as shown below:

Matrix	Post-cure	τ_i (MPa)	F_p (N)	G_i (kJ/m^2)	τ_{if} (MPa)	τ_w (MPa)
Polyester	nil	9.6	1.06	0.30	7 +/_ 7	5 +/_ 4
Polyester*	nil	11.7	0.73	0.14	2.5 +/_ 1.5	2 +/_ 2
Epoxy	nil	13.6	0.72	0.14	21 +/_ 5	10 +/_ 3
Epoxy*	nil	16.4	0.50	0.066	2.5 +/_ 1	2.5 +/_ 1

* silicone coated fibres

Table 10.2 Interfacial mechanical properties obtained from single fibre pull-out experiments. Glass fibres were embedded in epoxy and polyester matrixes. τ_{if} and τ_w refer to the maximum and the average shear stress respectively (Chua and Piggott 1985b).

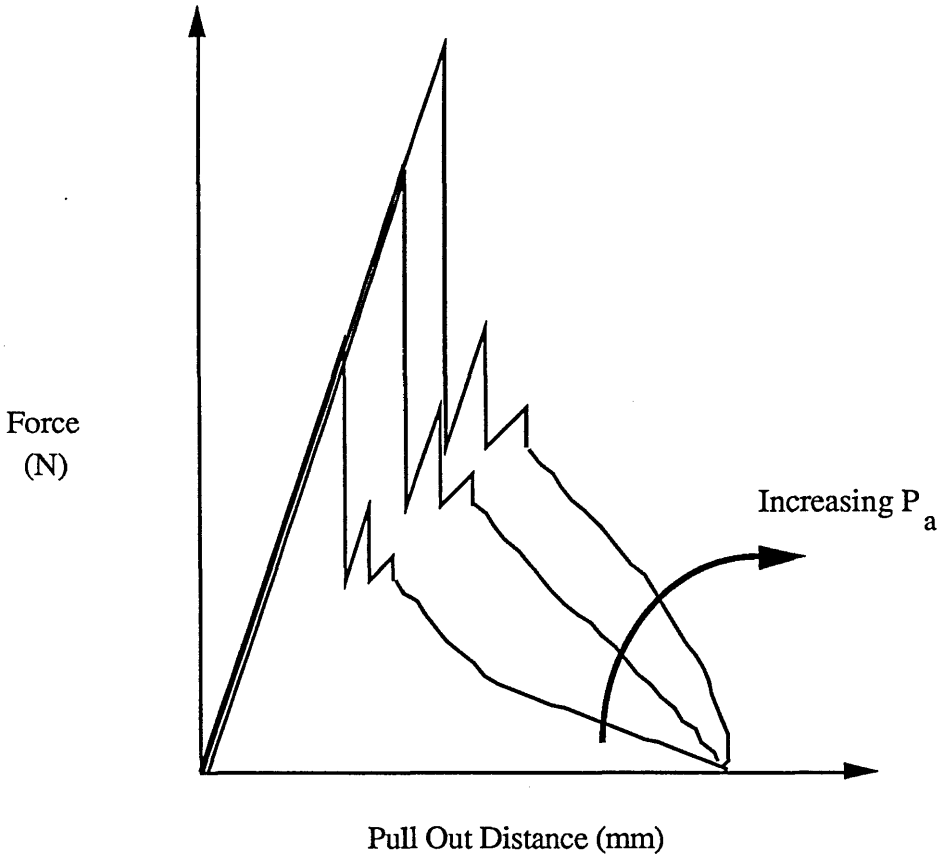


Figure 10.5 Force, **F**, versus displacement, **u**, trace for a single fibre pull-out experiment as a function of the external pressure, $\mathbf{P}_a$.(Chua and Piggott 1985c).

This study is the only reported work in which the surface mechanical properties of embedded fibres, in contact with polymeric matrixes, have been studied as a function of contact pressure $\mathbf{P}_a$. Values for the maximum shear stress τ_{if} were measured from the maximum slope of the pull-out traces at **u=L**. Both τ_{if} and the average shear stress, τ_w, were found to be independent of **L**, and both quantities increased in a linear fashion with $\mathbf{P}_a$. The frictional coefficients μ and μ_w were calculated for these materials using the dependence of τ_{if} and τ_w with $\mathbf{P}_a$ respectively. These results are shown in Table 10.3.

Matrix	Post-cure	μ	P_o (MPa)	μ_w	P_w (MPa)
Polyester	nil	0.28 +/_ 0.08	23 +/_ 10	0.38 +/_ 0.12	13 +/_ 6
Polyester*	nil	0.10 +/_ 0.02	25 +/_ 6	0.15 +/_ 0.05	16 +/_ 7
Epoxy	nil	0.54 +/_ 0.09	37 +/_ 10	0.34 +/_ 0.08	28 +/_ 9
Epoxy*	nil	0.07 +/_ 0.01	35 +/_ 10	0.09 +/_ 0.02	27 +/_ 10

* silicone coated fibres

Table 10.3 The coefficients of friction and the shrinkage pressures for a series of polyester/glass fibre and epoxy/glass fibre systems (Chua and Piggott 1985c).

The frictional coefficients were calculated using Equation 10.15, which is simply taken from Equations 10.1 and 10.5.

$$\tau_i = \mu (P_o + P_a) \qquad (10.15)$$

where μ = coefficient of friction

P_o = shrinkage pressure

P_a = applied pressure

The external pressure, P_a, gave reproducible changes in F_a as a function of **L** as below:

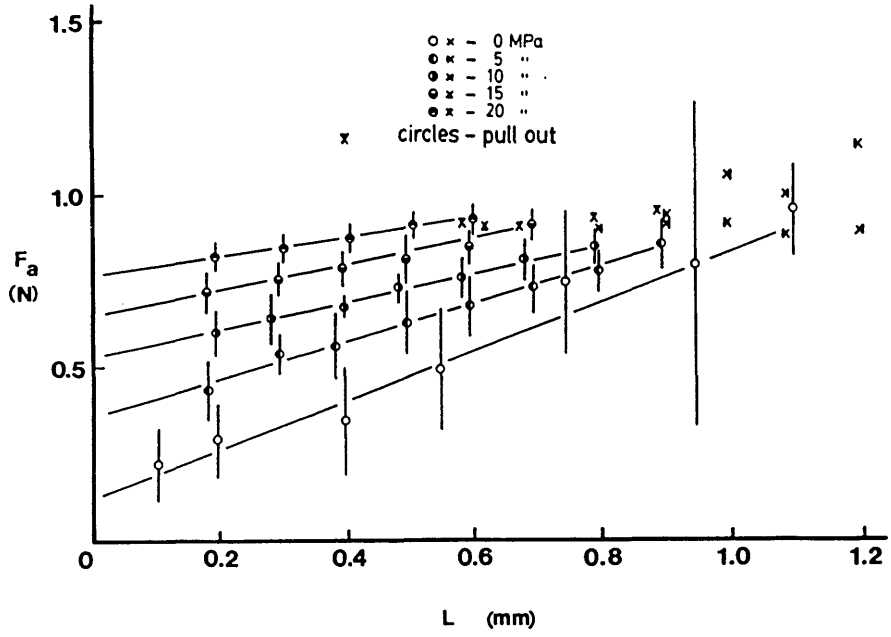


Figure 10.6 Adhesion force, $\mathbf{F}_a$, for a polyester matrix with glass fibres as a function of embedding depth **L** and external pressure $\mathbf{P}_a$. The data points represented by an (x) and an (o) denote fibre breakage and fibre pull-out respectively (Chua and Piggott 1985c).

These slopes, although similar in appearance for all fibre-matrix systems, actually reveal that the values of τ_i increased with the presence of the silicone coating. No reasons were given for this observation. The τ_i results show that the interfacial yield strength decreased with increasing external pressure, $\mathbf{P}_a$. This observation is a unexpected since in the shear yielding of thin polymeric films, the yield stress invariably increases with increasing hydrostatic stress or pressure (Smith 1979).

Although the single fibre pull-out method allows unique mechanical information to be determined, the fundamental significance of τ_i, τ_{if} or τ_w is unclear and certainly the factors which differentiate between these quantities are yet to be determined. Additional work needs to be undertaken to fully exploit the potential of this technique.

10.3.4 The Shearing of Micro-droplets on Fibres

Miller *et al.* (1987) have recently developed a new method for measuring τ_i. This

approach involves the formation of liquid epoxy micro-droplets onto a fibre, which are then allowed to cure *in situ* . These micro-droplets are then carefully debonded from the fibre using a pair of precision slits as schematically shown below :

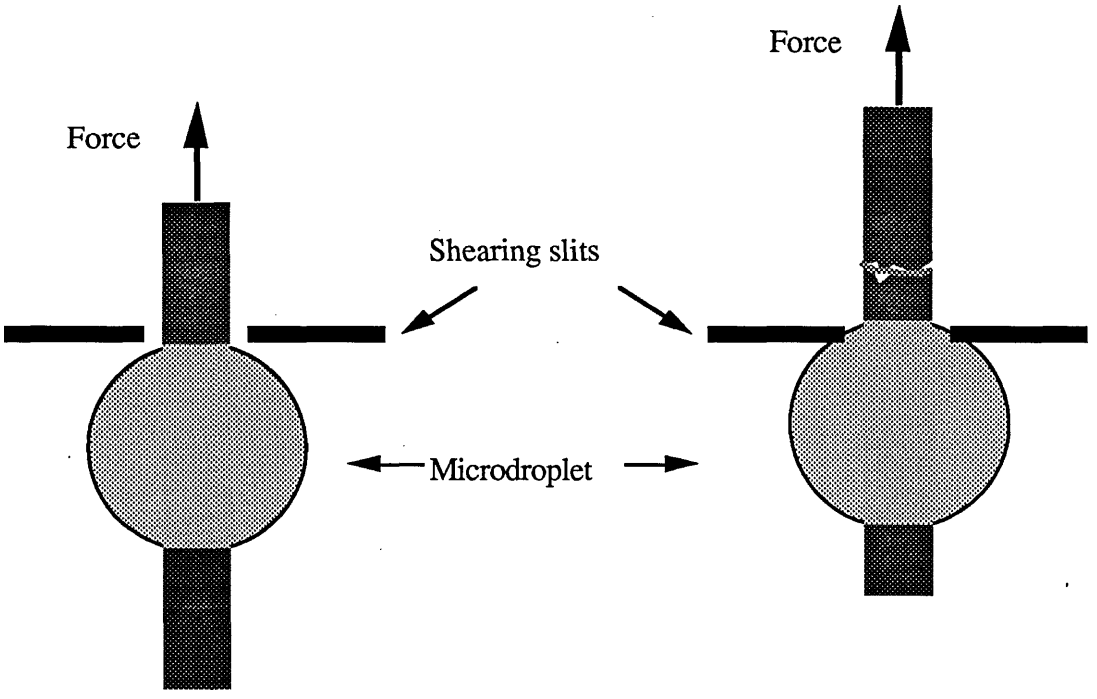


Figure 10.7 Measurement of τ_i using the micro-droplet debonding technique (Miller *et al.* 1985).

The droplet shearing force, **F**, is measured as a function of displacement, and the maximum shearing force is noted. By measuring the droplet length, and thus **A**, by microscopic examination, τ_i can be determined using Equation 10.9. Table 10.4 shows the values of τ_i for a number of fibre systems including "Kevlar" fibres.

Fibre and Treatment	Number of Droplets sheared	τ_i +/- σ (MPa)
"Kevlar 49" ("as received")	187	39 +/- 8
"Kevlar 49" (acetone washed)	107	39 +/- 8
"Kevlar 49" (MeOH/Acetone washed)	1158	41.4 +/- 0.3
"Kevlar 29" (MeOH/Acetone washed)	338	40.0 +/- 0.5
E-glass + silane	22	49 +/- 13
Carbon	37	57 +/- 10

Table 10.4 Measurement of τ_i using the shear droplet debonding technique for a various fibres with an epoxy polymer (Miller *et al.* 1985; Gaur and Miller 1989). σ is the standard deviation in the τ_i values.

The variations in the values of τ_i observed were argued by the authors to reflect the general heterogeneous nature of the fibre surface and were not the result of experimental errors. Gaur and Miller (1989) have recently established the effect of various experimental factors on this method for the measurement of τ_i. These factors included the initial fibre tension, the loading rate and the use of a second droplet to shear the first droplet. It was was concluded that none of these factors caused significant variations in τ_i.

Recently Favre (1989) has commented on the developments and improvements in the fibre pull-out method. He has astutely observed the ways in which these developments have significantly affected, by a factor of nearly three, the results which have been obtained within his own laboratory.

10.3.5 The Micro-debonding Method

Another technique which has been developed for the measurement of τ_i involves a fibre being pushed, rather than pulled, out of an interface (Mandell *et al.* 1980). A thin cross section of composite is polished and a small spherical indentor, approximately the same diameter of the fibre, is positioned above a fibre cross-section as shown below:

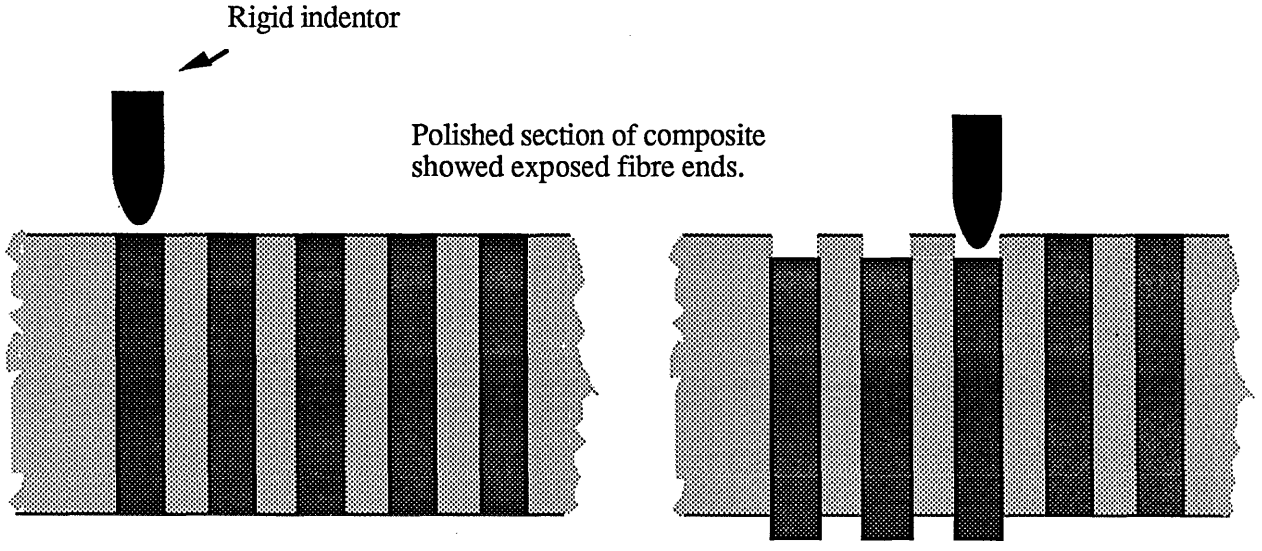


Figure 10.8 Schematic diagram of the micro-indentation method for measuring τ_i .

The indentor load on the fibre end is increased until the acoustic emission associated with interface rupture is sensed by a piezoelectric transducer. The load associated with the acoustic emission is noted and τ_i is calculated via Equation 10.9. Success has been claimed for fibres such as glass and "Kevlar", though problems with carbon fibres due to the presence of a skin-core morphology were encountered.

The primary advantage of this technique is that actual fibre composite materials can be studied. However there are a number of experimental problems associated with this method which include :

(i) the uncertain nature of relationship between the acoustic emission event and the load measured.

(ii) the possible mechanical damage to the interface that may occur during polishing of the surface, as well as chemical damage of the interface due due to water absorption.

(iii) the uncertain effects associated with axial fibre compression and the resultant Poisson radial expansion of the fibre.

(iv) the possible fracture and /or splitting of the fibre end due to the indentor stress.

More recently this technique has been applied to semi-infinite composite specimens rather than thin composite sections. This development was possible since Mandell *et al.* (1986) have established, using a finite element model, a relationship between the interfacial shear stress and the debonding force measured. Using this technique Netravali *et al.* (1989) have observed that an acoustic emission event associated with debonding was not observed for E-glass-epoxy specimens. The debonding process was thus presumed to be a slow continuous process. However, Caldwell *et al.* (1989) have reported on the automation of this technique and the successful characterisation of glass-epoxy interfaces.

10.3.6 Determination of Single Fibre Critical Length

Kelly (1964) developed a novel experimental method for measuring the stress transfer between matrix and the reinforcing fibres by embedding a single fibre with a low strain to failure (tungsten) into a matrix with a large strain to failure (copper). The samples were prepared by embedding single fibres into tensile dogbone coupons as shown in Figure 10.9. Under tensile loading, the test coupon was sufficiently strained so that fibre fragmentation could be expected as a result of the transfer of shear load from the matrix to the fibres. Dissolution of the copper revealed tungsten wire fragments whose length distribution could be determined. This length was defined as the critical fibre length, $\mathbf{L}_c$, and represents the minimum length of fibre possible to support the shear interfacial loading.

The relationship between L_c and τ_i is given below:

$$\tau_i = \sigma D / 2 L_c \quad (10.16)$$

where σ = tensile strength of the fibre for a gauge length of L_c

This technique has been applied to organic fibre composites by a number of authors. Due to the transparent nature of the matrix in many cases L_c could be measured directly with a microscope as is schematically shown in Figure 10.9. The mechanism for fibre fragmentation has been closely observed. As the tensile coupon is strained shear forces are transferred from the matrix to tensile loads in the fibre. This load builds up all along the fibre length until the transferred shear load exceeds the localised fracture strength of the fibre and results in fibre fracture. As the tensile coupon is further strained the fracture process continues with shorter fibre fragments being produced. This process continues until the fibre lengths become too short for interfacial shear to induce in fibre fracture. The resulting limiting length is described as L_c .

Initial studies with glass fibre composites were successfully undertaken by Ongchin *et al.* (1972). Later this technique was applied to carbon fibre materials firstly by Wadsworth and Spilling (1968) and later in more extensive studies by Drzal *et al.* (1980, 1981,1983). Recently DiBenedetto *et al.* (1989) have illustrated the more sophisticated treatments of data required to exploit fully this approach and have shown how this method can identify different failure modes in glass fibre materials.

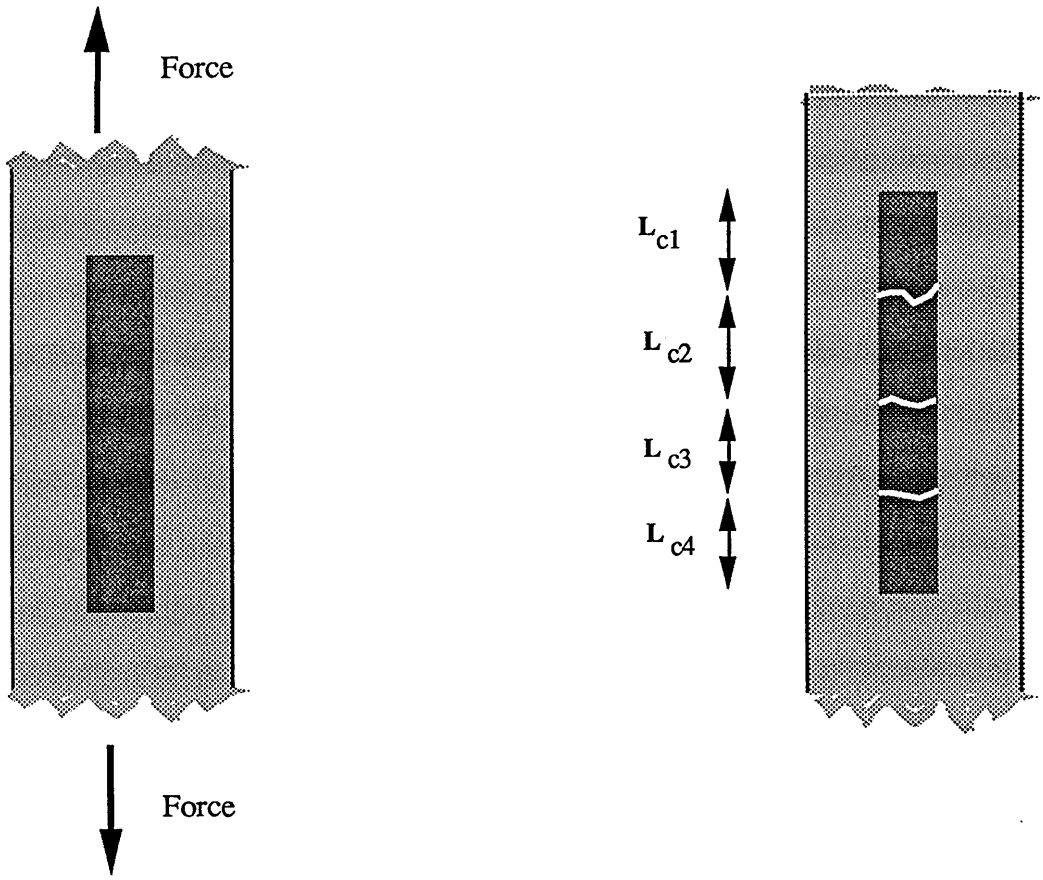


Figure 10.9 In the critical fibre length experiment a single fibre is embedded into a matrix phase. Upon matrix straining the fibre fragmentation occurs resulting in a distribution of fibre fragment lengths L_{c1} , L_{c2} ...L_{cn} .

Drzal's studies revealed that the histogram of L_c values provide a useful way of measuring τ_i . Measurements of L_c were found to be sensitive to various fibre surface modifications. Conclusions about the nature of the debonding process were also made by studying, in real time, debonding of a single fibre under polarised light .

Attempts to study "Kevlar"-epoxy systems with this method have been essentially unsuccessful (Drzal 1983). Unfortunately the non-brittle fracture process in the tensile failure of "Kevlar" fibres made it very difficult locate the fibre fracture surfaces, although regions of stronger polarised light intensity consistent with their existence were observed with polarised microscopy. Lee *et al.* (1989) have developed an experimental technique by

which the positions of fibre breakage, and thus the fibre lengths, may be determined via the use of two ultrasonic transducers. These are placed at each end of the fragmentation specimen and the transit times for the acoustic emissions associated with the fibre breaks are measured.

10.3.7 Raman Spectroscopic Studies of Micro-strain

When a beam on monochromatic light strikes a sample, light of two types will be scattered. Dominant in intensity will be the Rayleigh scattered light of the same wavelength as the excitation source. However a small amount of light will be inelastically scattered and this Raman scattering will be of a frequency shifted with respect to the excitation radiation. This frequency spectrum of the Raman scattered light will be the vibration spectrum of the sample. Application of this technique for studying polymers has been recently reviewed (Summerscales 1987).

An important class of Raman spectroscopy is resonance Raman spectroscopy in which the Raman band intensity is dramatically enhanced. This phenomena occurs if the sample has an electronic transition which coincides with the excitation wavelength. The application of resonance Raman spectral microscopy (RRSM) to the study of model single fibre composites is one of the most significant experimental advance in fibre micro-mechanics in the last 10 years.

Batcheldor, Galiotis, Young and their co-workers have successfully developed a spectroscopic technique in which the local strain field in model single fibre composites may be measured from the band shifts in the fibre's Raman vibration spectrum. Initially RRSM was used to study the micro-mechanics of a model composite consisting of a polydiacetylene single crystal within an epoxy matrix (Galiotis *et al.* 1984). It was established that the shift in the wavelength of the Raman band positions was a linear function of crystal strain. By using RRSM, the strain in localised sections along the fibre axis could be determined from the point by point variations in the wavelength of the

Raman vibration initially at 2085 cm-1. By straining the epoxy sample these workers were able to monitor the strain transfer to the fibre via these wavelength variations. They concluded that at low matrix strains, the fibre and matrix exhibited equal stresses and at higher strains the fibre strain equalled the matrix strain. In this case the strain variation along the fibre length was well approximated by the Cox's shear lag model and the critical length, $\mathbf{L}_c$, was confirmed to be a linear function of fibre diameter.

Later work by Robinson *et al.* (1987) investigated the effect of polymer matrix shrinkage on single fibre micro-mechanics. They concluded that, after the post-cure of the polymer, the compressive stresses associated with cooling of the material could cause the fibre to undergo elastic twinning. The twinning disappeared reversibly during tensile deformation and extent of matrix shrinkage could be determined by measuring the strain required to remove the twins.

Robinson *et al.* (1987) have suggested that a careful distinction should be made between $\mathbf{L}_c$ as measured by RRSM and as determined from fibre pull-out experiments. They argue that $\mathbf{L}_c$ measured by RRSM is an "elastic transfer length" which depends only on the fibre diameter, Young's modulus of the fibre and the matrix (Termonia 1987) and does not directly depend on τ_i . They thus suggest that if the fibre was surface treated then $\mathbf{L}_c$ from a fibre pull-out experiment will vary due to changes in τ_i, but values of $\mathbf{L}_c$ from RRSM will not change. This argument seems incorrect since Termonia clearly shows that $\mathbf{L}_c$ is strongly dependent on the fibre-matrix adhesion, and this quantity is directly identifiable with τ_i .

Galiotis *et al.* (1985) have shown that the resonance Raman frequencies of a "Kevlar" fibre are a linear function of the fibre strain. Jahankhani and Galiotis (1988) have studied model single fibre composites using "Kevlar" 49 fibres embedded in a room temperature cured epoxy resin. At low matrix strains of 0.8% the fibre behaved as a well bonded interface and gave a strain profile broadly in accord with the Cox model. However, as the matrix strain increased to 1.6% significant debonding has occurred with the fibre strain no

longer exhibiting a strain plateau, but a maximum strain in the central position along the fibre length. This observation suggests the fibre-matrix interface has failed at all but the centre section of the fibre, where some residual frictional forces are straining the middle of the fibre. Debonding was confirmed by a value of $\mathbf{L}_c$ = 1.46mm which corresponds to a **L/d** ratio of over 100. Most recently Jahankhani *et al.* (1989) have determined the variation of $\mathbf{L}_c$ with the matrix strain for "Kevlar" fibres embedded in an epoxy matrix.

Recently Fan and Hsu (1989) have applied RRSM to estimate the stress distribution along model fibre composites. They observed significant difference in the stress distributions between fibres with blunt ends and those with tapered ends. The results for those with blunt ends agreed with other studies. Melanitis *et al.* (1989) have shown that Raman Spectral Microscopy could be applied to carbon fibre systems. A range of carbon fibres was examined and the interfacial shear stresses were calculated for high modulus carbon fibres in an epoxy matrix. Raman Spectral Microscopy has recently been applied to model single fibre composites of poly(*p*-phenylene benzobisthiazol) in an epoxy matrix (Day *et al.* 1989).

10.3.8 Theoretical Aspects of Fibre-Matrix Micro-mechanics

To gain a fundamental understanding of the macroscopic mechanical performance and failure of fibre reinforced composites, a number of theoretical micromechanical models have been developed. These models are specific for different classes of composite materials and reflect the differing modes of stress transfer and energy dissipation possible in the interfacial regions.

Whilst these models can provide an important insight into the fibre matrix interface, they depend upon upon a number of simplifying assumptions. In general the following models assume that :

(i) the fibre and matrix behave elastically.

(ii) the interface is infinitesimally thin.

(iii) perfect bonding between fibre and the matrix occurs.

(iv) there are no variations in the mechanical properties of the matrix from the bulk to the interfacial regions.

(v) homogeneous surface topography and surface chemistry of the fibres is present.

Models to explain the reinforcing effect of fibres were firstly proposed by Cox (1952), and later by Dow (1963) and Rosen (1964). These are commonly referred to as the shear lag theories. Assuming that both the fibres and matrix behaved elastically, and that the fibre end does not participate in load transfer, then τ_i for a fibre with embedded length **L** at a distance **x** from the matrix surface was given by :

$$\tau_i = \mathbf{n} \,.\, \sigma_f \,.\, \{ \, (\cosh (\mathbf{n.L-n.x}) / \mathbf{r} \,)) \, / 2 \sinh (\mathbf{n.s}) \, \} \qquad (10.17)$$

where $\mathbf{n}^2 = \mathbf{E_m} / \{\mathbf{E_f} (1 + \nu_m). \ln(\mathbf{R} / \mathbf{r})\}$

$\mathbf{s} = \mathbf{L} / \mathbf{r}$

$\mathbf{R}$ = distance to nearest fibre

$\mathbf{r}$ = radius of fibre

ν_m = Poisson ratio for matrix

The fibre stress and interfacial shear stress for a model embedded fibre are shown in Figure 10.10.

For certain matrix systems such as metals, another mechanism for stress transfer between fibres and resins is dominant. Kelly and his co-workers (Kelly and Tyson 1965) have analysed the case of a fibre-matrix systems in which the matrix undergoes significant plastic yielding in the interfacial regions. In this case the shear stress is equal to the

shear yield stress of the metal. Thus for a single embedded fibre there will exist a slip point, ε_s ,which is a boundary between the fibre being rigidly held by the matrix and the onset of a region in which the plastic flow has occurred. This behaviour is illustrated in Figure 10.11.

Unlike the cases of elastic and plastic stress transfer, which assume perfect interfacial adhesion, for fibre reinforced polymers often the adhesion is poor and frictional slip can be expected to occur. Piggott (1978) has proposed a model which incorporated both elastic stress transfer and a slip stress τ_s which was arbitrarily defined in terms of τ_{my} .**a** in which is **a** is non dimensional adhesion constant. Beyond the slip region τ_i is controlled by the frictional coefficient and the normal stress.

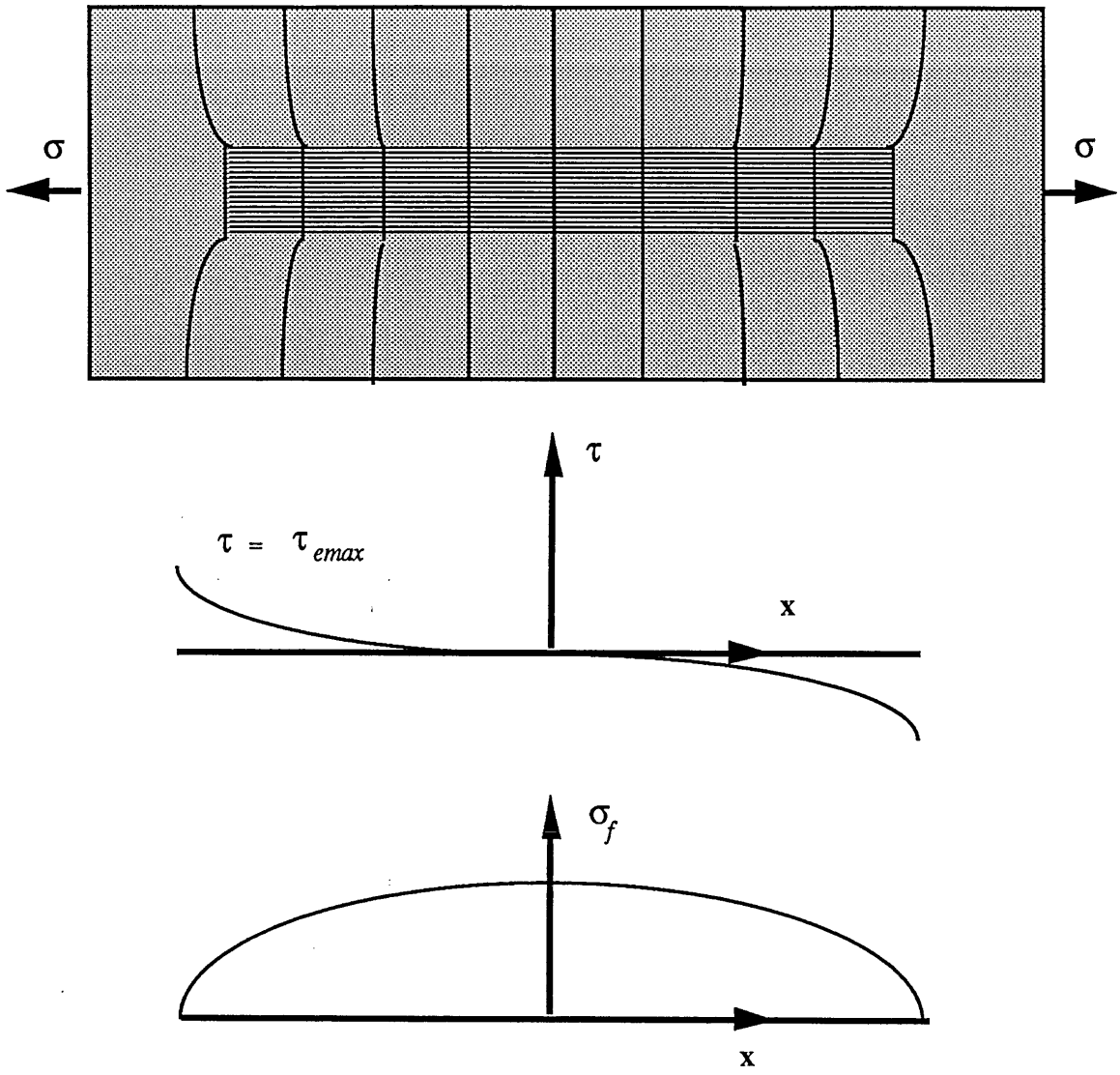


Figure 10.10 σ_f and τ_i as a function of position, x, for a single fibre subject to elastic stress transfer between fibre and matrix (Cox 1952; Piggott 1980).

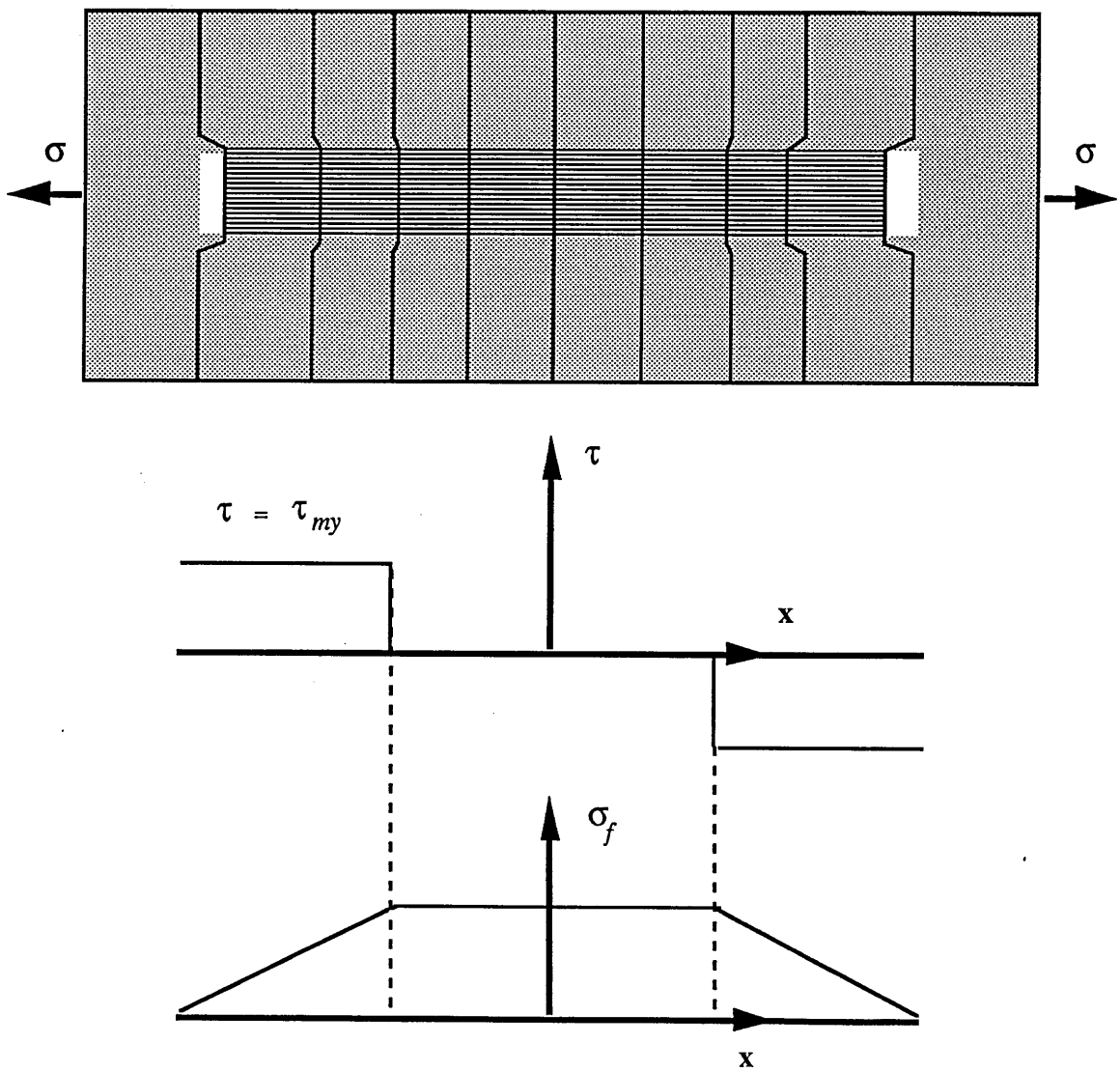


Figure 10.11 σ_f and τ_i as a function x for a single embedded fibre with plastic yielding between fibre and matrix (Kelly and Davies 1965; Piggott 1980).

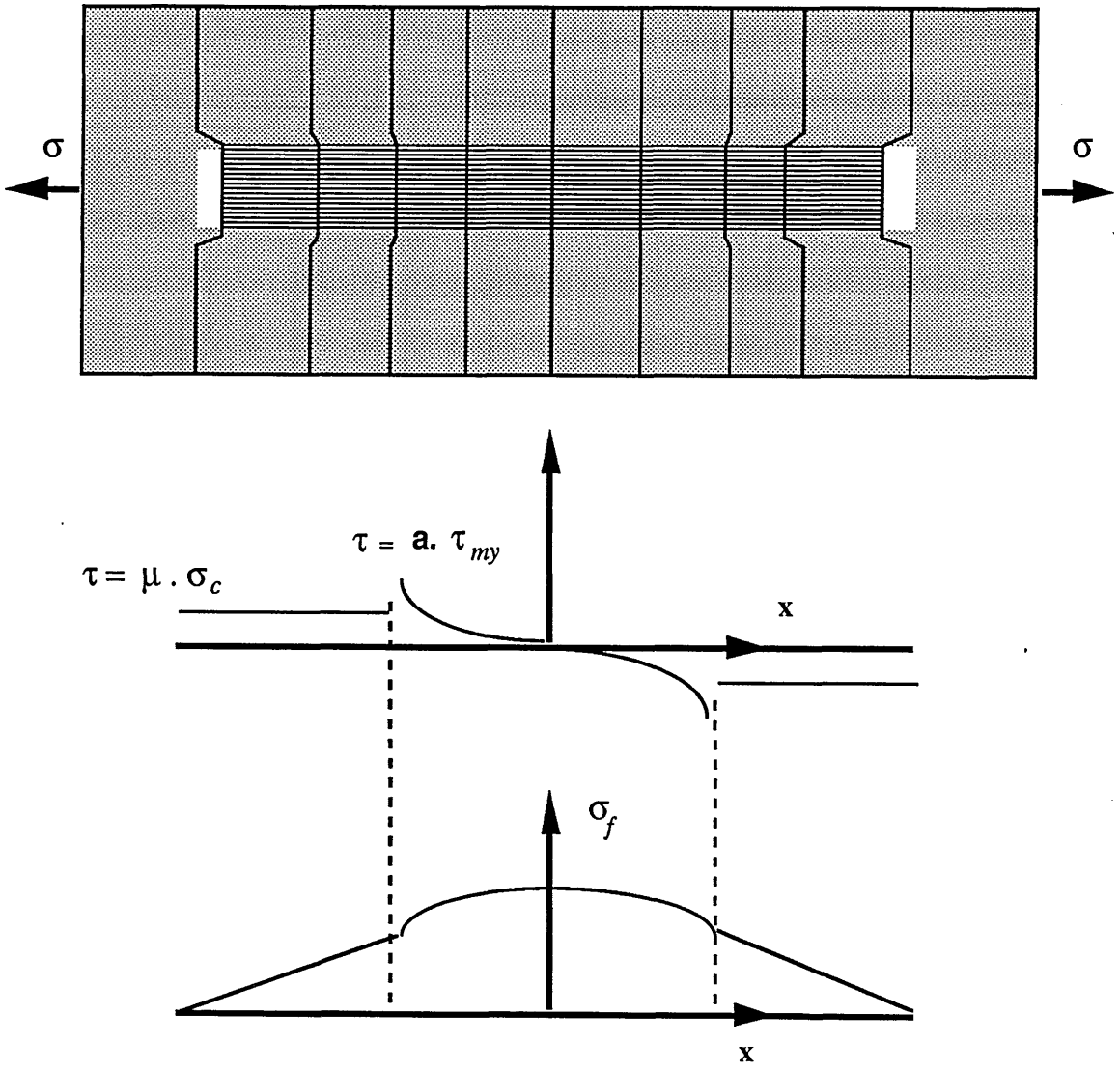


Figure 10.12 σ_f and τ_i as a function of **x** for a single embedded fibre with interfacial slippage between fibre and matrix (Piggott 1978) .

The stress transfer in a single fibre composite has been studied by Termonia (1987) using finite element modelling. His results show that $\mathbf{L}_c$ is a unique function of the ratio between $\mathbf{E}_f$ and $\mathbf{E}_m$ and is independent of fibre diameter. However, this result is only for a specified bonding efficiency between the fibre and the matrix, since $\mathbf{L}_c$ is directly dependent on the bonding efficiency. If the bonding efficiency falls below 30%, then $\mathbf{L}_c$ may increase by a factor of 2 or more over the case of complete bonding.

10.3.9 Conclusions

A large research effort has been directed towards gaining an understanding of the fibre-matrix interface via the use of various micro-mechanical experiments. Whilst an extensive range of experimental studies has been reported, most of these techniques yield values of τ_i with large experimental errors and in most cases this quantity is insensitive to changes in the fibre surface chemistry. Large variations between measured values of τ_i using different techniques have been also been reported. A serious need for a systematic study using the various micro-mechancial experimental methods with a specific fibre-matrix system thus exists.

Microscopic Raman spectroscopic techniques seem to offer a number of significant advantages over micro-mechanical methods and is currently one of the best available techniques for investigating the fibre-matrix interface.

A number of theoretical models of the fibre-matrix interface have been developed. Whilst these models seem to be theoretically sound, absolute experimental verification of their validity has not yet been reported.

To improve the fundamental understanding of the fibre-matrix interface, studies which consider interfacial pressure and the fibre-matrix interface chemistry need also to be undertaken.

10.4 A REVIEW OF FIBRE FRICTION

10.4.1 Introduction

Research in fibre friction has primarily resulted from the needs of the textile industry for the processing and manufacture of fibres. Generally, the frictional requirements for these applications are intermediate between the more popular interest in polymer tribology as typified by low friction engineering contacts in bearings, or the high friction required in brake linings. In fibre production, frictional forces must be sufficient so that reasonable fibre tensions can be produced for spinning and fibre processing. They should not however be too great so that fibre damage will occur.

Fibre friction is not currently an area of significant research interest and, as will be revealed in the following sections, the most important work in this area was done before 1970. Although a number of references quoted in this section are recent, they do not normally represent major advances in this field, but rather improvements in older established approaches. Few studies have been reported on the frictional behaviour of fibres important to the composite scientist, such as "Kevlar" or carbon fibres.

10.4.2 Single Fibre Friction Studies

Two experimental techniques have been developed which allow the friction of a single monofilament to be investigated. These techniques involve a monofilament in a point contact geometry, or in an extended line contact geometry.

The most important point contact experiment involves two monofilaments arranged orthogonally and is described as the "crossed fibre" experiment. One fibre is constrained at both ends whilst the other fibre has one end free to deform. By rubbing one fibre against the other, the bending of the free fibre allows the frictional force to be determined using beam bending theory. This technique has been extensively used by Tabor and his co-workers (Roselman and Tabor 1976; Pascoe and Tabor 1956) and more recently by

Briscoe and his co-workers (Kremnitzer 1978). These workers have studied the frictional properties of carbon, nylon, cellulose acetate and PET monofilaments.

The principal line contact methods are based on a single fibre passing over a cylindrical capstan. This type of experiment has found considerable usage in industry due to the relative experimental simplicity and expediency when compared to the point contact experiments. A number of variations in the experimental method and analysis have been investigated and they have been reviewed by Smith (1979). Schick (1975) has described an number of experimental systems which are used by industrial laboratories.

These studies generally support the adhesion model of friction described earlier (Chapter 7.2.2). For example with PET fibres the α and τ parameters provide a good means of predicting the form of dependency of μ in Equation 10.5.

10.4.3 Fabric Mechanics

In common with the previous section, most of the published work on the mechanics of fabrics in over 20 years old. Relatively few developments have been reported during the last few years suggesting a generally low level of current research interest. Where possible, recent work has been quoted in this review.

The seminal work on the modelling of fabric properties as a function of the geometry of fabric weave was reported by Peirce (1937). The basic nature of this model remains unchanged, though it has since been modified by a number of other workers. It forms the basis of most analyses of specific fabric mechanical properties. The mechanical properties of fabrics are mathematically described in terms of the yarn spacing, the weave angle, the yarn diameters, the crimp heights and the thread spacings.

Research on the tensile and bending properties of fabrics has been studied by a relatively small number of workers; Hearle, Grosberg, Leaf and Abbot. The tensile characteristics of typical fabrics have been analysed by Hearle *et al.* (1969) as well as by Grosberg (1977) and Leaf (1979). Bending properties of fabrics have been studied by

Grosberg (Grosberg and Swani 1966; Abbott *et al.* 1971,1972) as well as by Gibson and Postle (1978). In the cases of both tensile and bending deformations, these researchers have concluded that inter-fibre and inter-yarn friction is a very significant factor in the mechanical response of the fabrics. The ability of fibres and yarns to migrate, and thus accommodate the imposed stresses, directly depends on the frictional forces associated with these fibre interactions. However none of these models directly considers the effects of fibre friction, but rather include this behaviour within a general hysteresis parameter.

Fibre migration has been considered by a number of workers in the context of twisted yarn systems.These models have been reviewed by Motamedi (1989) who points out that none of these models account for the inter-fibre frictional forces. This author has demonstrated the importance of frictional effects in determining the mechanical behaviour of "Kevlar" fabrics under indentation loading. The effects of friction were successfully modelled on the basis of changes in the effective tensile modulus of the fibre assembly.

10.4.4 Conclusions

The frictional properties of single fibres may be measured via both point and line contact experiments. However, very little experimental work relevant to composite science has been reported. Although a number of models of the mechanical behaviour of fabrics have been developed, none of these models explicitly consider the inter-fibre friction and represent frictional phenomena within the macroscopic effects of hysteresis. However, it is now becoming accepted that inter-fibre friction is a critical factor determining the mechanical behaviour of fabrics under tensile, bending and indentation deformations. The surface chemical modifications described in Chapter 3 which were specifically designed to modify the fibre-matrix adhesion will clearly modify the mechanics of the yarn if these treatments have changed the fibre-fibre frictional characteristics. This prospect is considered further in a later section of this Chapter.

10.5 EXPERIMENTAL FIBRE MECHANICS STUDY

10.5.1 Introduction

The fibre pull-out, the fibre fragmentation and the micro-droplet debonding methods for the measurement of τ_i were all considered for use in this experimental study.

Initial experiments were conducted using the fibre fragmentation method using the methodology of the type described in Section 10.3.6. However, after a number of unsuccessful attempts to induce fibre fragmentation, these experiments were abandoned. The non-brittle fibre failure in aramid fibres, as observed by Drzal (1983), and the difficulty in achieving sufficiently large matrix strain to obtain fibre fractures seemed to be the major problems.

Considering the difficulties which have been historically associated with the fibre pull-out techniques, it was decided that the micro-droplet debonding method offered the best chance for the successful measurement of τ_i . This conclusion was supported by the small errors in τ_i recently reported by Gaur and Miller (1989). Another important prospect involved the untried possibility of measuring both the wettability of the droplets on the fibres using the Carroll drop profile method prior to curing the epoxy, followed by using the debonding method for the measurement of τ_i. Thus a unique opportunity for obtaining surface chemical and surface mechanical measurements within the one sample existed.

10.5.2 Micro-debonding Experiments

Preliminary experiments were conducted to establish the accuracy and repeatability of these types of experiments. Samples were prepared by wrapping single "Kevlar" monofilaments around a 25mm by 100mm rectangular frame made from glass rod. Micro-droplets of an epoxy polymer (Polysciences 812 epoxy, NMA co-monomer and DMP accelerator) were carefully deposited onto the monofilaments so that axi-symmetrical droplets formed on the fibre. On each 25mm piece of filament were placed two droplets.

The frames with the monofilaments were then placed into an oven and allowed to cure at 80° C overnight. The 25mm long fibre lengths were then carefully removed from the frame. One end of each fibre length was attached to a small aluminium tab, 4mm x 8mm, using a drop of epoxy adhesive. The tabs were hung onto a small capacity load cell of the Instron Testing machine via a small hole which had been drilled in each tab.

Initial experiments were conducted with a number of PDMS, metallated/cleaned and diol modified "Kevlar" fibres. Single fibre specimens were attached to the load cell and the free fibre end was allowed to fall between the debonding slits as formed between two razor blades. The Instron crosshead was raised at a rate of 0.5mm/minute and the slits were set at a width greater than the fibre diameter. As the droplet approached the debonding slit, the slit width was slowly decreased until a slight frictional resistance between the fibre and the slits was detected. This small frictional force was essentially constant in magnitude. When contact between the droplet and the slits was achieved, the force detected increased in a linear manner as shown below in Figure 10.13.

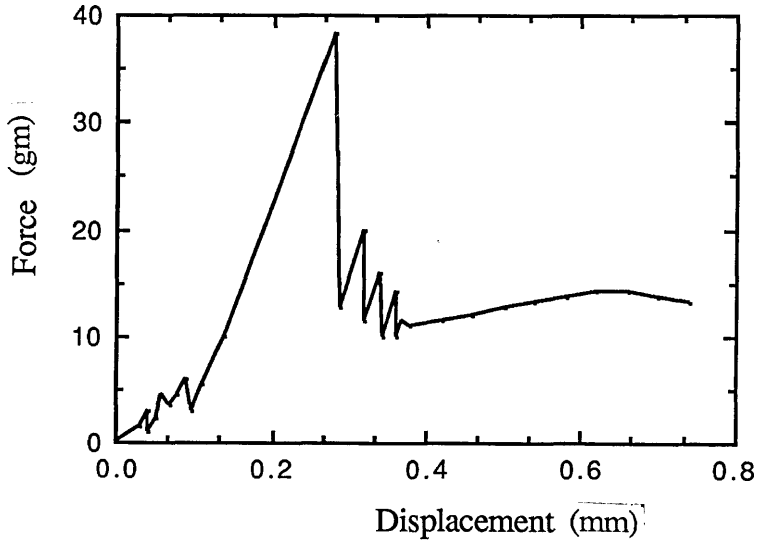


Figure 10.13 Typical trace of **F** versus **d** obtained by debonding an epoxy micro-droplet from a "Kevlar" fibre.

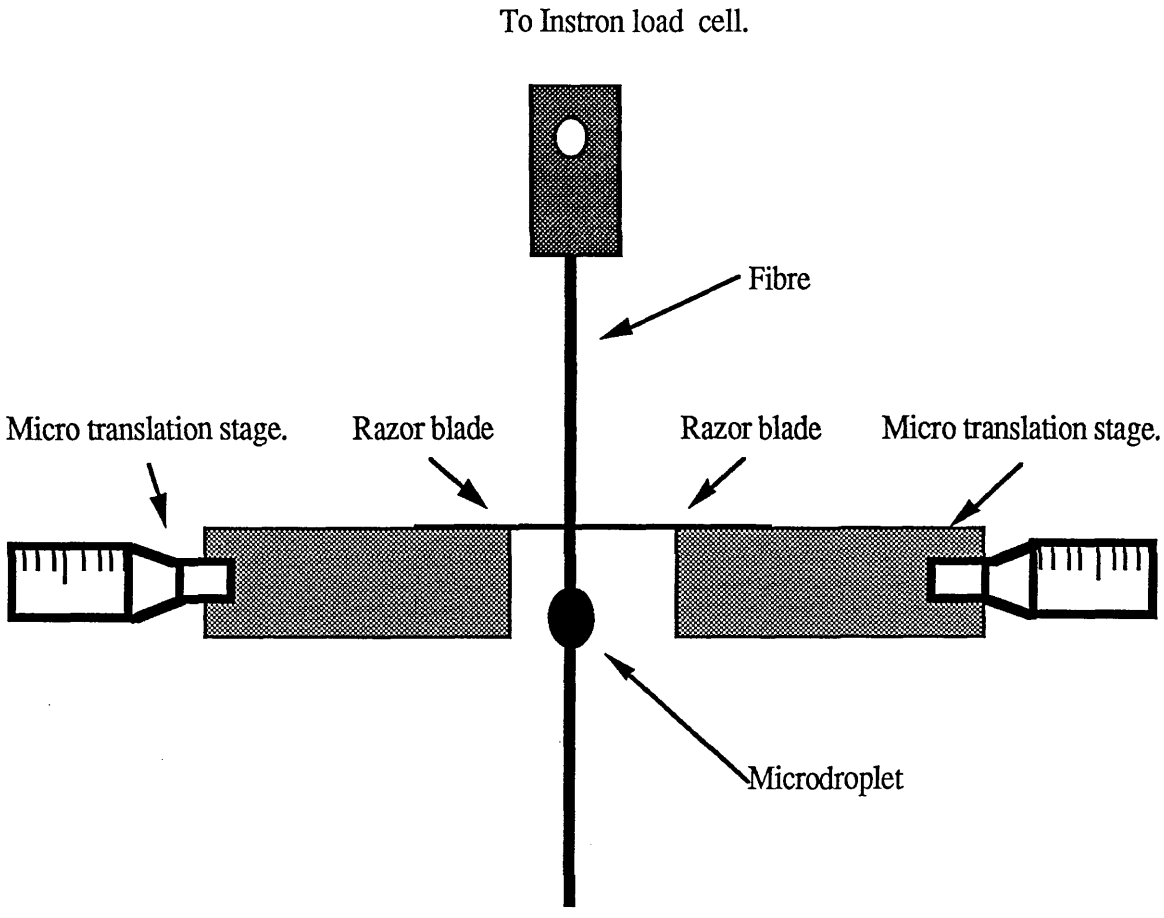


Figure 10.14 Apparatus for conducting the micro-debonding experiments.

At a critical force, fibre debonding occurs which results in a rapid decrease in the load. The maximum force was equated with the debonding force and τ_i was calculated using Equation 10.3. Figure 10.14 also illustrates the level of frictional force after the initial debonding. Though the PDMS treated fibres showed lower frictional forces after debonding, it was not possible to measure the coefficients of friction since the contact pressure was unknown.

Fibre Treatment	τ_i (MPa)	τ_i (MPa)	τ_i (MPa)	τ_i (MPa)	τ_i (MPa)
Diol Grafted	35.3	28.8	42.0	33.0	28.4
Metallated/clean	24.8	30.9	41.0	21.3	23.6
Poly(dimethyl siloxane)	27.0	30.9	35.7	25.1	34.0

Table 10.5 Individual measurements of τ_i using the shear droplet debonding technique for a range of surface treated "Kevlar" fibres with an epoxy polymer.

The results shown in Table 10.5 represent the measured τ_i values for 5 individual debonding experiments using three different surface treated "Kevlar" fibres. These results are in general agreement with those results already reported (Miller *et al.* 1985) and shown in Table 10.4. These workers reported values of 38 MPa. for τ_i . Although a statistical analysis of the experimental results shown in Table 10.5 has not been attempted, it is clearly evident that there is a large variation in the τ_i values for each type of sample. More significant is the similarity of the results for each of the three different types of sample. The level of accuracy and precision reported by other workers who have used this technique (Miller *et al* .1985; Gaur and Miller 1989) was not replicated by this study and thus the technique used in this laboratory requires additional development.

In view of these factors it was concluded that these measurements of τ_i, as performed in this study, were not sufficiently accurate to warrant a large scale study. The values of τ_i compare favourably with those obtained in thin film shear experiments assuming that the contact pressure is of the order of 10^7 to 10^8 Pa.

By considering the dependency of τ_i on factors such as polymer morphology, bulk yield stress and structure as established by Smith (1979), it is possible to postulate a qualitative ranking of τ_i for the various aramid fibre surfaces prepared in Chapter 3. This list is shown below in Table 10.6. For most of these materials in this list their ranking will primarily reflect the bulk shear properties of the material. "Kevlar" is known to have skin/core structure, with highly orientated crystalline material in the core regions and amorphous polymer in the outer skin regions of the fibres. In the case of the grafted "Kevlar" fibres, the removal of amorphous material from the surface of the fibres during the reaction (Takayagagi *et al.* 1987) would be expected to expose crystalline regions of PPTA with increased values for τ_i.

Fibre Surface Treatments	Typical τ_i values	
Poly(dimethyl siloxane) coated (PDMS)	10^3-10^4 Pa	↓ increasing τ_i
Poly(ethylene glycol) coated (PEG)		
"As received" fibres		
Epoxy coated	10^8 Pa	
Amine coated		
Clean		
Diol and Epoxy grafted		
Metallated/clean	10^8-10^9 Pa	↑ decreasing τ_i

Table 10.6 List of predicted values of τ_i decreasing in magnitude from the top of the list. Approximate values for τ_i are also shown based upon a subjective assessment of literature data.

10.5.3 Compressional Properties of "Kevlar" Fabrics

It was previously established in section 10.4.3, that the mechanical properties of fabrics are directly related to the inter-fibre friction. In this section the compressive properties of surface modified aramid fabrics are reported. The compressive deformation of aramid fabrics is a particularly relevant experiment for the study of composite materials. These fabrics undergo a similar deformation during the fabrication of laminate specimens in the autoclave.

The compressional properties of a number of the surface modified "Kevlar" fabrics were measured using an Instron Testing machine. Eight layers of the various "Kevlar" fabrics used in the fabrications of laminates were horizontally stacked together. The fabric stack was then compressed against a flat platen using a small circular indentor of 25mm in diameter, with a flat face. The rate of compressive straining was defined by the movement of the indentor attached to the instrument crosshead (0.5mm/min). The initial separation between the platen and the indentor was 3.5mm and the fabric stack was strained until a load of 60kg was recorded. This level of loading corresponds to a pressure of about 1.2 MPa. The impregnated fabrics used to fabricate the composite panels are subjected to a pressure of 0.6 MPa during autoclaving. The fabric samples were then unloaded at the same crosshead speed so that both the loading and unloading compressive properties of the fabric were measured.

The results obtained are shown below as a function of compressive strain and stress. The numbers in brackets after the fabric type denotes the compressive cycle number.

Figures 10.15 and 10.16 clearly show that the compressive properties of the various "Kevlar" fabrics are distinctly different. Figure 10.15 shows a dramatic difference in the shape of both the loading and unloading compressive cycles for four different surface treated fibre samples. In both Figures the fabrics were loaded until a strain of 45% was

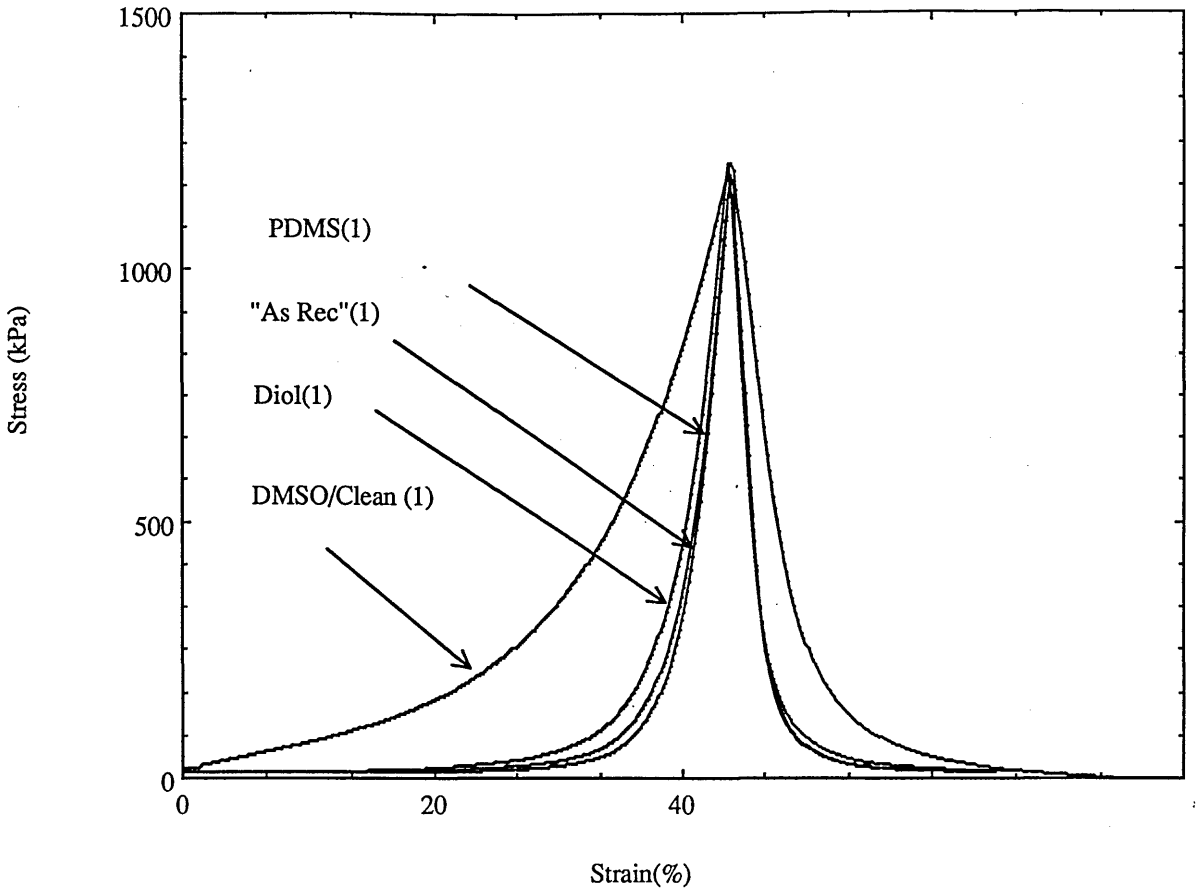


Figure 10.15 Compressive loading and unloading of a range of surface modified "Kevlar" fabrics.

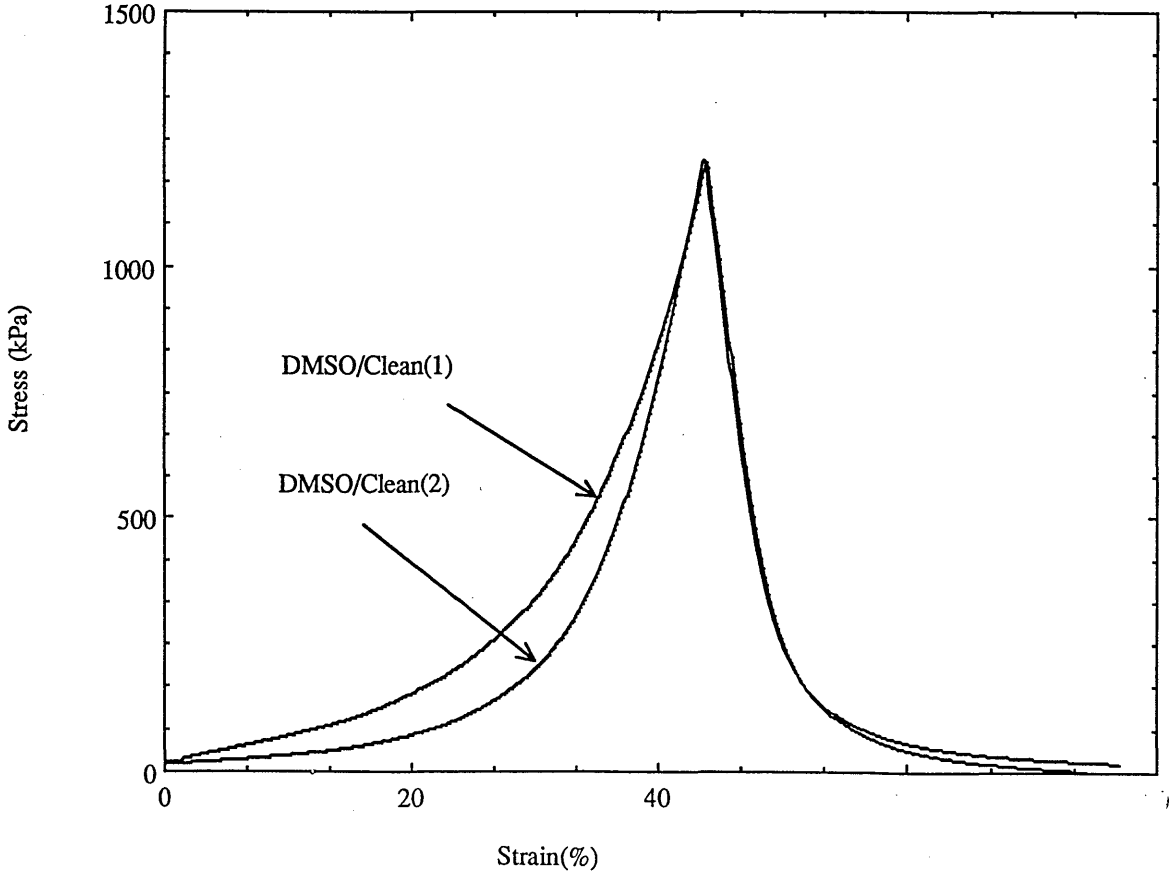


Figure 10.16 First and second compressive loading/unloading cycles for the metalled/clean "Kevlar" fabric.

recorded. Then the samples were unloaded at the the same strain rate.The shape of the loading curve indicates that the metallated/clean fabric is a significantly more compliant system than the other fabrics. The other three fabrics show a steeper gradient in the load versus strain curve indicating that these materials are effectively stiffer systems mechanically. This type of behaviour is normally associated with fibre assemblies in which the lubricated nature of the inter-fibre contact improves the effective stress transmission within the system. Using the compliance of the fibre assembly as a qualitative measure of the inter-fibre friction, an order of frictional coefficient can be estimated for the fibres:

Metallated /clean >> diol > "As Received" > PDMS

The compressive properties of these "Kevlar" fabrics were also determined as a function of the number of compressive loading/unloading cycles. The three samples with the smallest compliance showed no observable variation in the compressive properties as function of load cycle. However the metallated/clean fabric showed a pronounced effect which is evident in Figure 10.16. This response is commonly observed in assemblies which have high friction properties. During each loading cycle a number of the high friction inter-fibre junctions are ruptured and are not re-established during the unloading cycle. Consequently during the following loading cycle, the system is less compliant since a smaller number of junctions exist to resist the loading.

The compliance of the fabrics also shows a general agreement with the ranking of τ_i shown in Table 10.5.

Therefore it is clear that the surface modifications have affected the interfacial rheology and the friction properties as is reflected in the compression properties of the fabrics. Furthermore the order of fabric compliance in compression was consistent with the rankings shown in Table 10.5.

It is now appropriate to consider whether or not these changes in the mechanical

properties of the fabrics could be responsible for the subtle changes in the interlaminar fracture behaviour of the laminates. Chapter 8 provided a convincing argument of the importance of fibre-bridging effects and how this effect could be quantified in terms of the quantity a_b. The extent of fibre bridging was also found to be consistent with the observed appearance of the fracture surfaces. At that time it was noted that the surface modifications designed to improve fracture toughness appeared to produce the opposite effect. The lubricated fibres specifically designed to reduce adhesion (assuming that the surface coating remained in place during processing) between the fibre and the matrix based on surface energy considerations in fact produced the toughest specimens as shown by Table 8.4. It is extremely significant that the fracture mechanics toughness correlates with mechanical response of the fabrics under compression. The question now asked is as to how the interfacial and mechanical properties of the fabric influence the extent fibre bridging during fabrication.

At this point it should be noted that the extent of fibre-bridging should correlate with the work required to compress the fabric to a given stress. For discussion purposes it is useful to describe the transverse compressive work as the "resilient" of the fabric. That is, the fabric with the highest interfacial shear strength which provided the most "resilient" fabric would have the capability to maintain the fabric topographic features during compression. The rugosity of the fabric surface would not be "squashed out". If this type of model is to be pursued it is necessary to invoke another mechanism which would promote fibre migration during processing. It will be realised that the most "resilient" fabrics produced the weakest composites as distinguished by the interlaminar fracture results.

In order to proceed it is necessary to speculate that the important step is a fibre penetration process on a large scale, which would not produce a small number of large bridging points, but rather a process which would allow relatively small units of fabric or fibres to migrate into the adjacent fabric or matrix regions. The low friction system would,

in polymer parlance, have a less affine character. Relatively small units of the fibre would be able to migrate in a relatively free way independently of the neighbouring fibres. In this way a multitude of localised, and hence small, fibre migration events would occur.

This model could be likened to the process involved in diffusion enhanced adhesion (Chapter 2.2.2). In this case the diffusion of the low molecular weight species would correspond to the migration of short autonomous filament lengths which would be a characteristic of the low friction fabrics. The high friction systems would be analogous to the case of a crosslinked polymer where molecular diffusion is constrained by the crosslinks. Then only relatively large and infrequent bridges would be developed.

At this stage this proposition can only be regarded as reasonable speculation, but has the virtue of providing:

(i) self consistent rationalisation of the fracture mechanics

(ii) an explanation for the lack of correlation between the G_{IC} and the surface energy data.

10.5.4 Conclusion

Attempts to measure τ_i using the micro-droplet method were partially successful. Preliminary estimates of τ_i for the debonding of epoxy droplets for aramid fibres were made and these values agree with the literature values for similar systems. However, the technique employed in this study was too imprecise and a large scatter in the reported experimental results was observed.

The compressive properties of aramid fabrics was found to be strongly dependent on the type of surface treatments employed. It appears that the mechanics of these fabrics is strongly dependent on the fibre-fibre friction. This agrees with other work which has shown that the tensile, bending and indentation properties of fabrics is determined significantly by fibre frictional effects. The graft reactions had a particularly dramatic effect

on the mechanical response of the aramid fabric materials. This behaviour was probably due to additional surface roughness associated with these aggressive reactions. The ranking of frictional properties deduced from the compressive experiments was in general agreement with the ordering of τ_i reported in Table 10.6.

More work needs to be undertaken to clarify the interrelationship between fibre friction and the mechanical performance of surface modified fabrics. The present study however indicates that the surface chemical modifications do produce significant changes in the mutual interfacial shear stress of "Kevlar" fibres. These changes are clearly manifested in the compressive mechanical properties of the fabrics.

The relationship between friction, fracture mechanics and fabric mechanics has been established as discussed earlier in this Chapter. It is tentatively suggested that fibre migration is an important process which is apparently directly controlled in part by the fibre-fibre friction characteristics of the fabric

CHAPTER 11

CONCLUSIONS

This thesis has evaluated the effects of fibre surface modifications on the mechanical performance of aramid composites along research lines established by previous research workers. Like many of these workers, this study has not discovered the predicted correlations between the fibre surface properties and the mechanical performance based upon the classical models of adhesion which may be used to describe fibre-matrix adhesion.

A wide range of surface modifications were implemented for the aramid fibres studied and these fibres were characterised in a comprehensive and systematic manner. The surface characterisation, modifications, laminate fabrication and laminate testing were experimentally performed with as much care and accuracy as possible in this study so as to afford the best basis for obtaining accurate and appropriate data.

Fibre modifications were chosen so that a range of interface adhesive strengths could be prepared, from potentially weak to potentially strong interfaces. A range of new functionally grafted fibres surfaces was prepared for this purpose. The success of these surface reactions was confirmed by XPS and wettability results. The surface characteristics of the fibres were quantified in terms of the surface energies and heats of adsorption using wetting and gas adsorption measurements.

Virtually all of the currently available techniques for the physicochemical characterisation of solid surfaces have been used in this study to investigate the aramid fibre surface properties. The types of probes used to sense these surface properties included X-rays, gases, liquids and solids. All of these techniques were demonstrated to provide critical information about the state of the fibre surface. In many cases the information provided by each of these techniques is complementary and consistent.

XPS was found to be valuable in assessing the surface chemical composition of the

fibres and thus allowing the success, or not, of the various surface modifications to be quantified. The simplicity, sensitivity and continuing improvements in the experiment technique will maintain the importance of this method for polymer surface analysis.

Wettability measurements revealed information about not only the surface energetics of the fibres, but also on their surface topography. This technique was the primary source of thermodynamic data for the fibre surfaces as well as providing practical data on the likely wetting behaviour of the fabric by the epoxy polymer.

IGC yielded information of a fundamentally similar nature to that obtained from the wettability experiments. Although these experiments are difficult and more time consuming than wetting measurements, they can reveal subtle but important information about adsorption interactions. This technique is not complicated by the problems of fibre surface roughness and also allows characterisation information to be determined for a large fibre sample size. Further work is required to develop this technique so that it is suitable for routine characterisation and also to explore its full potential.

The only other techniques which may have provided additional useful information would have been the use of other vacuum spectroscopic techniques, especially those which would allow single fibres to be studied. Scanning secondary ion mass spectroscopy, spatially resolved XPS or thermal desorption mass spectroscopy would be three possible techniques. No single fibre high resolution electron microscopy were undertaken in this study.

Thus, this comprehensive characterisation of the fibre surfaces, prior to their impregnation with epoxy polymers, could have been expected to provide the necessary information from which the correlations with the mechanical performance of the laminates, expected by many workers, would be obtained. The accepted wisdom is that the nature of the fibre surface will influence the adhesive strength with the matrix and hence the composite mechanical properties.

The range of mechanical tests chosen in this study were of necessity a compromise since a very large number of potentially useful tests exist. Micro-mechanical measurements

were undertaken because of the strong precedents established by other workers. Fracture and interlaminar shear measurements are probably the most direct and best established mechanical tests for assessing the influence of the fibre-matrix adhesion. These were the major methods adopted in this work. Ballistic tests were chosen on the basis that they represent an important application area for aramid fibre reinforced composites.

Whilst the flexural deformation results for the "Kevlar" laminates were found to be insensitive to the quality of the fibre-matrix interface, small variations in the interlaminar shear strength, as measured by a short shear beam tests were found. Most laminates yielded interlaminar shear strengths of *ca.* 40 MPa, except both of the epoxy grafted and coated fabrics which gave results which were 10% higher, and the metallated/cleaned sample which was 20% lower in shear strength. However, these variations in shear strength did not directly correlate with the fibre surface energetics.

What is believed to be a new method for the analysis of the fracture mechanics of composites was developed based on the concept of a reduced crack length. This approach was demonstrated to be suitable for the analysis of a fracture where substantial fibre bridging occurs which constrains crack growth. The G_{IC} results and the derived values for the size of the fibre bridging zone, a_b, were found to be dependent on the nature of the fibre surface treatments. The values of G_{IC} varied from 0.90 kJ/m^2 in the case of the metallated/clean fibres to 2.85 kJ/m^2 in the case of the PDMS coated fabrics. The larger values of a_b were observed for those materials with the largest G_{IC} parameters. Microscopy revealed that the fracture surfaces which exhibited the largest values of G_{IC} exhibited the most fibre pull-out and disruption to the aramid fabric. The substrates with the lowest fracture energy showed few pulled-out fibres and "clean" epoxy fibre "beds".

The ballistic deformation experiments revealed that the increasing size of the damage zone caused by the impact of a high speed projectile generally correlated with a decrease in the interlaminar fracture energy of the laminate. However, the presence of larger interlaminar damage zones did not lead to an increased energy absorption on impact, but rather the contrary behaviour. This trend was presumably due to a more efficient energy

dissipation associated with mechanisms such as fibre bridging.

A limited study of single fibre micro-mechanics revealed similar values for the interfacial shear strength for the epoxy polymers with a number of the modified fibres. Debonded fibres revealed "clean" fibre surfaces with no apparent traces of the epoxy resin suggesting a predominantly interfacial failure. The measured values for τ_i were similar to other values reported for aramid fibres and comparable with results obtained for glass fibres. Preliminary fabric mechanics experiments showed significant variations between the compressibility of a number of the treated aramid fabrics. These differences were related to the fibre-fibre and yarn-yarn friction within the aramid fabric and are consistent with established analytical precedents in describing the mechanics of fabric assemblies. The various graft reactions led to increased friction due to the partial etching of the amorphous outer layers of the aramid fibres by the metallation reaction. The presence of PDMS resulted in fibres with low fibre-fibre friction. The interfacial shear strength of the various treated fibres was deduced on the basis of published data in this area. The fabric compressibility results indicate that the chemical changes instigated in Chapter 3 produced marked variations in the fabric compliance or "resilience".

Generally, the mechanical tests results did not reveal the predicted correlations between the composite material performance and the fibre surface properties. This observation seems to be generally true and many other workers have noted poor correlations between these properties. Two possible explanations for this conclusion exist. Firstly it is possible that the physical and chemical characteristics of the fibre surface are not maintained and the expected fibre-matrix interactions did not develop during the fabrication process. Or, secondly that phenomena other than those currently considered are critical in determining the material performance.

The strongest correlation obtain in this thesis was between the fibre bridging measured during interlaminar fracture with the fibre-fibre friction of the fabric and the tentatively deduced resultant structural changes in the composite laminate. Ironically, the fabric properties which gave the largest fracture energies corresponded to the systems with

the lowest predicted interface adhesive strength. These results indicated that the fibre-fibre friction critically affected the ultimate composite structure and hence were more important than the predicted simple adhesion strength of the interface. That is the simple notion of an expected composite performance based upon a structureless fabric where matrix-fibre interactions predominate is not an appropriate model.

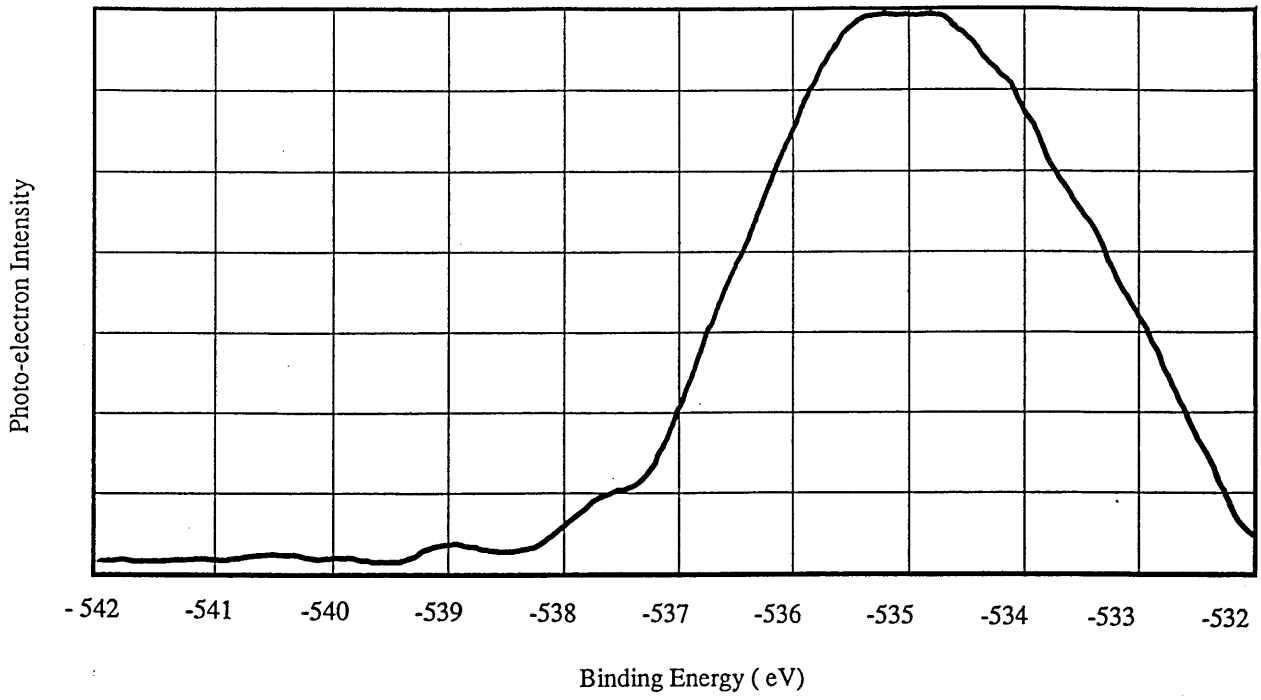
The later parts of Chapter 10 speculated upon the ways in which the magnitude of the fibre-fibre friction might, through its influence upon the mechanics of the fabric, influence the extent of fibre bridging in the resulting composite. Low friction fabrics, or rather fabrics comprising fibres with low mutual friction, may produce composites with many small dispersed fibre bridges. An analogy was offered with diffusion enhanced adhesive processes. Low friction systems have higher fibre migration rates or potential. The point of note is that the adhesion will be, as a result, controlled by the unfashionable "interlocking" processes introduced earlier (section 2.2.1). The final logical deduction is that in this case fibre-matrix adhesion will be of no consequence; *quod erat demonstrandum.*

JANUS

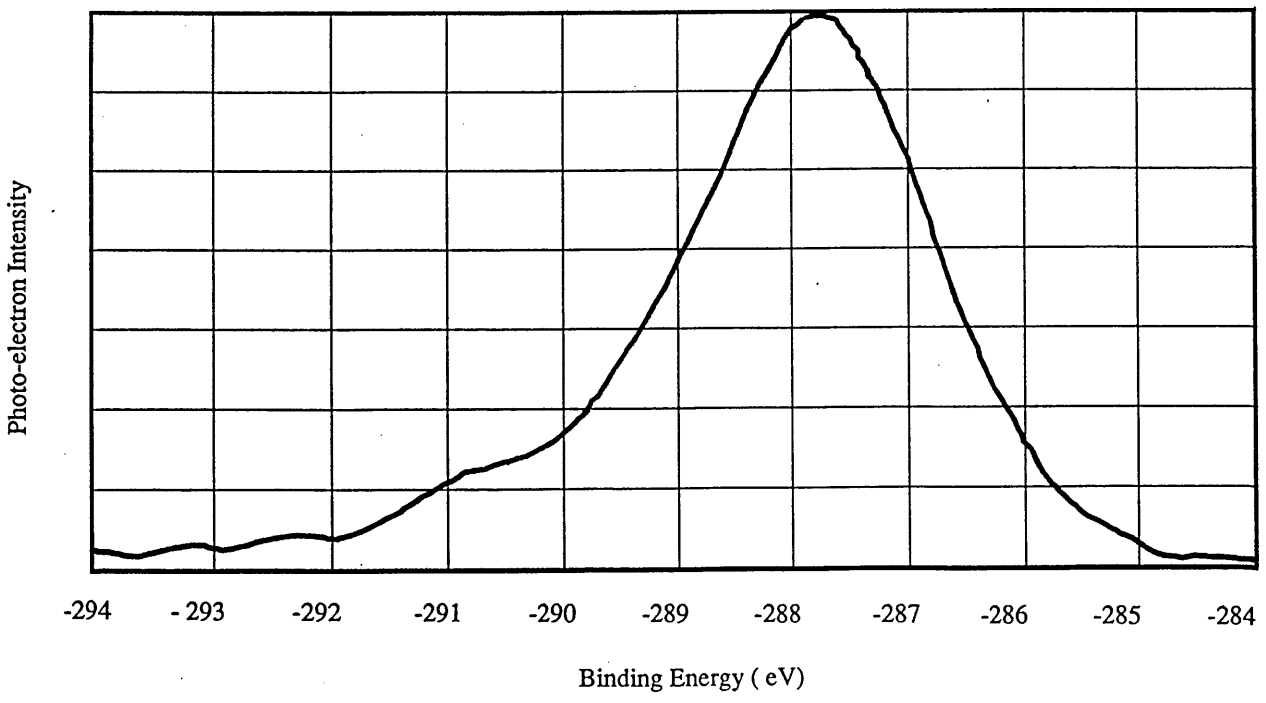
The study reported here has sought the Holy Grail of composite technology; the correlation between adhesion and mechanical performance. As in the classics the current search has been unsuccessful as the Grail has remained elusive. On the basis of this study it is not possible to dismiss the role of fibre-matrix adhesion. However its importance, like the Grail, must remain a matter of faith. This study suggests that another thing is of more relevance ; the structure of the system rather than the adhesion *per se'*. Whatever the truth , if a simple truth exists in such complex systems, it is perhaps of little scientific consequence. Like the medieval knight it is the cause of the quest which is the thing of value. The matters of practical significance are less easily dismissed. The thesis offered at the conclusion of work suggests a search for a causal phenomenon of arguably greater practical significance. At this time the proposed search for a structure mechanical property, rather than an adhesion-mechanical property correlation, may be misplaced in a commercial context. This remains to be seen. In any event it will provide an equally acceptable vehicle for scientific enquiry.

APPENDIX A

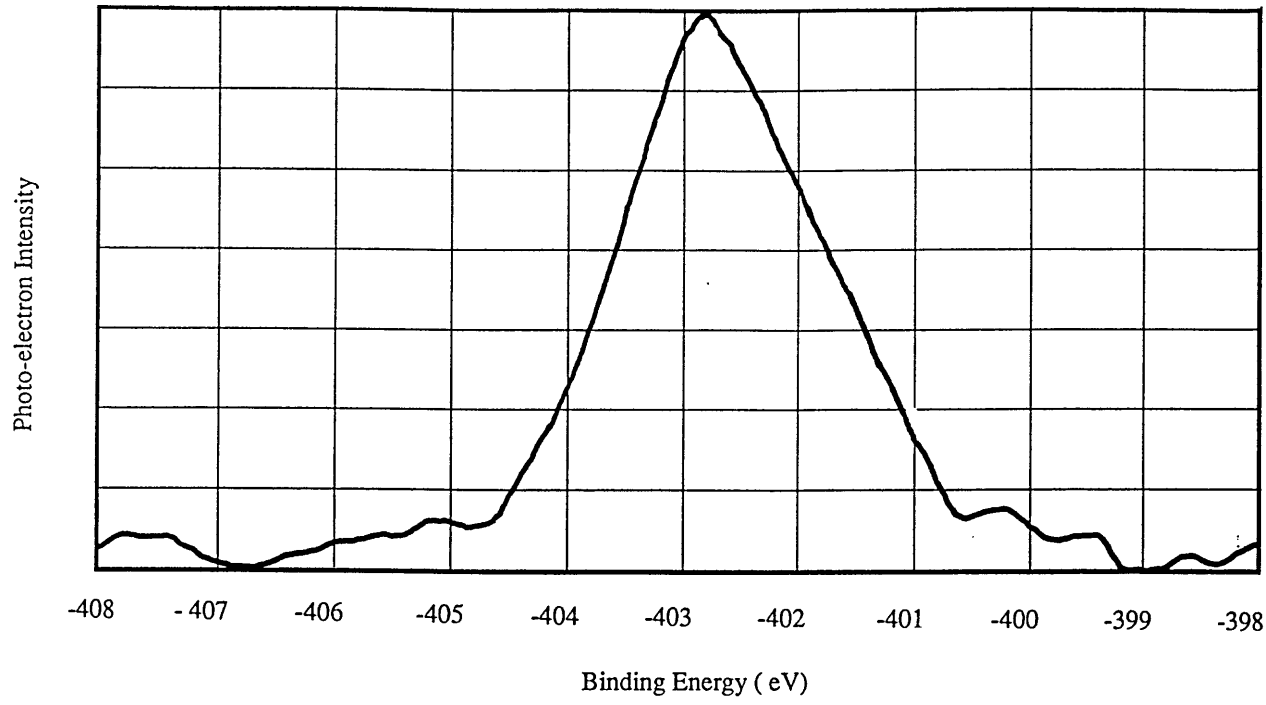
XPS Spectra of Surface Modified "Kevlar" Fibres



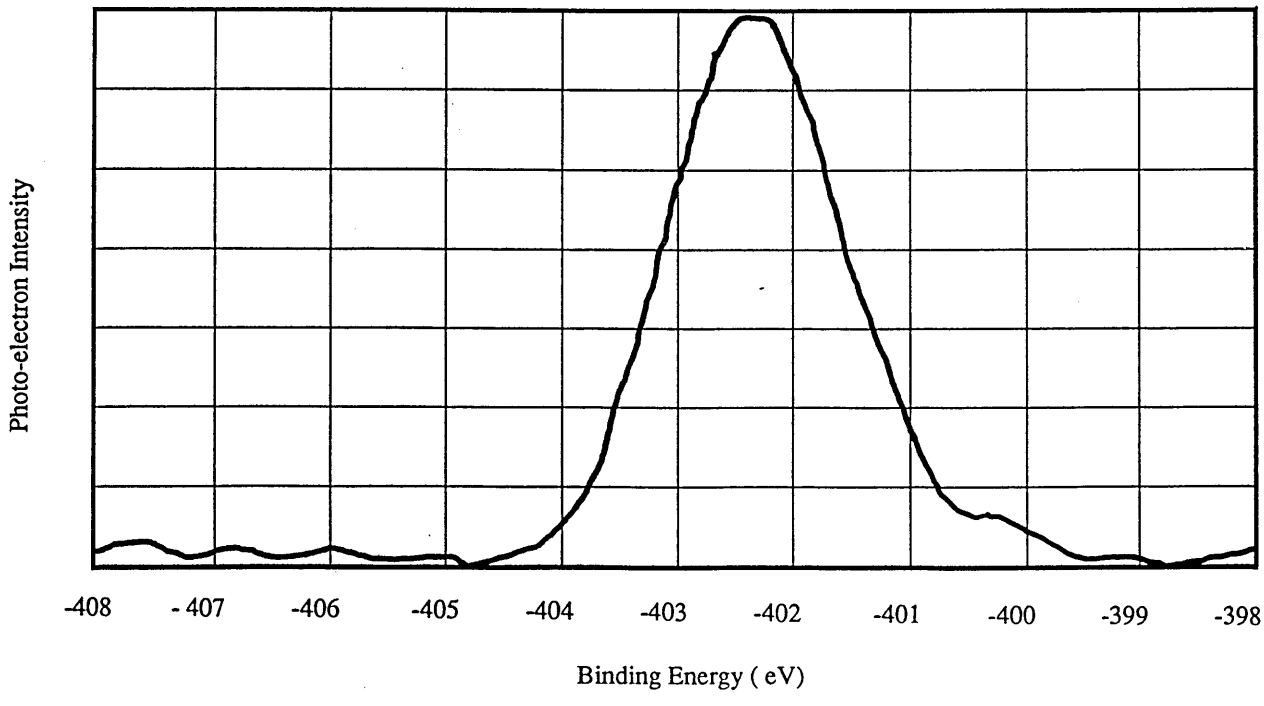
Oxygen 1s XPS spectrum of "as received" "Kevlar" fibres.



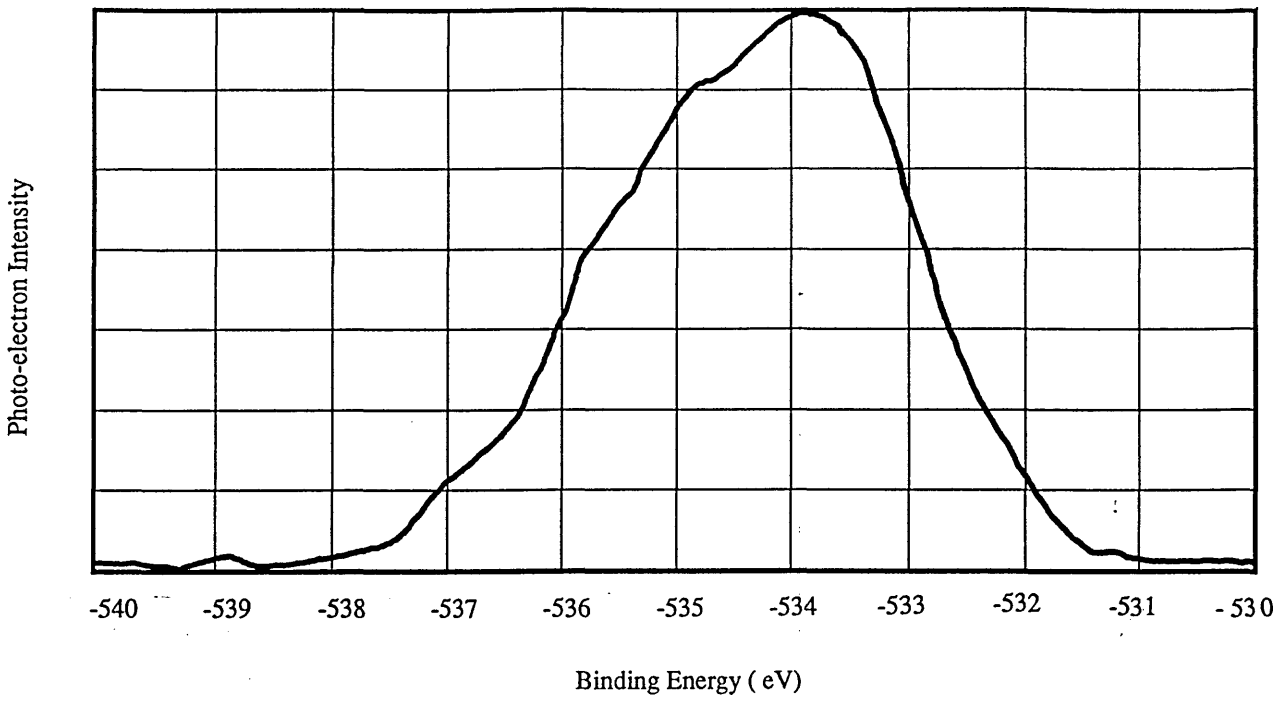
Carbon 1s XPS spectrum of "as received" "Kevlar" fibres.



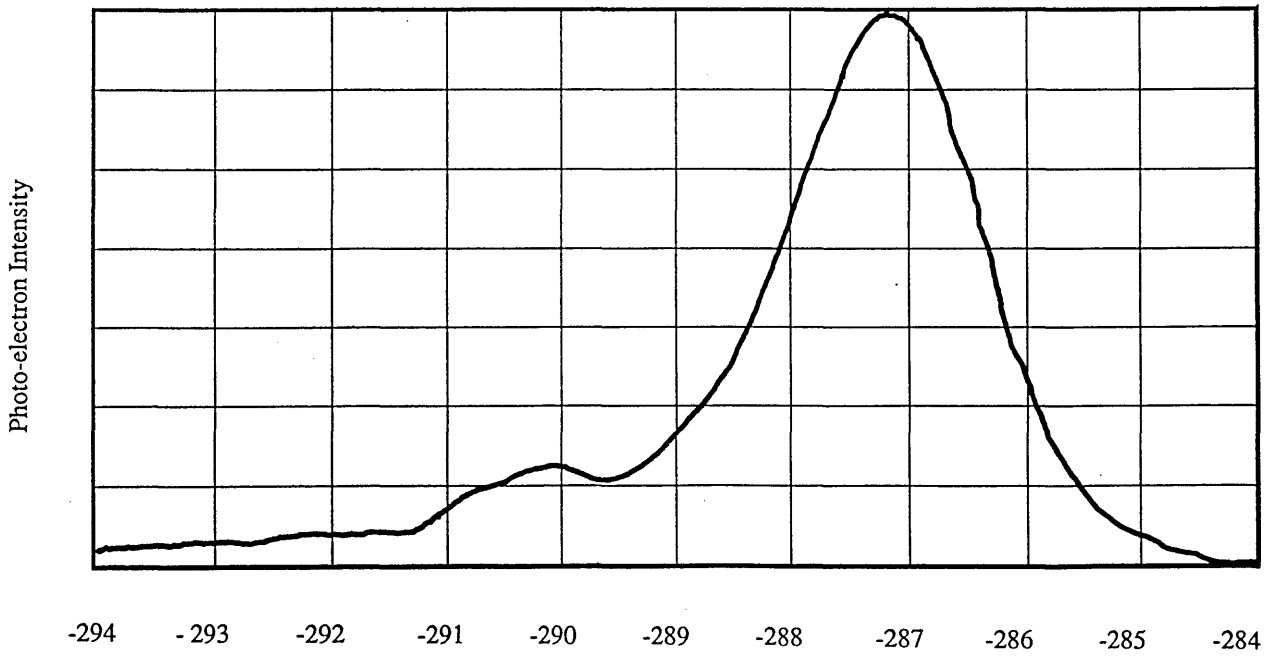
Nitrogen 1s XPS spectrum of "as received" "Kevlar" fibres.



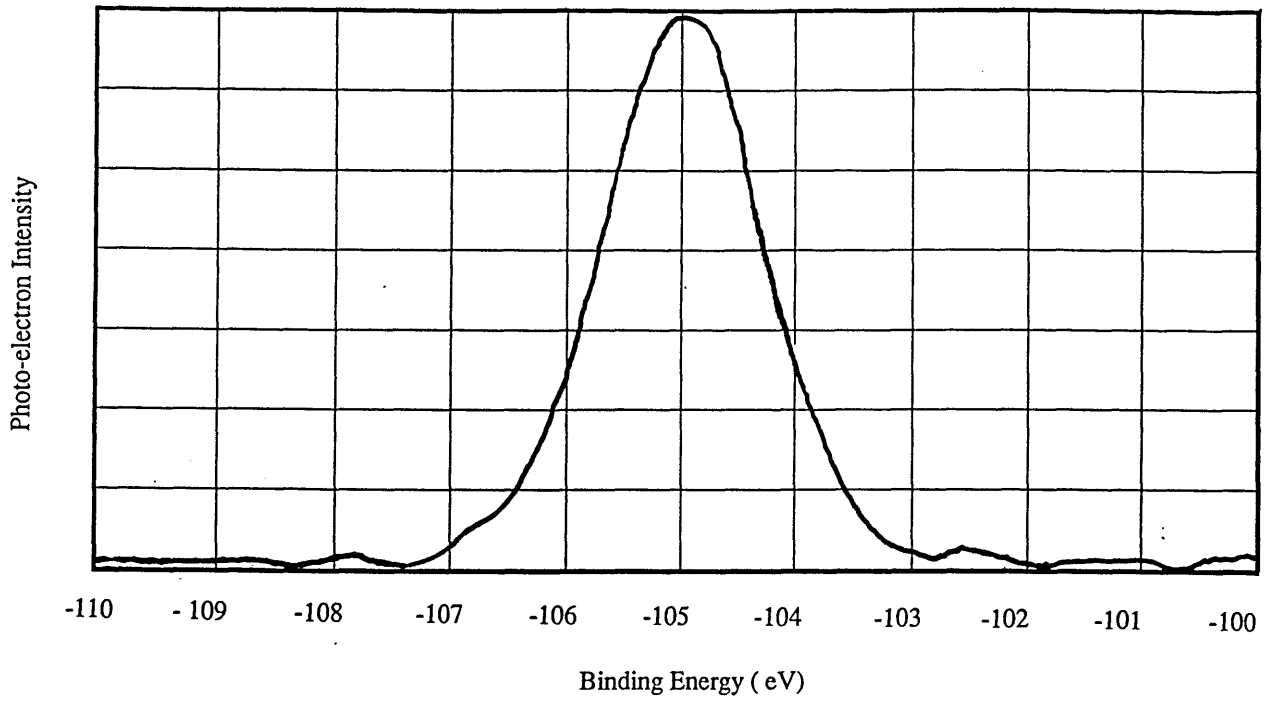
Nitrogen 1s XPS spectrum of cleaned "Kevlar" fibres.



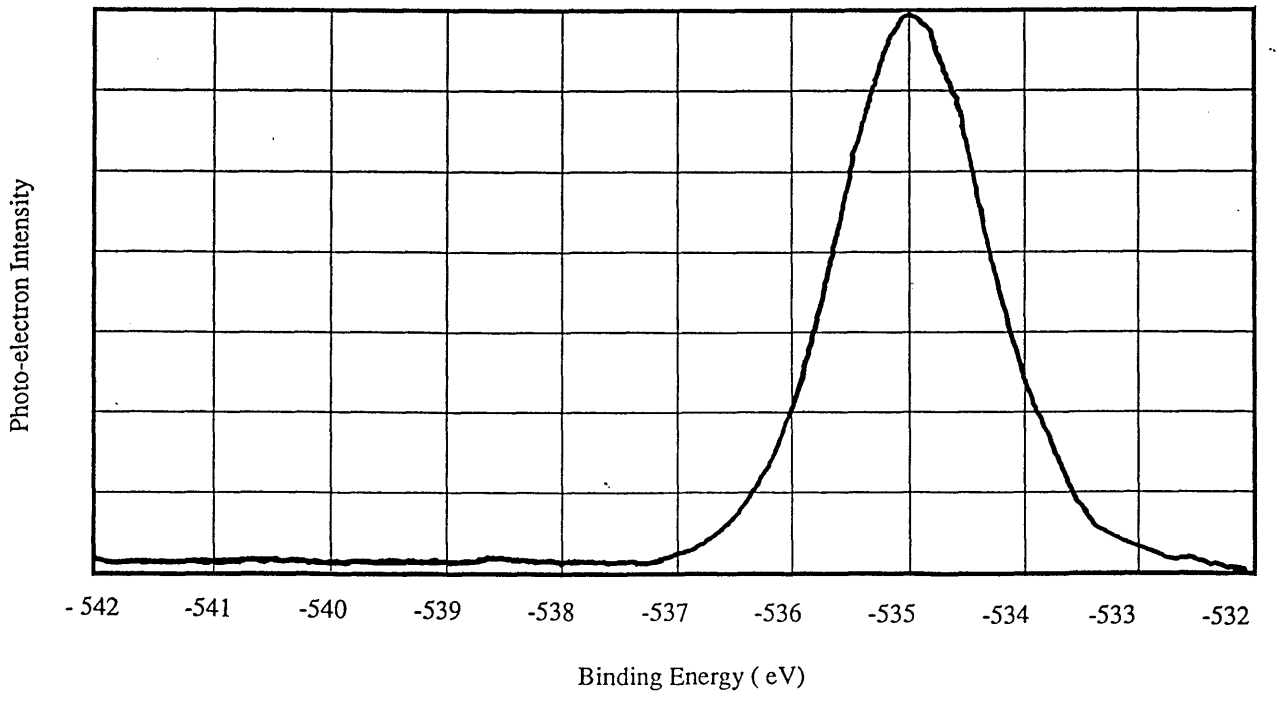
Oxygen 1s XPS spectrum of cleaned "Kevlar" fibres.



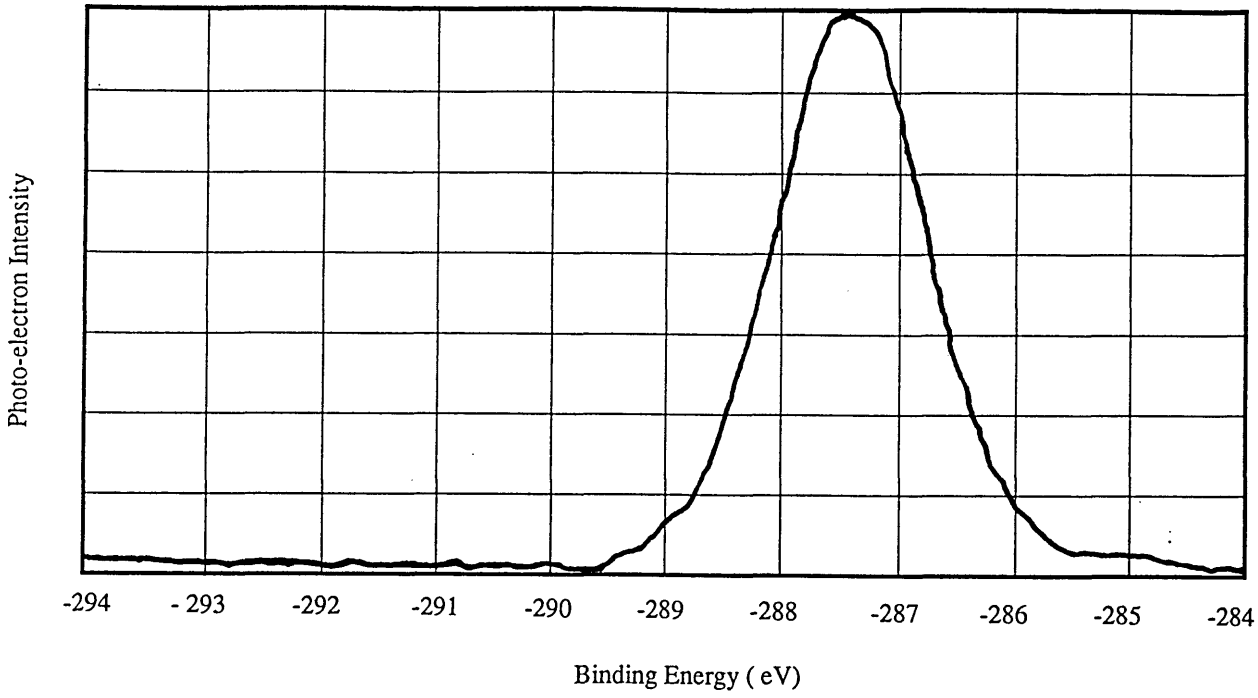
Carbon 1s XPS spectrum of cleaned "Kevlar" fibres.



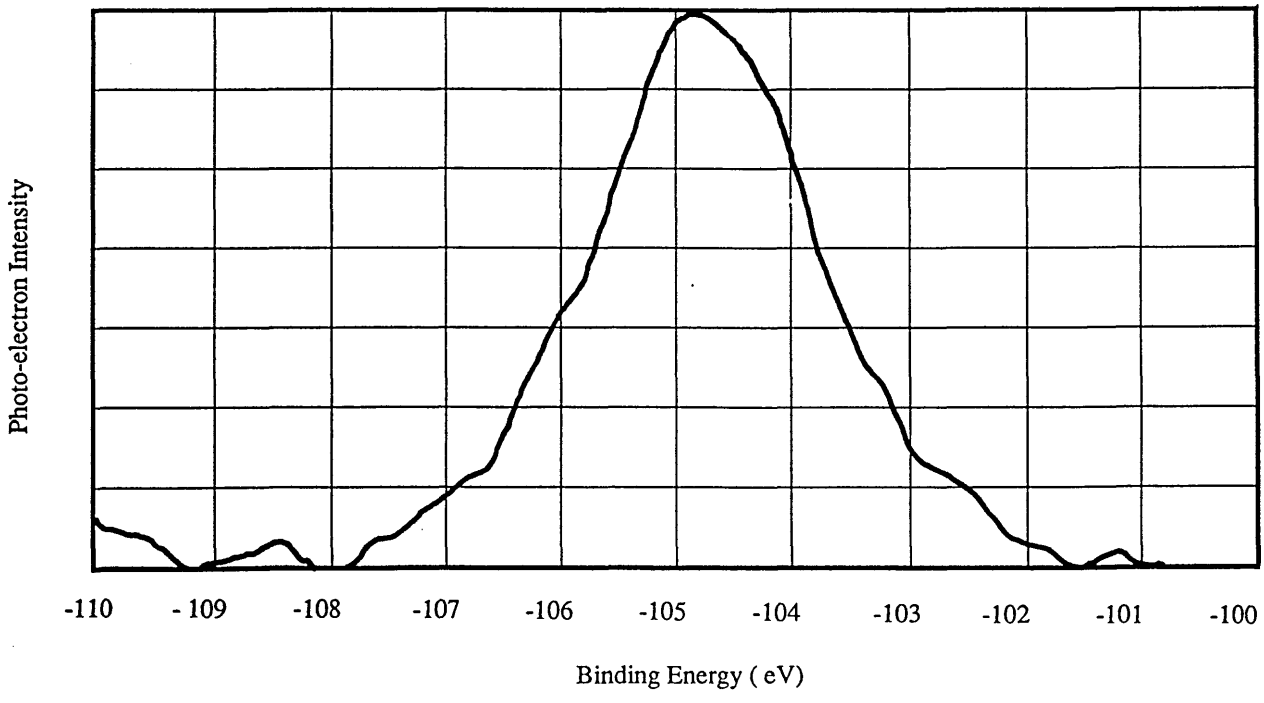
Silicon 1s XPS spectrum of polydimethyl siloxane coated "Kevlar" fibres.



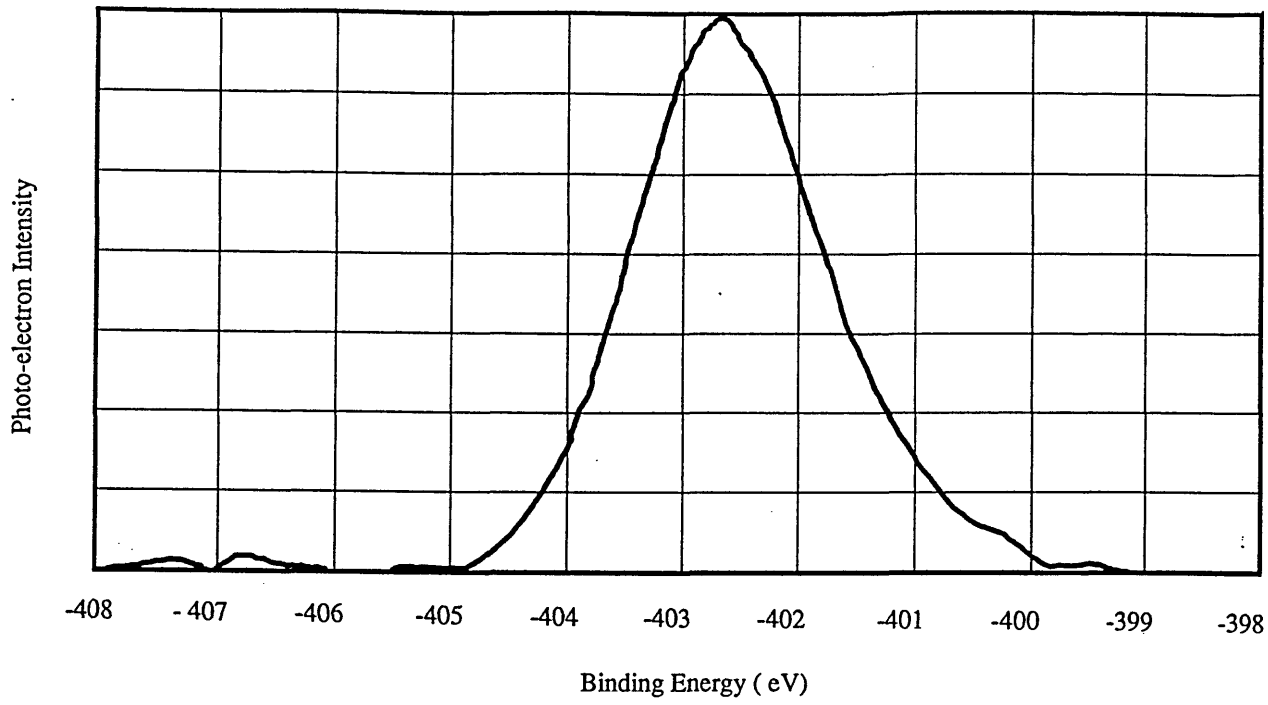
Oxygen 1s XPS spectrum of polydimethyl siloxane coated "Kevlar" fibres.



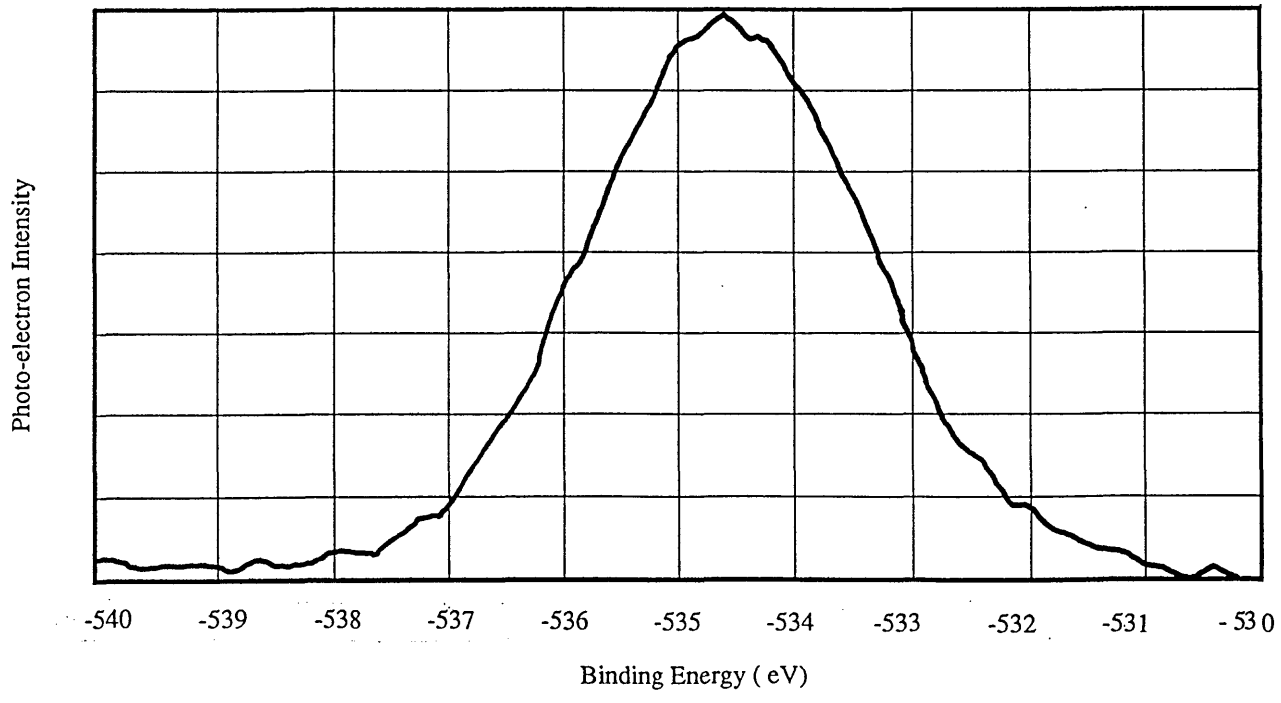
Carbon 1s XPS spectrum of polydimethyl siloxane coated "Kevlar" fibres.



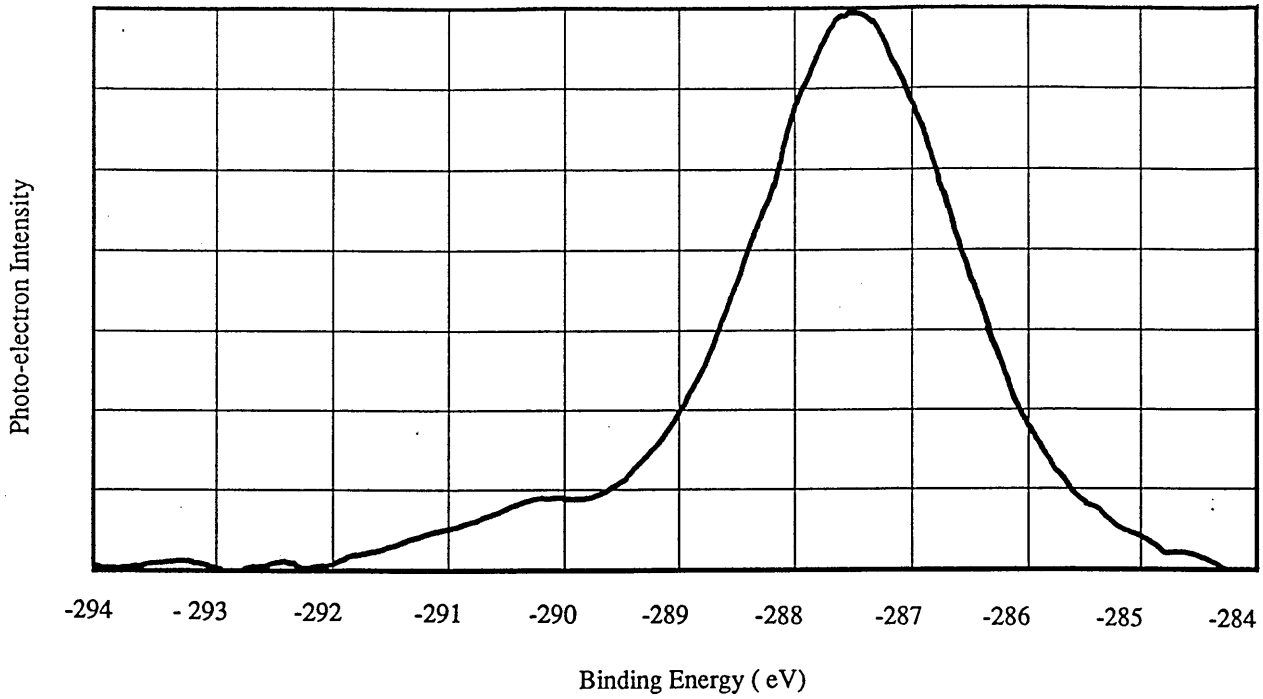
Silicon 1s XPS spectrum of methyl-silane grafted "Kevlar" fibres.



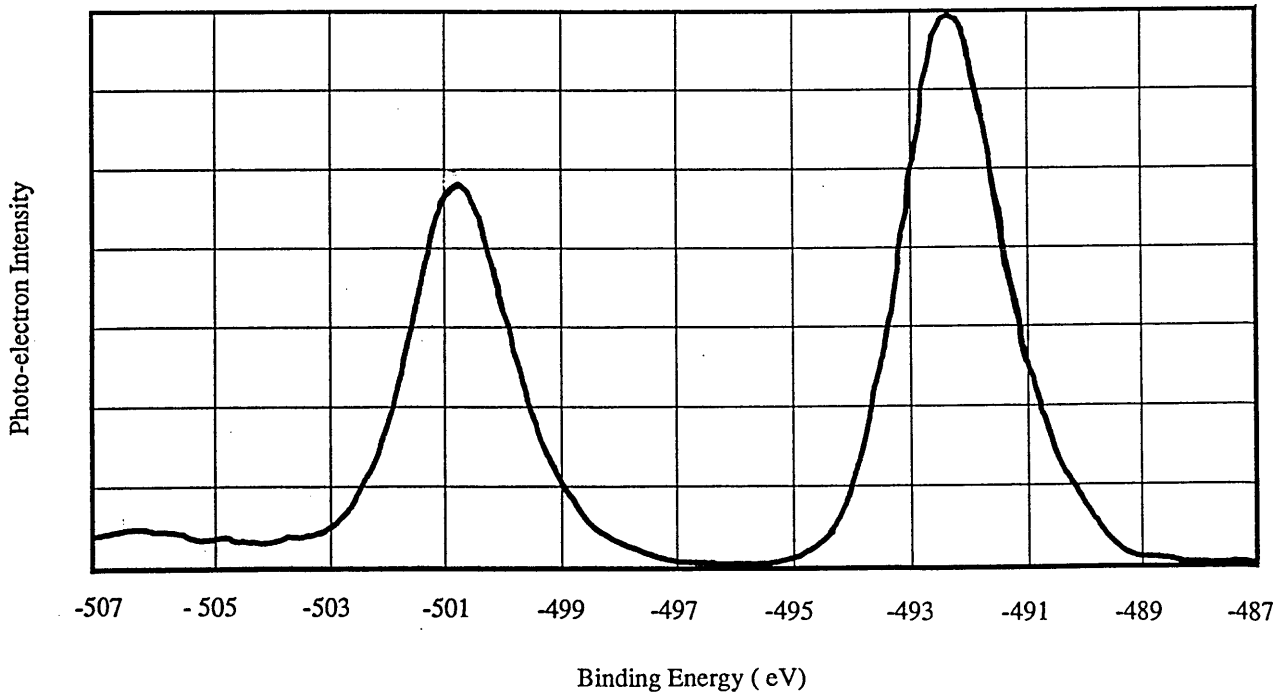
Nitrogen 1s XPS spectrum of methyl-silane grafted "Kevlar" fibres



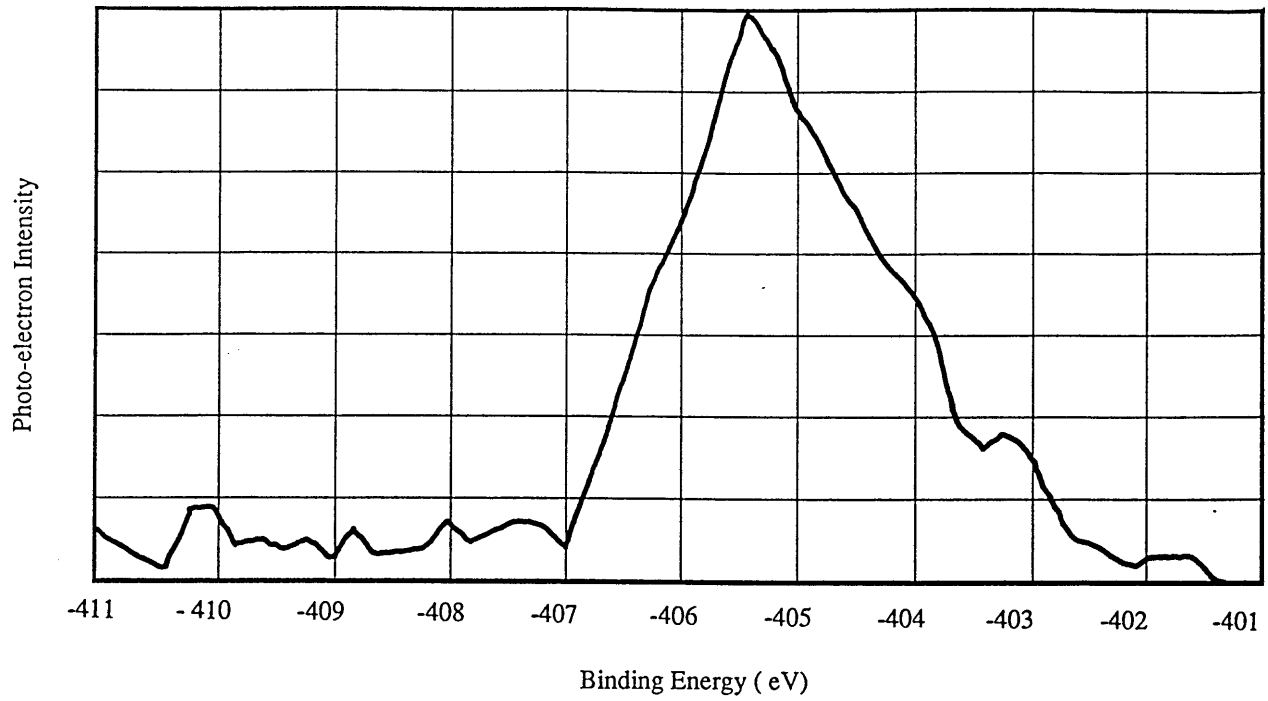
Oxygen 1s XPS spectrum of methyl-silane grafted "Kevlar" fibres.



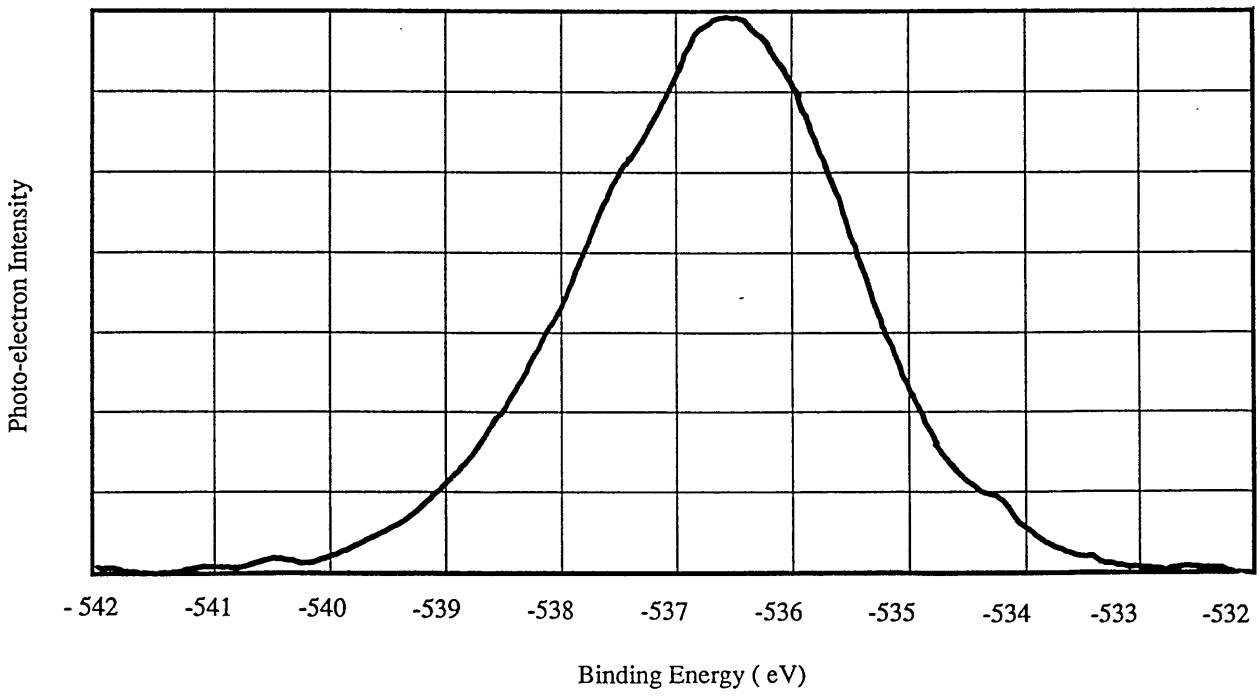
Carbon 1s XPS spectrum of methyl-silane grafted "Kevlar" fibres.



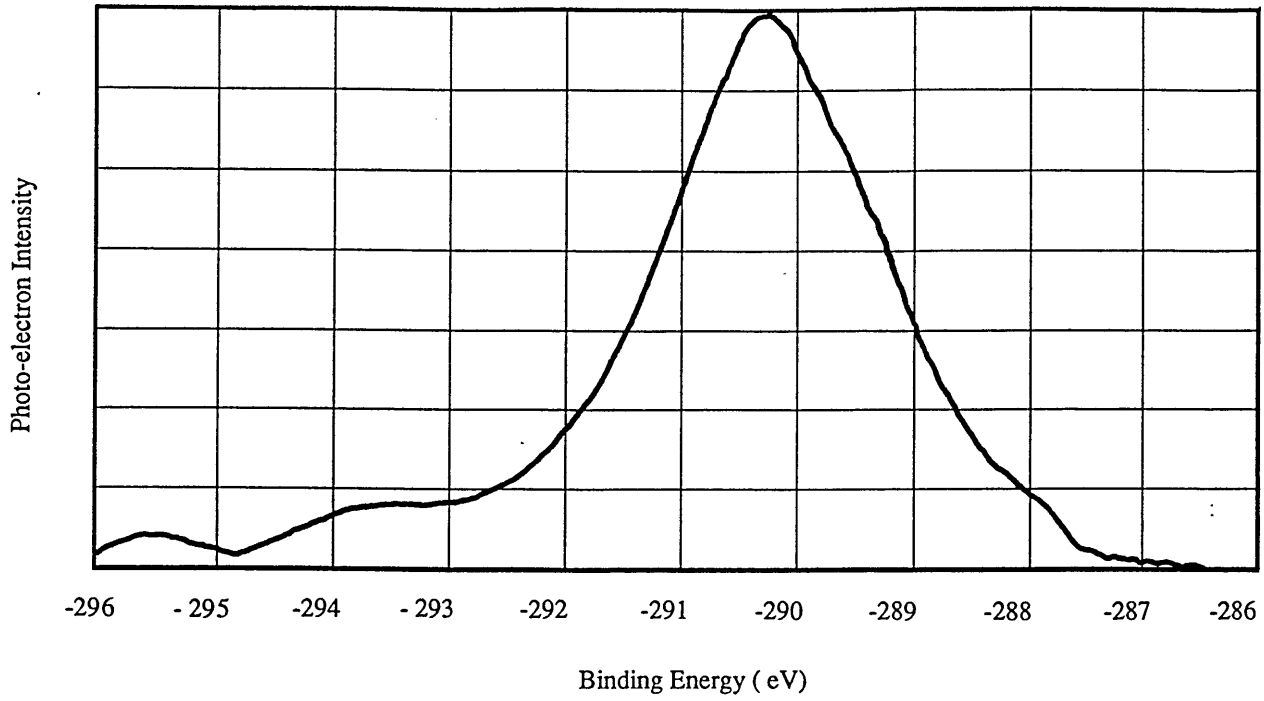
Tin 1s XPS spectrum of tin hydrosol coated "Kevlar" fibres.



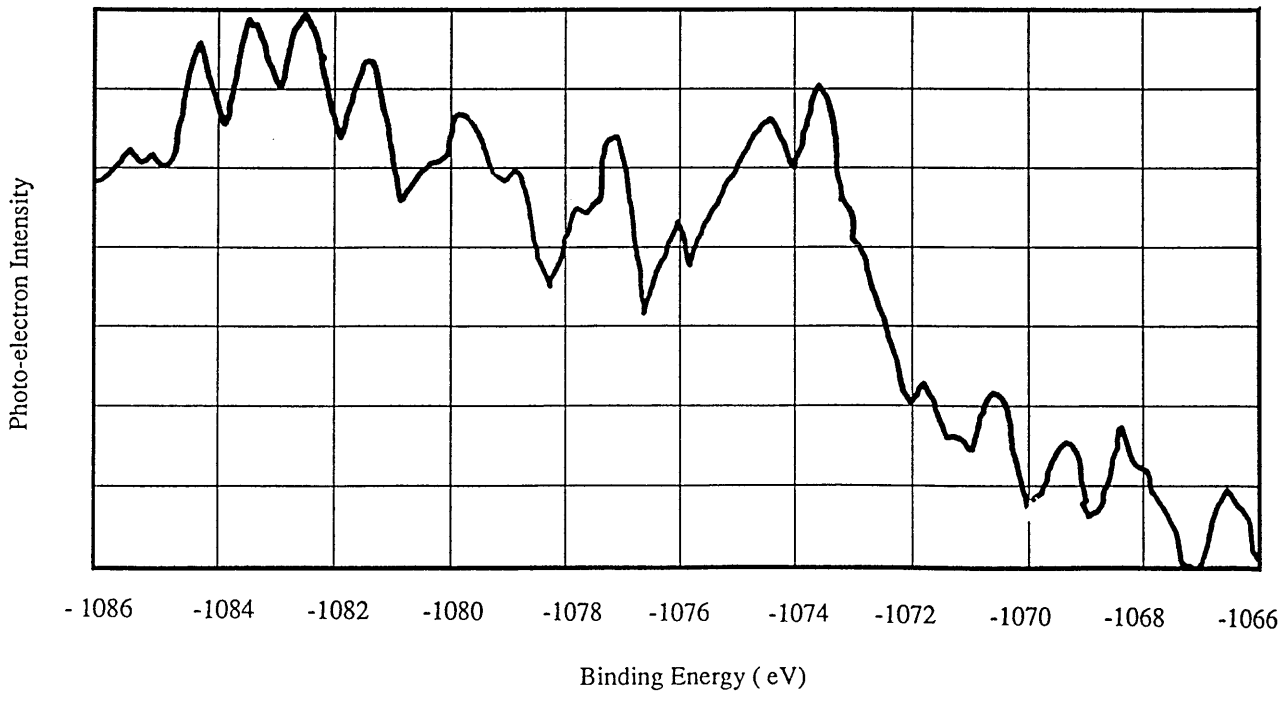
Nitrogen 1s XPS spectrum of tin hydrosol coated "Kevlar" fibres.



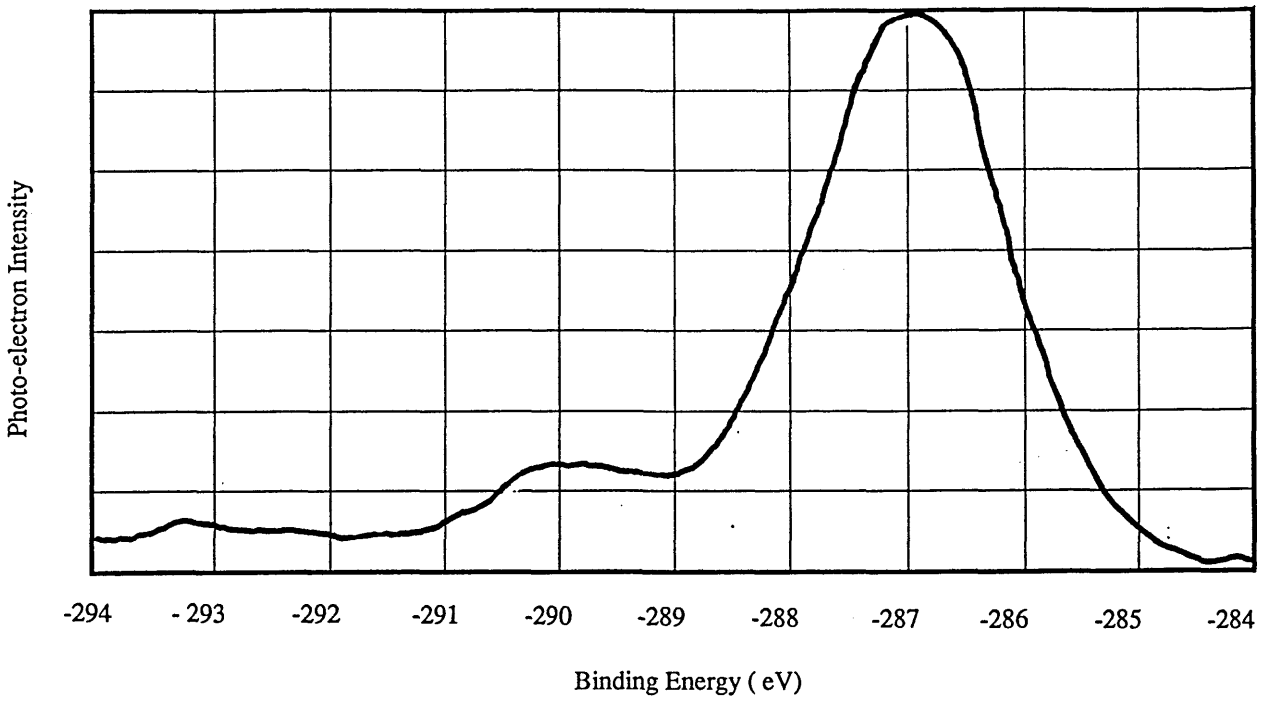
Oxygen 1s XPS spectrum of tin hydrosol coated"Kevlar" fibres.



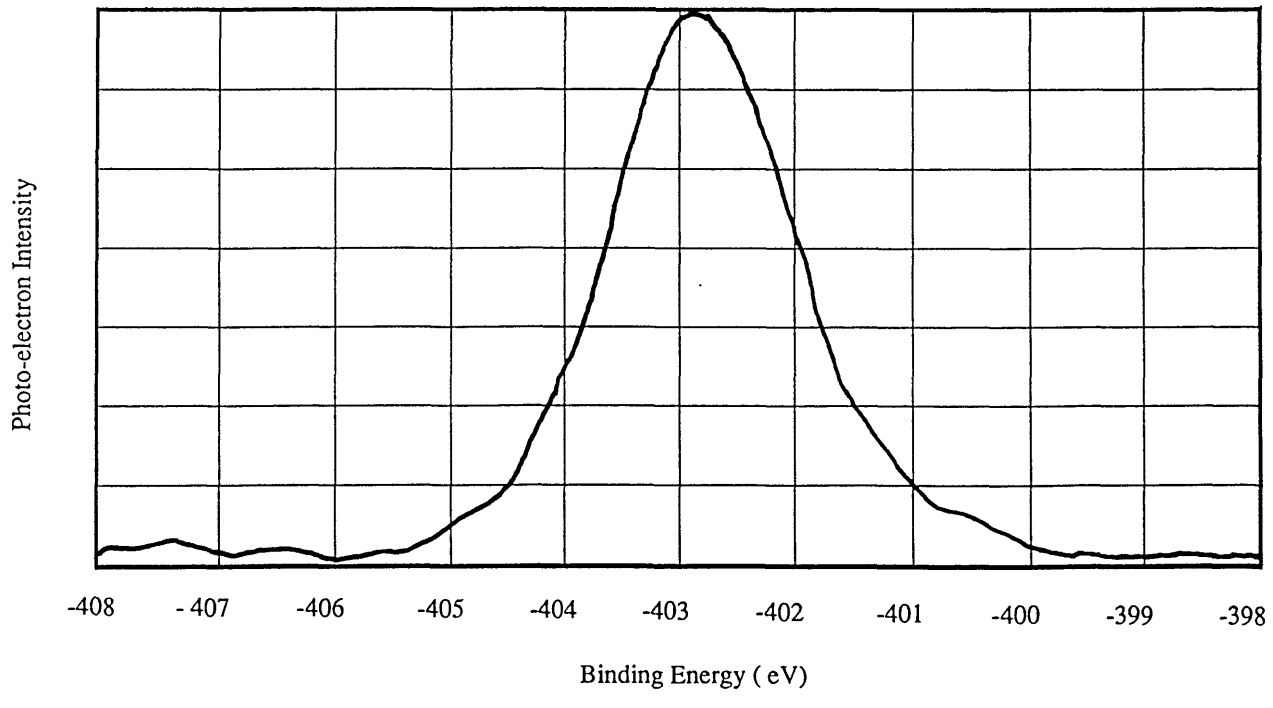
Carbon 1s XPS spectrum of tin hydrosol coated "Kevlar" fibres.



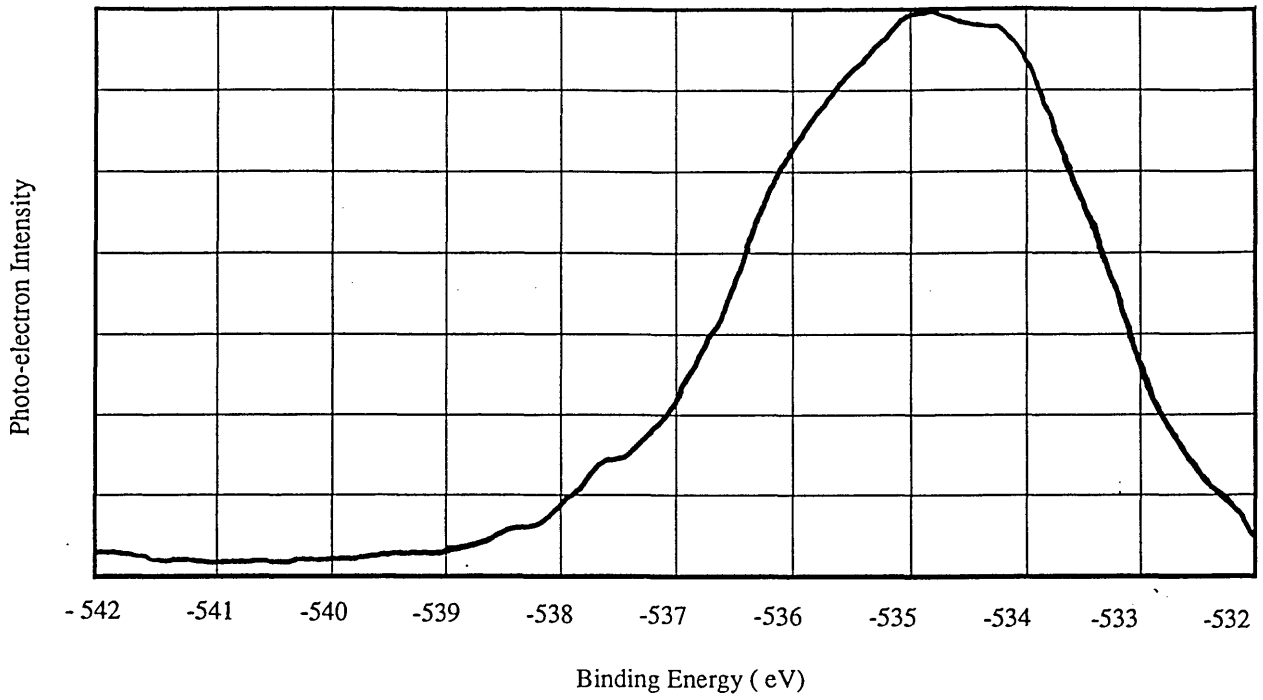
Sodium 1s XPS spectrum of metallisation /cleaned "Kevlar" fibres.



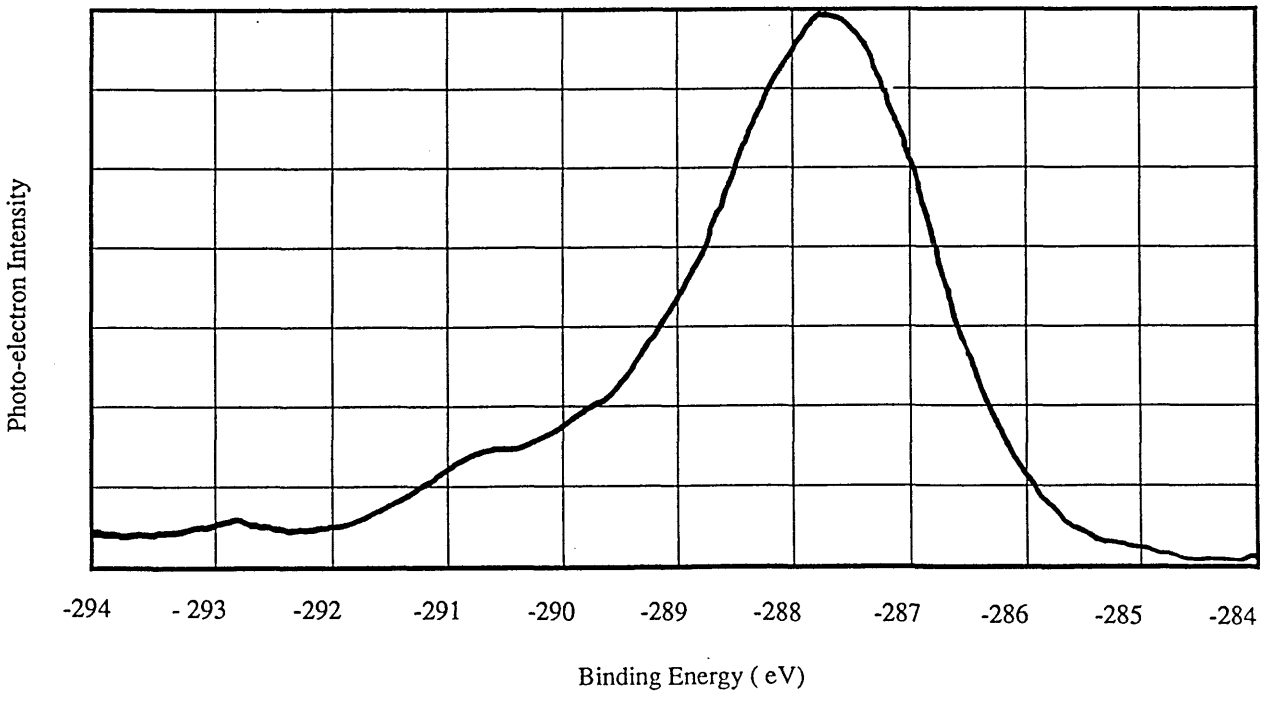
Carbon 1s XPS spectrum of metallisation /cleaned "Kevlar" fibres.



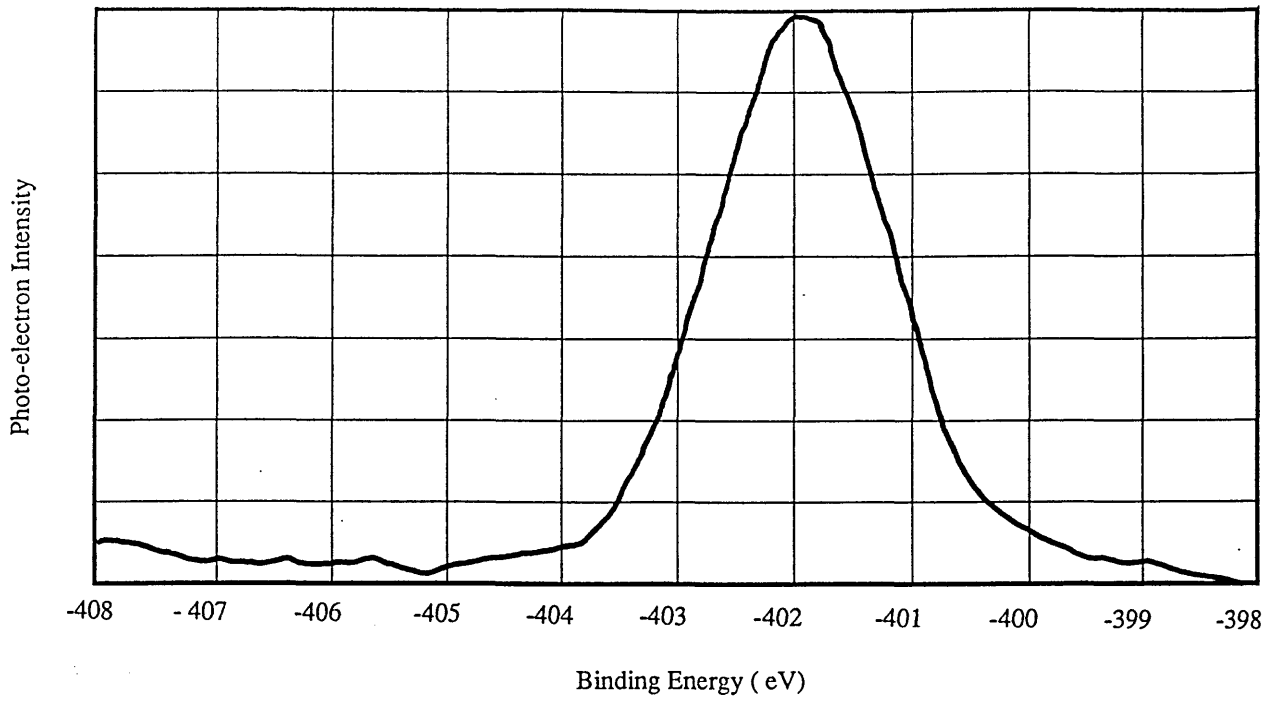
Nitrogen 1s XPS spectrum of epoxy grafted "Kevlar" fibres.



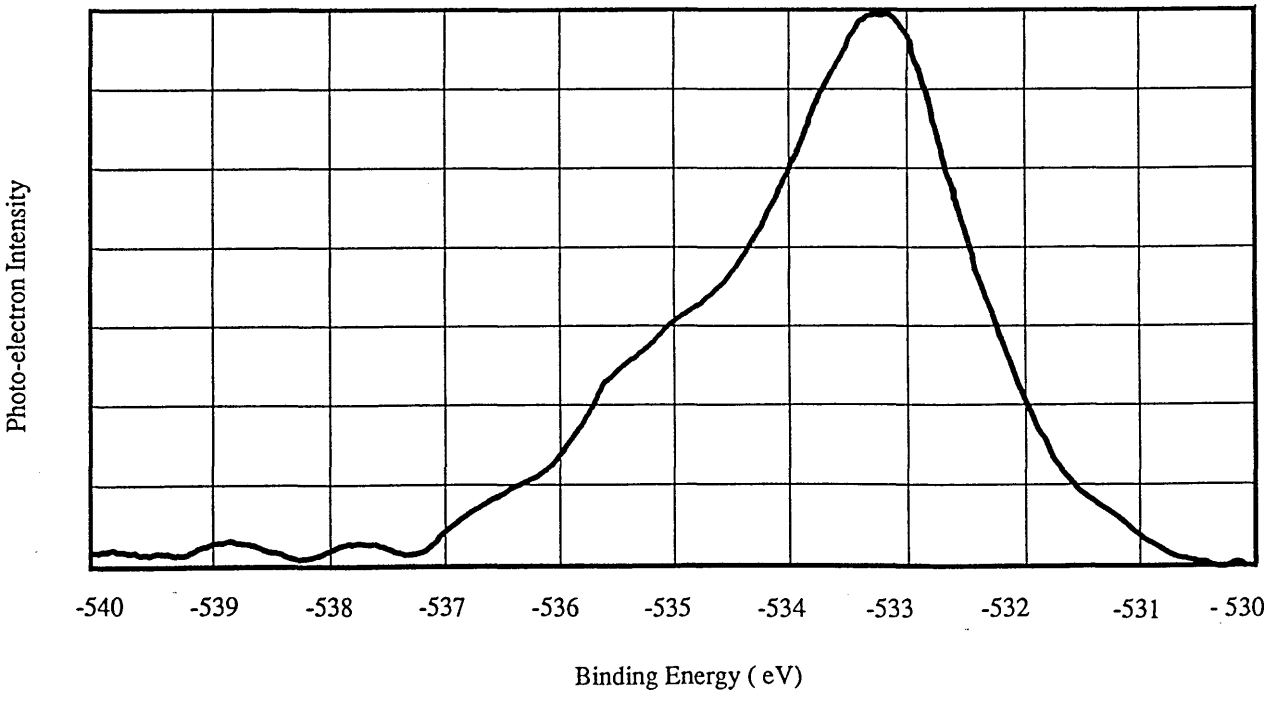
Oxygen 1s XPS spectrum of epoxy grafted "Kevlar" fibres.



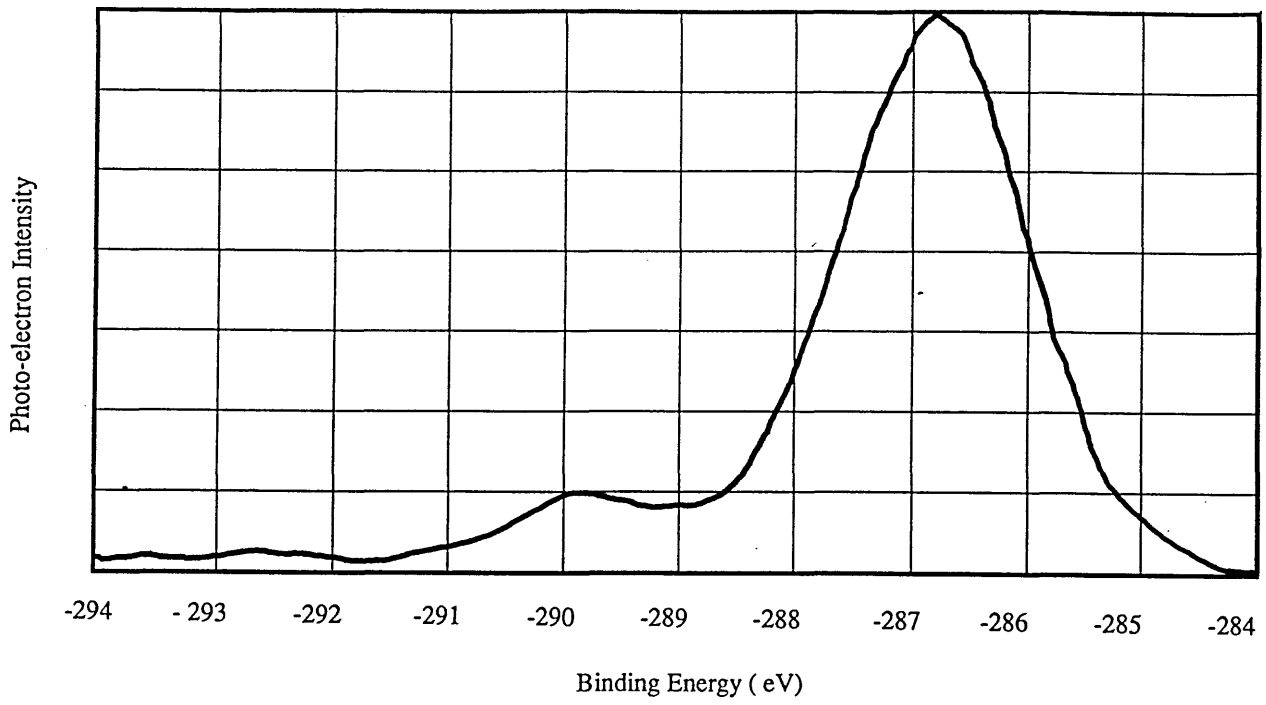
Carbon 1s XPS spectrum of epoxy grafted "Kevlar" fibres.



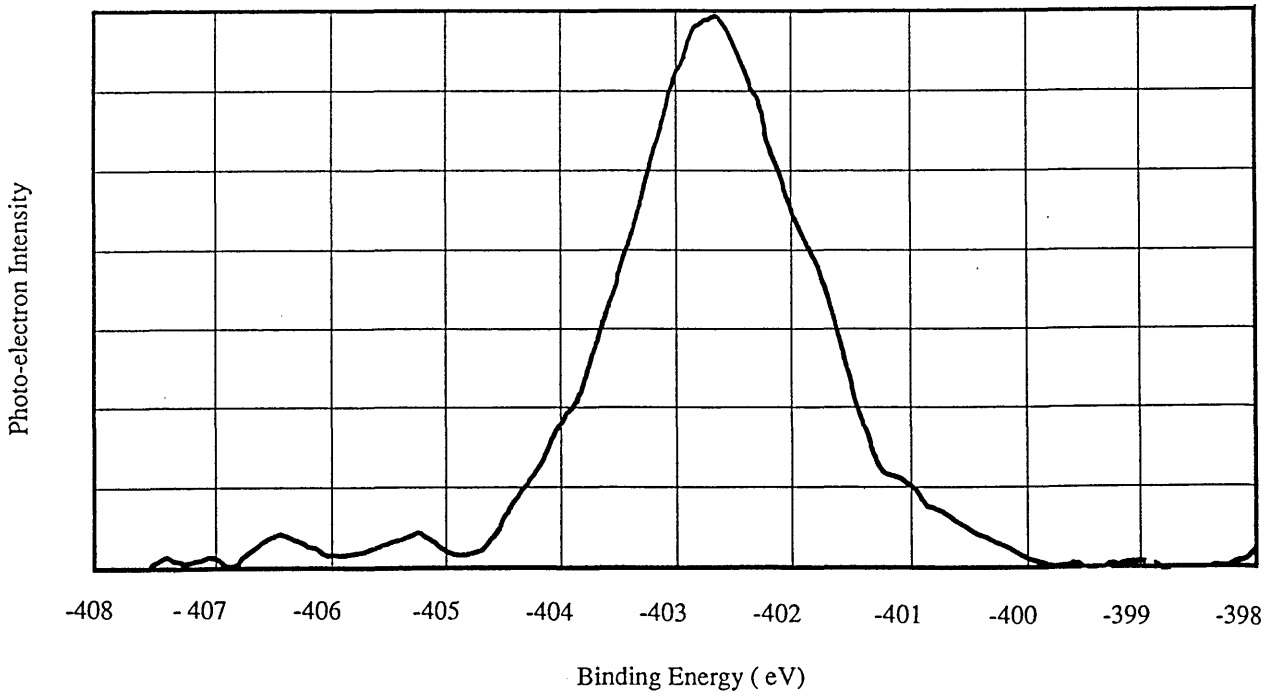
Nitrogen 1s XPS spectrum of nitrobenzene grafted "Kevlar" fibres.



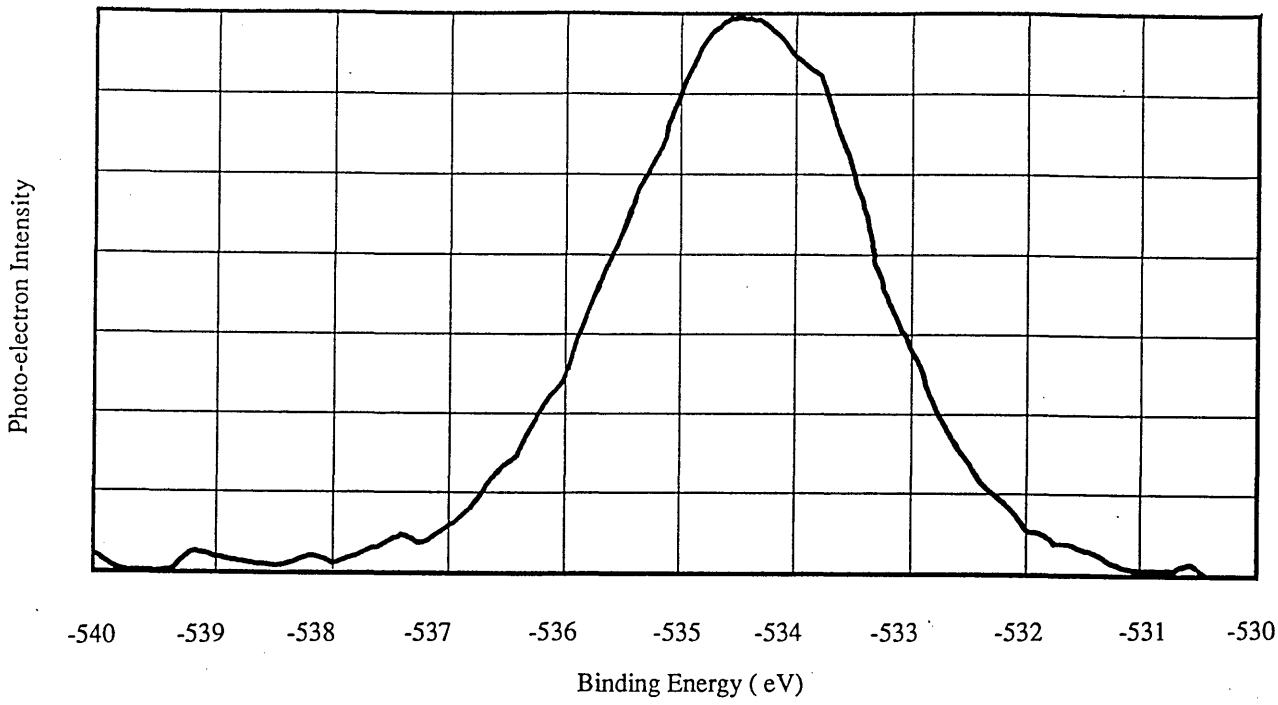
Oxygen 1s XPS spectrum of nitrobenzene grafted "Kevlar" fibres



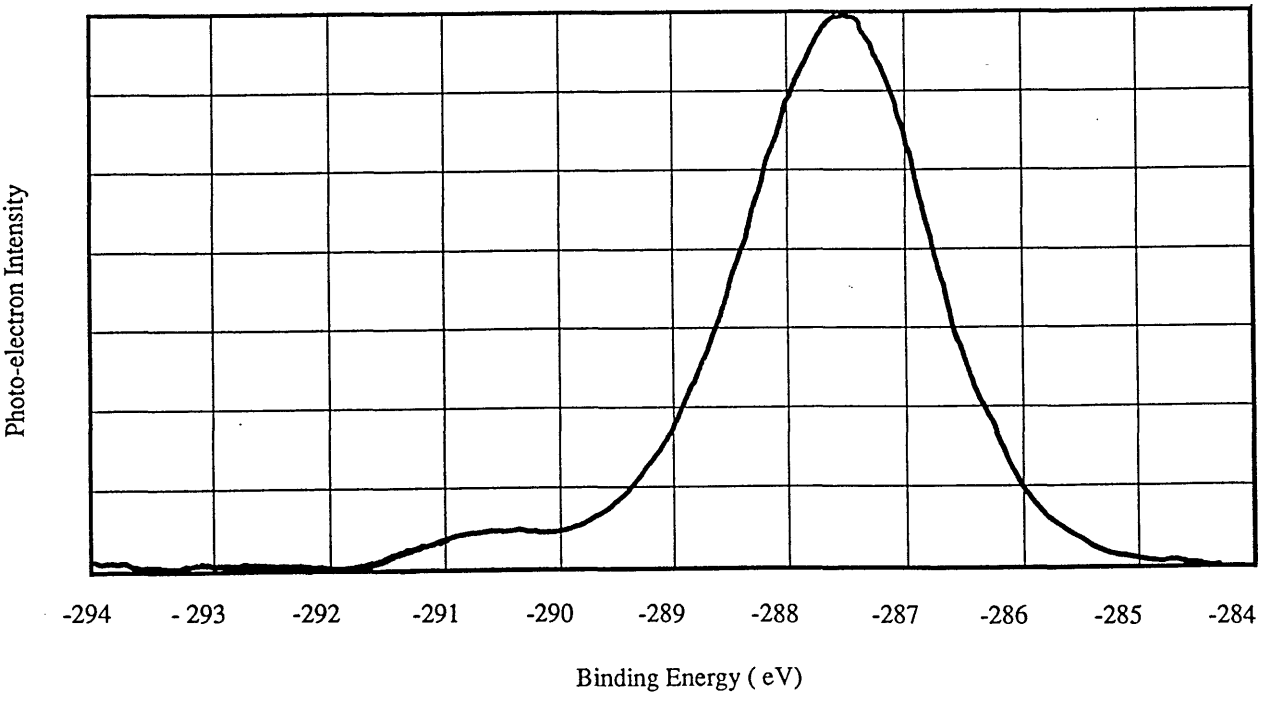
Carbon 1s XPS spectrum of nitrobenzene grafted "Kevlar" fibres.



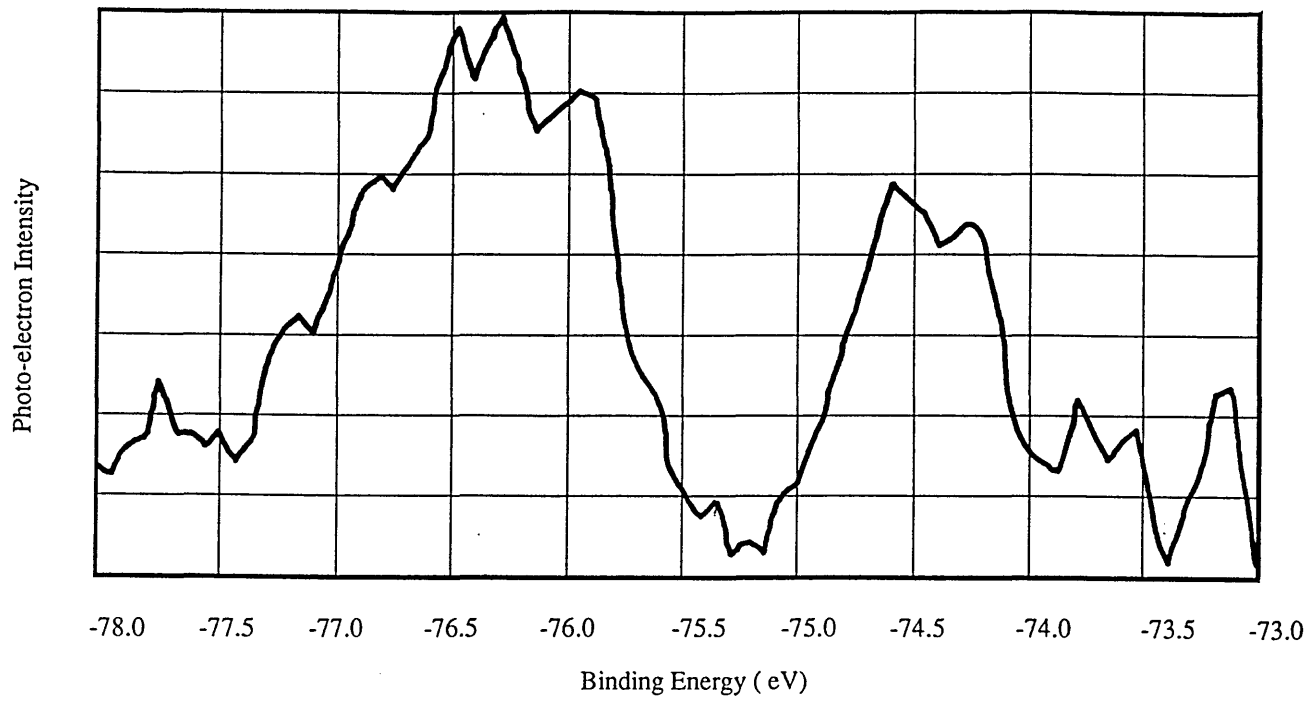
Nitrogen 1s XPS spectrum of octane grafted "Kevlar" fibres.



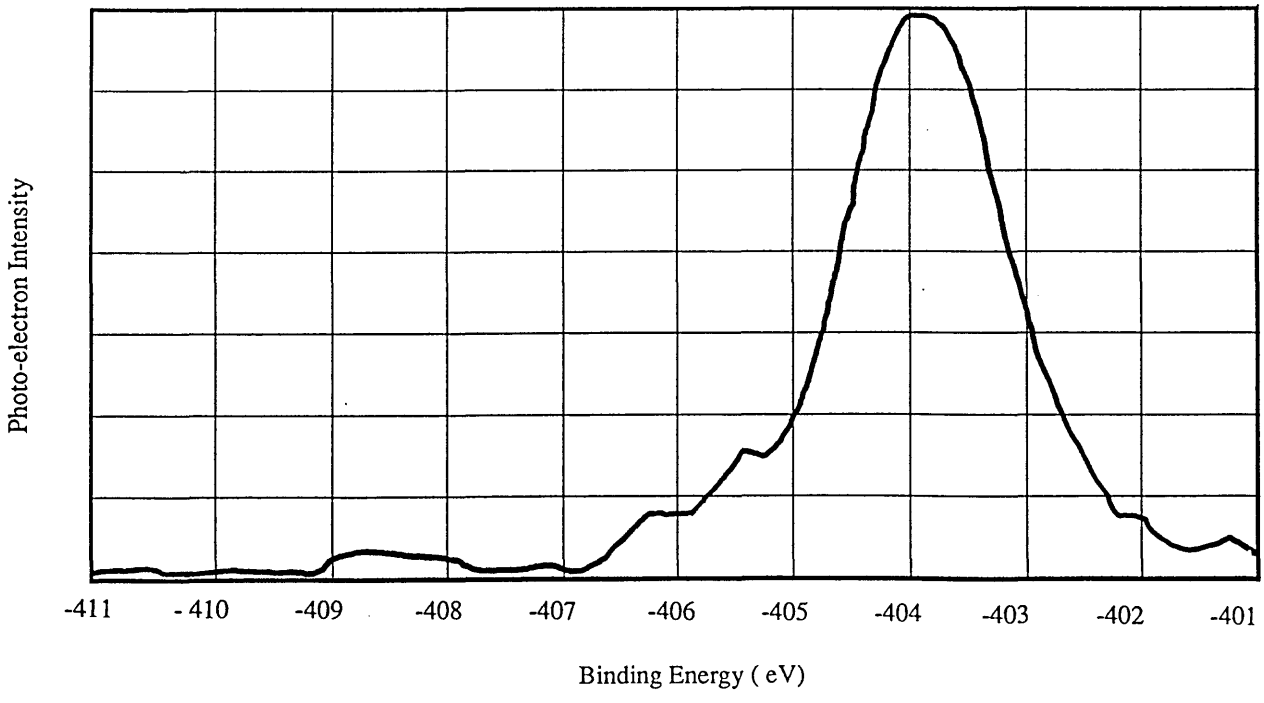
Oxygen 1s XPS spectrum of octane grafted "Kevlar" fibres.



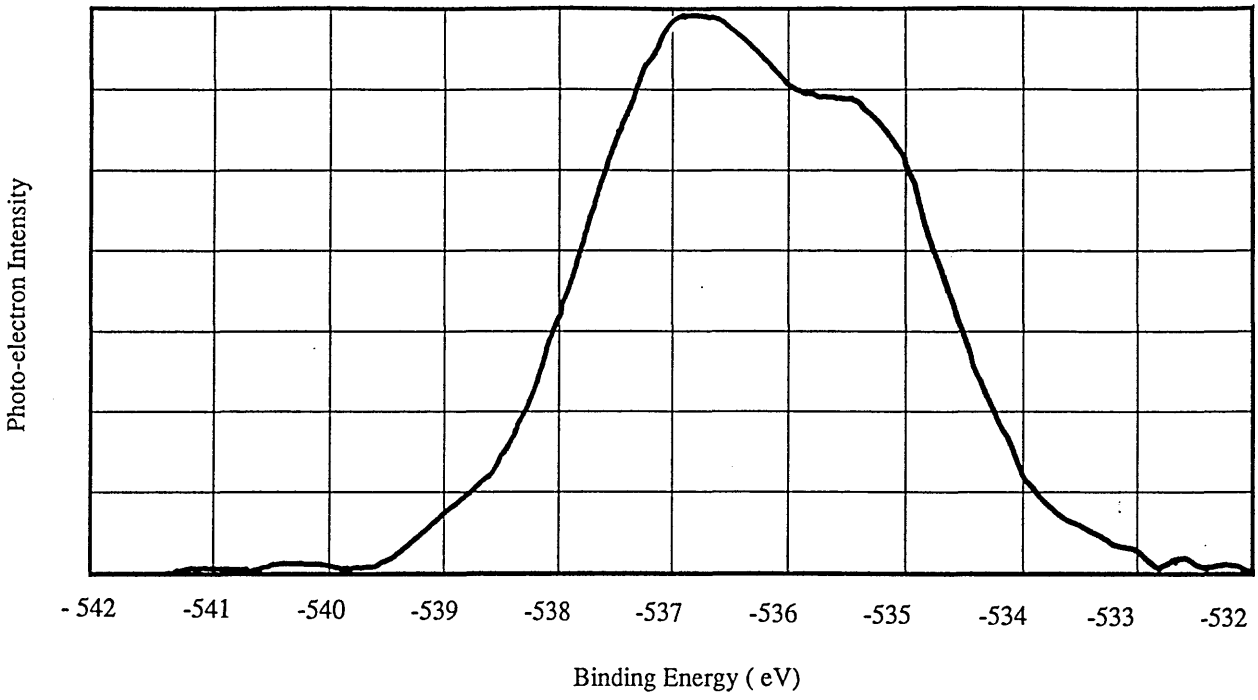
Carbon 1s XPS spectrum of octane grafted "Kevlar" fibres



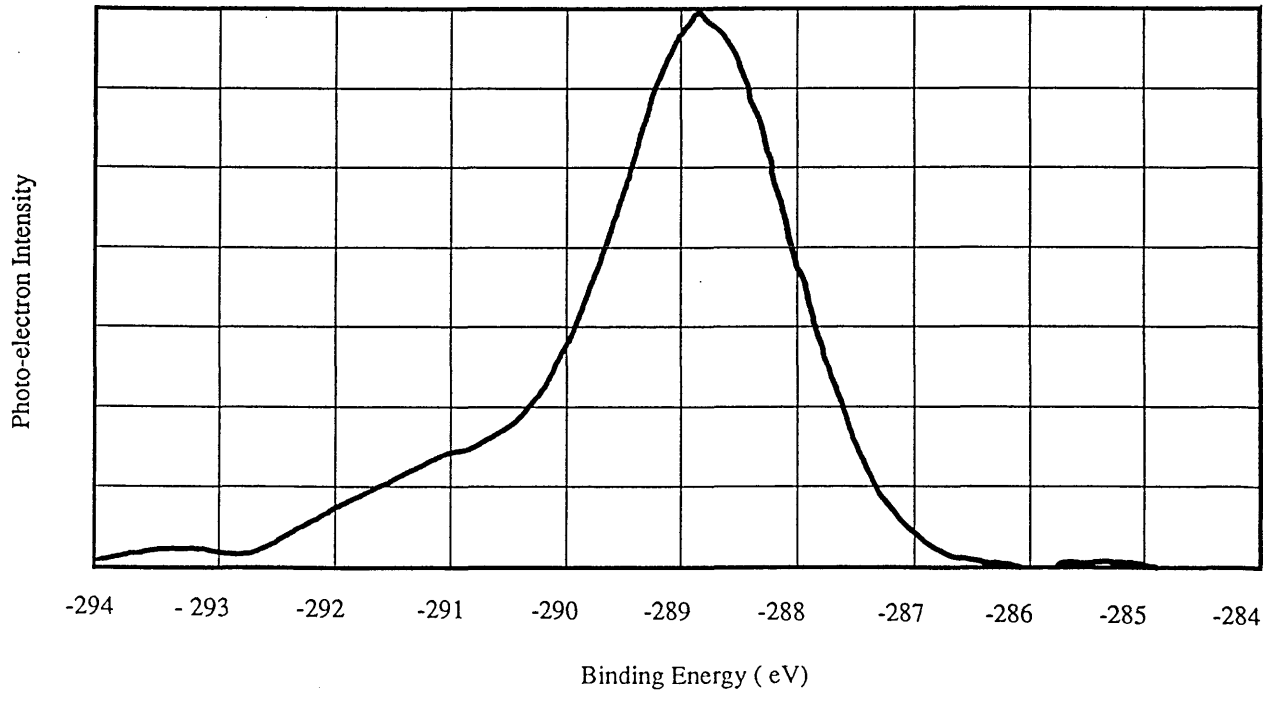
Bromine 1s XPS spectrum of diol grafted "Kevlar" fibres.



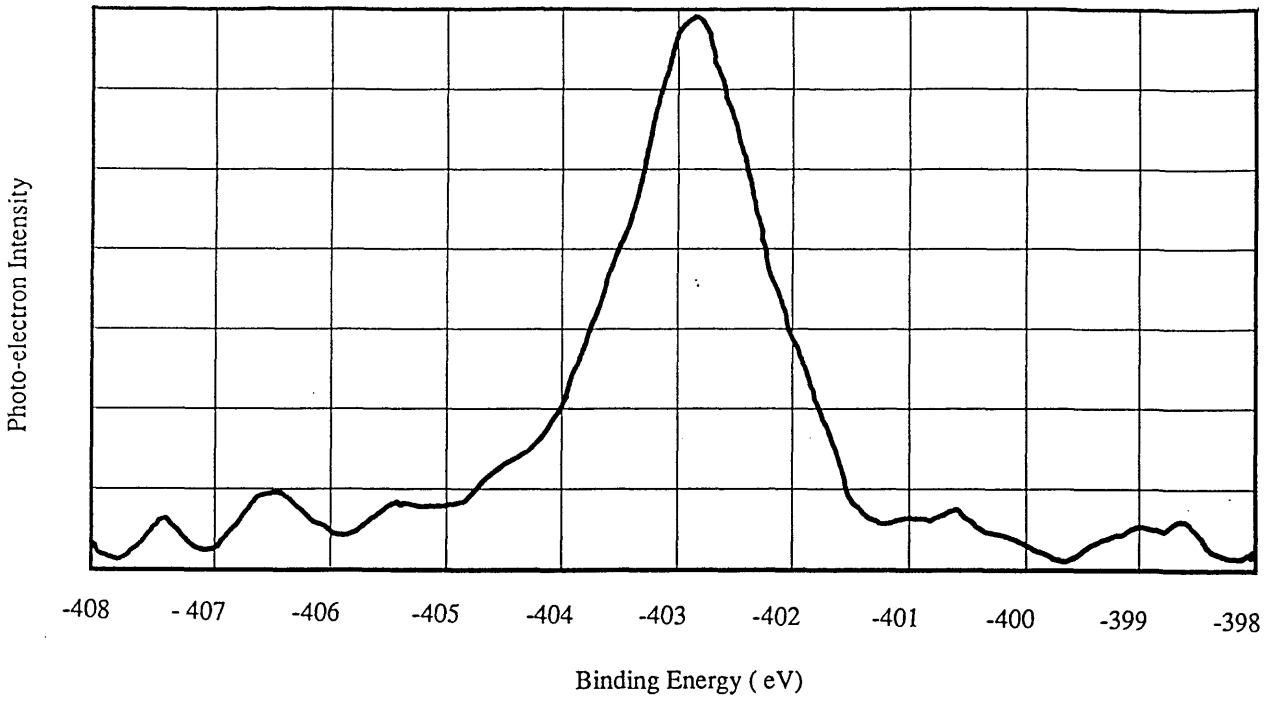
Nitrogen 1s XPS spectrum of diol grafted "Kevlar" fibres.



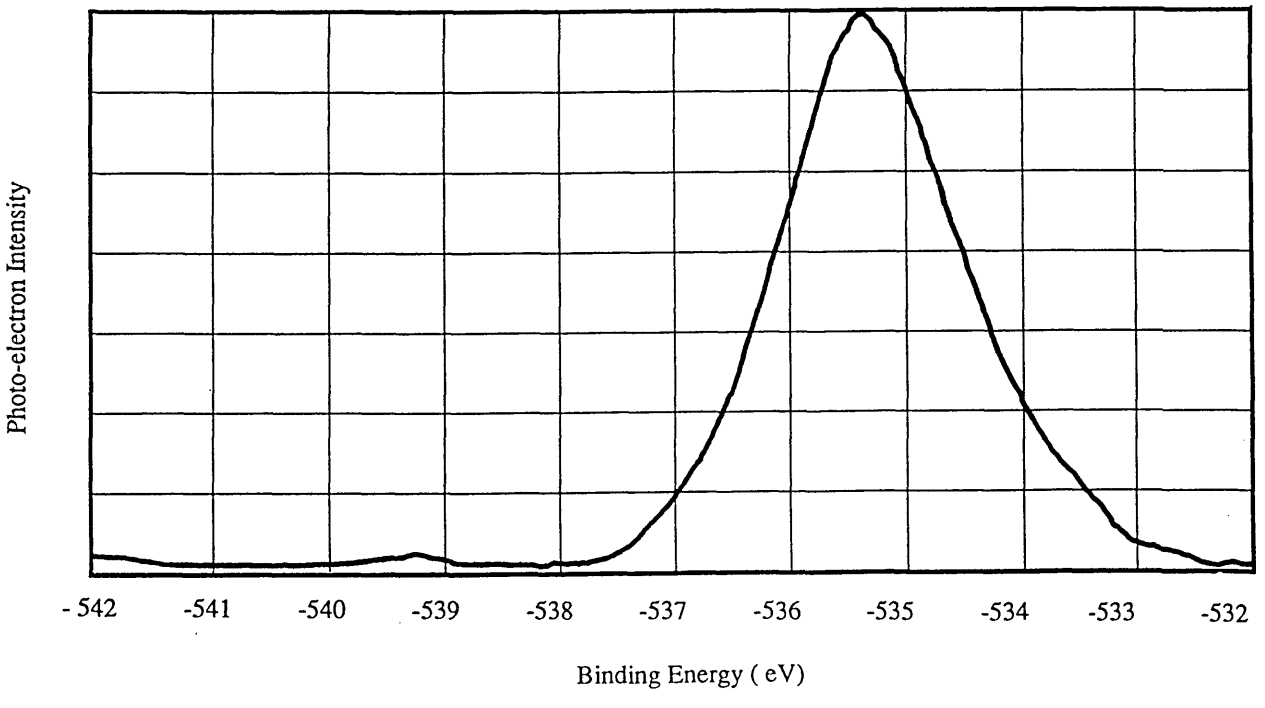
Oxygen 1s XPS spectrum of diol grafted "Kevlar" fibres.



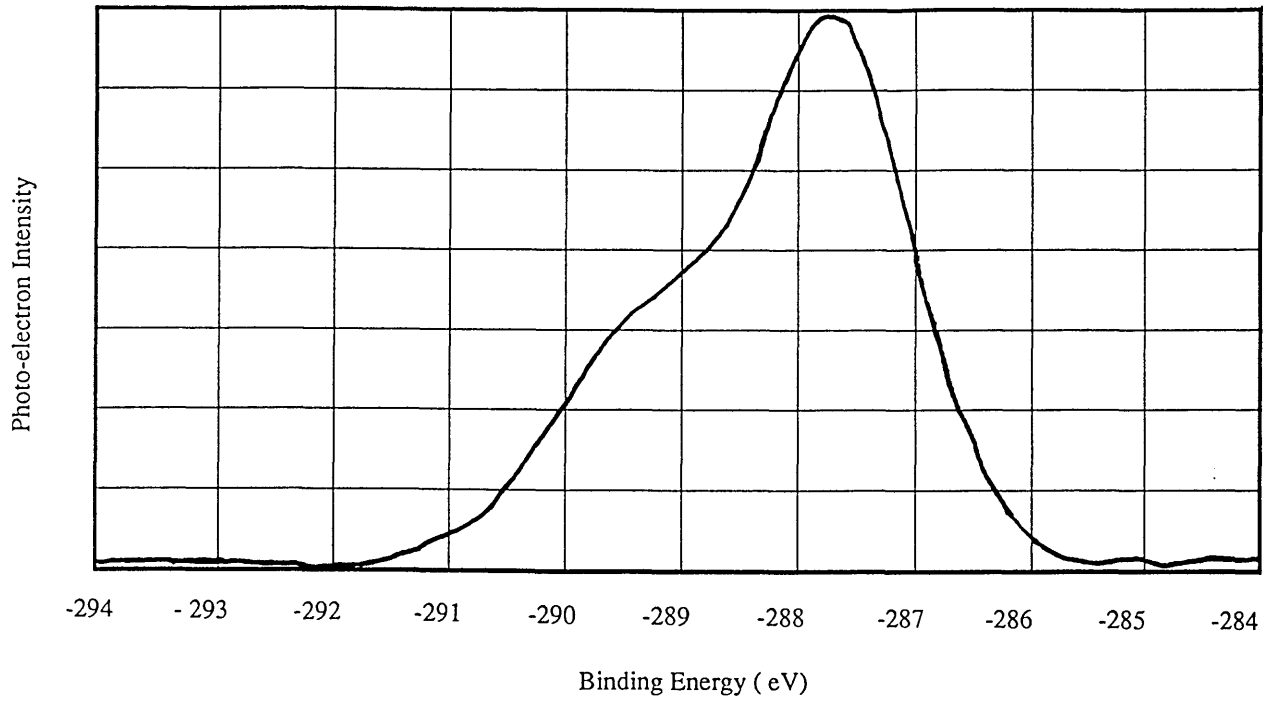
Carbon 1s XPS spectrum of diol grafted "Kevlar" fibres.



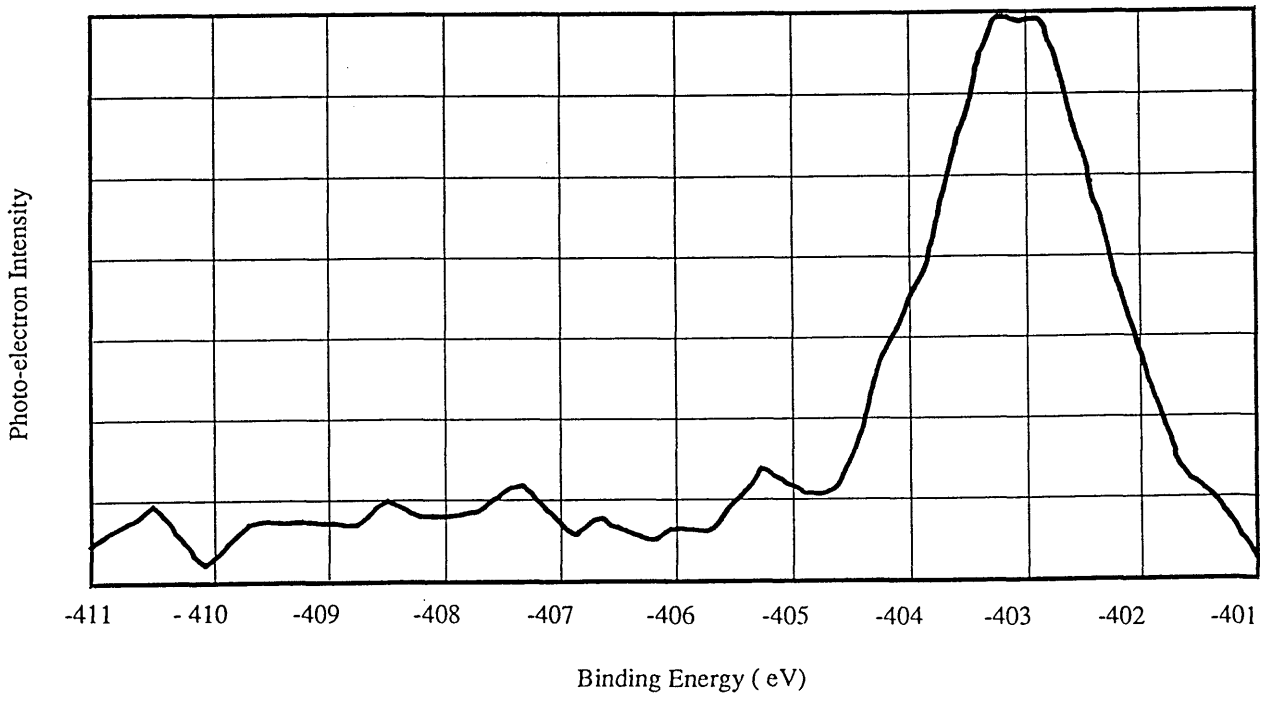
Nitrogen 1s XPS spectrum of polyethylene glycol coated "Kevlar" fibres.



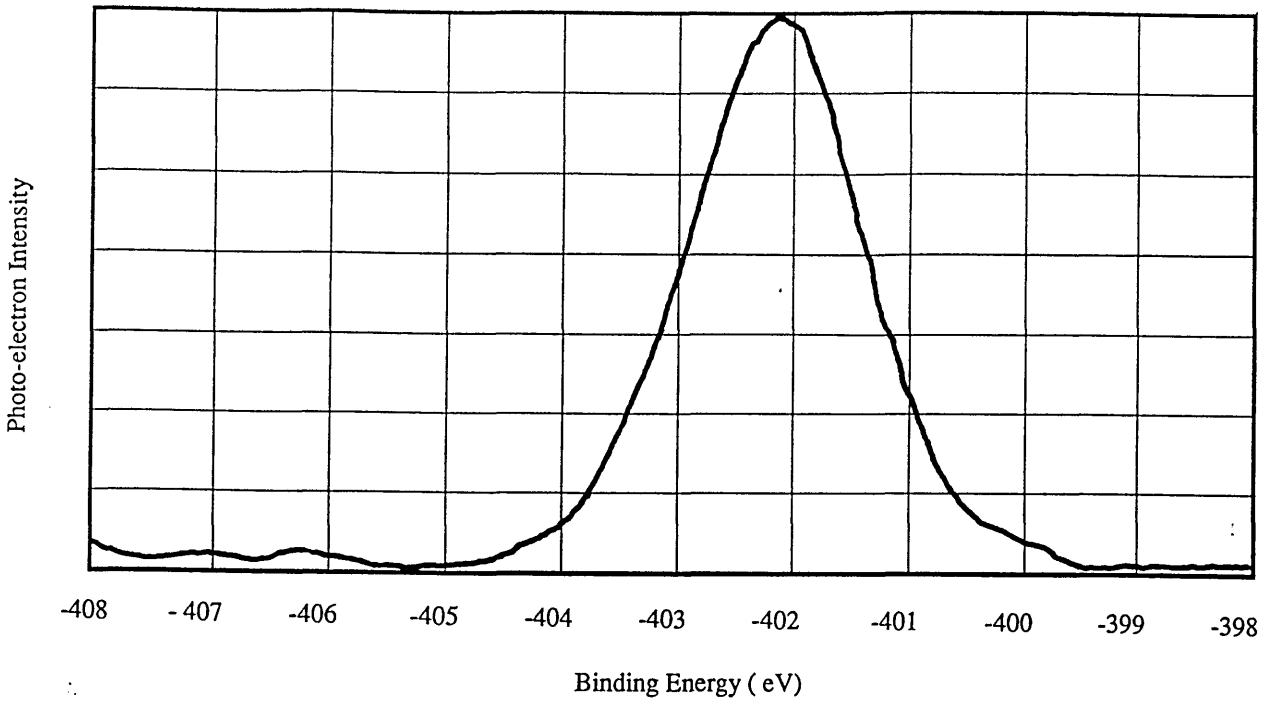
Oxygen 1s XPS spectrum of polyethylene glycol coated "Kevlar" fibres.



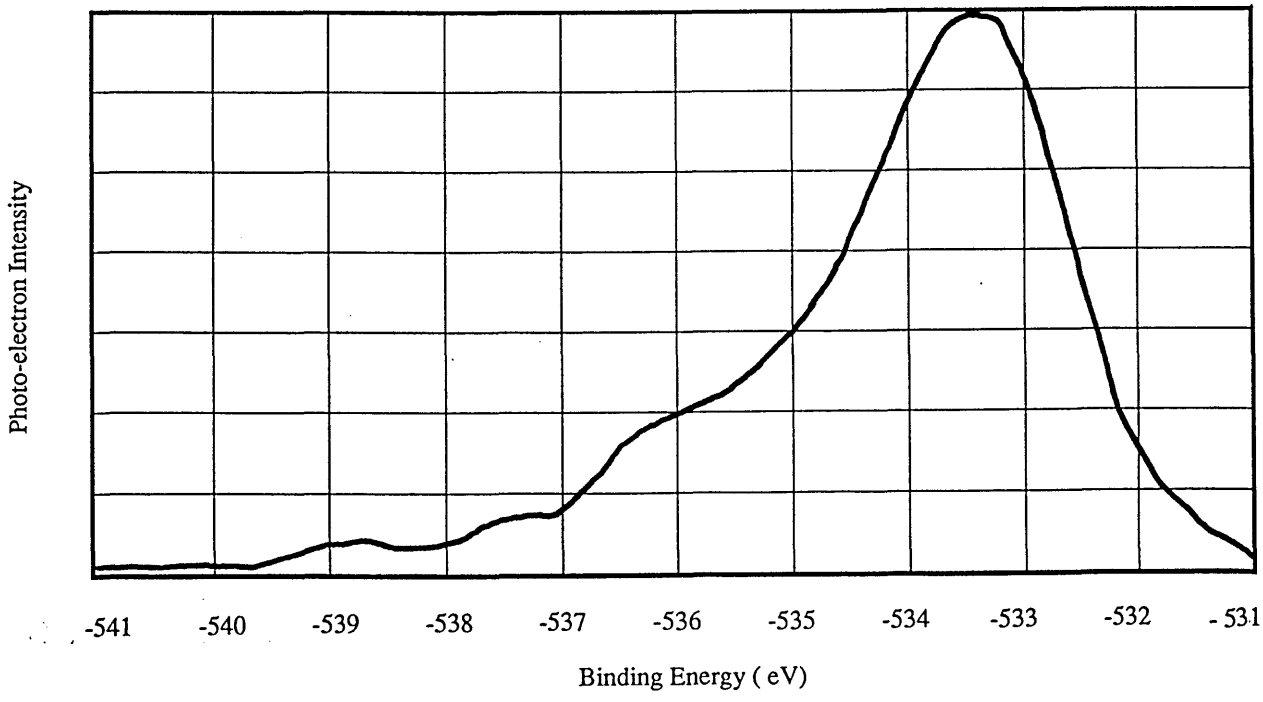
Carbon 1s XPS spectrum of polyethylene glycol coated "Kevlar" fibres.



Nitrogen 1s XPS spectrum of epoxy resin coated "Kevlar" fibres.



Nitrogen 1s XPS spectrum of metallisation /cleaned "Kevlar" fibres.



Oxygen 1s XPS spectrum of metallisation /cleaned "Kevlar" fibres.

REFERENCES

Abbott,C.M., Grosberg, P., Leaf, G.A.V., *Text.. Res.J.*, **41**, 4, 345 (1971).

Abbott, C.M., Grosberg, P., Leaf, G.A.V., *J.Text. Inst.*, **42**, 346 (1971).

Allan, A.J.G, *J. Colloid Science*, **13**, 273 (1958).

Allara, D.L., Fowkes, F.M., Noolandi, J.G., Rubloff, W. and Tirrell, M.V., "Bonding and Adhesion of Polymer Interfaces", *Mater. Sci. Eng.*, **83**, 213-26 (1986).

Allred, R.E., Street, K.H. and Martinez, R.J., "Improvement of Transverse Composite Strengths: Test Specimen and Materials Development", Proceedings of the 24th National SAMPE Symposium, Azusa, California, pp.31 (1979).

Allred, R.E. and Lindrose, A.M., " Room Temperature Moisture Kinetics of Kevlar 49 Fabric- Epoxy Laminates", in Composite Materials : Testing and Design , ASTM STP 674, American Society for Testing and Materials, Philadelphia, 313 (1979).

Allred, R.E., "Surface Modification of Polyaramid Filaments with Amine Plasmas", Doctor of Science Thesis, Massachusetts Institute of Technology (1983).

Amuzu, J.K.A., Briscoe, B.J. and Tabor, D., Transactions of the Institute of Mechanical Engineers (1976).

Amuzu, J.K.A., Briscoe, B.J. and Tabor, D., 1977a, Trans. ASLE, **20**, 152.

Amuzu, J.K.A., Briscoe, B.J. and Tabor, D., 1977b, Trans. ASLE, **20**, 354.

Andrews, E.H. and Kinlock, A.J., *Proceeding of the Royal Society-London,* **A332**, 401 (1973).

Andrade, J.D., King, R.N., Gregonis, D.E. and Coleman, D.L., "Surface Characterisation of PHEMA. Contact Angles in Water", *Journal of Polymer Science Symposium*, **66**, 313 (1979).

Andrade, J.D., Smith, L.M. and Gregonis, D.E. , "The Contact Angle and Interface Energetics", in Physicochemical Aspects of Polymer Surfaces, Plenum,N.Y. (1983).

Anhang, J. and Gray, D.G., "Surface Characterisation of Poly(ethylene Terephthalate) Film by Inverse Gas Chromatography", Journal of Applied Polymer Science, **27**, 71 (1982).

Armistead, J.P., Snow, A.W. and Bascom, W.D., "Butadiyne Vapour Deposition Polymerisation on Carbon Fibers", Int. SAMPE Tech. Conf., **19** (Nations Future Mat. Needs) 644 (1987).

Arrowsmith, D.J., *Transactions of the Institure of Metals Finishing*, **48**, 88 (1970).

ASTM Standard D 790 M , "Flexural Properties of Unreinforced and Reinforced Plastics and Electrical Insulating Materials(Metric)".

Bailey,. A.I. and Courtney-Pratt, J.S, *Proc. Roy. Soc.*, **A227**, 500 (1955).

Bascom, W.D. and Jensen, R.M., "Stress Transfer in Single Fiber/Resin Tensile Tests" , *J.Adhesion*, **19**(3-4),219-39, (1986).

Bascom, W.D. and Drzal, L.T., "The Surface Properties of Carbon Fibers and Their Adhesion to Organic Polymers", NASA Contract Rep. NASA-CR-4084, NAS1.26:4084 (1987).

Bascom, W.D., Jensen, R.M. and Cordner L.W., "The Adhesion of Carbon Fibers to Thermoplastic Polymers", Proceedings of the 6th International Conference on Composite Materials, London, Elsevier, Volume **5**, pp 424-38 (1987).

Bascom, W.D., Timmons, C.O. and Jones, R.L., "Apparent Interfacial Failure in Mixed Mode Adhesive Fracture", *Journal of Material Science,* **10**, 1037 (1975).

Batchelder, D.N. and Bloor D., "Strain Dependance of the Vibrational Modes of a Diacetylene Crystal", *Journal of Polymer Science: Polymer Physics Edition*, **17**, 569 (1979).

Batich, C.P. and Wendt R.C., "Chemical Labels to Distinguish Surface Functional Groups using XPS", Photon, Electron and Ion Probes of Polymer Structure and Properties, (Ed. Dwight D.W., Fabish T. J. and Thomas H.R.), ACS Symposium Series No. **162**, 221 (1981).

Beaumont, P., IBM Polymer Symposium, Imperial College, September (1989).

Bendure R.L., Dynamic Adhesion Tension Measurement, *Journal of Colloid and Interface Science*, **42**(1), 137-144, (1973).

Bhatnagar, A., Lin, L.C., Lang, D.C. and Chang, H.W., "Comparison of Ballistic Performance of Composites", 34th International SAMPE Conference (1989).

Bolvari, A.E. and Ward, T.C., "Determination of Fiber-Matrix Adhesion and Acid-Base Interactions, in, Inverse Gas Chromatography, (Ed. Lloyd, D.R., Ward, T.C. and Schreiber, H.P.) ACS Symposium Series **391**, ACS Washington, D.C., 217 (1989).

Borroff, E.M. and Wake, W.C., "Adhesion of Rubber to Textiles", *Tranactions of the Institute of the Rubber Industry,* **25** , 190 (1949).

Bowden, F.P. and Tabor, D., "The Friction and Lubrication of Solids", Part 1, Clarendon Press, Oxford (1950)

Bowden, F.P. and Tabor, D., "The Friction and Lubrication of Solids" , Part 11, Clarendon Press, Oxford (1964)

Boywer, S., Proceedings of the Third International Conference on Composite Materials, Paris (1980).

Bridgman, P.W., *Phys. Rev.*, **48**, 825 (1935).

Briggs, D., IBM Polymer Symposium, Imperial College, September (1989).

Briggs, D., Rance, D.G. and Briscoe, B.J.,"Surface Properties", Comprehensive Polymer Science, Chapter 23, Volume 2, Pergamon Press (1988).

Briscoe,B.J., "Interfacial Friction of Polymer Composites : General Fundamental Principles", in Friction and Wear of Composite Materials (Ed. K. Freidrich), Elsevier (1985).

Briscoe,B.J., Galvin, K.G. and Williams, D.R., Patent applied for (1989).

Briscoe, B.J., Motamedi, F. and Williams, D.R., "A Static Model of th Transverse Ballistic Capture Efficiencies of Modified Aramid Fabrics", *Proceed. Conf. "Technology and Tommorrow's Fibres"*, Textile Institute, Coventry (1988).

Briscoe,B.J., Scruton, B and Willis, F.R., *Proc. Roy. Soc.*, **A333**, 99. (1973)

Briscoe, B.J. and Tabor, D., "General Outlines of the Mechanisms of Polymer Friction and Wear", in Polymer Surfaces (Ed. Clark , D and Feast, W.J.), (1978)

Brochard,V., "Spreading of Liquid Drops on Thin Cylinders : The "Manchon/Droplet" Transition", *Journal of Chemical Physics*, **84**(8), 4664-4672 (1986).

Broutman. L.J., "Measurement of the Fiber-Polymer Matrix Interfacial Strength", in Interfaces in Composites ASTM STP 327, American Society. Testing and Materials, Phil. Pa., 133. (1963).

Broutman, L.J., "Glass-Resin Joint Strengths and Their Effect on Failure Mechanisms in Reinforced Composites", *Polymer Science and Engineering*, **6**, 263 (1966).

Broutman L.J., "Measurement of the Fiber-Polymer Matrix Interfacial Strength. in, Interfaces in Composites, ASTM STP 452, American Soc. Testing .Mater. Phil. Pa. ,pp27 (1969).

Broutman L.J., "Mechanical Properties of the Fiber Matrix Interface", Proceedings of the 25th Annual Technical Conference of the Society of Plastics Industry, Section 13-B, 1 (1970).

Bueche, F., *Journal of Chemical Physics*, **20**, 1959 (1952).

Caldwell, D.L., Babbington, D.A. and Johnson, C.F., "Interfacial Bond Strength Determination in Manufactured Composites", in Interfacial Phenomena in Composite Materials '89 (Ed. F.R. Jones), Butterworth, pp 44-52 (1989).

Carroll B.J., "The Accurate Measurement of Contact Angle, Phase Contact Area, Drop Volume and Laplace Excess Pressure in a Drop-on-Fibre Systems", *Journal of Colloid and Interface Science*, **57**(3), 488-495 (1976).

Carroll B.J., "The Determination of the Contact Angle of a Liquid Droplet on a Thin Fiber", *Textile Research Journal*, **47**(8), 561-562 (1977).

Carroll B.J., "The Equilibrium of Liquid Drops on Smooth and Rough Circular Cylinders", *Journal of Colloid and Interface Science*, **97**(1), 195-200 (1984).

Cassie A.B.D., "Contact Angles", *Discussions of the Faraday Society*, **3**,11 (1948).

Castells, R.C. and Mazza, G.D., Journal of Applied Polymer Science, **32**, 5917 (1986).

Chabert, B. and Edel, G., C.R. Acad.Sci. Paris, Ser C **267**, 54 (1958).

Chang, H.W., Smith R.P., Li, S. K. and Neumann, A.W. , "Wetting of Reinforcing Fibres" in, Molecular Characterisation of Composite Interfaces, (Eds. H. Ishida and G.Kumar), Plenum Press, pp 413-421 (1985).

Chappell, P.J.C. , Personal Communication, 1989.

Chappell, P.J.C.,Williams, D.R.and George, G.A., "XPS Analysis of Model p-Aramid Compounds and Poly(p-phenylene Terephthalamide) Fibres", Journal of Colloid and Interface Science, in press (1989).

Chappell, P.J.C. and Williams, D.R., "Surface Thermodynamic Analysis of Finishes on Kevlar 29 Fabrics by Inverse Gas Chromatography", Journal of Adhesion Science and Technology, in press (1989a).

Chappell, P.J.C. and Williams, D.R., "Determination of Poly(p-phenylene Terephthalamide) Fibre Surface Cleanliness by Inverse Gas Chromatography", Journal of Colloid and Interface Science,**128**, 501-7 (1989b).

Chase, V.A., "Investigation of Reinforced Plastics for Naval Aircraft Electromagnetic Windows", Whittaker Corp. Report, Naval Airsystems Command Contract N00019-74-C-0055, January (1975).

Chatzi, E.G., Tidrick, S.L. and Koenig, J.L. , "Characterisation of the Surface Hydrolysis of Kevlar 49 Fibers by Diffuse Reflectance FTIR Spectroscopy.", *J. Poly. Sci. Part B.*, **26**, 1585-1593 (1988).

Chen, F., "Study of Donor-Acceptor Interactions at the Polymer Interface by IGC Data Analysis", *Macromolecules,* **21**(6), 1640-43, 1988.

Chiao, T.T. and Moore, R.L., *Composites,* 1, (1973).

Chua, P.S. and Piggott, M.R., "The Glass-Fibre-Polymer Interface: I, Theoretical Consideration for Single Fibre Pull-out Tests", *Composite Science and Technology,* **22**, 33-42 (1985).

Chua, P.S. and Piggott M.R., "The Glass Fibre-Polymer Interface : II" , *Composite Science and Technology,* **22**, 107-119 (1985).

Chua, P.S. and Piggott M.R., "The Glass Fibre-Polymer Interface : III Pressure and Coefficient of Friction", *Composite Science and Technology*, **22**,185-196 (1985).

Chua, P.S. and Piggott M.R. "The Glass Fibre-Polymer Interface : IV" *Composite Science and Technology*, **22**,185-196 (1985).

Clark, D.T. , in Advances in Characterisation of Polymer and Metal Surfaces, (Ed. Lee, L.H.) Academic Press, New York (1977).

Clark, D.T., "The Investigation of Polymer Surfaces by means of ESCA", in Polymer Surfaces (Ed. Clark, D.T. and Feast, W.J.) John Wiley and Sons, Chichester, pp309 (1978).

Collins, G.E. *Journal of the Textile Institute*, **38**, T73 (1947).

Condor, J.R. and Young, C.L., Physicochemical Measurement by Gas Chromatography, John Wiley and Sons, Chichester, 1979.

Corten, H.T., "Micromechanics and Fracture Behaviour of Composites" , in Modern Composite Materials, (Ed.Broutman, L.J. and Krock, R.H.) Addison-Wesley, New York, pp 27-105 (1967).

Cox, H.L.,"The Elasticity and Strength of Paper and other Fibrous Materials", *British Journal of Applied Physics*, **3**,72 (1952).

"Cutting and Machining Kevlar", Du Pont de Nemours International, Industrial Fibres Department, Geneva, Switzland.

Dann, J.R., "Forces in the Adhesive Process I. Critical Surface Tension of Polymers Solids as Determined by Polar Liquids", *Journal of Colloid and Interface Science*, **32**, 302 (1970).

Davidovitz, M., Mittelman, A., Roman, I and Marom, G., "Failure Modes and Fracture Mechanisms in Flexure of Kevlar-epoxy Composites", *Journal of Materials Science*, 19, 377-384 (1984).

Davies, P.C., Cantwell, and Kausch, H.H., "Measurement of Initiation Values of G_{IC} in IM6/PEEK Composites", *Composites Science and Technology*, **35**, 301, 1989.

Day, R.J., Zakikhani, M., Ang,P.P. and Young, R.J., "Studies of Model Poly (p-phenylene benzobisthiazole) Composites using Raman Spectroscopy" in Interfacial Phenomena in Composite Materials '89 (Ed. F.R. Jones), Butterworth, pp.121-124 (1989).

de Charentenay, F.X., Harry J.M., Prel, Y., Benzeggagh, M.L., " Characterising the Effect of Delamination Defect on Mode I Delamination Defect", ASTM STP 386, 84 (1984).

de Charentenay, F.X., Benzeggagh, M.L and Davies, P. "Fracture Mechanics Applied to the Delamination of Composites", *Proceedings of the European Symposium on Damage Development and Failure Processes in Composite Materials*, Departement Metaalkunde en Toegapaste Materiaalkunde, Katolic Universiteit Leuven (1987).

de Gennes, P.G., *Macromolecules*, **9**, 587 (1976).

Delhalle, J., Andre, J.M., Delhalle, S., Pireaux, J.J.,Caudano, R. and Verbist, J.J., "Electronic Structure of Polyethylene: Theory and ESCA Measurements", *Journal of Chemical Physics*, **60**(12), 595, (1974).

Deryaguin, D.V., Krotova, N.A., V.V. Karassev and Kivillova, Y.M. , Proceedings of the 2nd International Congress on Surface Activity III, Butterworths, London, 417 (1957).

Deryaguin, B.V. and Smilga,V.P., Adhesion, Fundamentals and Practice, McLaren and Son, London (1969).

Deryaguin, D.V., Zherrebkov, S.K. and Medvedddeva, A.M. , *Colloid Journal USSR*, **18**, 404 (1956).

Dettre, R.H. and Johnson, R.E., "Contact Angle Hysteris : Part II", in Contact Angle, Wettability and Adhesion, (Ed. Fowkes, F.M.), Advances in Chemistry Series,43 , pp112 (1964).

Dettre, R.H. and Johnson, R.E., "Contact Angle Hysteris : Part IV", *Journal of Physical Chemistry*, **69**, 1507 (1965).

Devitt, D.F., Schapery, R.A. and Bradley, W.L., " A Method for Determining the Mode I Fracture Toughness of Elastic and Viscoelastic Composite Materials", *Journal of Composite Materials*, **14**, 270 (1980).

Di Benedetto, L., Haddad, G., Schilling,C. and Osterholtz,F., Evaluation of Silane Coupling Agents for Glass Fibres in Composite Materials, in Interfacial Phenomena in Composite Materials '89 (Ed. F.R. Jones), Butterworth, pp181-187 (1989).

Di Benedetto, L., Nicolais, A.T. N., Ambrosia, L. and Groeger, J., Stress Transfer and Fracture in Single Fiber/Epoxy Composites, Proceeding of the First International Conference on Composite Interfaces, (Eds. H. Ishida and J.L. Koenig), Elsevier, pp 45-55 (1986).

Di Landro L.and Pegoraro, M., " Carbon fibre-Thermoplastic Matrix Adhesion",*J. Mater. Sci.* **22**,1980-86 (1987).

Dilks,V., in Photon, Electron and Ion Probes of Polymer Structure and Properties, (Ed. Dwight, D.W., Fabish, T.J. and Thomas, H.R.), ACS Symposium Series No. 162, 293 (1981).

Dorey, G., "Impact Damage in Composites- Development, Consequences and Prevention", Proceedings of the 6th International Conference on Composite Materials, London, Elsevier, Volume **3**, pp 1-26 (1987).

Dorey, G., Sidey, G.R. and Hutchins, D, "Impact Properties of carbon/Kevlar 49 hybrid composites", *Composites*, 25 (1978).

Dorris, Gilles M. and Gray, Derek G., "Adsorption, Spreading Pressure, and London Force Interactions of Hydrocarbons on Cellulose and Wood Fiber Surfaces", Journal of Colloid and Interface Science, **71**(1) 93 (1979).

Dorris, Gilles M. and Gray, Derek G., "Adsorption of n-Alkanes at Zero Surface Coverage on Cellulose and Wood Fiber Surfaces", Journal of Colloid and Interface Science, **77**(2) 353, 1980.

Dow, N.F., "Study of the Stresses Near a Discontinuity in a Filament Reinforced Composite Metal", General Electric Report TIS R635D61, AD-414673 (1963).

Drago , R.S. and Wayland, B.B., "A Double Scale Equation for Correlating Enthalpies of Lewis Acid-Base Interactions", *Journal of the American Chemical Society*, **87**(16), 3571 (1965).

Drago, R.S. and Epley, T.D., " Enthalpies of Hydrogen Bonding and Changes in $\Delta\nu$OH for a Series of Adducts with Substituted Phenols", *Journal of the American Chemical Society*, **91**, 2883 (1969).

Drago, R.S., Vogel, G.C,. and Needham, T.E. *Journal of the American Chemical Society*, **93**, 6014 (1971).

Drzal, L.T, "The Interphase in Epoxy Composites", in Epoxy Resin and Composites II, Advances in Polymer Science Series (Ed. K.Dusek), Springer-Verlag, Berlin, 3 (1985).

Drzal, L.T., Rich, M.J., Camping, J.D. and Park, W.J., "Interfacial Shear Strength and Failure Mechanisms in Graphite Fiber Composites", Proceedings of the 35th Annual Technical Conference of the Society of Plastics Industry, Section 20-C, 1 (1980)

Drzal, L.T., Rich, M.J. and Hall, D.L., "Structure-Property Relationships at the Composite Interphase", 15th Biennial Conference on Carbon, American Carbon Society, June (1981).

Drzal, L.T., Rich, M.J. and LLoyd, P.F., "Adhesion of Graphite Fibres to Epoxy matrixes I: The Role of the Fibre Surface Treatment", *J. Adhesion* , **16,** 1-30 (1982)

Drzal, L.T., Rich, M.J., Koenig, M.F. and LLoyd, P.F., "Adhesion of Graphite Fibres to Epoxy matrixes II: The Effect of Fibre Finish", *J. Adhesion* ,**16** 133-152 (1983)

Drzal, L.T., "Adhesion of Graphite Fibers to Epoxy Matrixes. III. The Effect of Hygrothermal Exposure", *J. Adhesion*, **18**(1), 49-72 (1985).

Drzal, L.T., 15th National SAMPE Technical Conference, 190-201, October (1983).

Dwight, D.W. and Thomas, H.R., "Developments in ESCA Analysis of Polymers", *Polymer Preprints*, **22**, 302-305 (1981).

Dwight, D.W., McGrath, J.E. and Wightman, J.P., "ESCA Analysis of Polymer Structure and Bonding I.", *Polymer Preprints*, **18**, 123 (1977).

Eagles.D.B., Blumentritt,B.F. and Cooper,S.L., *J. Applied. Poly.Sci.*, **20**, 435 (1976).

Edel, G. and Chabert, B., *C.R. Acad.Sci. Paris, Ser C* **268**, 226 (1959).

Engelberg, I. and Marom, G., "Some Observations on Transverse Fracture Energies of Unidirectional Composites", *Fibre Science and Technology*, **9**, 63 (1976)

Erickson, P.W. and Plueddeman, E.P., in, Composite Materials (Ed. Broutman and Krock) Chapter 6 ,Volume 6, Academic Press, New York, (1974).

Evans, J.R. and Packham, D.E., in Adhesion 1, (Ed. K.W.Allen), Applied Science Publishers, London (1977).

Fan, C.F. and Hsu, S.L., "A Spectroscopic Analysis of the Stress Distribution along the Reinforcement Fibers in Model Composites : End Effects", *Macromolecules*, **22**, 1474 (1989).

Favrè, J.P. " Review of Test Methods and Testing for Assessment of Fibre-Matrix Adhesion", in Interfacial Phenomena in Composite Materials '89 (Ed. F.R. Jones), Butterworth, pp.7-12 (1989).

Favre, J.P. and Perrin, J., "Carbon Fiber Adhesion to Organic Matrices", *J. Matèr. Sci.*, **7**, 1113 (1972).

Favre, J., "The Role of the Fibre-Matrix Interface", *Proceedings of the European Symposium on Damage Development and Failure Processes in Composite Materials*, Departement Metaalkunde en Toegapaste Materiaalkunde, Katolic Universiteit Leuven (1987).

Finchmun, D.R., Newman, S. and Wiggle, R., *Journal of Applied Polymer Science,* **14**, 2411 (1970).

Fisher, S and Marom, G., "The Flexural Behaviour of Aramid Fibre Hybrid Composite Materials", *Composites Science and Technology, 28, 291-314 (1987).*

Fisher, S and Marom, G., "A Complete Elastic-Plastic Analysis of Aramid Fibre Composites", *Composites Science and Technology*, 20, 91-98 (1984).

Fisher, S, Rosensaft, M. and Marom, G., "Dependence of the Interlaminar Shear Strength on the Loading Span-to-depth Ration in Aramid Fibre-reinforced Beams", *Composites Science and Technology*, 25, 69-73 (1986).

Fitzer,E. *et al. , Carbon*, **18**, 389 (1980).

Fowkes, F.M., *Ind. Eng. Chem.*, **56**, 40 (1964).

Fowkes, F.M., McCarthy, D.C. and Mostafa, M.A., "Contact Angles and the Equilibrium Spreading Pressures of Liquids on Hydrophobic Solids", *Journal of Colloid and Interface Science*, **78**(1), 200 (1980).

Fowkes, F.M. and Maruchi, S., "Surface Acidity and Basicity of Polymers", *Coatings Plastic Preprints*, **37**, 605, (1977).

Fowkes, F.M. and Mostafa, M.A., "Acid-Base Interactions in Polymer Adsorption Industrial and Engineering Chemistry", *Product Research and Development*, **17**,3, (1978)

Fowkes, F.M., "Donor-Acceptor Interactions at Interfaces", in Adhesion and Adsorption of Polymers , Part A , (Ed. Lee, L.H.) Plenum Publishing, New York, 43 (1980).

Fowkes, F.M., "Acid-Base Interactions in Polymer Adhesion", in Physicochemical Aspects of Polymer Surfaces (Ed. K.L. Mittal) , Plenum Pub. New York, Volume 2, 583 (1983).

Fowkes, F.M., Tischler, D.O., Wolfe, J.A., Lannigan, L.A., Ademu-John, C.M. and Halliwell, M.J., "Acid-Base Complexes of Polymers", *Journal of Polymer Science: Polymer Chemistry Ed.*, **22**, 547 (1984).

Fowkes, F.M., "Role of Acid-base Interfacial Bonding in Adhesion", *J.Adhes. Sci. Technol.* **1**(1), 7-27 (1987).

Fox, H.W. and Zisman, W.A., "The Spreading of Liquids on Low Energy Surface Part 1: Polyterafluoroethylene", *Journal of Colloid Science*, **5**, 514 (1950).

Fox , H.W.and Zisman, W.A., "The Spreading of Liquids on Low Energy Surface Part 2: Modified Terafluoroethylene Polymers", *Journal of Colloid Science*, **7**, 109 (1952a).

Fox, H.W. and Zisman, W.A., "The Spreading of Liquids on Low Energy Surface Part 3: Hydrocarbon Surfaces", *Journal of Colloid Science*, **7**, 428, (1952b)

Furlong, D.N.and Hartland S.,"Wall Effect in the Determination of Surface Tension using A Wilhelmy Plate", *Journal of Colloid and Interface Science*, **71**, 301-315 (1979).

Galiotis, C., Young, R.J., Young, P.H.J. and Batchelder, D.N. "The study of model polydiacetylene/epoxy composites: Part 1 The axial strain in the fibre" , *J. Mater. Sci.*, **19**, 3640-3648 (1984).

Galiotis, C., Robinson, I.M., Young, R.J., Smith, B.J.E. and Batchelder, D.N. Strain dependance of the Raman frequencies of a Kevlar 49 fibre, *Polymer Communications* , **26**, 354-55, (1985).

Garton, A., Stevenson, W.T.K. and Wang, S.P., "The Crosslinking of Epoxy Resins at Interfaces V. Amine Cured Resins at Carbon and Graphite Surfaces, *J. Polymer Sci. Part A: Polymer Chemistry,* **26**, 1377-1391 (1988).

Gaymans R.J., Tijssen, J., Harkema, S., and Bantjes,A., "Elastic Molulus in the Crystalline Region of Poly(p-Phenylene Terephthalamide)", *Polymer*, **17**, 517-18 (1976).

Gibson, V.L. and Postle, R., *Text. Res.J.*, **48**, 1,14 (1978)

Gilbert , S.G.and Paik, S.W., "Water Sorption Isotherms on Sucrose and Starch by Modified Inverse Frontal Gas Chromatography", *J. Chromatography*, 351(3), 417-23 (1986).

Good, R.J., "Contact Angles and the Surface Free Energy of Solids", in Surface and Colloid Science, (Eds. R.J. Good and R.R. Stromberg), Plenum Pub. New York, Vol. 11, 1,1979.

Gray , D.G. and Guillet, J.E., "A Gas Chromatographic Method for the Study of Sorption on Polymers", *Macromolecules*, **5**,316 (1972).

Gray, R.J. " Analysis of the Effect of Embedded Fibre Length on Fibre Debonding and Pull-out from an Elastic Matrix", *J. Mater. Sci.*, **19**, 1680 (1984).

Gregg, S.G.and Sing, K.S.W., Adsorption, Surface Area and Porosity, Academic Press, New York, 1967.

Griffith, A.A., "The Phenomena of Rupture and Flow in Solids", *Proceedings of the Royal Society*, **A221**, 163 (1921).

Griffith, A.A., "The Theory of Rupture", *Proceedings of the First International Congress on Applied Mechanics*, Delft (1924).

Grosberg, P. and Swani, N.M., *Text. Res. J.*, **36**, 4, 332 (1966)

Grosberg, P., "Surface Characteristics of Fibres and Textles", Ch.15 (1977)

Gaur, U. and Miller, B., "Microbond Method for Determination of the Shear Strength of a Fiber/Resin Interface: Evaluation of Experimental Parameters", *Composites Science and Technology* , **34**, 35-51 (1989).

Guedra, D., Lang, D., Rouchon, J., Marais, C. and Sigety, P., "Fracture Toughness in Mode I : A Comparison of Various Test Methods", Proceedings of the 6th International Conference on Composite Materials, London, Elsevier, Volume **3**, pp 346-357 (1987).

Gutmann, V., The Donor-Acceptor Approach to Molecular Interactions, Plenum Press, New York, (1978).

Hamilton, R.G., "The Effect of Couple-Stress on the Initiation of Fracture in Composite Materials", Massachusetts Institute of Technology, M.S. Thesis (1970).

Hammer, G.E. and Drzal, L.T., "Graphite Fiber Surface Analysis by X-Ray Photoelectron Spectroscopy and Polar/Dispersive Free Energy Analysis", *Applications of Surface Science*, **4**, 340-355 (1980).

Harvey, J., Kozlowski, C.and Sherwood, P., "X-ray Photoelectron Spectroscopic Studies of Carbon Fibre Surfaces : Part 6: Pilot Plant Surface Treatment and Epoxy Resin Composites" *J. Mat. Sci.*, **22**, 1785-1596 (1987).

Hasemi, S., Kinloch, A.J. and Williams, J.G., "Interlaminar Fracture of Composite Materials", Proceedings of the 6th International Conference on Composite Materials, London, Elsevier, Volume **5**, pp 254-264 (1987).

Hearle, J.W.S., Grosberg, P.and Backer, S., "Structural Mechanics of Fibres, Yarns and Fabrics" (1960)

Hiemenz, P.C., Principles of Colloid and Surface Chemistry, pp235, Marcel Dekker, New York (1977).

Hildebrand, J.H. and Scott, R.L., Regular Solutions, Prentice Hall, Edgewood Cliffs, N.J. (1962).

Hu, P. and Adamson, A.W., "Adsoption and Contact Angle Studies 2. Water and Organic Substances on Polished Polytetrafluoroethylene", *Journal of Colloid and Interface Science*, **59**(3), 605 (1977).

Huang, X.N.and.Hull, D. "Effects of Fibre Bridging on G_{IC} of a Unidirectional Glass/Epoxy Composite", *Composites Science and Technology*, **35**, 283 (1989).

Hunston, D.L., Bascon, W.D.,Moulton, R.J. and Johnson, N.J., "Matrix Resin Effects in Composite Delamination-Mode I Fracture Aspects"., ASTM Special Technical Publication 937 (Toughened Composites), 74-94 (1987).

Inglis, C.E., "Stresses in a Plate due to the Presence of Cracks and Sharp Corners", *Transactions of the Institute of Naval Architects*, **55**(1), 219 (1913)

Irwin, G.R. "Analysis of Stresses and Strains near the End of a Crack Traversing a Plate", *Journal of Applied Mechanics*, **24**, 361 (1957).

Irwin, G.R. , "Analytical Aspects of Crack Stress Field Problems", TAM Report No. 213, University of Illinois (1962).

Irwin, G.R., "Fracture Dynamics", Fracturing of Metals, American Society of Metals, Cleveland, USA, 1948.

Israelachvili, J.N. and Tabor, D., *Wear*, **24**, 386 (1973)

Iyengar, Y. and Erickson, D.E., *Journal of Applied Polymer Science*, **11**, 2311 (1967).

Jahankhani, J.,Vlattas, C. and Galiotis, C. "Interfacial Studies in Aramid/epoxy Systems with Laser Raman Spectroscopy", in Interfacial Phenomena in Composite Materials '89 (Ed. F.R. Jones), Butterworth, pp.125-131 (1989).

James, A.T. and Martin, A.J.P., Biochemistry Journal, **50**, 679 (1952).

Jaworske, D.A. and Maciag, C., "Improving the Interlaminar Shear Strength of Carbon Fiber Epoxy Composites Through Carbon Fibre Bromination", NASA Technical Memo., NASA-TM-100248, E-3870 (1987).

Jennings, C.W., "Surface Preparation for Adhesive Bonding", *Applied Polymer Symposium,* **19**, 49 (1972).

Jensen, W.B. The Lewis Acid-Base Concepts, Wiley Interscience, New York (1980).

Johnson, R.E. and Dettre, R.H., "Contact Angle Hysteris : Part I",in Contact Angle, Wettability and Adhesion, (Ed. F.M. Fowkes), Advances in Chemistry Series, ACS, **43** , p.112 (1964a).

Johnson, R.E and Dettre, R.H., "Contact Angle Hysteris : Part III", *Journal of Physical Chemistry*, **68**, 1744 (1964b).

Johnson, W.S. and Mangalgiri, P.D., "Investigation of Fiber Bridging in DCB Specimens", NASA Technical Memorandum, 87716 (1986).

Jones, F.R., Interfacial Aspects of Glass Fibre Reinforced Plastics, in Interfacial Phenomena in Composite Materials '89 (Ed. F.R. Jones), Butterworth, pp.25-34 (1989).

Kaeble, D.H. "Analysis of Interfacial Bonding Critea for Fibre Composite Fracture Energy", 16th National SAMPE Technical Conference (1984).

Kaelble, D.H., "Dispersion-Polar Surface Tension Properties of Organic Solids", *Journal of Adhesion*, **2** , 66 (1970).

Kaelble, D.H.and Uy, K.C., "A Reinterpretation of Organic Liquid-Polytetrafluoroethylene Surface Interactions", *Journal of Adhesion*, **2** ,50 (1970).

Kaelble, D.H., Dynes, P.J. and Maus, L., "Surface Energy Analysis of Treated Graphite Fibres", *Journal of Adhesion*, **6**, 239 (1974).

Kaelble, D.H., Dynes, P.J. and Cirlin, E.H., "Interfacial Bonding and Environmental Stability of Polymer Matrix Composites", *Journal of Adhesion*, **6**, 23 (1974).

Kaelble, D.H. "Interface Degradation Processes and Durability", *Polymer Science and Engineering*, **17**(7), 474 (1977).

Kageyama, K.,Kobayashi,V and Chou, T.W., "Analytical Compliance Method for Mode I Interlaminar Fracture Toughness Testing of Composites", *Composites*, **18**(5), 393 (1987).

Kamath, Y.K., Dansizer, C.J., Hornby, S. and Weighmann, H.D., "Surface Wettability Scanning of Long Filaments by a Liquid Membrane Technique", *Textile Research Journal*, **57**(4), 205-213 (1987).

Katz, S. and Gray, D.G., "The Adsorption of Hydrocarbons on Cellophane : I. Zero Coverage Limit", *Journal of Colloid and Interface Science*, **82**(2), 318 (1981).

Katz, S. and Gray, D.G., "The Adsorption of Hydrocarbons on Cellophane : II. Finite Coverage Region", *Journal of Colloid and Interface Science*, **82**(2), 326 (1981).

Keller, T.S., Hoffman, A.S., Ratner, B.D. and McElroy, B.J., "Chemical Modification of Kevlar Surfaces for Improved Adhesion to Epoxy Resin Materials : I. Surface Characterisation", in Physicochemical Aspects of Polymer Surfaces, (Ed. K.L. Mittal), Plenum, Volume 2 (1984).

Kelly, A., The Strengthening of Metals by Dispersed Particles, *Proceedings of the Royal Society* 19282 , 63 (1964).

Kelly, A. and.Tyson, W.R., "Tensile Properties of Fibre Reinforced Metals : Copper Tungsten and Copper/ Molybdenum", *Journal of the Physics and Mechanics of Solids*, **13**, 329 (1965).

Kelly, A., Strong Solids, Oxford University Press, Oxford, 1966.

Kelly, A., "Interface effects and the work of fracture of fibrous composite" *Proceeding of the Royal Society* , **A.319**, 95-116 (1970).

Kinloch, A.J. and Young, R.J., Fracture Behaviour of Polymers, Applied Science Publishers, London (1983).

Kinloch, A.J., "Mechanics and Mechanisms of Fracture of Thermosetting Epoxy Polymers", *Advances in Polymer Science*, **72**, 45 (1985).

Kiselev, A.V. and Yashin, Y.I., Gas Adsorption Chromatography, Plenum, New York (1969).

Klein, J. and Briscoe, B.J., *Proceeding of the Royal Society-London,* **A365**, 53 (1979).

Kodokian, G.K.A. and Kinloch, A.J.,"Surface Pretreatment and Adhesion of Thermoplastic Fibre-Composites", *Journal of Material Science Letters*, **7**, 625 (1988).

Konish, H.J.,Swedlow, J.L. and Cruse, T.A., "Experimental Investigation of Fracture in Advanced Fiber Composite", *Journal of Composite Materials*, 114 (1972).

Kremnitzer, S.L. "The Adhesion, Friction and Lubrication of Polyethylene Terephthalate Fibres", PhD. Dissertation, University of Cambridge (1978).

Kruger, R., "Aramid Fibres in Ballistic Materials", Polymers in Defence : International Conference, Bristol, (1983).

Larsen, J.V., "Fracture Energy of CTBN/Epoxy-Carbon Fibre Composite", 26th Annual Conference, Society of Plastics Industry, Reinforced Plastics Division, 10-D (1971).

Lastnik, A.L., Text. Ser. Report., No.32, HQ QMR and D. Comm., Natick, MA, USA (1962).

Leach, D., "Tough and Damge Resistant Composites", *Proceedings of the European Symposium on Damage Development and Failure Processes in Composite Materials*, Departement Metaalkunde en Toegapaste Materiaalkunde, Katolic Universiteit Leuven p136 (1987).

Leaf, G.A.V., in "Mechanics of Flexible Fibre Assemblies" Ed. Hearle, Thwaites and Amirbayat, (1979)

Lee, W. , Personal Communication, 1989.

Lee, S.M A., "Comparison of Fracture Toughness of Matrix Controlled Failure Modes : Delamination and Transverse Cracking", *Journal of Composite Materials*, **20**, 185 (1986).

Lee, W.J., Berg, J.C. and Seferis, J.C., "Characterizing High Performance Composite Processability with Dynamic Fiber Wettability Measurements", *Polymer Composites* (1987).

Mai, Y.M. and Castino, F., "Fracture Toughness of Kevlar-Epoxy Composites with Controlled Interfacial Bonding", *Journal of Material Science*, **19**, 1638 (1984).

Malpass, B.W., Packham, D.E. and Bright, K. , *Journal of Applied Polymer Science,* **18**, 3249 (1974).

Mandell, J.F., "Fracture Toughness of Fiber Reinforced Composites", PhD.Thesis, Massachusetts Institute of Technology (1971).

Mandell, J.F., Chen, J.F. and McGarry, F.J., *International Journal of Adhesion and Adhesives*, **1**(1), 40 (1980).

Mandell, J.F., Grande, D.N., Tsiang,T.H. and McGarry, F.J., "Modified Microdebonding Test for Direct in situ Fiber-Matrix Bond Strength Determinations in Fiber Composites", ASTM STP 893, Test and Design (7th. Conference) (Ed. J. Whitney), ASTM Philladelphia, 87 (1986).

Mandell, J.F. and McGarry, F.J. , "Microdebonding Test for *in situ* Bond Strength Measurement", Summary of Presentation at the 3rd Annual Army Composite Research Review, October (1980).

Marks, A.P. and Drago, R.S., "Justification for the E and C Equation", *Journal of the American Chemical Society,* **97**, 3324 (1975).

Marom, G. and White, E.F.T., "Improvements in the Transverse Properties of Composites : Part I Fracture Surface Energy and Mechanism of Transverse Fracture in Glass Fibre Composites", *Journal of Material Science*, **7**,1299 (1978).

McCarthy, D.C. and Fowkes, F.M., "Predicting Energies of Polymer-Filler Interaction", 40th Annual Conference Preprint, Society of Plastics Industry, Section 17-D (1985).

McKenna, G.B., Mandell, J.F. and McGarry, F.J., "Interlaminar Strength and Toughness of Fibreglass Composites", Society of Plastics Industry, 29th Annual Technical Conference, Section 13c (1974).

McMahon, P.E. and Ying, L., "Effects of Fiber/Matrix Interactions on the Properties of Graphite/Epoxy Composites", NASA Contractor Report 3607 (1982).

Megerdigian, C., Robinson, R. and Lehmann, S., "Carbon Fibre/Resin Matrix Interphase : Effect of Carbon Fibre Surface Treatment and Environmental Conditioning on Composite Performance", Int SAMPE Sym. Exhibition., **33** (Mater. Pathway Future) 571-582 (1988).

Melanitis, N., Tetlow, P., Galiotis, C. and Davies, C.K.L., "Characterisation of Carbon Fibre Surfaces and Examination of Carbon/Epoxy Interfaces with Laser Raman Microscopy", in Interfacial Phenomena in Composite Materials '89 (Ed. F.R. Jones), Butterworth, pp.97-104 (1989).

Menard, H., Lefebvre, Y. and Khorami, J., "Study of the Adsoption of Organic Substances on Asbestos By GC", *Talanta*, **34**(6), 589-92 (1987).

Mijovic, J.S. and Koutsky, J.A. , *Polymers-Plastic Technology Engineering*, **9**(2), 139 (1977).

Miller, B.,. Penn, L.S and Hedvat, S., "Wetting Force Measurements on Single Fibers", *Colloids and Surfaces* , **6**, 49-61 (1983).

Miller, B.,.Muri, P and Rebenfeld, L., "A Microbond Method for Determination of the Shear Strength of a Fiber/Resin Interface", *Composites Science and Technology*, **28**, 17-32 (1987).

Mohlin, U.B. and Gray, D.G., "Gas Chromatography on Polymer Surfaces : Adsorption on Cellulose", *Journal of Colloid and Interface Science*, **47**(3), 747 (1974).

Motamedi, F.M., "Interfacial Friction in Fabric Mechanics", Doctor of Philosophy Thesis, Imperial College (1989).

Mujin, S., Baorong, H., Yisheng, W.. Ying, T., Weiqiu, H. and Youxian, D., "The Surface of Carbon Fibres Continuously Treated by Cold Plasma", *Composites Science and Technology*, **34**, 353-364 (1989).

Nardin, M. and Ward. I.M., "Influence of Surface Treatment on Adhesion of Polyethylene Fibers", *Mater. Sci. Technology.*, **3**(10),814-26,(1987).

Nayar, B.C. and Adamson, A. W., "Adsorption and Contact Angle Studies. 4. Alcohols and Water on Polypropylene and Polycarbonate", in Physicochemical Aspects of Polymer Surfaces, (Ed. LK.Mittal), Plenum, New York, Volume 2, 612-23 (1983).

Netravali, A.N., Stone, D., Ruoff, S. and Topoleski, L.T.T., "Continuous Micro-indenter Push-through Technique for Measuring Interfacial Shear Strength of Fibre Composites", *Composites Science and Technology* , **35** , 289-303 (1989).

Neumann, A.W., "Contact Angles and their Temperature Dependence", *Advances in Colloid and Interface Science*, **4**, 105, (1974).

Noel , L. and Menard, H., "Improved method for Determining Adsoption Isotherms by LC on Long and Short Fibrous Material", *J.Chromatography*, **436**(3) 391-7 (1988).

Olster, E.F. and Jones, R.C., "Toughening Mechanisms in Fiber Reinforced Plastics", Massachusetts Institute of Technology, Civil Engineering Report R70-75 (1970).

Ongchin, L., Olender W.K. and Ancher, F.E., " Fiber Matrix Adhesion and the Fracture Behaviour of Glass Reinforced High Density Polyethylene", Proceedings of the 27th Annual Technical Conference of the Society of Plastics Industry, Section 11-A (1972).

Orchard, A.F. in Handbook of X-ray and Ultraviolet Photoelectron Spectroscopy, (Ed. D.Briggs), Heyden, London, Chapter 1 (1977).

Orowan, E., "Fracture and Strength of Solids", Reports on the Progress in Physics, **12**, 185 (1949).

Osmont, E. and Schreiber, H.P., "Surface Characteristics of Glass Fibers", in, Inverse Gas Chromatography, (Ed. Lloyd, D.R., Ward, T.C. and Schreiber, H.P.) ACS Symposium Series **391**, ACS Washington, D.C., 230 (1989).

Outwater, J.O. and Murphy, M.C., "The Influences of Environment and Glass Finishes on the Fracture Energy of Glass Epoxy Joints", Proceedings of the 25th Annual Technical Conference of the Society of Plastics Industry, Section 16-D, 1 (1970).

Outwater, J.O. and Murphy, M.C., "On the Fracture Energy of Unidirectional Laminates", Proceedings of the 24th Annual Technical Conference of the Society of Plastics Industry, Section 11-C, 1 (1969).

Outwater, J.O. and Murphy, M.C., "On the Fracture Energy of Unidirectional Laminates" *Modern Plastics*, 160 (September 1970).

Owens, D.K. and Wendt, R.C., "Estimation of the Surface Free Energy of Polymers", *Journal of Applied Polymer Science*, **13**, 1741 (1969).

Packham, D.E., Bright, K. and Malpass, B.W., "Mechanical Factors in the Adhesion of Polyethylene to Aluminium", *Journal of Applied Polymer Science,* **18**, 3237 (1974).

Papirer, E., "Characterisation of Fibres and Fillers for Composite Materials Using IGC", in Composite Interfaces (Proc. Int. Conf. 1st.), (Ed. H.Ishida and J. Koenig), North Holland, N.Y., N.Y. pp.203-213 (1986).

Papirer,E., Vidal, A. and Balard,H., "Analysis of Solid Surface Modification", in, Inverse Gas Chromatography, (Ed. Lloyd, D.R., Ward, T.C. and Schreiber, H.P.) ACS Symposium Series **391**, ACS Washington, D.C., 248 (1989).

Papirer, E., Ballard, H., Rahmani, Y., Legrand, A.P L., Facchini, L. and Hommel, H., "Characterisation by IGC of the Surface properties of Silicas Modified by Poly(ethylene Glycolls) and their model Oligomer", *Chromatographia*, **23**(9) 639 (1987).

Pascoe, M.W. and Tabor, D., *Research,* 8, S15 (1955)

Pashley, R.M.and Kitchener, J.A., *Journal of Colloid and Interface Science*, **71**, 491 (1979).

Peirce, F.T., *J. Text. Inst.*, **28**, T45 (1937)

Penn, L.S and Liao, T.K., "Studies on Bonding at the Aramid-Epoxy Interface", *Composites Technology and Review* , 133 (1984).

Penn, L. and Larsen, F. "Physicochemical Properties of Kevlar 49 Fiber ", *Journal of Applied Polymer Science*, **23**(1) 59-74 (1979).

Penn, L.S. and Miller, B., "Advancing, Receding and "Equilibrium" Contact Angles", *Journal of Colloid and Interface Science*, **77**(2), 574-576 (1980).

Penn, L.S. and Lee, S.M., "Interpretation of the Force Trace for Kevlar/Epoxy Single Filament Pull-out Tests", *Fibre Science and Technology*, **17**, 91-97 (1982).

Penn, L.S., Bystry, F.A. and Marchionni, H.J. , "Relaxation of Interfacial Adhesion in Kevlar/Epoxy Systems to Surface Characterisation and Composite Performance", *Polymer Composites* , **4**(1), 26-31 (1983).

Penn, L., Bystry, F., Karp, W. and Lee, S. "Aramid/Epoxy vs. Graphite Epoxy: Origin of the Difference in Strength at the Interface", in Molecular Characterisation of Composite Interfaces ", (Ed. H.Ishida and G. Kumar), Elsevier, 93-109 (1985).

Penn, L.S., Bystry, T.J. and Liao, T.K., " The Study of Reactive Functional Groups in Adhesive Bonding at the Aramid-Epoxy Interface", *J. Adhesion*,, **23**, 163-185 (1987).

Peters, P.W.M. and Springer, G. S., "Effects of Cure and Sizing on Fibre-Matrix Bond Strength", *J.Composite Materials*, **21**, 157-171, (1987).

Petrie, E.M. and Chottiner, J.C., "Plasma Treatment of Aramid Fibers for Improved Composite Properties", Proceedings of the 40th Annual SPE Conference, St.Louis, Minnesota, p.777, (1982).

Phillips, D.C. and Wells, G.M., "The Stability of Transverse Cracks in Fibre Composites", *Journal of Materials Science Letters*, **1**, 321 (1982).

Piggott, M.R. and Dai, S.R., "Brittle Failure at the Fibre-Matrix Interface, in Interfaces in Polymeric, Ceramic and Metal Matrix Composites (Proceedings of the Second International Conference on Composite Interfaces) (Ed. H. Ishida), Elsevier New York, 481-488 (1988).

Piggott,M.R., Load Bearing Fibre Composites, Pergamon, Oxford (1980).

Piggott, M.R., Sanadi, A., Chua, P.S. and Andison, D.,"Mechanical Interactions in the Interphasial region of Fibre Reinforced Thermosets", *in* Proceeding of the First International Conference on Composite Interfaces (H. Ishida and J.L. Koenig Eds), Elsevier, 10 (1986).

Piggott, M.R., "Debonding and Friction at Fibre Polymer Interfaces: Criteria for Failure and Sliding", *Composites Science and Technology*, **30** , 295-306 (1987).

Piggott, M.R., "Debonding and Friction at Fibre Polymer Interfaces:, Macroscopic Model Experiments", *Composites Science and Technology*, **31** , 15-24 (1988).

Piggott, M.R. and Reboredo, M.M., "The Properties of the Interface Between Fibres and Polymers", 34th International SAMPE Symposium (1989).

Pireaux, J.J., Riga, J., Caudano, R. and Verbist, " Electronic Structure of Polymers : XPS Valence Band Spectroscopy", J. Photon, Electron and Ion Probes of Polymer Structure and Properties, (Ed. D.W. Dwight, T.J. Fabish and H.R. Thomas), ACS Symposium Series No. **162**, 169 (1981).

Pooley, C.M. and Tabor, D., *Proc. Roy. Soc.*, **A329**, 251 (1972)

Prevorsek, D.C., Kwon, Y.D., Harpell, G.A. and H.L. Li, ""Spectra" Composite Armor: Dynamics of Absorbing the Kinetic Energy of Ballistic Projectiles", 34th International SAMPE Conference (1989).

Rabinowicz, E. and Tabor, D., *Proc. Roy. Soc.*, **A208**, 455 (1951)

Reilly, C.N., Everhart, D.S. and Ho, F.F.L., "ESCA Analysis of Functional Groups on Modified Polymer Surfaces", *Anal. Chem.*, **53**, 665 (1981).

Rhee,C.K., Ferry, J.D. and Fetters, L.J., *Journal of Applied Polymer Science*, **21**, 783 (1977).

Rich, M.J. and Drzal, L.T. "Interfacial Properties of some High Strain Rate Carbon Fibers in an Epoxy Matrix", *J. Reinf. Plast. Compos.*, **7**(2), 145-54 (1988).

Robinson, I.M., Yeung, P.H.J., Galiotis, C., Young, R.J. and Batchelder, D.N. " Stress Induced Twinning of Polydiacetylene Single Crystal Fibres in Composites", *J. Mater. Sci.*, **21**, 3440-3444 (1986).

Robinson, I.M., Young, R.J., Galiotis, C. and Batchelder, D.N., "The Study of Model Polydiacetylene/epoxy Composites: Part 2 Effect of Resin Shrinkage", *J. Mater. Sci.*, **22**, 3642-3646 (1987).

Roselman, I.C. and Tabor, D., "The Friction of Carbon Fibres", *J. Phys.D: Appl. Phys.*, **9**, 2517 (1976)

Rosen, B.W., "Tensile Failure of Fibrous Composites", *AIAA. Journal*, **2**(11),1985 (1964).

Roylance, D. and Wang, S.S, "Influence of Fibre Properties on Ballistic Penetration of Textile Panels", *Fibre Science and Technology*, **14**, 183 (1981).

Rueda, G., Matthews, F.L. and Godwin, E.W., "An Experimental Comparison of Standard Test Method for the Determination of Tensile, Compressive and Flexural Properties of 'Kevlar" Fibre/Epoxy Laminates", Report of the Centre for Composite Materials, Imperial College (1988).

Rugger, G. and Fenter, J.R. "Ceramic Composite Armour", Kirk-Ottimer Encyclopedia of Chemical Technology, 2ed Supplement, pp 138, Washington DC, (1971).

Saczalski, T.K., "Determination of Multivariate G_{IC} and G_{IIC} Fracture Toughness Response Functions for Fiber/Resin Composites", 34th International SAMPE Meeting (1989).

Saint Flour, C. and Papirer, E., "Gas-Solid Chromatography, A Method of Measuring Surface Free Energy Characteristics of Short Glass Fibers : 1. Through Adsorption Isotherms", *Industrial and Engineering Chemistry Research and Development*, **21**,337 (1982).

Saint Flour, C. and Papirer, E., Gas-Solid Chromatography, "A Method of Measuring Surface Free Energy Characteristics of Short Glass Fibers : 2. Through Retention Volumes Measured near Zero Surface Coverage", *Industrial and Engineering Chemistry Research and Development*, **21**, 666 (1982).

Saint Flour , C. and Papirer, E., "Gas-Solid Chromatography :A Quick Method for Estimating Surface Free Energy Variations Induced by the Treatment of Short Glass Fibers", *Journal of Colloid and Interface Science*, **91**(1), 69 (1982).

Savage, G.M., "Fabric and Fibre Reinforced Laminate Armours", *Metals and Materials*, 285 (May 1989).

Schick, M.J., "Surface Characteristics of Fibres and Textiles", *Fibre Science Series*, Chapter 1 (1975)

Schulman, F. and Zisman, W.A., *Journal of Colloid Science*, **7**, 465 (1952).

Schultz, W.J. *et al.* , "Fracture Toughness of FRP Laminated Plates", Massachusetts Institute of Technology, Civil Engineering Report (1970).

Schultz, J. and Lavielle, L., "Interfacial Properties of Carbon Fiber-Epoxy Matrix Composites", in, Inverse Gas Chromatography, (Ed. Lloyd, D.R., Ward, T.C. and Schreiber, H.P.) ACS Symposium Series **391**, ACS Washington, D.C., 185 (1989).

Schultz, J., Lavielle, L. and C. Martin , "The Role of the Interface on Carbon Fibre-Epoxy Composites", *Journal of Adhesion*, **23**(1), 45 (1987).

Schultz, J., Lavielle, L. and Martin , C., "Surface Properties of Carbon Fibres determined by Inverse gas Chromatography", *J. Chim. Phys. Phys.-Chim. Biol.*, **84**(2), 231-7 (1987).

Scola, D.A., "High-Modulus Fibers and the Fiber-Resin Interface in Resin Composites", in Interfaces in Polymer Matrix Composites, (Ed. E.P. Pluddemann) Academic Press, New York, p217 (1974).

Scott, J.M. and Phillips, D.C., "Carbon Fibre Composites with Rubber Toughened Matrices", *Journal of Material Science*, **10**, 551 (1975).

Scruton, B. Ph.D.Thesis, University of Cambridge, (1971)

Seletti C., Vargui S., Martuscelli E. and Fabbro, D., "Wettability of Glass Fibers with Different Sizes and their Adhesion to unsaturated Polyester Matrixes", *J.Mater. Sci.*, **22**(10), 3477-84 (1987).

Sell, P.J., "Wetting Properties of Carbon Fibres", *Umschau*, **72**(13) , 433 (1972).

Seo, K.S., Fornes, R.E., Gilbert, R.D. and Memory, J.D., " Effects of Ionising Radiation on Epoxy, Graphite Fibre and Epoxy/Graphite Composites : Part 1 Surface Energy Changes", *J.Poly. Sci., Part B: Polym. Phys.*, **26**(2), 245-55 (1988).

Shephard R.G, "The use of Polymers in Personal Ballistic Protection", Polymers in Defence : International Conference, Bristol (1983).

Shih, G.C. and Chen, E.P., "Fracture Analysis of Unidirectional Composites", *Journal of Composite Materials*, 230 (1973).

Shiriajeva, G.V. and Andreevskaya, G.D., *Soviet Plastics*, **4**, 40-42 (1962).

Sidney, G.R. and Bradshaw, F.J., "Some Investigations on Carbon-Fibre Reinforced Plastics under Impact Loading, and Measurements of Fracture Energy", in Proceedings of the International Conference on Carbon Fibres, The Plastics and Rubber Institute, London (1971).

Siegbahn, K *et al.* , *Nova Acta R. Soc. Sci. Uppsala*, Series IV, **20** (1967).

Siegmund, A.J. and Kukanskis, P., *Adhesives Age,* **19**(2), 29 (1976).

Slepetz, J.M. and Carlson, L., "Fracture of Composite Compact Tension Specimens", in Fracture Mechanics of Composites, ASTM STP 593, 143 (1975).

Smith, A.C., " Interfacial Shear Properties of Thin Polymer Films ", PhD Dissertation, Imperial College, (1979)

Snyder, L.R., Principles of Adsorption Chromatography, Marcel Dekker, New York (1968).

Stull, D.R.,Westrum, E.F. and Sinke,U.C., in The Chemical Thermodynamics of Organic Compounds, John Wiley, New York (1969).

Summerscales, J., "Non-destructive Testing By Raman Spectroscopy", in Proceedings of the 6th International Conference on Composite Materials, London, Elsevier, Volume **1**, pp 321-331 (1987).

Tadros, M.E., Hu, P. and Adamson, A.W.," Adsorption and Contact Angle Studies 1. Water on Smooth Carbon, Linear Polyethylene and Steric Acid-Coated Copper ", *Journal of Colloid and Interface Science* , **49**(2), 184 (1974).

Tagiaferri, V., Crivelli Visconti, I. and Di Ilio, A., "Machining of Fibre Reinforced Materials with Laser Beam : Cut Quality Evaluation", in Proceedings of the 6th International Conference on Composite Materials, London, Elsevier, Volume **1**, pp 190-198 (1987).

Takayanagi, M. and Katayose, T., " N. Substituted Poly(p-Phenylene Terephthalamide)", *J.Poly. Sci. Poly. Chem. Ed.*, **19**, 1133 (1981).

Takayanagi, M., Kajiyama, T. and Katayose, T., "Surface-Modified Kevlar Fiber Reinforced Polyethylene and Ionomer", *J. Appl. Poly. Sci.*, **27**, 3903 (1982).

Takayanagi, M., Ueta, S., Lei, W.Y. and Koga, K., "A New Chemical Method of Surface Treatment of Kevlar Fiber for Composites with Epoxy Resin", *Polymer Journal,* **19**(5), 467-474 (1987).

Termonia, Y., "Theoretical study of the stress transfer in single fibre composites", *J. Mater. Sci.*, **22**, 504-508 (1987)

Tetelman, A.S., "Fracture Processes in Fiber Composite Materials", in Composite Materials : Testing and Design, ASTM STP 460, 473, 1969.

Thomas, H.R. and O'Malley, J.J., " Surface Studies on Multicomponent Polymers Systems by XPS : PS-PEO Diblock Copolymers", *Macromolecules*, **12**, 323 (1979).

Tse, J. and Adamson, A.W., "Adsorption and Contact Angle Studies 3. Organic Substances on Polished Polyethylene", *Journal of Colloid and Interface Science*, **72**(3), 515 (1979).

Tseng, C.S., LLoyd, D.R. and Ward, L.C., *Journal of Applied Polymer Science*, **30**,1815 (1985).

Ulrich, H.H., *Faserforsch Textiltech,* **22** (10), 501 (1971).

van Oss, C.J., Good, R.J. and Chaudhury, M.K., "Additive and Nonadditive Surface Tension Components and the Interpretation of Contact Angles", *Langmuir*, **4**, 884 (1988)

Varma, D.S., Needles, H.L., Kourtides, D.A. and Fish, R.H. , "Interlaminar Shear Properties of Graphite Fiber High Perfprmance Composites", *Polymer Composites*, **4**, 99 (1983).

Verpoest, I, "Interfaces in Aramid-Fibre Reinforced Plastics", *Proceedings of the European Symposium on Damage Development and Failure Processes in Composite Materials*, Departement Metaalkunde en Toegapaste Materiaalkunde, Katolic Universiteit Leuven (1987).

Voyutskii, S.S., Autoadhesion and Adhesion of High Polymers, John Wiley and Son, New York, 1963.

Vukov, A.J. amd Gray, D.G., "Properties of Carbon Fiber Surfaces", in, Inverse Gas Chromatography, (Ed. Lloyd, D.R., Ward, T.C. and Schreiber, H.P.) ACS Symposium Series **391**, ACS Washington, D.C., 168 (1989).

Wadsworth,N.J. and Spilling,I, "Load Transfer from Broken Fibres in Composite Materials", *British Journal of Applied Physics*, Series 2, **1**, 1049 (1968).

Waltersson, K., "ESCA Studies of Carbon Fibres Part 1 -The Chemical Composition of a Coarbon Fibre Subsurface", *Fibre Science and Technology*, **17**, 289-302 (1982)

Waltersson, K., "ESCA Studies of Carbon Fibres Part 2 - Surface Reactions of Carbon Fibres with Epoxides", *Composites Science and Technology*, **22**, 223-239 (1985).

Waltersson, K., "ESCA Studies of Carbon Fibres Part 3 - Surface Reactions of Carbon Fibres with Amines", *Composites Science and Technology*, **23**, 303-321 (1985).

Wardle, M.W. and Steenkamer, D.A., "Special Considerations in Testing Advanced Composite Materials Reinforced with "Kevlar" Aramid Fibres", in Proceedings of the 6th International Conference on Composite Materials, Elsevier, Volume 1,199 (1987).

Weinberg, M., "Surface Energy Measurements of Graphite and Glass Filaments", in Toughened Composites, ASTM Conference, Houston (1985).

Wenzel, R.N., *Industrial and Engineering Chemistry*, **28**,988 (1936).

Wertheimer, M.R. and Schreiber, H.P., "Surface Property Modification of Aromatic Polyamides by Microwave Plasmas", *Journal of Applied Polymer Science*, **26**, 2087 (1981).

Wesson, S.P. and Allred, R.E., "Surface Energetics of Plasma-Treated Carbon Fiber", in, Inverse Gas Chromatography, (Ed. Lloyd, D.R., Ward, T.C. and Schreiber, H.P.) ACS Symposium Series **391**, ACS Washington, D.C., 203 (1989).

Wesson, S.P. and Tarantino, A., "Wetting Characteristics of E-Glass Textile Filaments", *Journal of Non-Crystalline Solids*, **38/39** 619-624 (1980).

Westerlind, B.S. and Berg, C., "Surface Energy of Untreated and Surface-Modified Cellulose Fibers", *Journal of Applied Polymer Science*, **36**, 523-534 (1988).

Williams, D.R. and Fowkes, F.M., "The Acid-Base and Wettability Behaviour of some Polymer Surfaces", submitted to *Journal of Colloid and Interface Sci.*, 1989.

Williams, J.G. , Fracture Mechanics of Polymers, Ellis Horwood, Chichester (1984) .

Williams, J.G., "Large Displacement Effects in the DCB Test for Interlaminar Fracture in Modes I and II", in Proceedings of the 6th International Conference on Composite Materials, London, Elsevier Volume 3, 233 (1987).

Williams, J.G., " On the Calculation of Energy Release Rates for Cracked Laminates", *International Journal of Fracture,* 36, 101 (1988).

Wu, E.M., "Fracture Mechanics of Anistropic Plates", in Composite Materials Workshop, (Ed. Tsia, S.T., Halpin, J.C. and Pagano, N.J.), Technomic Pub., Westport Conneticut, pp 20-43 (1968).

Wu, S., *J. Applied Polymer Science*, C**34**, 19 (1971).

Wu, S., Polymer Interface and Adhesion, Dekker, New York (1982).

Wu, E.M., in Composite Materials, Volume 5, Academic Press, N.Y., (1974).

Yamaki, J.I. and Katayama,Y.,*J.Applied Poly. Sci.* , **19**, 2897 (1975).

Young, T., *Proc.Royal. Soc.,* December 1804; *Philos. Trans.*, **95**, 65-84 (1805).

Zisman, W.A., in Advances in Chemistry Series., ACS, **43**, 1 (1964).

Zweben, C., "The Flexural Strength of Aramid Fibre Composites", *Journal of Composite Materials*, **12**, 422 (1978).